frontiers | Research Topics

Innate immunity: Platelets and their interaction with other cellular elements in host defense and disease pathogenesis

Edited by
Meganathan Kannan, Firdos Ahmad, Esaki M. Shankar and Kopperuncholan Namachivayam

Published in
Frontiers in Immunology

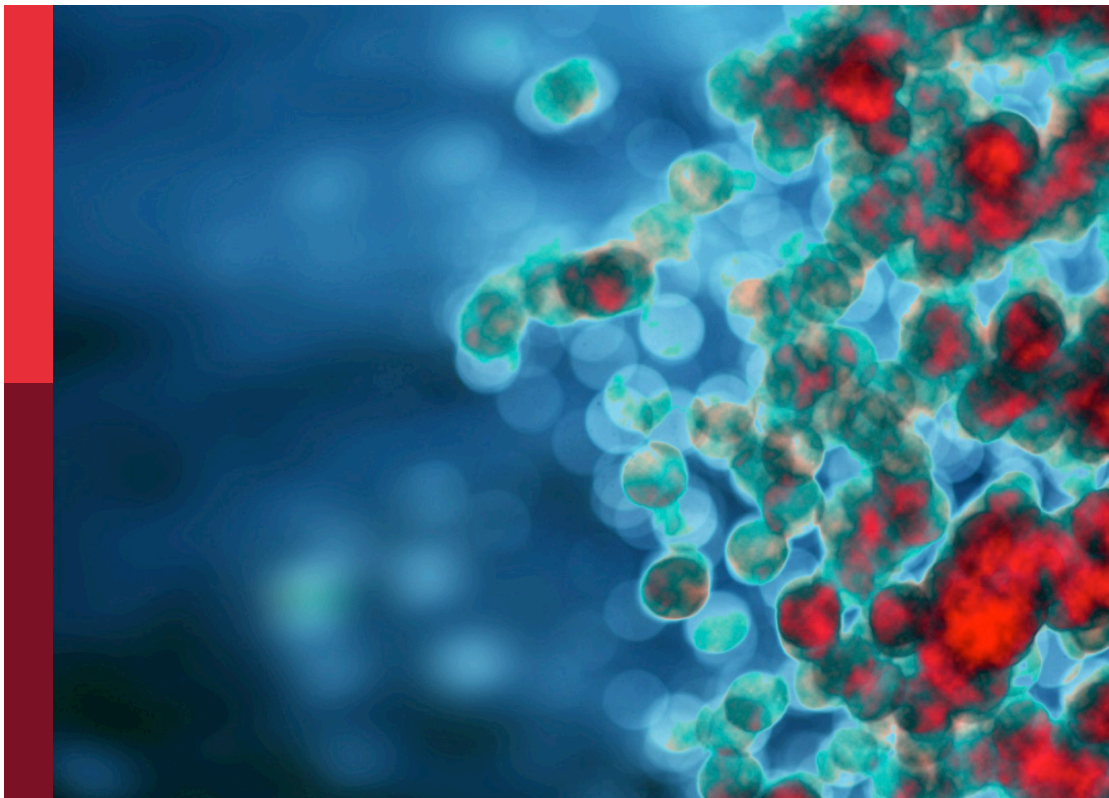

ISSN 1664-8714
ISBN 978-2-8325-3872-2
DOI 10.3389/978-2-8325-3872-2

About Frontiers

Frontiers is more than just an open access publisher of scholarly articles: it is a pioneering approach to the world of academia, radically improving the way scholarly research is managed. The grand vision of Frontiers is a world where all people have an equal opportunity to seek, share and generate knowledge. Frontiers provides immediate and permanent online open access to all its publications, but this alone is not enough to realize our grand goals.

Frontiers journal series

The Frontiers journal series is a multi-tier and interdisciplinary set of open-access, online journals, promising a paradigm shift from the current review, selection and dissemination processes in academic publishing. All Frontiers journals are driven by researchers for researchers; therefore, they constitute a service to the scholarly community. At the same time, the *Frontiers journal series* operates on a revolutionary invention, the tiered publishing system, initially addressing specific communities of scholars, and gradually climbing up to broader public understanding, thus serving the interests of the lay society, too.

Dedication to quality

Each Frontiers article is a landmark of the highest quality, thanks to genuinely collaborative interactions between authors and review editors, who include some of the world's best academicians. Research must be certified by peers before entering a stream of knowledge that may eventually reach the public - and shape society; therefore, Frontiers only applies the most rigorous and unbiased reviews. Frontiers revolutionizes research publishing by freely delivering the most outstanding research, evaluated with no bias from both the academic and social point of view. By applying the most advanced information technologies, Frontiers is catapulting scholarly publishing into a new generation.

What are Frontiers Research Topics?

Frontiers Research Topics are very popular trademarks of the *Frontiers journals series*: they are collections of at least ten articles, all centered on a particular subject. With their unique mix of varied contributions from Original Research to Review Articles, Frontiers Research Topics unify the most influential researchers, the latest key findings and historical advances in a hot research area.

Find out more on how to host your own Frontiers Research Topic or contribute to one as an author by contacting the Frontiers editorial office: frontiersin.org/about/contact

Innate immunity: Platelets and their interaction with other cellular elements in host defense and disease pathogenesis

Topic editors

Meganathan Kannan — Central University of Tamil Nadu, India
Firdos Ahmad — University of Sharjah, United Arab Emirates
Esaki M. Shankar — Central University of Tamil Nadu, India
Kopperuncholan Namachivayam — Johns Hopkins University, United States

Citation

Kannan, M., Ahmad, F., Shankar, E. M., Namachivayam, K., eds. (2023). *Innate immunity: Platelets and their interaction with other cellular elements in host defense and disease pathogenesis*. Lausanne: Frontiers Media SA.
doi: 10.3389/978-2-8325-3872-2

Table of contents

frontiers | Frontiers in Immunology

TYPE Editorial
PUBLISHED 28 September 2023
DOI 10.3389/fimmu.2023.1292316

OPEN ACCESS

EDITED AND REVIEWED BY
Francesca Granucci,
University of Milano-Bicocca, Italy

*CORRESPONDENCE
Meganathan Kannan
meganathank@cutn.ac.in

RECEIVED 11 September 2023
ACCEPTED 21 September 2023
PUBLISHED 28 September 2023

CITATION
Kannan M, Ahmad F and Shankar EM (2023) Editorial: Innate immunity: platelets and their interaction with other cellular elements in host defense and disease pathogenesis.
Front. Immunol. 14:1292316.
doi: 10.3389/fimmu.2023.1292316

Editorial: Innate immunity: platelets and their interaction with other cellular elements in host defense and disease pathogenesis

Meganathan Kannan[1]*, Firdos Ahmad[2] and Esaki M. Shankar[3]

[1]Blood and Vascular Biology Research Lab, Department of Biotechnology, Central University of Tamil Nadu, Thiruvarur, India, [2]Department of Basic Medical Sciences, College of Medicine, University of Sharjah, Sharjah, United Arab Emirates, [3]Infection and Inflammation, Department of Biotechnology, Central University of Tamil Nadu, Thiruvarur, India

KEYWORDS

platelet, innate immunity, cell-cell interactions, microparticle, inflammatory responses

Editorial on the Research Topic

Innate immunity: platelets and their interaction with other cellular elements in host defense and disease pathogenesis

Platelets are the anucleate cells that impact the immune system by releasing their cellular contents (1). Immunological reactions are responsible for effectively clearing foreign particles from the body. However, immune responses, at times, can lead to adverse pathological manifestations in the host (2). Platelets play a critical role in innate immunity via encasement of microbial intruders by necessitating the coagulation process, preventing them from disseminating further in the host system. Because platelets can interact with other cellular elements and trigger immune responses either directly or indirectly, they are often regarded as one of the first-line defenders against microbial invasion (3). Further, activated platelets express certain proteins on their surface and release granular contents that provide the ability to cross-talk with immune cells contributing to innate immune responses. When platelets are activated, they release microvesicles called platelet microparticles that play a crucial role in enhancing inflammatory responses (4). These microparticles communicate with immune cells and other cellular elements in the host, thereby contributing significantly to immune responses. Understanding the role of platelet microparticles in the pathogenesis of clinical conditions is essential for effective disease management. This Research Topic has addressed the role of platelets and other associated cellular and soluble elements in host defense and surveillance mechanisms. We invited research related to key areas such as the mechanism and sources of platelet activation, the role of platelets and other cellular elements in defense mechanisms, association of activated platelets in infections, role of platelet activation against viral agents, platelet-microvesicles as immune mediators in health and diseases, Platelet interaction with complement mediators and many other relevant topics. In response to these topics, a total of nine articles were submitted by researchers.

In this Research Topic, Lee et al. proposed that activated platelets promote the expression of CD16+ on CD14+ monocytes. It is known that monocytes and macrophages are the key components of the innate immune system playing a crucial role in the pathogenesis of various inflammatory disorders including rheumatoid arthritis (RA). However, the mechanism of induction of CD16+ on monocytes and its significance remain ambiguous. This study demonstrated that activated platelets play an important role in the expression of CD16 on monocytes, which possibly alters their phenotypical and functional features. Further, this study identified that soluble CD62P, a marker of activated platelets, was elevated in RA patients which justifies the increased expression of CD16+ on CD14+ monocytes in these patients.

Another study by Saris et al. demonstrated that platelets can serve as potential immune modulators contributing to the transfusion-related immune modulation (TRIM) in platelet transfusions. They showed that the platelet releasate inhibits the pro-inflammatory properties of dendritic cells thus decreasing the T cell responses. This study adds value to transfusion-related immune modulation.

Viral infections alter the morphological and biochemical features of platelets to facilitate their participation in defense mechanisms (5, 6). While such alterations of platelets are necessary for the inflammation response, these alterations also trigger hypercoagulation (7). Kim et al. demonstrated that platelet-mediated neutrophil extracellular trap (NET) amplifies coagulopathy that contributes to lung immunopathogenesis during influenza virus A infection. The study strongly indicates that thrombin is a key molecule connecting coagulation and inflammation in infection.

Nanodiamonds (NDs) have potential biomedical applications such as drug delivery and bioimaging (8). Hung et al. tested the induction and rescue of thrombocytopenia in mice with various sizes of NDs and found that those NDs with 50 nm in size promote cell death leading to thrombocytopenia. Further, they found that these NDs induce stronger platelet aggregation, pyroptosis, and apoptosis suggesting the scope for the therapeutic development of thrombocytopenia.

Interleukin 8 (IL-8) is a member of the chemokine family and is one of the early indicators of bacterial infections (9). While IL-8 is secreted by various cells, the mechanism of release was unclear, Quach et al. unraveled the role of platelets in potentiating bacterial-induced IL-8 release from monocytes in human whole blood.

The complete blood count (CBC) parameters, though routine, have become very important in the accurate diagnosis of some of the clinical diseases in the early stage. For example, recent studies have associated dysregulation of mean platelet volume (MPV) with tuberculosis (10, 11). Multiple parameters and cell indices are being associated with clinical outcomes to verify whether these can serve as biomarkers. Weng et al. in this Research Topic, reported that the white blood cell counts to mean platelet volume ratio (WMR) is an important prognostic indicator for acute ischemic stroke outcomes (AIS). The authors studied a total of 549 AIS patients to conclude the above. Additionally, when CBC is combined with the cellular components/releasates, they become critical indicators of various diseases. Urban-Solano et al. studied both latent and active tuberculosis and found that platelet count is correlated very much with the high levels of platelet factor 4 (PF4) and vascular endothelial growth factor (VEGF-A) in active tuberculosis. Baier et al. provided evidence that low platelet count is correlated with the markers of kidney injury and decreased complement C3. The study concluded the link between platelets, complement activation system, and clinical outcome. All three studies reported in this Research Topic strongly suggest that the cellular subpopulations are gaining value in clinical outcomes.

Activated platelets release tiny particles known as platelet microparticles (PMP) that are less than 1 μm in size. These microparticles are thrombogenic and participate in the pathogenesis of various diseases including cancer (12). Elevated PMP, an indicator of activated platelets in circulation, has been identified in several clinical conditions such as hypertension, diabetes, etc (13, 14). Gharib et al. studied the role of PMP in the progression of chronic lymphocytic leukemia (CLL) using cell lines. The study concluded that PMP provokes CLL through metabolic reprogramming.

All the above studies strongly suggest that platelets are the major contributors of the pathogenesis of many clinical conditions. Thus measurement of activated platelets, utilizing a reliable diagnostic tool, in many pathological conditions may undoubtedly benefit the effective management of diseases.

Author contributions

MK: Conceptualization, Writing – original draft, Writing – review & editing. FA: Writing – review & editing. ES: Writing – review & editing.

Acknowledgments

The authors thank the researchers who contributed their work to this Research Topic.

Conflict of interest

The authors declare that the research was conducted in the absence of any commercial or financial relationships that could be construed as a potential conflict of interest.

The author(s) declared that they were an editorial board member of Frontiers, at the time of submission. This had no impact on the peer review process and the final decision.

Publisher's note

References

1. Koupenova M, Clancy L, Corkrey HA, Freedman JE. Circulating platelets as mediators of immunity, inflammation, and thrombosis. *Circ Res* (2018) 122(2):337–51. doi: 10.1161/CIRCRESAHA.117.310795

2. Conroy M, Naidoo J. Immune-related adverse events and the balancing act of immunotherapy. *Nat Commun* (2022) 13(1):392. doi: 10.1038/s41467-022-27960-2

3. Mezger M, Nording H, Sauter R, Graf T, Heim C, von Bubnoff N, et al. Platelets and immune responses during thromboinflammation. *Front Immunol* (2019) 10:1731. doi: 10.3389/fimmu.2019.01731

4. Di L, Zha C, Liu Y. Platelet-derived microparticles stimulated by anti-β_2GPI/β_2GPI complexes induce pyroptosis of endothelial cells in antiphospholipid syndrome. *Platelets* (2023) 34(1):2156492. doi: 10.1080/09537104.2022.2156492

5. Schrottmaier WC, Schmuckenschlager A, Pirabe A, Assinger A. Platelets in viral infections - brave soldiers or trojan horses. *Front Immunol* (2022) 13:856713. doi: 10.3389/fimmu.2022.856713

6. Meena AA, Amudhan M, Sopnajothi S, Yong YK, Ganesh PS, Vimali IJ, Vignesh R, Elanchezhiyan M, Kannan M, Dash AP, Shankar EM. Increase of plasma TNF-α is associated with decreased levels of blood platelets in clinical dengue infection. *Viral Immunology* (2020) 33(1):54–60. doi: 10.1089/vim.2019.0100

7. Al-Tamimi AO, Yusuf AM, Jayakumar MN, Ansari AW, Elhassan M, AbdulKarim F, et al. SARS-CoV-2 infection induces soluble platelet activation markers and PAI-1 in the early moderate stage of COVID-19. *Int J Lab Hematol* (2022) 44(4):712–21. doi: 10.1111/ijlh.13829

8. Chauhan S, Jain N, Nagaich U. Nanodiamonds with powerful ability for drug delivery and biomedical applications: Recent updates on in vivo study and patents. *J Pharm Anal* (2020) 10(1):1–12. doi: 10.1016/j.jpha.2019.09.003

9. Selvavinayagam ST, Aswathy B, Yong YK, Frederick A, Murali L, Kalaivani V, et al. Plasma CXCL8 and MCP-1 as biomarkers of latent tuberculosis infection. *MedRxiv (Cold Spring Harbor)* (2023) doi: 10.1101/2023.08.07.23293767

10. Xu F, Qu S, Wang L, Qin Y. Mean platelet volume (MPV): new diagnostic indices for co-morbidity of tuberculosis and diabetes mellitus. *BMC Infect Dis* (2021) 21 (1):461. doi: 10.1186/s12879-021-06152-1

11. Wei Y, Tang S, Xie Z, He Y, Zhang Y, Xie Y, et al. Pulmonary tuberculosis-related ischemic stroke: A retrospective case control study. *J Inflammation Res* (2022) 15:4239–49. doi: 10.2147/JIR.S368183

12. Moreau J, Pelletier F, Biichle S, Mourey G, Puyraveau M, Badet N, et al. Increased levels of circulating platelet-derived microparticles are associated with metastatic cutaneous melanoma. *Exp Dermatol* (2017) 26(10):961–3. doi: 10.1111/exd.13339

13. Kannan M, Ahmad F, Saxena R. Platelet activation markers in evaluation of thrombotic risk factors in various clinical settings. *Blood Rev* (2019) 37:100583. doi: 10.1016/j.blre.2019.05.007

14. Maphumulo SC, Pretorius E. Role of circulating microparticles in type 2 diabetes mellitus: implications for pathological clotting. *Semin Thromb hemostasis* (2022) 48 (2):188–205. doi: 10.1055/s-0041-1740150

frontiers in Immunology

ORIGINAL RESEARCH
published: 07 January 2021
doi: 10.3389/fimmu.2020.611133

Activated Platelets Convert CD14$^+$CD16$^-$ Into CD14$^+$CD16$^+$ Monocytes With Enhanced FcγR-Mediated Phagocytosis and Skewed M2 Polarization

*Su Jeong Lee[1,2], Bo Ruem Yoon[3], Hee Young Kim[3,4], Su-Jin Yoo[5], Seong Wook Kang[5] and Won-Woo Lee[1,3,4,6,7,8]**

[1] Laboratory of Autoimmunity and Inflammation (LAI), Department of Biomedical Sciences, Seoul National University College of Medicine, Seoul, South Korea, [2] BK21Plus Biomedical Science Project, Seoul National University College of Medicine, Seoul, South Korea, [3] Department of Microbiology and Immunology, Seoul National University College of Medicine, Seoul, South Korea, [4] Institute of Infectious Diseases, Seoul National University College of Medicine, Seoul, South Korea, [5] Department of Internal Medicine, Chungnam National University School of Medicine, Daejeon, South Korea, [6] Cancer Research Institute, Seoul National University College of Medicine, Seoul National University Hospital Biomedical Research Institute, Seoul, South Korea, [7] Ischemic/Hypoxic Disease Institute, Seoul National University College of Medicine, Seoul, South Korea, [8] Seoul National University Hospital Biomedical Research Institute, Seoul, South Korea

OPEN ACCESS

Edited by:
Fabrice Cognasse, Groupe Sur L'immunité Des Muqueuses Et Agents Pathogènes (GIMAP), France

Reviewed by:
Cyril Clavel, Université Toulouse III Paul Sabatier, France
Arnaud Millet, INSERM U1209 Institut pour l'Avancée des Biosciences (IAB), France

***Correspondence:**
Won-Woo Lee
wonwoolee@snu.ac.kr

Specialty section:
This article was submitted to Inflammation, a section of the journal Frontiers in Immunology

Received: 28 September 2020
Accepted: 20 November 2020
Published: 07 January 2021

Citation:
Lee SJ, Yoon BR, Kim HY, Yoo S-J, Kang SW and Lee W-W (2021) Activated Platelets Convert CD14$^+$CD16$^-$ Into CD14$^+$CD16$^+$ Monocytes With Enhanced FcγR-Mediated Phagocytosis and Skewed M2 Polarization. Front. Immunol. 11:611133. doi: 10.3389/fimmu.2020.611133

Monocytes are important cellular effectors of innate immune defense. Human monocytes are heterogeneous and can be classified into three distinct subsets based on CD14 and CD16 expression. The expansion of intermediate CD14$^+$CD16$^+$ monocytes has been reported in chronic inflammatory diseases including rheumatoid arthritis (RA). However, the mechanism underlying induction of CD16 and its role in monocytes remains poorly understood. Here, we demonstrate that activated platelets are important for induction of CD16 on classical CD14$^+$CD16$^-$ monocytes by soluble factors such as cytokines. Cytokine neutralization and signaling inhibition assays reveal that sequential involvement of platelet-derived TGF-β and monocyte-derived IL-6 contribute to CD16 induction on CD14$^+$CD16$^-$ monocytes. Activated platelet-induced CD16 on monocytes participates in antibody-dependent cellular phagocytosis (ADCP) and its level is positively correlated with phagocytic activity. CD14$^+$CD16$^-$ monocytes treated with activated platelets preferentially differentiate into M2 macrophages, likely the M2c subset expressing CD163 and MerTK. Lastly, the amount of sCD62P, a marker of activated platelets, is significantly elevated in plasma of RA patients and positively correlates with clinical parameters of RA. Our findings suggest an important role of activated platelets in modulating phenotypical and functional features of human monocytes. This knowledge increases understanding of the immunological role of CD14$^+$CD16$^+$ cells in chronic inflammatory diseases.

Keywords: TGF-β, IL-6, phagocytosis, platelet, CD14$^+$CD16$^+$ monocytes, M2 macrophages, rheumatoid arthritis, MerTK

INTRODUCTION

Monocytes are circulating blood leukocytes typically regarded as systemic precursors of macrophages and dendritic cells (DCs) (1–3). Besides their primary role as precursors, monocytes also act as important innate effectors in the pathogenesis of various inflammatory diseases as well as in the inflammatory response against infectious pathogens through phagocytosis, production of reactive oxygen species (ROS), secretion of proinflammatory soluble factors, and the activation of adaptive immunity (4, 5). In humans, peripheral monocytes are heterogeneous and classified into three functionally distinct subsets depending on the expression of CD14, a coreceptor for LPS, and CD16 (also known as FcγRIII). These include classical $CD14^+CD16^-$, intermediate $CD14^+CD16^+$, and nonclassical $CD14^{dim}CD16^+$ monocytes (6–9). *In vivo* deuterium labeling experiments revealed that $CD14^+CD16^-$ monocytes have the potential to become $CD14^+CD16^+$ monocytes before finally differentiating into $CD14^{dim}CD16^+$ monocytes under steady state and experimental endotoxemic conditions (10). Moreover, $CD16^+$ monocytes are expanded in patients with inflammatory disorders including several autoimmune diseases (11–13), and platelets are a major factor contributing to the induction of CD16 expression on human monocytes (14). However, the mechanisms underlying the induction of CD16 are not fully understood.

Platelets are circulating, tiny, anucleate cells that play a prominent role in hemostasis and thrombosis (15). However, platelets are also involved in aiding and modulating inflammatory reactions and immune responses. This occurs through immune ligands and receptors on the platelet surface and through release of an abundance of secretory molecules, including inflammatory mediators and cytokines (16). Upon activation, platelets change their shape and form aggregates. In addition, P-selectin (CD62P) expressed on activated platelets mediates the formation of monocyte-platelet aggregates (MPAs), which is an essential pathophysiological mechanism that mediates the induction of inflammatory events by activated platelets (17, 18). Several studies have shown increased levels of circulating MPAs in the peripheral blood of patients with atherosclerosis, type I diabetes, and end-stage renal diseases (19–22). In several autoimmune diseases, including rheumatoid arthritis (RA) and systemic lupus erythematosus (SLE), platelets are considered active players that produce serotonin and IL-1-containing microparticles (23–26). Further, platelets promote macrophage polarization toward the proinflammatory phenotype in response to LPS stimulation resulting in increased survival of septic mice (27), whereas platelet-lymphocyte interactions mediate anti-inflammatory events in rheumatoid arthritis (RA) (28). Together this suggests platelets play a regulatory role in innate as well as adaptive immune responses (15, 29).

In our previous study we demonstrated that $CD14^+CD16^+$ monocytes are markedly expanded in peripheral blood and synovial fluid of RA patients. Further, CD16 expression on $CD14^+$ monocytes is induced by TGF-β without additive effects of co-treatment with IL-1β, TNF-α or IL-6, which are typical proinflammatory cytokines produced by activated monocytes (11). Given the involvement of platelets in the pathophysiology of RA and their role as a major reservoir of TGF-β (30), we sought to investigate the underlying mechanisms of CD16 induction on monocytes and the immunological role of this receptor under co-culture conditions with activated, autologous platelets.

In the present study, we demonstrate that CD16 expression is induced by exposure to the cytokine milieu generated in monocyte and ADP-activated platelet co-cultures. Exogenous cytokine treatment and neutralization assay showed that both platelet-derived TGF-β and monocyte-derived IL-6 are sequentially involved in the induction of CD16 expression on purified $CD14^+CD16^-$ monocytes. Induced CD16 participates in IgG-mediated phagocytosis, as shown by the correlation between the level of CD16 expression by monocytes co-cultured with activated platelets and the CD16-dependent uptake of latex beads coated with FITC-labeled IgG. In addition, monocytes pretreated with activated platelets preferentially differentiate into M2c-like macrophages in the presence of M-CSF. Lastly, the amount of sCD62P, a marker of platelet activation, was found to be significantly elevated in plasma of RA patients compared with that of healthy controls and positively correlated with clinical parameters of RA patients. These findings underscore the important role of activated platelets in modulating phenotypical and functional features of human monocytes. Together these findings increase understanding of the immunological role of $CD14^+CD16^+$ monocytes in various inflammatory disorders.

MATERIALS AND METHODS

Cell Preparation

The study protocols were approved by the institutional review board (IRB) of Seoul National University Hospital and Chungnam National University Hospital. Peripheral blood of RA patients and healthy controls (HCs) was drawn after obtaining written, informed consent. The methods were performed in accordance with the approved guidelines. The patient characteristics of RA patients enrolled in this study are summarized in **Table 1**. To obtain platelets, platelet-rich plasma (PRP) was prepared from whole blood by centrifugation at 190 *g* for 15 min at room temperature (RT). Subsequently, platelet pellet was prepared from PRP by centrifugation at 2,400 *g* for 5 min and was resuspended with 25mM HEPES-buffered Tyrode's solution (Sigma-Aldrich, St. Louis, MO). Peripheral blood mononuclear cells (PBMC) were isolated from blood by density gradient centrifugation (Bicoll separating solution; BIOCHROM Inc., Cambridge, UK). To purify $CD14^+CD16^-$ monocytes, $CD16^+$ monocytes were negatively depleted from PBMC with $CD16^+$ Monocyte Isolation Kit (Miltenyi Biotec Inc., Auburn, CA) and $CD14^+$ monocytes were positively purified from $CD16^+$ cell-depleted PBMC using anti-CD14 microbeads (Miltenyi Biotec Inc.).

Co-Culture of Monocytes and Activated Platelets

Purified $CD14^+CD16^-$ monocytes were cultured in RPMI 1640 medium supplemented with 10% charcoal stripped fetal bovine

TABLE 1 | The characteristics of RA patients.

Patient Characteristics (Value)	Age (years), means ± SD	57.84 ± 8.81
	Sex (female/male), *N* (%)	24/8 (75.00/ 25.00)
	Disease duration, months	5.48 ± 5.12
	Rheumatoid factor – no. of positive (%)	28/32 (87.50)
	Rheumatoid factor titer (IU/ml), means ± SD	122.90 ± 87.70
	Anti-citrullinated protein antibody, no. of positive (%)	25/32 (78.13)
	Anti-citrullinated protein antibody titer (IU/ml), means ± SD	357.88 ± 161.59
	ESR (mm/h), means ± SD	26.81 ± 23.98
	CRP (mg/dl), means ± SD	2.00 ± 6.17
	DAS28 ESR, means ± SD	3.36 ± 1.62
	DAS28 CRP, means ± SD	2.42 ± 1.29
Medications [No. (%)]	Steroid (Prednisolone)	25/32 (78.13)
	Methotrexate	27/32 (84.38)
	Sulfasalazine	10/32 (31.25)
	Hydroxychloroquine	15/32 (46.88)
	Leflunomide	1/32 (3.13)
	TNF inhibitor (Infliximab)	1/32 (3.13)

ESR, erythrocyte sedimentation rate.
CRP, C-reactive protein.
DAS28, Disease Activity Score-28.
DAS28-ESR, DAS28 for RA based on ESR.
DAS28-CRP, DAS28 for RA based on CRP.

serum, 1% penicillin/streptomycin, and 1% L-glutamine. Platelets were activated with ADP (10 μg/ml) for 5 min at RT. $CD14^+CD16^-$ monocytes were co-cultured with activated platelets at 1:100 ratio for 18 h at 37°C in polystyrene tubes. In some experiments, $CD14^+CD16^-$ monocytes and activated platelets were placed in lower- and upper-chamber of Transwell cell culture plate (0.4 μm pore size) (Corning-Costar, Lowell, MA), respectively and cultured for 18 h at 37°C. To prepare human monocyte-derived macrophage (HMDM), purified monocytes were pretreated for 18 h with or without ADP-activated platelets and were differentiated into macrophages for 6 days in the presence of recombinant human M-CSF (50 ng/ml; PeproTech, Rocky Hill, NJ) without washing platelets.

Cytokine Neutralization Assay and Signaling Inhibition Assay

Purified $CD14^+CD16^-$ monocytes were pre-incubate for 30 min at 37°C with anti-IL-6, anti-TGF-β 1,2,3, or anti-IL-10 neutralizing Ab (all from R&D systems, Minneapolis, MN) to examine the effect of above cytokines on CD16 induction by activated platelets. In some experiments, $CD14^+CD16^-$ monocytes were pre-incubate for 30 min at 37°C with 5,15-DPP (STAT3 inhibitor VIII), SIS3 (SMAD3 inhibitor), or SB431542 (TGF-βRI inhibitor) (all from MERCK, Burlington, MA) to examine the effect of TGF-β and IL-6-mediated signal transduction on CD16 induction by activated platelets.

Flow Cytometric Analysis

Cultured monocytes and HMDM were stained for 30 min at 4°C with following fluorochrome-conjugated Abs: PE-Cy5-anti-HLA-DR, FITC- or APC-Cy7-anti-CD14, PE-anti-CD16, APC-anti-CD62P (all from BD Bioscience, San Jose, CA), and APC-anti-CD80 (BioLegend, San Jose, CA). The stained cells were acquired using a BD LSR Fortessa (BD Bioscience) and analyzed using Flowjo software (Tree Star, Ashland, OR).

Quantitative RT-PCR

Total RNA was extracted from freshly isolated or cultured cells using TRIzol reagents (Life technologies, Grand Island, NY), and cDNA was synthesized by GoScript reverse transcription system (Promega, Madison, WI). Real-time quantitative RT-PCR was performed in triplicates on a 7500 PCR system (Applied Biosystems, Grand Island, NY) using following primers: *CD16*: 5′-GCTCCGGATATCTTTGGTGA-3′ and 5′-TTCCAGCTGTGACACCTCAG -3′; *TGF-β*: 5′- AAGTGGAC ATCAACGGGTTC -3′ and 5′-GTCCTTGCGGA AGTCAATGT-3′; *IL-6*: 5′-AGGAGACTTGCCTGGTGAAA-3′ and 5′-CAGGGGTGGTTATTGCATCT-3′; *IL-10*: 5′-TGCCTTCAGCAGAGTGAAGA-3′ and 5′-GGTCT TGGTTCTCAGCTTGG-3′; *CD80*: 5′-GGGAAAGTGT ACGCCCTGTA-3′ and 5′-GCTACTTCTGTGCCCACCAT-3′; *CXCL10*: 5′-CAGCAGAGGAACCTCCAGTC-3′ and 5′-CAAAATTGGCTTGCAGGAAT-3′; *TNF-α*: 5′-AGCCCAT GTTGTAGCAAACC-3′ and 5′-TGAGGTACAG GCCCTCTGAT-3′; *MRC1*: 5′-TGACACACTT TTGGGGATCA-3′ and 5′-AAACTTGAACGGGAATGCAC-3′; *Dectin-1*: 5′-GGGCTCTCAAGAACAATGGA-3′ and 5′-CCAAGCATAGGATTCCCAAA-3′; CD163: 5′-TTT GCTCAAAGGGAGCAGAT-3′ and 5′-GTTGGACATC CCAGTTGCTT-3′; *MerTK*: 5′-GGGTGAAGGAGAG TTTGGGTC-3′ and 5′-ACGCTGCCTCACTGAGAAAC-3′; and β-*actin*: 5′-GGACTTCGAGCAAGAGATGG-3′ and 5′-AGCACTGTGTTGGCGTACAG-3′. The levels of gene expression were normalized to the expression of β-actin. The comparative CT method (*ΔΔ*CT) was used for the quantification of gene expression.

Enzyme-Linked Immunosorbent Assay

The amount of TGF-β, IL-6, and IL-10 in culture supernatant and soluble CD62P in plasma of RA patients and HCs was quantified by enzyme-linked immunosorbent assay (ELISA) kits (all from Thermo Fisher Scientific, Waltham, MA). The measurement of OD (Optical density) was performed using the infinite 200 pro multimode microplate reader (Tecan Group Ltd., Seestrasse, Switzerland).

Immunoblot Analysis

Total proteins were prepared by RIPA buffer (150 mM NaCl, 10 mM Na_2HPO_4, pH 7.2, 1% Nonidet P-40, and 0.5% deoxycholate) containing PMSF (phenylmethylsulfonyl fluoride) (Millipore Sigma, Burlington, MA), EDTA, and protease and phosphatase inhibitor cocktail (Thermo Fisher scientific). Cell lysates were separated on an 8–10% SDS-PAGE

gel and blotted onto a PVDF membrane (Bio-Rad, Hercules, CA). The membrane was incubated overnight at 4°C with rabbit anti-human pSTAT3, anti-STAT3, anti-pSMAD3 or anti-SMAD3 polyclonal Ab (all from Cell Signaling Technology, Danvers, MA), followed by incubation with the HRP-conjugated secondary Abs for 1 hr. The membranes were developed by SuperSignal West Femto Maximum Sensitivity substrate kit (Thermo Fisher Scientific, Waltham, MA).

Phagocytosis Assay

CD16-dependent phagocytic activity of monocytes co-cultured with platelets were assessed by flow cytometry using Phagocytosis Assay Kit (Cayman Chemical Company, Ann Arbor, MI). Cultured monocytes were pre-incubated at 37°C for 30 min with anti-CD64 and anti-CD32 neutralizing Abs (all from BioLegend) in the presence or absence of anti-CD16 neutralizing Ab (BD Bioscience). After washing, Latex beads coated with FITC labeled rabbit IgG were added at 1:400 ratio into the cultured monocytes, followed by incubation at 37°C for 15 min. The phagocytic activity was evaluated using a BD LSR Fortessa (BD Bioscience).

Statistics

A paired *t*-test, unpaired *t*-test, or Pearson correlation analysis was done to analyze data using Prism 7 software (GraphPad Software Inc., La Jolla, CA) as indicated in the figure legends. *P*-values of less than 0.05 were considered statistically significant.

RESULTS

Induction of CD16 on $CD14^+CD16^-$ Monocytes by Activated Platelets

The expansion of $CD14^+CD16^+$ monocytes has been reported in a variety of inflammatory disorders including rheumatoid arthritis (RA) and inflammatory bowel disease (IBD) (11, 12, 31), implying an important role of these cells in disease pathogenesis. Our previous study demonstrated that TGF-β predominantly induces CD16 expression on conventional $CD14^+$ monocytes isolated from healthy controls (11). Considering that platelets are a major reservoir of TGF-β, we first tested whether platelets induce CD16 expression on human monocytes. Highly purified $CD14^+CD16^-$ monocytes were co-cultured with autologous platelets pretreated with or without adenosine diphosphate (ADP) to activate platelets. Our FACS analysis using CD62P, a marker of platelet activation, showed that around 10% of platelets were spontaneously activated before adding ADP, probably by physical stress during isolation. However, ADP treatment markedly induced the activation of platelets (**Supplementary Figure 1**). We found that platelets significantly increased the expression of CD16 on $CD14^+$ monocytes as previously depicted (14). This induction was intensified by ADP-treatment of platelets (**Figure 1A**) in a transcription-dependent manner (**Figure 1B**), with markedly elevated CD16 mRNA expression 18 h after co-culture. Monocytes treated with ADP alone did not induce CD16 expression on $CD14^+CD16^-$ monocytes (**Supplementary Figure 2**) although it has been known that P2Y12, a receptor for ADP, is expressed on THP-1 human monocyte cells (32). Activated platelets give rise to an increase of the $CD14^+CD16^+$ subset, but had no effect on the appearance of nonclassical $CD14^{dim}CD16^+$ monocytes (**Figure 1A**). Although stimulated platelets are a main source of TGF-β, the adherence of platelets to monocytes is also known to influence the production of cytokines such as IL-10 and TNF-α (33). Therefore, we extended our analysis to examine which cytokines, in addition to TGF-β, induce CD16 expression and compared these findings with the platelet-treatment group. In agreement with previous studies, $CD14^+$ monocytes treated with exogenous TGF-β and IL-10 exhibited significantly enhanced CD16 expression (**Figure 1C**) (11, 14, 33, 34). However, the major pro-inflammatory cytokines produced by activated monocytes, IL-1β and TNF-α, exhibited no effect on CD16 induction. Of note, in contrast to other monocyte-derived pro-inflammatory cytokines, such as IL-1β and TNF-α, IL-6 was found to induce CD16 to a degree similar to that induced by TGF-β or platelet treatment (**Figure 1C**). These findings demonstrate that cytokines derived from monocyte-platelet co-cultures are responsible for induction of CD16 on conventional $CD14^+$ human monocytes.

TGF-β and IL-6 Are Involved in Activated Platelet-Mediated Induction of CD16 on Monocytes

We next investigate whether the induction of CD16 expression on monocytes by activated platelets is directly attributable to endogenously secreted TGF-β, IL-10, or IL-6 in the co-culture. The expression of IL-10 and IL-6 mRNA was significantly increased in a time-dependent manner during the co-culture, whereas the TGF-β mRNA level was not changed until 18 h after co-culture (**Figure 2A**). ELISA revealed that TGF-β was mainly secreted by activated platelets and was minimally produced by monocytes cultured with activated platelets and thus, a high level of TGF-β was maintained over time (**Figure 2B**). This finding was confirmed using a transwell system in which direct contact between monocytes and activated platelets mediated by CD62P was found to be dispensable for CD16 induction at 18 h after co-culture (**Supplementary Figure 3**). In stark contrast to TGF-β, platelets have no ability to produce IL-10 or IL-6 regardless of their activation state. Consistent with its mRNA expression, the amount of IL-6 in the co-culture supernatant increased greatly over time compared with the culture of monocytes alone (**Figure 2B**). In contrast, IL-10 was detected in the supernatant a later time-point, although at a relatively low level, and the amount of IL-1β released from the co-culture was minimal (< 10 pg/ml). Moreover, the production of IL-1β and TNF-α was comparable between co-culture of monocytes and platelets and culture of monocytes alone (data not shown). This suggests that TGF-β and IL-6, not IL-10, are the main contributors to the induction of CD16 expression on $CD14^+$ monocytes co-cultured with activated platelets. To confirm this finding, purified $CD14^+$ monocytes were cultured with ADP-activated platelets in the presence of

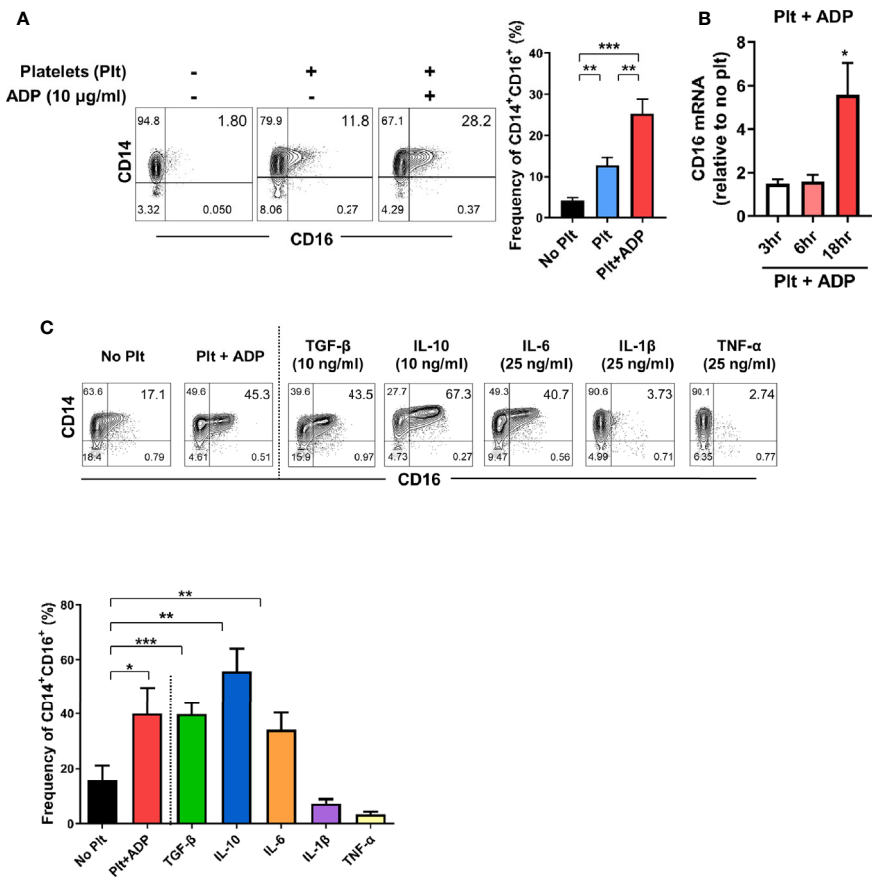

FIGURE 1 | Activated platelets induce CD16 expression on $CD14^+CD16^-$ monocytes. **(A)** Representative contour plots of CD16 expression on monocytes co-cultured with or without activated platelets (right). Highly purified $CD14^+CD16^-$ monocytes were co-cultured for 18 h with resting platelets or ADP-activated platelets. Frequencies (%) of $CD14^+CD16^+$ monocytes were analyzed using flow cytometry (left) (n = 7). **(B)** Quantitative RT-PCR analysis of CD16 in monocytes co-cultured with activated platelets for the indicated times. mRNA expression of CD16 was normalized to that in monocytes incubated without platelets at the same time points (n = 5 or 6). **(C)** Representative contour plot of CD16 expression on monocytes co-cultured with activated platelets for 18 h or treated with the indicated cytokines for 18 h (upper panel). Frequencies (%) of $CD14^+CD16^+$ monocytes under the indicated conditions were analyzed using flow cytometry (lower panel) (n = 4). Bars show the mean ± S.E.M. $^*p < 0.05$, $^{**}p < 0.01$, and $^{***}p < 0.001$ by two-tailed paired t-test.

neutralizing antibodies for cytokines related to induction of CD16. As expected, neutralization of TGF-β and IL-6 significantly diminished the induction of CD16 expression, whereas no inhibitory effect on CD16 expression by IL-10 was observed (**Figures 2C, D**). Our data suggest that endogenously secreted TGF-β and IL-6 are predominantly involved in activated platelet-mediated induction of CD16 on monocytes.

Activated Platelet-Induced CD16 Expression Is Mediated by SMAD3 and STAT3

To further investigate the molecular mechanisms underlying activated platelet-mediated induction of CD16 by monocytes, we sought to investigate whether SMAD3 and STAT3, which are directly phosphorylated by receptor binding of TGF β and IL-6, respectively, were involved in CD16 induction. Due to the technical difficulty of separating monocytes and platelets during the co-culture, the phosphorylation levels of STAT3 and SMAD3 were analyzed in the co-culture samples and were compared with monocytes or platelet-alone culture groups. STAT3 phosphorylation increased in the co-culture supernatant starting at 3 h, at which time IL-6 was also increased (**Figure 2B**) (**Figure 3A**). SMAD3 was immediately phosphorylated in platelets upon stimulation with ADP, likely in an autocrine manner. When co-cultured with monocytes, activated platelets enhanced the level of SMAD3 phosphorylation over time (**Figure 3A**). These findings were corroborated by a signal transduction inhibitor assay. SIS3, a SMAD3 inhibitor, and 5,15-DPP, a STAT3 inhibitor, significantly suppressed activated platelet-mediated induction of CD16 by monocytes (**Figure 3B**). Our data illustrate that activated platelets induce TGF-β and IL-6 *via* the SMAD3 and STAT3 pathways, respectively, which are responsible for the induction of CD16 on monocytes.

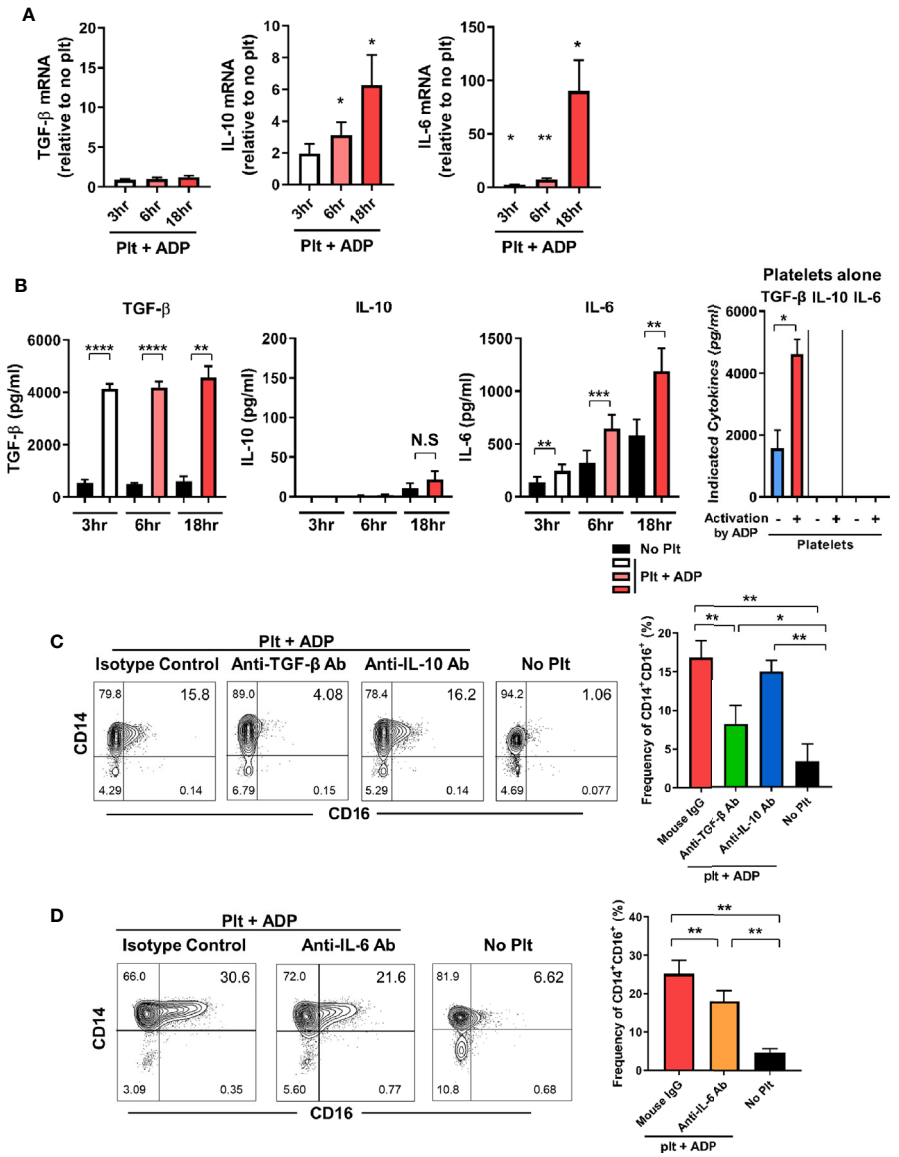

FIGURE 2 | TGF-β and IL-6 are responsible for activated platelet-mediated induction of CD16 on monocytes. **(A)** Quantitative RT-PCR analysis of TGF-β, IL-10, and IL-6 in monocytes co-cultured with activated platelets at the indicated time points. mRNA expression of each gene was normalized to that in monocytes incubated without platelets at the same time points (n = 5 or 6). **(B)** The amount of TGF-β, IL-10, and IL-6 in supernatants of monocytes co-cultured with or without ADP-activated platelets (n = 6 or 7) or unstimulated platelets (n = 3) were quantified (ELISA). **(C, D)** Representative contour plot of CD16 expression on monocytes co-cultured with activated platelets in the presence of anti-TGF-β (10 μg/ml), anti-IL-10 (10 μg/ml), or anti-IL-6 (10 μg/ml) neutralizing antibodies (left panels of **C** and **D**). Purified $CD14^+CD16^-$ monocytes were incubated with each neutralizing antibody for 30 min, followed by addition of ADP-activated platelets into the culture. Frequencies (%) of $CD14^+CD16^+$ monocytes under the indicated conditions were analyzed using flow cytometry (right panels of **C** and **D**) (n = 4 or 5). Bars show the mean ± S.E.M. $^*p < 0.05$, $^{**}p < 0.01$, $^{***}p < 0.005$, and $^{****}p < 0.001$ by two-tailed paired t-test. NS, not significant.

Activated Platelet-Induced CD16 Expression Is Involved in CD16-Dependent Phagocytosis in Monocytes

CD16 is an Fc gamma receptor (FcγR) that binds IgG molecules through their Fc portion. FcγRs recognize IgG-coated targets, such as opsonized pathogens or immune complexes (ICs), and provoke antibody-mediated effector functions in innate immune cells. These include antibody-dependent cell-mediated cytotoxicity (ADCC), antibody-dependent cellular phagocytosis (ADCP), and complement-dependent cytotoxicity (CDC) (35, 36). To assess the phagocytic activity of CD16-expresssing monocytes, we utilized a flow cytometry-based phagocytosis assay with latex beads coated with FITC-labeled rabbit IgG. To rule out CD64 and CD32-mediated phagocytosis, monocytes were pretreated with

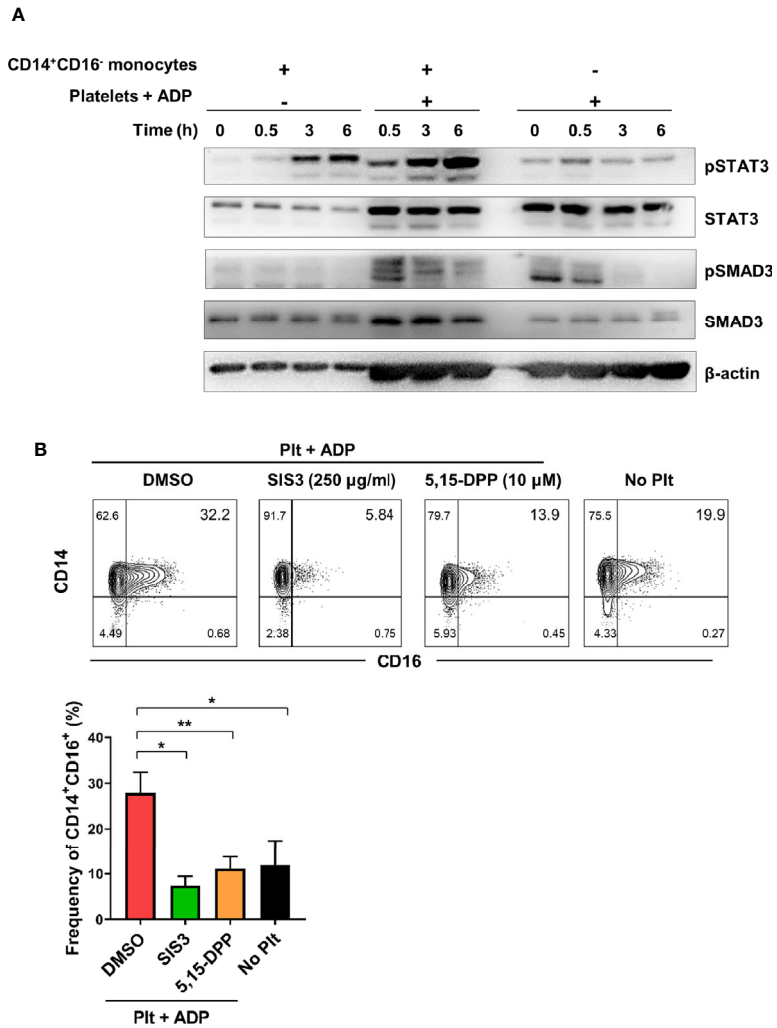

FIGURE 3 | Activated platelet-induced CD16 expression is mediated by phospho-SMAD3 and phospho-STAT3. **(A)** Immunoblot analysis of phosphorylated and total protein expression of STAT3 and SMAD3 in cell lysates from activated platelets alone, monocytes co-cultured with ADP-activated platelets, and monocytes alone at the indicated time points (n = 3). **(B)** Representative contour plot of CD16 expression on monocytes co-cultured for 18 h with activated platelets in the presence of SIS3 (SMAD3 inhibitor) or 5,15-DPP (STAT3 inhibitor) (upper panel). Frequencies (%) of $CD14^+CD16^+$ monocytes treated with SIS3 or 5,15-DPP were analyzed using flow cytometry (lower panel) (n = 4). 0.1% DMSO was used as a vehicle. Bars show the mean ± S.E.M. $^*p < 0.05$ and $^{**}p < 0.01$ by two-tailed paired t-test.

anti-CD64/32 neutralizing antibodies and their phagocytic activity was quantified following culture with platelets or ADP-treated platelets (**Figure 4A** and **Supplementary Figure 4**) with or without anti-CD16 neutralizing antibody (**Figures 4A, B**). Monocytes co-cultured with ADP-activated platelets showed significantly higher phagocytic activity than those incubated with resting platelets. Furthermore, blockade of CD16 with a neutralizing Ab revealed that CD16 partially contributes to the enhanced phagocytic activity of monocytes co-cultured with activated platelets. As seen in **Figure 4C**, the frequency of the $CD14^+CD16^+$ subset 18 h after co-culture significantly correlated with phagocytic activity (**Figure 4C**, $p < 0.05$). These data demonstrate that activated platelet-mediated induction of CD16 contributes to CD16-dependent phagocytosis by monocytes.

$CD14^+$ Monocytes Treated With Activated Platelets Preferentially Differentiate Into M2 Macrophages

Depending on the microenvironmental stimuli and signals, circulating monocytes can differentiate into macrophages with functional heterogeneity (37–39). To examine whether the cytokine milieu generated by monocyte-platelet co-culture influences macrophage differentiation, highly purified $CD14^+$ $CD16^-$ monocytes were pre-treated with ADP-stimulated platelets for 18 h followed by stimulation with M-CSF for 6 days to allow differentiation into macrophages. On day 6, the expression of typical M1 and M2-related genes was analyzed by quantitative PCR in human monocyte-derived macrophages (HMDMs) in the presence of ADP-activated platelets (**Figure 5A**). The expression of

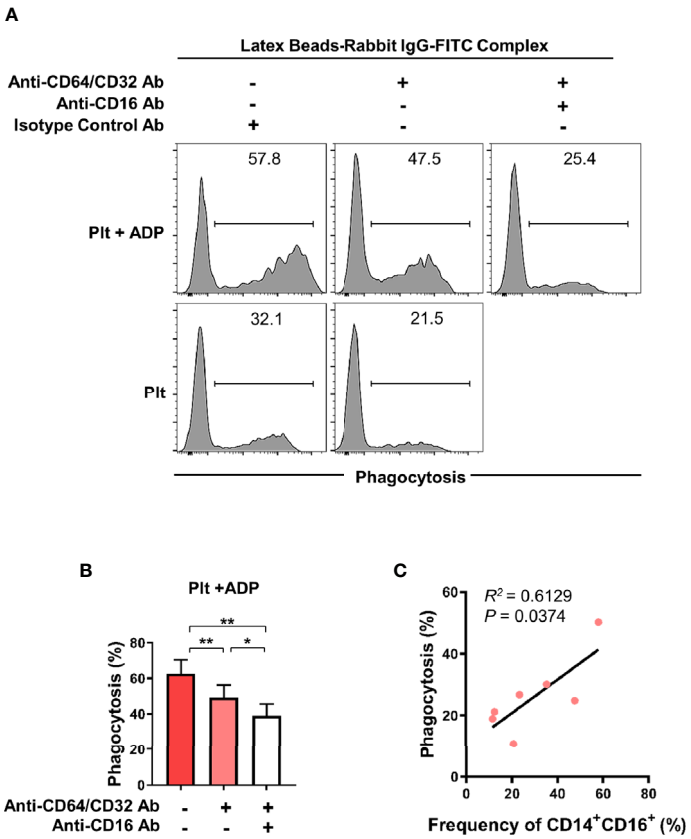

FIGURE 4 | Activated platelet-induced CD16 expression on monocytes is involved in CD16-dependent phagocytosis. Purified $CD14^+CD16^-$ monocytes were co-cultured with resting platelets or APD-activated platelets for 18 h Monocytes were incubated for 15 min with latex beads coated with FITC-labeled rabbit IgG. The phagocytic activity of monocytes was analyzed using flow cytometry. **(A)** Representative histogram plots of latex bead-based phagocytic activity of monocytes. To evaluate CD16-dependent phagocytic activity, CD64 and CD32, both Fcγ receptors, were blocked for 30 min by anti-CD64 and anti-CD32 neutralizing antibodies (10 μg/ml of each antibody) and their phagocytic activity was quantified in monocytes co-cultured with resting platelets or ADP-activated platelets and with or without anti-CD16 neutralizing antibody (10 μg/ml). **(B)** Frequency (%) of monocyte phagocytosis of latex beads coated with FITC-labeled rabbit IgG under the indicated conditions. (n = 6) **(C)** Correlation between CD16-dependent phagocytic activity and the frequency of $CD14^+CD16^+$ monocytes after 18 h-co-culture with ADP-activated platelets (n = 7). P value was obtained using the Pearson correlation analysis. Bars show the mean ± S.E.M. *$p < 0.05$ and **$p < 0.01$ by two-tailed paired t-test.

M1-related genes, such as CXCL10, CD80 and TNF-α, was significantly lower in HMDMs pretreated with activated platelets than in untreated HMDMs. However, the expression of some M2-related genes, such as CD16 and CD163, was increased in HMDMs pretreated with activated platelets. Of note, MerTK, a marker of M2c macrophages, was significantly upregulated in HMDMs pretreated with activated platelets. This finding was confirmed through flow cytometric analysis and ELISA (**Figures 5B, C**). These data suggest that the cytokine milieu generated by monocyte-activated platelet co-cultures potentiates a polarization to M2 macrophages, and probably M2c macrophages.

Clinical Relevance of Enhanced Soluble CD62P, a Marker of Platelet Activation in RA Patients

Since our previous study revealed an expansion of $CD16^+CD14^+$ monocytes in peripheral blood of RA patients (11), we next asked whether activated platelets are associated with increased CD16 expression on peripheral monocytes in RA patients. The patient characteristics of RA patients enrolled in this study are summarized in **Table 1**. A number of soluble factors, such as platelet factor 4 (PF4), soluble CD62P (sCD62P), β-thromboglobulin, and thromboxane, are known to be released from activated platelets (40, 41). In the present study, sCD62P was quantified in plasma and compared between RA patients and age-matched healthy controls (**Figure 6A**). Consistent with previous reports (42, 43), RA patient plasma (mean ± S.D.: 245.7 ± 48.3 ng/ml, n = 32) had a significantly higher amount of sCD62P than did that of HCs (126.4 ± 48.3 ng/ml, n = 18) ($p < 0.0001$), suggesting that the presence of activated platelets is related to the expansion of $CD14^+CD16^+$ monocytes in RA patients. Lastly, we sought to examine whether elevated levels of sCD62P in plasma are associated with clinical parameters and disease activity of RA patients. The amount of sCD62P in plasma had a significant positive correlation with the Disease Activity Score-28 (DAS28) for RA based on erythrocyte sedimentation rate (DAS28-ESR) and C-reactive protein (DAS28-CRP), which

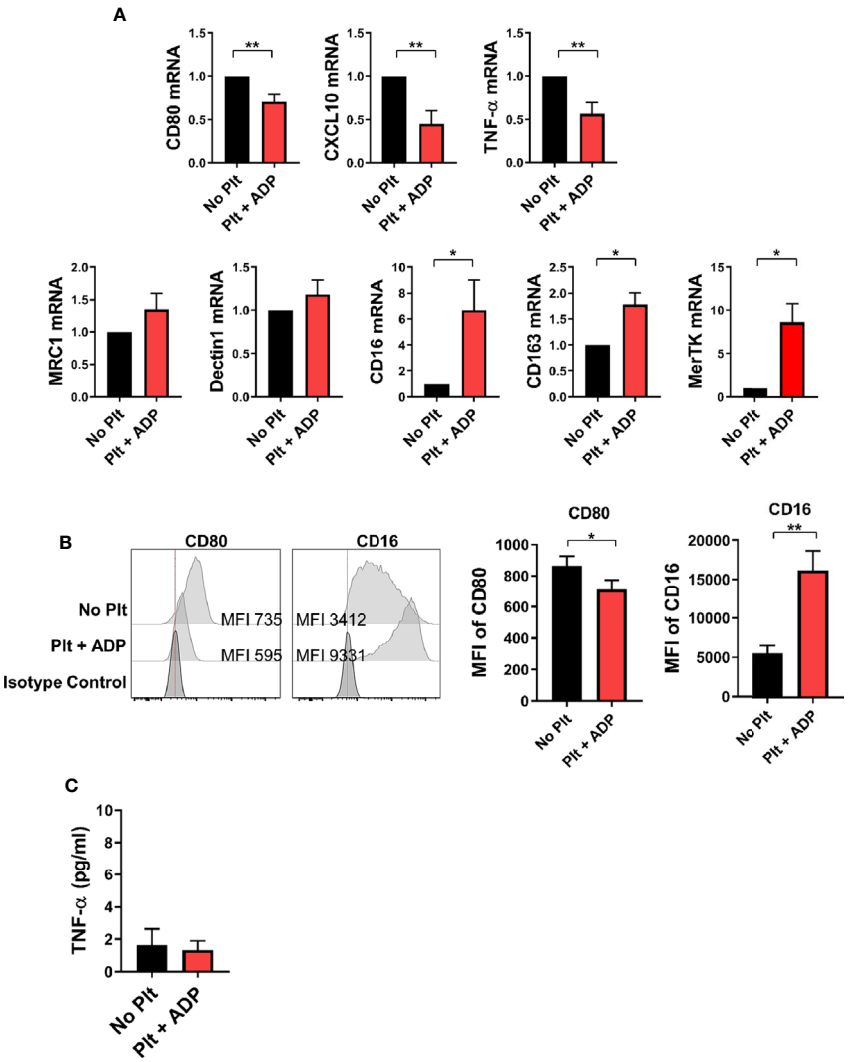

FIGURE 5 | CD14$^+$ monocytes treated with activated platelets preferentially differentiate into M2 macrophages. Purified CD14$^+$ CD16$^-$ monocytes were pre-co-cultured with ADP-activated platelets for 18 h followed by stimulation with M-CSF (50 ng/ml) for 6 days to induce differentiation into macrophages. **(A)** Quantitative RT-PCR analysis of typical M1- (upper panel) and M2-related genes (lower panel) in human monocyte-derived macrophages (HMDMs) (n = 5 ~ 8). **(B)** Representative histogram plots of CD80 and CD16 expression in HMDMs differentiated under the indicated conditions (left panel). Mean fluorescent intensities (MFIs) of CD80 and CD16 expression on HMDMs pre-cultured with ADP-activated platelets compared with their expression on HMDMs cultured without platelets (right panel) (n = 6). **(C)** TNF-α in culture supernatants (ELISA) (n = 9). Bars show the mean ± S.E.M. *p < 0.05 and **p < 0.01 by two-tailed paired t-test.

represent enhanced inflammatory responses (**Figure 6B**, $p = 0.0138$ and $p = 0.0476$, respectively). Together, these findings demonstrate that increased activity of platelets, which is represented by higher level of sCD62P in plasma, is positively correlated with RA clinical parameters. This suggests a possible mechanism for the accumulation of CD14$^+$CD16$^+$ monocytes in RA patients.

DISCUSSION

Monocytes are a versatile and dynamic cell population critical for the innate immune response during infections and autoimmune diseases (2, 4, 10, 44). Surface molecule expression patterns and transcriptomic profiles demonstrate that murine equivalents of classical CD14$^+$CD16$^-$ and nonclassical CD14^{dim}CD16$^+$ subsets in humans are the proinflammatory Ly6C^{hi}CX$_3$CR1^{mid}CCR2$^+$ and patrolling Ly6C^{lo}CX$_3$CR1^{hi}CCR2$^-$ populations, respectively. The CD14$^+$CD16$^-$ subset mediates classical monocyte roles, such as initiation of the inflammatory response, recognition and phagocytosis of pathogens and production of proinflammatory cytokines, whereas nonclassical monocytes have anti-inflammatory properties and are involved in maintenance of vascular homeostasis (4, 44). In addition to the two monocyte subsets, a substantial number of intermediate CD14$^+$CD16$^+$ monocytes exist in human peripheral blood. CD14$^+$CD16$^+$ monocytes exhibit both phagocytic

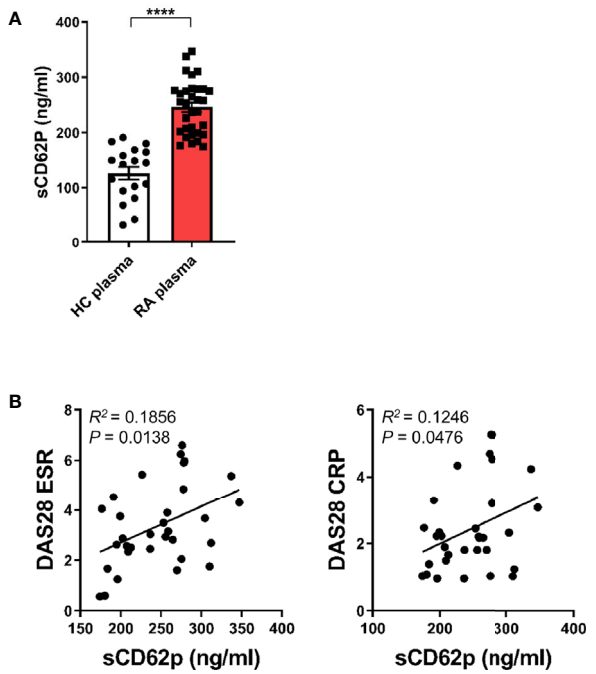

FIGURE 6 | Clinical relevance of enhanced soluble CD62P, a marker of platelet activation, in RA patients. **(A)** sCD62P in plasma of HCs (n = 18) and RA patients (n = 32) was quantitated by ELISA. Scatter plots show the mean ± S.E.M. ****$p < 0.0001$ by two-tailed unpaired t-test. **(B)** Correlation between sCD62P levels in the plasma of RA patients and RA clinical parameters (n = 32). sCD62P levels were plotted against DAS28 ESR and DAS28 CRP. P value was obtained using Pearson correlation analysis.

function and anti-inflammatory effects, as well as higher levels of intracellular IL-1β and TNF-α at steady state (45, 46). Research on the developmental trajectories of the three monocyte subsets in humans and in humanized mice suggests that intermediate monocytes exist in a transitory stage from classical to nonclassical monocytes at steady state and under experimental endotoxemic conditions (10). A number of studies have shown that $CD14^+CD16^+$ monocytes are expanded in peripheral blood and inflamed tissues during acute and chronic inflammation such as is seen with inflammatory bowel disease (IBD) and rheumatoid arthritis (RA) (11–13, 34). Since the murine analog to $CD14^+CD16^+$ monocytes has not been clearly identified, little is known about mechanism underlying expression of CD16 and the immunological role of intermediate monocytes.

CD16 expression has been shown to be upregulated on monocytes in response to a number of different factors including platelets and several cytokines (11, 14, 34). In agreement with an early report, our data show that activated platelets lead to a marked induction of CD16 expression on classical $CD14^+$ monocytes in a transcription-dependent manner (**Figures 1A, B**) (14). Several studies have demonstrated that induction of CD16 expression on monocytes is mediated by activated platelet-dependent COX-2 upregulation and consequent PGE2 synthesis in monocytes. Moreover, COX-2 synthesis is modulated by adhesion and signaling in response to cytokines such as platelet-derived TGF-β1 or monocyte-derived IL-1β (47–49). Since MPAs are involved in secretion of soluble factors, including various cytokines (15, 50), we sought to determine which cytokines are capable of inducing CD16 on monocytes. Besides TGF-β1, a well-known inducer of CD16 on monocytes (11, 14), STAT3-activating cytokines IL-10 and IL-6 noticeably enhance CD16 expression, whereas IL-1β and TNF-α, major monocyte-derived pro-inflammatory cytokines, had an inhibitory effect on CD16 induction. Our previous study showed that TGF-β-induced CD16 expression on monocytes was inhibited by IL-1β and TNF-α, but not IL-6 (11). Kinetics of cytokine production by MPA reveal that TGF-β and IL-6 are involved in activated platelet-mediated induction of CD16 monocytes (**Figure 2**). Although exogenous IL-10 is a potent inducer of CD16 on monocytes, as described previously and in the present study (**Figure 1C**) (34), activated platelets have no ability to produce IL-10, nor do monocytes induce IL-10 production within 18 h after co-culture. Moreover, an IL-10 neutralization assay corroborated our findings as IL-10 blockade had no effect on CD16 induction by MPAs (**Figure 2C**). It has been demonstrated that $CD14^+CD16^+$ intermediate monocytes are induced by IL-10 and positively correlate with disease activity in rheumatoid arthritis (RA) (34). IL-10 is broadly produced by many types of immune cells (51), and it has been suggested that CD16 expression on monocytes is maintained by IL-10 produced by human naïve $CD4^+$ T cells (52). Induction of CD16 by IL-10 may occur in chronic inflammatory conditions including RA or during interactions with T cells. We showed that the majority of the TGF-β was rapidly secreted from ADP-stimulated platelets in a transcription-independent manner and its production by monocytes in MPAs was minimal (**Figure 2B**). Thus, hindrance of direct contact in the transwell system had no effect on CD16 induction on monocytes. However, IL-6 was produced solely by activated monocytes in MPAs in a transcription-dependent manner as seen in the **Figure 2B**. Immunoblotting of phosphorylation of the downstream mediators, SMAD3 and STAT3, revealed an obvious difference in the pattern and kinetics of TGF-β and IL-6 production in MPA. SMAD3 in monocytes is rapidly (before 30 min) phosphorylated only when cells are co-cultured with platelets, whereas phosphorylation of STAT3 was enhanced at later time points *via* IL-6 autocrine signaling. The critical role of TGF-β and IL-6 for CD16 induction in MPA was clearly shown by inhibition with SB431542, SIS3, or 5, 15-DPP, which selectively inhibit TGF-βRI, SMAD3, and STAT3, respectively (**Supplementary Figure 5** and **Figure 3B**). It should be noted that IL-6 induced expression of COX2, which is important for CD16 induction on monocytes by activated platelets, is mediated by STAT3 in monocytic THP1 cells and prostatic tumor cells (47, 53, 54).

Recent work has highlighted a cardinal role for platelets in inflammatory and immune responses by expressing and secreting many potent immunological mediators, such as FcγRIIA (CD32), CD154, TLRs, MHC class I molecules, cytokines, chemokines, and several granules including platelet factor 4 (PF4), glutamate, serotonin, and ADP (15, 18). Activated

platelets shed microparticles that bud from their membranes (30) extending the reach of the activated platelet to sites distant from the cell itself (55). Besides their well-known pathogenic role in atherosclerosis, platelets have been identified as active players in the pathogenesis of RA and SLE (30, 55, 56). Anti-citrullinated protein antibodies (ACPA), which recognize a group of post-transcriptionally modified autoantigens in RA, contribute to platelet activation and activated platelets release ADP themselves, further causing platelet activation (57). Of note, serum soluble selectin levels including sCD62P are elevated in RA and systemic sclerosis. Thus, sCD62P has been suggested as a circulating biomarker in RA with thrombocytosis, indicating the presence of a continuous underlying inflammatory stimulus (42, 43). We previously reported that $CD14^+CD16^+$, but not $CD14^{dim}CD16^+$, monocytes were predominantly expanded in peripheral blood and synovial fluid of RA patients compared with healthy controls (11). As seen in **Figure 6A**, the concentration of sCD62P, a biomarker of activated platelets, was significantly increased in plasma of RA patients compared with that of healthy controls, implicating activated platelets in the induction of CD16 on classical monocytes in RA. It should be noted that the expression of CD16 on $CD14^+$ monocytes is induced by synovial fluid in a dose-dependent manner and this upregulation is greatly inhibited by SB431542, a TGF-βRI inhibitor (11). In RA patients, the proportion of $CD14^+CD16^+$ monocytes is positively correlated with clinical parameters, such as CRP and DAS28-ESR, and is significantly decreased after a 12-week treatment with methotrexate (MTX), a gold standard, disease-modifying anti-rheumatic drug (DMARD) (34). This is supported by our findings showing sCD62P concentration is significantly and positively correlated with RA clinical parameters including DAS28-ESR and DAS28-CRP (**Figure 6B**).

Human CD16 exists in two different isoforms, FcγRIIIA (CD16A) and FcγRIIIB (CD16B), encoded by separate genes (58). Phillips et al. showed that CD16 expressed on platelet-activated monocytes is structurally similar to the transmembrane-anchored CD16B polypeptide expressed on NK cells but is associated with the FcεRI-γ subunit in a manner identical to that of human basophils (14). Therefore, it has been suggested that CD16 on monocytes contributes to antibody-dependent cellular cytotoxicity (ADCC) for targeting and killing virus-infected or transformed cells coated with specific antibodies (59). ADCC by $CD16^+$ monocytes requires cell-cell contact facilitated *via* β2-integrins and mediated by TNF-α (59). Besides ADCC, CD16 induced by activated platelets mediates antibody-dependent cellular phagocytosis (ADCP), showing that this phagocytic activity is comparable to that of CD64/CD32-mediated phagocytosis in monocytes (**Figure 4B**). Our data illustrate that the phagocytic capacity largely depends on the platelet activity and the proportion of CD16+CD14+ monocytes induced (**Figures 4B, C**). Given that ADCC, ADCP, and complement-dependent cytotoxicity (CDC) are FcR-mediated effector functions which contribute to removal of antibody-opsonized target cells or molecules, induction of CD16 on monocytes is likely involved in regulation of immune responses and inflammatory reactions. Although not examined in our study, expanded $CD14^+CD16^+$ monocytes in RA may result in an increased responsiveness to immune complex(IC)-stimulation (60). Given that IgG-containing immune complexes (IC) including those containing rheumatoid factors (RFs) and cyclic citrullinated peptide (CCP) autoantibodies are found abundantly in serum and synovial fluid of patients with RA, it could be one potential pathophysiological role of intermediate $CD14^+CD16^+$ monocytes in RA.

A large number of circulating monocytes migrate into an inflamed tissue and generally differentiate into inflammatory macrophages during an inflammatory reactions (6, 61). Macrophages can be phenotypically and functionally polarized into proinflammatory M1 or anti-inflammatory/pro-resolving M2 macrophages depending on the surrounding microenvironmental stimuli and signals (37, 38). It has been recently demonstrated that M2 macrophages can be further subcategorized as M2a, M2b, M2c, or M2d based on the applied stimuli, the resultant transcriptional changes, and their functions (39). Moreover, recent single-cell transcriptome sequencing (scRNA-seq) analyses have shown that synovial monocytes/macrophages of RA patients and RA mouse model are heterogeneous and these distinct subsets are closely linked to diverse homeostatic, regulatory, and inflammatory functions (62–64). Leukocyte-rich RA synovia have a greater abundance of $IL1B^+$ monocytes but a reduced $NUPR1^+$ monocytes, whereas $MerTK^+$ macrophages are associated with remission and maintenance of RA (62, 63). In present study, we found that incubation with activated platelets lead to skewing of monocytes toward differentiation into macrophages with an M2 propensity (**Figure 5**). It is still debated whether platelet interactions with monocytes/macrophages elicit proinflammatory or anti-inflammatory responses upon various stimulations (27, 65–67). Of note, activated platelets alone induce anti-inflammatory responses of monocytes/macrophages *via* PGE_2 and cytokines (67). In our study, ADP-activated monocytes appear to differentiate into $CD16^+CD163^+MerTK^+$ M2c macrophages that are polarized by IL-10, TGF-β, or glucocorticoid and play crucial roles in the phagocytosis of apoptotic cells (68). M-CSF is capable of inducing polarization of M2 macrophages that express CD16 and CD163 on monocytes during differentiation (69). However, we found that monocytes pre-treated with ADP-platelets further increased the expression of CD16 and CD163 during differentiation in the presence of M-CSF compared to control. Furthermore, MerTK, a marker of M2c macrophages, was significantly upregulated in HMDMs pretreated with activated platelets. A recent study demonstrated that M2c-like cells are detectable among circulating $CD14^+CD16^+$, but not $CD14^{dim}CD16^+$, monocytes (70).

In summary, we provide evidence that activated platelets are important for induction of CD16 expression on classical $CD14^+CD16^-$ monocytes through sequential involvement of platelet-derived TGF-β and monocyte-derived IL-6. Induced CD16 on monocytes participates in IgG-mediated phagocytosis. In addition, monocytes pretreated with activated platelets preferentially differentiate into M2c-like macrophages in the presence of M-CSF. In RA patients, the plasma level of sCD62P, a marker of activated platelets, was significantly elevated, which may explain the accumulation of $CD14^+CD16^+$ monocytes in RA patients. Furthermore, the sCD62P level in plasma is positively correlated with RA clinical parameters. These findings underscore

a key role of activated platelets for regulating phenotypical and functional features of human monocytes and shed light on the immunological role of $CD14^{+}CD16^{+}$ cells in a variety of inflammatory disorders.

DATA AVAILABILITY STATEMENT

All datasets generated in this study are included in the article/ **Supplementary Material**. Further inquiries can be directed to the corresponding author.

ETHICS STATEMENT

The studies involving human participants were reviewed and approved by the Institutional Review Board (IRB) of Seoul National University Hospital and of Chungnam National University Hospital. The patients/participants provided their written informed consent to participate in this study.

AUTHOR CONTRIBUTIONS

SL: participated in the design of the study, performed most of the experiments, data collection and analysis, and drafted the manuscript. BY and HK: participated in the design of the study, performed the experiments, data collection and analysis. SK and S-JY: participated in study design and performed data analysis. W-WL: conceived of the study, participated in its design and coordination, performed data analysis and writing of manuscript, and has full access to all the data in this study and financial support. All authors contributed to the article and approved the submitted version.

FUNDING

This work was supported by grant (NRF-2018R1A2B2006310 to W-WL) from the National Research Foundation of Korea (NRF) funded by Ministry of Science and ICT (MSIT).

ACKNOWLEDGMENTS

The authors thank Jiyeon Jang (Seoul National University College of Medicine) for assisting in the recruitment of human subjects and thank Core Lab, Clinical Trials Center, Seoul National University Hospital for drawing blood.

SUPPLEMENTARY MATERIAL

The Supplementary Material for this article can be found online at: https://www.frontiersin.org/articles/10.3389/fimmu.2020.611133/full#supplementary-material

REFERENCES

1. Randolph GJ, Inaba K, Robbiani DF, Steinman RM, Muller WA. Differentiation of phagocytic monocytes into lymph node dendritic cells in vivo. *Immunity* (1999) 11(6):753–61. doi: 10.1016/S1074-7613(00)80149-1
2. Geissmann F, Jung S, Littman DR. Blood monocytes consist of two principal subsets with distinct migratory properties. *Immunity* (2003) 19(1):71–82. doi: 10.1016/S1074-7613(03)00174-2
3. Varol C, Landsman L, Fogg DK, Greenshtein L, Gildor B, Margalit R, et al. Monocytes give rise to mucosal, but not splenic, conventional dendritic cells. *J Exp Med* (2007) 204(1):171–80. doi: 10.1084/jem.20061011
4. Cros J, Cagnard N, Woollard K, Patey N, Zhang SY, Senechal B, et al. Human CD14dim monocytes patrol and sense nucleic acids and viruses via TLR7 and TLR8 receptors. *Immunity* (2010) 33(3):375–86. doi: 10.1016/j.immuni.2010.08.012
5. Auffray C, Sieweke MH, Geissmann F. Blood monocytes: development, heterogeneity, and relationship with dendritic cells. *Annu Rev Immunol* (2009) 27:669–92. doi: 10.1146/annurev.immunol.021908.132557
6. Shi C, Pamer EG. Monocyte recruitment during infection and inflammation. *Nat Rev Immunol* (2011) 11(11):762–74. doi: 10.1038/nri3070
7. Geissmann F, Auffray C, Palframan R, Wirrig C, Ciocca A, Campisi L, et al. Blood monocytes: distinct subsets, how they relate to dendritic cells, and their possible roles in the regulation of T-cell responses. *Immunol Cell Biol* (2008) 86(5):398–408. doi: 10.1038/icb.2008.19
8. Ingersoll MA, Platt AM, Potteaux S, Randolph GJ. Monocyte trafficking in acute and chronic inflammation. *Trends Immunol* (2011) 32(10):470–7. doi: 10.1016/j.it.2011.05.001
9. Wong KL, Yeap WH, Tai JJ, Ong SM, Dang TM, Wong SC. The three human monocyte subsets: implications for health and disease. *Immunol Res* (2012) 53 (1-3):41–57. doi: 10.1007/s12026-012-8297-3
10. Patel AA, Zhang Y, Fullerton JN, Boelen L, Rongvaux A, Maini AA, et al. The fate and lifespan of human monocyte subsets in steady state and systemic inflammation. *J Exp Med* (2017) 214(7):1913–23. doi: 10.1084/jem.20170355
11. Yoon BR, Yoo SJ, Choi Y, Chung YH, Kim J, Yoo IS, et al. Functional phenotype of synovial monocytes modulating inflammatory T-cell responses in rheumatoid arthritis (RA). *PloS One* (2014) 9(10):e109775. doi: 10.1371/journal.pone.0109775
12. Koch S, Kucharzik T, Heidemann J, Nusrat A, Luegering A. Investigating the role of proinflammatory CD16+ monocytes in the pathogenesis of inflammatory bowel disease. *Clin Exp Immunol* (2010) 161(2):332–41. doi: 10.1111/j.1365-2249.2010.04177.x
13. Rossol M, Kraus S, Pierer M, Baerwald C, Wagner U. The CD14(bright) CD16 + monocyte subset is expanded in rheumatoid arthritis and promotes expansion of the Th17 cell population. *Arthritis Rheumatol* (2012) 64 (3):671–7. doi: 10.1002/art.33418
14. Phillips JH, Chang CW, Lanier LL. Platelet-induced expression of Fc gamma RIII (CD16) on human monocytes. *Eur J Immunol* (1991) 21(4):895–9. doi: 10.1002/eji.1830210406
15. Semple JW, Italiano JEJr., Freedman J. Platelets and the immune continuum. *Nat Rev Immunol* (2011) 11(4):264–74. doi: 10.1038/nri2956
16. von Hundelshausen P, Weber C. Platelets as immune cells: bridging inflammation and cardiovascular disease. *Circ Res* (2007) 100(1):27–40. doi: 10.1161/01.RES.0000252802.25497.b7
17. Celi A, Pellegrini G, Lorenzet R, De Blasi A, Ready N, Furie BC, et al. P-selectin induces the expression of tissue factor on monocytes. *Proc Natl Acad Sci USA* (1994) 91(19):8767–71. doi: 10.1073/pnas.91.19.8767
18. Morrell CN, Aggrey AA, Chapman LM, Modjeski KL. Emerging roles for platelets as immune and inflammatory cells. *Blood* (2014) 123(18):2759–67. doi: 10.1182/blood-2013-11-462432

19. Allen N, Barrett TJ, Guo Y, Nardi M, Ramkhelawon B, Rockman CB, et al. Circulating monocyte-platelet aggregates are a robust marker of platelet activity in cardiovascular disease. *Atherosclerosis* (2019) 282:11–8. doi: 10.1016/j.atherosclerosis.2018.12.029
20. Tay HM, Yeap WH, Dalan R, Wong SC, Hou HW. Increased monocyte-platelet aggregates and monocyte-endothelial adhesion in healthy individuals with vitamin D deficiency. *FASEB J* (2020) 34(8):11133–42. doi: 10.1096/fj.202000822R
21. Zahran AM, El-Badawy O, Mohamad IL, Tamer DM, Abdel-Aziz SM, Elsayh KI. Platelet Activation and Platelet-Leukocyte Aggregates in Type I Diabetes Mellitus. *Clin Appl Thromb Hemost* (2018) 24(9_suppl):230S–9S. doi: 10.1177/1076029618805861
22. Ashman N, Macey MG, Fan SL, Azam U, Yaqoob MM. Increased platelet-monocyte aggregates and cardiovascular disease in end-stage renal failure patients. *Nephrol Dial Transplant* (2003) 18(10):2088–96. doi: 10.1093/ndt/gfg348
23. Knijff-Dutmer EA, Koerts J, Nieuwland R, Kalsbeek-Batenburg EM, van de Laar MA. Elevated levels of platelet microparticles are associated with disease activity in rheumatoid arthritis. *Arthritis Rheumatol* (2002) 46(6):1498–503. doi: 10.1002/art.10312
24. Cloutier N, Allaeys I, Marcoux G, Machlus KR, Mailhot B, Zufferey A, et al. Platelets release pathogenic serotonin and return to circulation after immune complex-mediated sequestration. *Proc Natl Acad Sci U S A* (2018) 115(7):E1550–E9. doi: 10.1073/pnas.1720553115
25. Boilard E, Blanco P, Nigrovic PA. Platelets: active players in the pathogenesis of arthritis and SLE. *Nat Rev Rheumatol* (2012) 8(9):534–42. doi: 10.1038/nrrheum.2012.118
26. Burbano C, Villar-Vesga J, Orejuela J, Munoz C, Vanegas A, Vasquez G, et al. Potential Involvement of Platelet-Derived Microparticles and Microparticles Forming Immune Complexes during Monocyte Activation in Patients with Systemic Lupus Erythematosus. *Front Immunol* (2018) 9:322. doi: 10.3389/fimmu.2018.00322
27. Carestia A, Mena HA, Olexen CM, Ortiz Wilczynski JM, Negrotto S, Errasti AE, et al. Platelets Promote Macrophage Polarization toward Pro-inflammatory Phenotype and Increase Survival of Septic Mice. *Cell Rep* (2019) 28(4):896–908 e5. doi: 10.1016/j.celrep.2019.06.062
28. Zamora C, Canto E, Nieto JC, Bardina J, Diaz-Torne C, Moya P, et al. Binding of Platelets to Lymphocytes: A Potential Anti-Inflammatory Therapy in Rheumatoid Arthritis. *J Immunol* (2017) 198(8):3099–108. doi: 10.4049/jimmunol.1601708
29. Koupenova M, Clancy L, Corkrey HA, Freedman JE. Circulating Platelets as Mediators of Immunity, Inflammation, and Thrombosis. *Circ Res* (2018) 122(2):337–51. doi: 10.1161/CIRCRESAHA.117.310795
30. Boilard E, Nigrovic PA, Larabee K, Watts GF, Coblyn JS, Weinblatt ME, et al. Platelets amplify inflammation in arthritis via collagen-dependent microparticle production. *Science* (2010) 327(5965):580–3. doi: 10.1126/science.1181928
31. Kapellos TS, Bonaguro L, Gemund I, Reusch N, Saglam A, Hinkley ER, et al. Human Monocyte Subsets and Phenotypes in Major Chronic Inflammatory Diseases. *Front Immunol* (2019) 10:2035. doi: 10.3389/fimmu.2019.02035
32. Micklewright JJ, Layhadi JA, Fountain SJ. P2Y12 receptor modulation of ADP-evoked intracellular Ca(2+) signalling in THP-1 human monocytic cells. *Br J Pharmacol* (2018) 175(12):2483–91. doi: 10.1111/bph.14218
33. Gudbrandsdottir S, Hasselbalch HC, Nielsen CH. Activated platelets enhance IL-10 secretion and reduce TNF-alpha secretion by monocytes. *J Immunol* (2013) 191(8):4059–67. doi: 10.4049/jimmunol.1201103
34. Tsukamoto M, Seta N, Yoshimoto K, Suzuki K, Yamaoka K, Takeuchi T. CD14(bright)CD16+ intermediate monocytes are induced by interleukin-10 and positively correlate with disease activity in rheumatoid arthritis. *Arthritis Res Ther* (2017) 19(1):28. doi: 10.1186/s13075-016-1216-6
35. Bournazos S, Wang TT, Dahan R, Maamary J, Ravetch JV. Signaling by Antibodies: Recent Progress. *Annu Rev Immunol* (2017) 35:285–311. doi: 10.1146/annurev-immunol-051116-052433
36. Junker F, Gordon J, Qureshi O. Fc Gamma Receptors and Their Role in Antigen Uptake, Presentation, and T Cell Activation. *Front Immunol* (2020) 11:1393. doi: 10.3389/fimmu.2020.01393
37. Murray PJ. Macrophage Polarization. *Annu Rev Physiol* (2017) 79:541–66. doi: 10.1146/annurev-physiol-022516-034339
38. Yoon BR, Oh YJ, Kang SW, Lee EB, Lee WW. Role of SLC7A5 in Metabolic Reprogramming of Human Monocyte/Macrophage Immune Responses. *Front Immunol* (2018) 9:53. doi: 10.3389/fimmu.2018.00053
39. Wang LX, Zhang SX, Wu HJ, Rong XL, Guo J. M2b macrophage polarization and its roles in diseases. *J Leukoc Biol* (2019) 106(2):345–58. doi: 10.1002/JLB.3RU1018-378RR
40. Gurney D, Lip GY, Blann AD. A reliable plasma marker of platelet activation: does it exist? *Am J Hematol* (2002) 70(2):139–44. doi: 10.1002/ajh.10097
41. Kannan M, Ahmad F, Saxena R. Platelet activation markers in evaluation of thrombotic risk factors in various clinical settings. *Blood Rev* (2019) 37:100583. doi: 10.1016/j.blre.2019.05.007
42. Ates A, Kinikli G, Turgay M, Duman M. Serum-soluble selectin levels in patients with rheumatoid arthritis and systemic sclerosis. *Scand J Immunol* (2004) 59(3):315–20. doi: 10.1111/j.0300-9475.2004.01389.x
43. Ertenli I, Kiraz S, Arici M, Haznedaroglu IC, Calguneri M, Celik I, et al. P-selectin as a circulating molecular marker in rheumatoid arthritis with thrombocytosis. *J Rheumatol* (1998) 25(6):1054–8.
44. Ingersoll MA, Spanbroek R, Lottaz C, Gautier EL, Frankenberger M, Hoffmann R, et al. Comparison of gene expression profiles between human and mouse monocyte subsets. *Blood* (2010) 115(3):e10–9. doi: 10.1182/blood-2009-07-235028
45. Wong KL, Tai JJ, Wong WC, Han H, Sem X, Yeap WH, et al. Gene expression profiling reveals the defining features of the classical, intermediate, and nonclassical human monocyte subsets. *Blood* (2011) 118(5):e16–31. doi: 10.1182/blood-2010-12-326355
46. Kratofil RM, Kubes P, Deniset JF. Monocyte Conversion During Inflammation and Injury. *Arterioscler Thromb Vasc Biol* (2017) 37(1):35–42. doi: 10.1161/ATVBAHA.116.308198
47. Passacquale G, Vamadevan P, Pereira L, Hamid C, Corrigall V, Ferro A. Monocyte-platelet interaction induces a pro-inflammatory phenotype in circulating monocytes. *PloS One* (2011) 6(10):e25595. doi: 10.1371/journal.pone.0025595
48. Eligini S, Barbieri SS, Arenaz I, Tremoli E, Colli S. Paracrine up-regulation of monocyte cyclooxygenase-2 by platelets: role of transforming growth factor-beta1. *Cardiovasc Res* (2007) 74(2):270–8. doi: 10.1016/j.cardiores.2006.12.013
49. Dixon DA, Tolley ND, Bemis-Standoli K, Martinez ML, Weyrich AS, Morrow JD, et al. Expression of COX-2 in platelet-monocyte interactions occurs via combinatorial regulation involving adhesion and cytokine signaling. *J Clin Invest* (2006) 116(10):2727–38. doi: 10.1172/JCI27209.
50. Lam FW, Vijayan KV, Rumbaut RE. Platelets and Their Interactions with Other Immune Cells. *Compr Physiol* (2015) 5(3):1265–80. doi: 10.1002/cphy.c140074
51. Saraiva M, O'Garra A. The regulation of IL-10 production by immune cells. *Nat Rev Immunol* (2010) 10(3):170–81. doi: 10.1038/nri2711
52. Liu Y, Yang B, Ma J, Wang H, Huang F, Zhang J, et al. Interleukin-21 maintains the expression of CD16 on monocytes via the production of IL-10 by human naive CD4+ T cells. *Cell Immunol* (2011) 267(2):102–8. doi: 10.1016/j.cellimm.2010.12.003
53. Basu A, Das AS, Sharma M, Pathak MP, Chattopadhyay P, Biswas K, et al. STAT3 and NF-kappaB are common targets for kaempferol-mediated attenuation of COX-2 expression in IL-6-induced macrophages and carrageenan-induced mouse paw edema. *Biochem Biophys Rep* (2017) 12:54–61. doi: 10.1016/j.bbrep.2017.08.005
54. Liu XH, Kirschenbaum A, Lu M, Yao S, Klausner A, Preston C, et al. Prostaglandin E(2) stimulates prostatic intraepithelial neoplasia cell growth through activation of the interleukin-6/GP130/STAT-3 signaling pathway. *Biochem Biophys Res Commun* (2002) 290(1):249–55. doi: 10.1006/bbrc.2001.6188
55. Andersson G, Axell T, Larsson A. Impact of consumption factors on soft tissue changes in Swedish moist snuff users: a histologic study. *J Oral Pathol Med* (1990) 19(10):453–8. doi: 10.1111/j.1600-0714.1990.tb00786.x
56. Davi G, Patrono C. Platelet activation and atherothrombosis. *N Engl J Med* (2007) 357(24):2482–94. doi: 10.1056/NEJMra071014
57. Habets KL, Trouw LA, Levarht EW, Korporaal SJ, Habets PA, de Groot P, et al. Anti-citrullinated protein antibodies contribute to platelet activation in rheumatoid arthritis. *Arthritis Res Ther* (2015) 17:209. doi: 10.1186/s13075-015-0665-7

58. Zhang Y, Boesen CC, Radaev S, Brooks AG, Fridman WH, Sautes-Fridman C, et al. Crystal structure of the extracellular domain of a human Fc gamma RIII. *Immunity* (2000) 13(3):387–95. doi: 10.1016/S1074-7613(00)00038-8
59. Yeap WH, Wong KL, Shimasaki N, Teo EC, Quek JK, Yong HX, et al. CD16 is indispensable for antibody-dependent cellular cytotoxicity by human monocytes. *Sci Rep* (2016) 6:34310. doi: 10.1038/srep34310
60. Cooper DL, Martin SG, Robinson JI, Mackie SL, Charles CJ, Nam J, et al. FcgammaRIIIa expression on monocytes in rheumatoid arthritis: role in immune-complex stimulated TNF production and non-response to methotrexate therapy. *PloS One* (2012) 7(1):e28918. doi: 10.1371/journal.pone.0028918
61. Italiani P, Boraschi D. From Monocytes to M1/M2 Macrophages: Phenotypical vs. Functional Differentiation. *Front Immunol* (2014) 5:514. doi: 10.3389/fimmu.2014.00514
62. Alivernini S, MacDonald L, Elmesmari A, Finlay S, Tolusso B, Gigante MR, et al. Distinct synovial tissue macrophage subsets regulate inflammation and remission in rheumatoid arthritis. *Nat Med* (2020) 26(8):1295–306. doi: 10.1038/s41591-020-0939-8
63. Zhang F, Wei K, Slowikowski K, Fonseka CY, Rao DA, Kelly S, et al. Defining inflammatory cell states in rheumatoid arthritis joint synovial tissues by integrating single-cell transcriptomics and mass cytometry. *Nat Immunol* (2019) 20(7):928–42. doi: 10.1038/s41590-019-0378-1
64. Culemann S, Gruneboom A, Nicolas-Avila JA, Weidner D, Lammle KF, Rothe T, et al. Locally renewing resident synovial macrophages provide a protective barrier for the joint. *Nature* (2019) 572(7771):670–5. doi: 10.1038/s41586-019-1471-1
65. Olumuyiwa-Akeredolu OO, Page MJ, Soma P, Pretorius E. Platelets: emerging facilitators of cellular crosstalk in rheumatoid arthritis. *Nat Rev Rheumatol* (2019) 15(4):237–48. doi: 10.1038/s41584-019-0187-9
66. Andia I. Rheumatoid arthritis: The ins and outs of platelets in RA. *Nat Rev Rheumatol* (2017) 13(5):262–4. doi: 10.1038/nrrheum.2017.52
67. Linke B, Schreiber Y, Picard-Willems B, Slattery P, Nusing RM, Harder S, et al. Activated Platelets Induce an Anti-Inflammatory Response of Monocytes/Macrophages through Cross-Regulation of PGE2 and Cytokines. *Mediators Inflammation* (2017) 2017:1463216. doi: 10.1155/2017/1463216
68. Roszer T. Understanding the Mysterious M2 Macrophage through Activation Markers and Effector Mechanisms. *Mediators Inflammation* (2015) 2015:816460. doi: 10.1155/2015/816460
69. Sierra-Filardi E, Vega MA, Sanchez-Mateos P, Corbi AL, Puig-Kroger A. Heme Oxygenase-1 expression in M-CSF-polarized M2 macrophages contributes to LPS-induced IL-10 release. *Immunobiology* (2010) 215(9-10):788–95. doi: 10.1016/j.imbio.2010.05.020
70. Zizzo G, Hilliard BA, Monestier M, Cohen PL. Efficient clearance of early apoptotic cells by human macrophages requires M2c polarization and MerTK induction. *J Immunol* (2012) 189(7):3508–20. doi: 10.4049/jimmunol.1200662

Conflict of Interest: The authors declare that the research was conducted in the absence of any commercial or financial relationships that could be construed as a potential conflict of interest.

frontiers in Immunology

ORIGINAL RESEARCH
published: 25 February 2021
doi: 10.3389/fimmu.2021.631285

Inhibition of Dendritic Cell Activation and Modulation of T Cell Polarization by the Platelet Secretome

Anno Saris[1,2†‡], *Juulke Steuten*[1‡], *David P. Schrijver*[1], *Gijs van Schijndel*[1], *Jaap Jan Zwaginga*[3,4], *S. Marieke van Ham*[1,5] *and Anja ten Brinke*[1*]

[1] Department of Immunopathology, Sanquin Research and Landsteiner Laboratory, Amsterdam University Medical Center, University of Amsterdam, Amsterdam, Netherlands, [2] Department of Infectious Disease, Leiden University Medical Center, Leiden, Netherlands, [3] Center for Clinical Transfusion Research, Sanquin Research, Leiden, Netherlands, [4] Department of Hematology, Leiden University Medical Center, Leiden, Netherlands, [5] Swammerdam Institute for Life Sciences, University of Amsterdam, Amsterdam, Netherlands

Platelet transfusions are a frequently administered therapy for especially hemato-oncological patients with thrombocytopenia. Next to their primary function in hemostasis, currently there is increased attention for the capacity of platelets to affect the function of various cells of the immune system. Here, we investigate the capacity of platelets to immuno-modulate monocyte-derived dendritic cells (moDC) as well as primary dendritic cells and effects on subsequent T cell responses. Platelets significantly inhibited pro-inflammatory (IL-12, IL-6, TNFα) and increased anti-inflammatory (IL-10) cytokine production of moDCs primed with toll-like receptor (TLR)-dependent and TLR-independent stimuli. Transwell assays and ultracentrifugation revealed that a soluble factor secreted by platelets, but not microvesicles, inhibited DC activation. Interestingly, platelet-derived soluble mediators also inhibited cytokine production by human *ex vivo* stimulated myeloid CD1c+ conventional DC2. Moreover, platelets and platelet-derived soluble mediators inhibited T cell priming and T helper differentiation toward an IFNγ+ Th1 phenotype by moDCs. Overall, these results show that platelets are able to inhibit the pro-inflammatory properties of DCs, and may even induce an anti-inflammatory DC phenotype, with decreased T cell priming capacity by the DC. The results of this study provide more insight in the potential role of platelets in immune modulation, especially in the context of platelet transfusions.

Keywords: platelet immunomodulation, transfusion-related immune modulation, platelet releasate, monocyte-derived dendritic cells, primary dendritic cell, T cell priming

OPEN ACCESS

Edited by:
Alexandre Corthay,
Oslo University Hospital, Norway

Reviewed by:
Kitti Pázmándi,
University of Debrecen, Hungary
Niels Schaft,
University Hospital Erlangen, Germany
Jurjen Tel,
Eindhoven University of Technology, Netherlands

***Correspondence:**
Anja ten Brinke
a.tenbrinke@sanquin.nl

[†]***ORCID:***
Anno Saris
orcid.org/0000-0003-0493-9501

[‡]*These authors have contributed equally to this work and share first authorship*

Specialty section:
This article was submitted to Molecular Innate Immunity, a section of the journal Frontiers in Immunology

Received: *19 November 2020*
Accepted: *20 January 2021*
Published: *25 February 2021*

Citation:
Saris A, Steuten J, Schrijver DP, van Schijndel G, Zwaginga JJ, van Ham SM and ten Brinke A (2021) Inhibition of Dendritic Cell Activation and Modulation of T Cell Polarization by the Platelet Secretome. Front. Immunol. 12:631285. doi: 10.3389/fimmu.2021.631285

Abbreviations: CFSE, Carboxyfluoresceïne succinimidyl ester; DAMP, damage-associated molecular pattern; FNHTR, febrile non-hemolytic transfusion reactions; IFNγ; interferon γ; IL-1β; interleukin 1β; LTBP, latent TGF-β binding protein; MPLA, monophosphoryl lipid A; PAM3CSK4, pam3CysSerLys4; PAMP, pathogen-associated molecular pattern; PGE_2, prostaglandin E2; PMA, phorbol myristate acetate; TGFβ; transforming growth factor β; TNFα; tumor necrosis factor α; TRALI, transfusion related acute lung injury; TRAP-6, thrombin receptor-activating peptide 6; TRIM, transfusion related immune modulation; TT, tetanus toxoid.

INTRODUCTION

Up to three million platelet transfusions are administered every year in Europe, and the majority (up to 65%) of these transfusions are administered to hemato-oncological patients (1–7). Prophylactic administration of platelet transfusions in patients not at direct risk of bleeding is currently subject of debate (6–9). Next to the fact that platelet transfusions are costly and involve complicated logistics, they are associated with adverse reactions like alloimmunization, febrile non-hemolytic transfusion reactions (FNHTR), transfusion related acute lung injury (TRALI), as well as the still somewhat elusive transfusion related immune modulation (TRIM) (8, 10–13). TRIM associates with increased risk of infections, decreased graft rejection and recurrence of tumor growth in patients receiving transfusions (14–16). Even though a number of studies have investigated TRIM, the underlying mechanisms remain largely unresolved (17–20).

Platelets are anucleate megakaryocyte-derived cell fragments packed with secretory granules containing many hemostatic and angiogenic factors, but also a collection of mediators that affect the immune system, ranging from chemokines (e.g. chemokine ligand 5 (CCL5)) to microbicidal molecules (e.g. thrombocidin-1 and 2) (21, 22). Platelets also express many molecules such as toll-like receptors (TLRs), integrins and costimulatory molecules through which they can sense pathogen-associated molecular patterns and interact with leukocytes (23–26). Moreover, platelets are the main source of (s)CD40L in plasma, and in CD40L deficient mice transfer of wildtype platelets increased virus-specific IgG titers (27, 28). In contrast, platelet derived active transforming growth factor β (TGF-β), together with lactate, was found to inhibit T cell anti-tumor functions (29). Due to increased understanding of the potential immune functions of platelets, the question arises to what extent transfused platelets will affect the recipient's immune system (12, 17, 20, 30, 31), which would be especially relevant for hematological patients that are frequently strongly immune-compromised (7).

Dendritic cells (DCs) are instrumental for the initiation and skewing of the adaptive immune response. DCs are equipped with many pattern recognition receptors (PRRs) that recognize various pathogen- and danger- associated molecular patterns (PAMP/DAMP). Upon encounter of pathogenic antigens, DCs can engulf and process these antigens and present antigenic peptides in the context of MHC molecules to T cells. The upregulation of costimulatory molecules and secretion of cytokines is directed by the signaling pathways of the engaged PRR(s), whereby DCs prime and skew the antigen-specific T cells toward a particular immune response (32). Due to the central role of DCs in the adaptive immune response it is important to study the potential immune modulatory effect of platelets on DC effector functions. Previous studies describe variable effects of platelets on DC effector function depending mostly on the presence or absence of an additional activating stimulus (33–43). Although some studies have shown that platelets may reduce DC activation, lipopolysaccharide (LPS) was almost exclusively used for DC stimulation (33, 34, 36–38). Therefore, questions remain on the generalizability and consistency of these effects and more importantly what are the consequences on T cell activation and priming.

In the present study we aimed to advance our understanding of platelet-mediated inhibition of human DCs and how this affects subsequent T cell responses. Our studies revealed that upon activation platelets release soluble factors (platelet releasate) that affect both moDC and primary myeloid CD1c+ conventional DC2 (cDC2) cytokine production induced by a range of TLR-dependent and TLR-independent stimuli with minimal effects on co-stimulatory marker expression. Furthermore, moDCs stimulated in presence of platelets or platelet releasate show less ability to induce T cell proliferation and have decreased capacity to skew naïve T cells toward a Th1 IFNγ^+ phenotype. Overall, we show here that mediators derived from activated platelets directly impair DC effector functions, which may contribute to the occurrence of TRIM upon transfusion of platelets.

MATERIALS AND METHODS

Human Blood Samples

Leukapheresis products or buffy coats obtained from anonymized Sanquin blood donors were used to isolate monocytes and T cells after written informed consent by donors. Citrated whole blood was obtained to isolate fresh platelets and platelet releasate. All procedures were approved by the Sanquin Ethical Advisory Board and are in accordance with the declaration of Helsinki and Dutch regulations.

Isolation of Human Monocytes and Differentiation to Immature moDC

Monocytes were isolated using the Elutra Cell Separation System (Gambro, Lakewood, CO, USA) from fresh leukapheresis material or from PBMCs isolated from buffy coats using CD14+ magnetic cell separation (Miltenyi Biotech, Leiden, Netherlands) and subsequently frozen until further use as previously described (13, 44). Purity of monocytes was >90% as determined using flow cytometry with APC labeled anti-CD14 (clone MϕP9, BD biosciences). Upon initiation of culture, monocytes were thawed and differentiated into immature dendritic cells (DCs) as previously described (13, 44).

Platelet Isolation and Production and Ultracentrifugation of Platelet Releasate

Platelets were isolated from citrated whole blood by centrifugation at 200g for 10 min and supernatant platelet rich plasma was washed (5 min, 1650g) 1:2 with sequestrine buffer (17.5 mM Na2HPO4, 8.9 mM Na2EDTA, 154 mM NaCl, pH 6.9, containing 0.1% [wt/vol] bovine serum albumin, all obtained from Merck Millipore, Amsterdam, Netherlands). After washing, platelets were resuspended in GMP DC serum-free medium (Cellgenix, Freiburg, Germany) containing 100 U/ml penicillin and 100 U/ml streptomycin (Gibco). To collect platelet releasate, platelets were incubated 30 min with 250 μM thrombin receptor-activating

peptide 6 amide (TRAP-6) (Bachem, Bubendorf, Switzerland) after which platelets were removed by centrifugation: first 5 min at 1,650 g and subsequently 10 min at 4,000g. If indicated, platelet releasate was hereafter centrifuged to remove microparticles at 100,000g for 1 h in Optima L-100 XP Ultracentrifuge (Beckman Coulter, IN, United States). Experiments that directly compared whole platelets and releasate used releasate and whole platelets from the same donor. Otherwise, releasate was pooled from four or five whole blood donors, aliquoted and stored at −20°C until further use.

Stimulation of DCs

Immature moDCs were stimulated in the absence or presence of platelets or platelet releasate with a platelet:DC ratio ranging from 80:1 to 1:1 (or equivalent amount of releasate) in GMP DC serum-free medium (Cellgenix, Freiburg, Germany) containing 100 U/ml penicillin and 100 U/ml streptomycin (Gibco). When indicated, DCs were stimulated using 2.5 μg/ml monophosporyl lipid A (MPLA) (Sigma Aldrich, Zwijndrecht, Netherlands), 5 μg/ml pam3CysSerLys4 (PAM3CSK4) (Invivogen, San Diego, CA, USA), 2.5 μg/ml resiquimod (R848) (Alexis Biochemical, Paris, France) or 0.25 μg/ml flagellin *bacillus subtilis* (Invivogen) in combination with 1,000 U/ml IFNγ (Boehringer Ingelheim, Alkmaar, Netherlands) or a cytokine maturation cocktail consisting of 10 ng/ml TNFα, 10 ng/ml IL-1β (both Cellgenix, Freiburg, Germany), and 1 μg/ml prostaglandin E2 (PGE_2) (Sigma Aldrich, Zwijndrecht, Netherlands). When indicated, releasate or recombinant human TGF-β (R&D Systems, Minneapolis, MN, United States) was pre-incubated with blocking antibody against TGF-β (Clone 1D11, 10 μg/ml, BioXCell, NH, United States) for 30' at 37°C, 5% CO_2. For transwell experiments, moDCs were stimulated with MPLA/IFNγ in a 96-well transwell system (Corning, pore size ≤0.3 μM) in absence or presence of TRAP-6 activated platelets (platelet:DC ratio 40:1) that were either below the transwell (i.e. in the same compartment as the DCs) or separated by the transwell. After 24 or 48 h at 37°C, 5% CO_2 culture supernatant was harvested and frozen at −20°C until cytokine measurements.

Cytokine Measurements

The levels of IL-6 and IL-10 in culture supernatants were measured using compact PeliKine Cytokine ELISA kits (Sanquin Reagents, Amsterdam, Netherlands); the level of TNF-α was determined with Human TNF-α ELISA set (Diaclone, Besançon, France). To determine production of IL-12p40, a combination of two anti-IL-12p40 antibodies was used (coat: clone C11.79 and detection: clone C8.6, Sanquin Reagents, Amsterdam, Netherlands) and recombinant IL-12p40 was used as calibration. The level of human TGF-β1 was measured using DuoSet ELISA kit (R&D Systems, Minneapolis, MN, United States) either after or without chemical activation of the samples according to manufacturer's protocol. Absorbance was measured at 540nm with SynergyTM 2 (BioTek, Winooski, VT, USA).

Phenotyping DCs

After 48 h of stimulation, DCs were harvested with 0.4% trisodium citrate (Merck Millipore, Amsterdam, Netherlands) in PBS supplemented with 4 mg/ml human albumin (Albuman, Sanquin Reagents, Amsterdam, Netherlands). DCs were stained 30 min at room temperature with LIVE/DEAD Fixable near-IR Dead Cell Stain Kit (Thermo Fisher Scientific) and subsequently with either PE-labeled anti-HLA-DR (Clone G46-6) or with FITC-labeled anti-CD80 (Clone L307.4), PE-labeled anti-CD40 (Clone 5C3), APC-labeled anti-CD83 (Clone HB15e) and BV421-labeled anti-CD86 (Clone 2331) (all from BD Biosciences) in the presence of 3 mg/ml human γ-globulin (Nanogam, Sanquin, Amsterdam, Netherlands). Samples were measured with BD FACSCanto II and analyzed using Flowjo VX (Beckton, Dickinson & Company, Ashland, OR, United States). Gating strategy involved selection of DCs on FSC/SSC, single cells and viable cells.

Isolation of Human T Cells

Total human lymphocytes were isolated using the Elutra Cell Separation System (Gambro, Lakewood, CO, USA) from fresh leukapheresis material and frozen until further use. Naïve human CD4+ T cells were isolated from buffy coats. First, the PBMC fraction was isolated by density gradient centrifugation (Lymphoprep, Axis-shield, Alere Technologies AS, Oslo, Norway). From PBMC fraction, CD4+ cells were isolated by negative selection using magnetic separation followed by negative selection of CD45RA population (both Miltenyi Biotech, Leiden, Netherlands). Purity of isolated naïve CD4+ T cells ≥95% as determined by staining with FITC-labeled anti-CD45RA (Clone HI100, eBioscience) and BV421-labeled anti-CD45RO (Clone UCHL1, BD Bioscience).

Isolation and Stimulation of Primary Blood DCs

Primary blood DCs were isolated from buffy coats as previously described (45). In short, PBMCs were enriched for blood DCs by elutriation with JE-5.0 elutriator (Beckman Coulter, Brea, CA, USA), followed by sorting on FACSAria IIIu or III cell sorter (BD Bioscience, San Jose, CA, USA). For sorting, the cells were stained with APC-labeled anti-CD3 (clone HIT3a), anti-CD14 (clone MϕP9), anti-CD19 (clone SJ25-C1) (all BD Biosciences), PE-Cy7-labeled anti-CD1c (clone L161, Biolegend) and FITC-labeled 6-sulfo LacNAc (Slan)-specific antibody (clone M-DC8, Miltenyi Biotech) and LIVE/DEAD fixable Near-IR Dead Cell Stain Kit (Invitrogen). Different DC subtypes were gated as follows: Slan+ non-classical monocytes as $CD3^-CD14^-CD19^-$ $M\text{-}DC8^+$ and myeloid cDC2 as $CD3^-CD14^-CD19^-CD1c^+$ (see **Supplementary Figure S3** for gating strategy). Purity after sort was >90% as tested by flow cytometry. Primary DCs were rested overnight in GMP DC serum-free medium (Cellgenix) containing 100 U/ml penicillin and 100 U/ml streptomycin (Gibco) at 37°C and 5% CO_2. After overnight rest, DCs were stimulated with R848 (Alexis Biochemical, Paris, France) at a concentration of 5 μg/ml in absence or presence of platelets or platelet releasate in a 50:1 platelet:DC ratio.

T Cell Proliferation Assay

After thawing and 1 h resting total T cells or naïve CD4+ CD45RA + T cells were washed twice with PBS and incubated with 5μM

CFSE (Invitrogen) for 20 min at room temperature. After washing, T cells were resuspended in IMDM+5%HS medium and incubated 10:1 (T:DC ratio) with autologous (TT-loaded) or allogeneic DCs. If indicated, DCs were first incubated 1 h at 37° C with 5 μg/ml tetanus toxoid (AJVaccines, Copenhagen, Denmark) before stimulation with MPLA/IFNγ. After maturation with MPLA/IFNγ or IL-1β/TNFα/PGE_2, moDCs were washed twice with IMDM + 5%HS medium to remove potential remaining platelets or platelet-derived factors. After 8 days, total T cells were harvested, labeled with LIVE/DEAD Fixable near-IR Dead Cell Stain Kit (Thermo Fisher Scientific) and subsequently with PE-labeled anti-CD4 (Clone SK3) and APC-labeled anti-CD8 (Clone SK1) (both from BD biosciences) in FACS buffer (PBS + 0.5% BSA + 0.02% Azide). After 9-10 days, naïve T cells were stimulated with PMA (100 ng/ml) and ionomycin (1 μg/ml) in presence of Brefeldin A (10 μg/ml) (all from Sigma Aldrich) for 5 h. T cells were harvested and washed, labeled with LIVE/DEAD Fixable near-IR Dead Cell Stain Kit (Thermo Fisher Scientific) at RT and subsequently with BUV395-labeled anti-CD4 (clone SK3, BD Bioscience). Hereafter, cells were fixed for 15 min with 4% paraformaldehyde (Merck, Darmstadt, Germany) after which cells were stained with PECy7-labeled anti-IFNγ (Clone B27, BD Bioscience), APC-labeled anti-TNFα (clone Mab11, Biolegend) in Brilliant Stain buffer (BD Bioscience) in permeabilization buffer containing 0.5% Saponin, 1%BSA, and 0.02% azide. Cells were washed and measured on Canto II (total T cells) or LSR Fortessa (both from BD Bioscience). Data were analyzed in Flowjo VX (Beckton, Dickinson & Company, Ashland, OR, United States), gating involved selection of lymphocytes based on FSC/SSC, single cells, live CD4+ cells, proliferation dye dilution and positivity for specific cytokines.

Statistical Analysis

Graphical presentation and statistical analyses were performed using GraphPad prism v8.02 (GraphPad Software Inc, La Jolla, California, USA). Paired t-tests, repeated measures one-way ANOVA and two-way ANOVA with Tukey post test were used to determine statistical differences in DC and T cell cytokine production, DC co-stimulatory marker expression and viability, and T cell proliferation. *$p \leq 0.05$, **$p \leq 0.01$, ***$p \leq 0.001$.

Data Sharing Statement

For original data, please contact a.tenbrinke@sanquin.nl

RESULTS

Platelets Decrease moDC Pro-Inflammatory Cytokine Production Upon DC Activation With Different Stimuli

To investigate if and to what extent platelets affect human DC function, monocyte-derived DCs (moDCs) were stimulated with several stimuli to mimic various types of physiological activation, including MPLA (TLR4; **Figure 1A**), PAM3CSK4 (TLR1/2; **Figure 1C**), R848 (TLR7/8; **Figure 1D**) or flagellin (TLR5; **Figure 1E**) in the presence of IFNγ or with a cytokine maturation cocktail containing IL-1β, TNF-α; and PGE_2 (**Figure 1B**, TNF-α not measured as this was added with stimulation cocktail). After stimulation, moDCs produced pro-inflammatory cytokines TNF-α, IL-12, and IL-6. In the presence of platelets however, pro-inflammatory cytokine production reduced significantly after all stimulations with an average residual cytokine production of 18.9%, 19.7%, and 43.4% for TNFα, IL-12p40, and IL-6 respectively after MPLA/IFNγ stimulation. Platelet-mediated inhibition of cytokine production was not observed for IL-6 production after R848/IFNγ stimulation and IL-12p40 production upon flagellin/IFNγ or cytokine cocktail stimulation, which both failed to induce a strong IL-12p40 response. The decrease in cytokine production was dependent on the number of platelets present (**Supplementary Figure S1A**). Additionally, in presence of platelets anti-inflammatory IL-10 production was induced for R848/IFNγ and IL-1β/TNFα/PGE_2 stimulated moDCs (**Figures 1B, D**). MoDCs stimulated with MPLA/IFNγ and PAM3CSK/IFNγ display a non-significant trend of IL-10 induction in the presence of platelets (**Figures 1A, C**), whereas IL-10 production was not detectable for moDCs stimulated with Flagellin/IFNγ (**Figure 1E**). When immature moDCs were cultured with platelets without additional maturation stimulus, some donors showed an increase in cytokine production. This non-significant trend was most clear for IL-6 and IL-10 production by immature moDCs in presence of platelets (**Supplementary Figure 1B**).

Stimulation with MPLA/IFNγ or IL-1β/TNFα/PGE_2 induced the highest expression of co-stimulatory molecules as measured by flow cytometry. Interestingly, platelets minimally affected the phenotype of MPLA/IFNγ or IL-1β/TNFα/PGE_2 stimulated DCs, with only limited changes in expression of CD83 or CD40 and CD86, respectively (**Supplementary Figure S1C**; for gating strategy see **Supplementary Figure S2A**). In summary, platelets reduced moDC pro-inflammatory cytokine production after various DAMP/PAMP stimulations, despite minimal effects on co-stimulatory molecule expression.

The Effect of Platelets on moDC Cytokine Production Is Mediated by a Soluble Factor

Next, the contact dependency of platelet mediated inhibition of DC cytokine production was investigated. When platelets were cultured with DCs in a transwell system to prevent direct cell-cell contact, IL-12p40, IL-6, and TNF-α production by stimulated moDCs was also reduced although to a slightly lower extent, which possibly can be explained by a concentration gradient-induced effect of the transwell itself (**Figure 2A**). Hence platelets inhibited pro-inflammatory cytokine production by moDCs also without direct cell-cell contact.

To further explore the involvement of platelet-derived soluble mediators, the releasate secreted by activated platelets was tested. For this, isolated platelets were activated with the PAR1 agonist thrombin receptor activator peptide-6 (TRAP-6). After activation, the platelet suspension was centrifuged twice to remove whole platelets and cell fragments. Whole platelets and

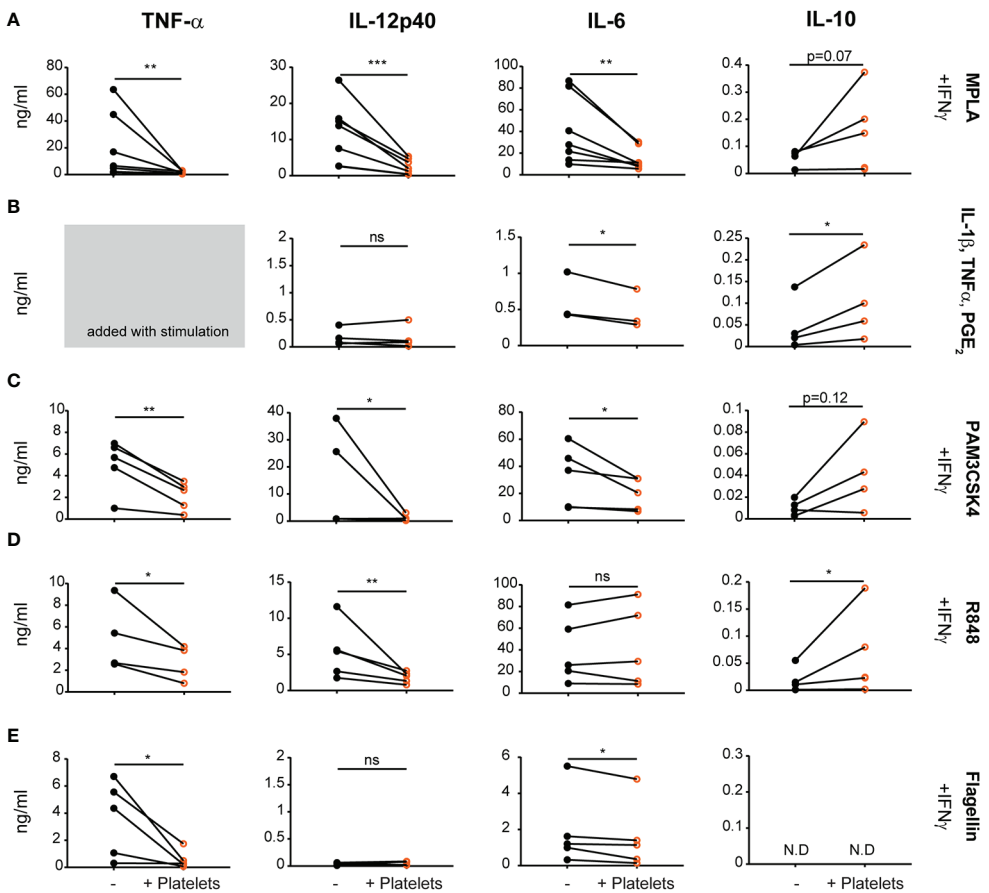

FIGURE 1 | Platelets decrease monocyte-derived dendritic cells (moDC) pro-inflammatory cytokine production upon activation with different stimuli. moDCs were stimulated with **(A)** monophosporyl lipid A (MPLA), **(B)** a cytokine cocktail containing IL-1β, TNFα and prostaglandin E2 (PGE_2), **(C)** pam3CysSerLys4 (PAM3CSK), **(D)** R848, or **(E)** Flagellin **(A, C–E)** in the presence of IFNγ **(A–E)** in absence or presence of platelets (platelet:DC ratio 40:1). After 48 h, supernatant was harvested and production of TNF-α, IL-12p40, IL-6, and IL-10 was determined by ELISA. Differences in cytokine production (mean ± SEM) were determined by paired t-tests, **(A, C–E)** *n*=5 donors; five independent experiments **(B)** *n*=4 donors; two independent experiments. **(A–E)** IL-6 panel B and IL-10 panel E fewer replicates due to values below detection limit. N.D. not detectable. *p ≤ 0.05, **p ≤ 0.01, ***p ≤ 0.001.

platelet releasate from the same platelet donor induced a comparable decrease of pro-inflammatory cytokine production by MPLA/IFNγ stimulated moDCs (**Figure 2B**), while TRAP-6 itself did not affect moDC viability or cytokine production (**Supplementary Figures S2B, C**). Lastly, to exclude involvement of microvesicles, the releasate was ultracentrifuged at 100,000 *g*. Releasate with or without ultracentrifugation equally inhibited pro-inflammatory cytokine production by stimulated moDCs (**Figure 2C**). Overall, platelets inhibit MPLA/IFNγ-stimulated moDC pro-inflammatory cytokine production *via* a soluble factor, and not through release of microvesicles.

As platelets are a major source of DC-tolerizing active TGF-β in plasma (46–50) and platelet-derived TGF-β was shown to inhibit the anti-tumor T cell response in a murine model (29, 51), we investigated the involvement of TGF-β in platelet-mediated DC inhibition. Both platelets and DCs possess machinery to activate latent TGF-β and release the mature 25-kDa dimer (29, 48). Upon chemical activation, inducing dissociation of the mature TGF-β dimer from latent TGF-β binding proteins (LTBPs), we could detect active TGF-β1 in platelet releasate (**Supplementary Figure S3A**), indicating that latent TGF-β is present and may potentially be activated in our culture system. However, blocking TGF-β in platelet releasate could not restore cytokine production by moDCs (**Supplementary Figure S3B-C**), indicating that TGF-β is not the responsible factor in the releasate for the inhibition of cytokine production by moDC.

Platelet Releasate Affects Myeloid Conventional DC2 TNFα Production

In human blood, two types of myeloid or conventional DCs (myeloid cDC1 (CD141+) and cDC2 (CD1c+)) can be distinguished (32) and there is a subset of slan+ non-classical monocytes that show DC-like characteristics (52). To investigate to what extent our findings translate to human primary blood DCs, we isolated human myeloid CD1c+ conventional DC2 and slan+ non-classical monocytes from blood (**Supplementary Figure S4**).

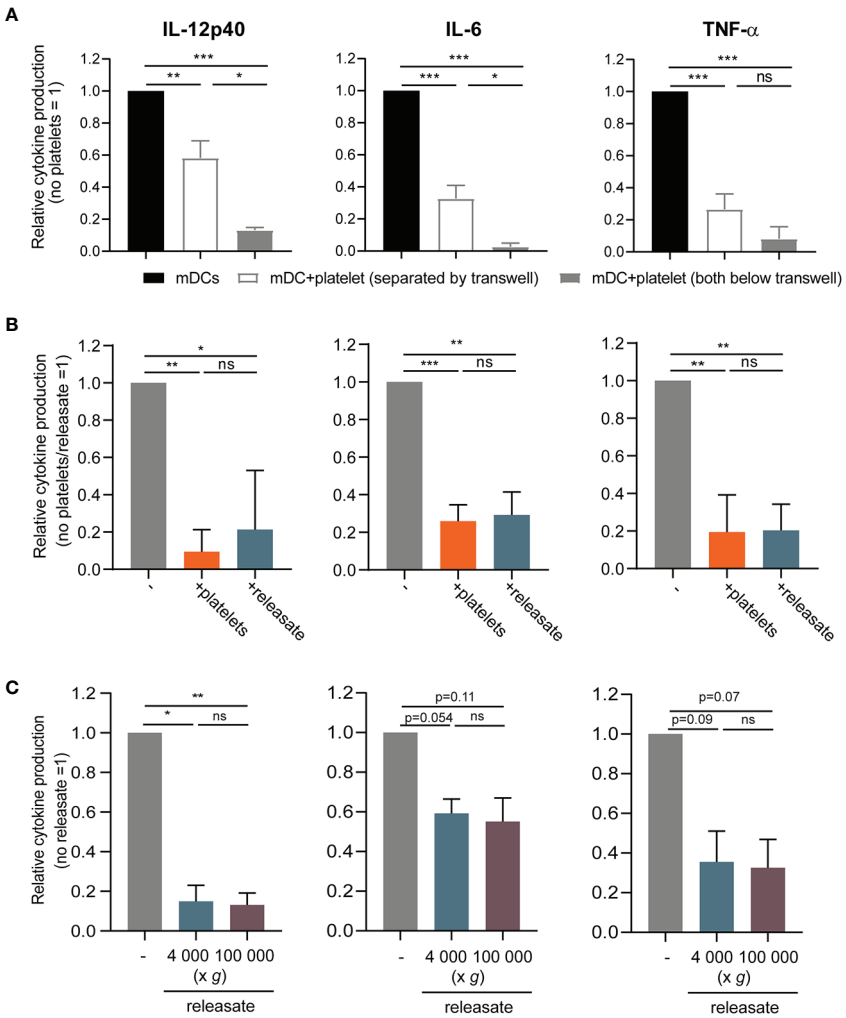

FIGURE 2 | The effect of platelets on monocyte-derived dendritic cells (moDC) cytokine production is mediated by a soluble factor. **(A)** moDCs were stimulated with monophosporyl lipid A (MPLA)/IFNγ in a transwell system (pore size ≤ 0.3 μm) in absence or presence of thrombin receptor-activating peptide (TRAP)-activated platelets (platelet:DC ratio 40:1) that were either below the transwell (i.e. in the same compartment as the DCs) or separated by the transwell (n=4 donors; four independent experiments) (no platelets: IL-12p40 211-110714 pg/ml mean 23,068 pg/ml; IL-6 927.0 -127446 pg/ml mean 34,503 pg/ml; TNFα 352-44501 pg/ml mean 14,471 pg/ml). **(B, C)** moDCs were stimulated with MPLA/IFNγ **(B)** in absence or presence of TRAP-activated whole platelets or platelet releasate centrifuged at 4,000 × g for 10 min ((equivalent) platelet:DC ratio 50:1 (n=4 donors; two independent experiments)) (no platelets: IL-12p40 24568-495930 pg/ml mean 233,399 pg/ml; IL-6 35500-62984 pg/ml mean 51,077 pg/ml; TNFα 6670-42400 pg/ml mean 24,768 pg/ml) or **(C)** in absence or presence of platelet releasate (equivalent platelet:DC ratio 50:1) centrifuged at 4000 g for 10 min (microvesicles in suspension) or additionally at 100 000 g for 1 h (no microvesicles in suspension) (n=3 donors; three independent experiments) (no platelets: IL-12p40 3370-10800 pg/ml mean 6,220 pg/ml; IL-6 5230-34900 pg/ml mean 17,168 pg/ml; TNFα 7540-32400 pg/ml mean 15,427 pg/ml). **(A–C)** After 48 h, supernatant was harvested and production of TNF-α, IL-12p40, and IL-6 was determined by ELISA. Differences in relative cytokine production (mean ± SEM) were determined using repeated measures one-way ANOVA with Tukey post testing. *p ≤ 0.05, **p ≤ 0.01.

After overnight rest, isolated myeloid cDC2's and slan+ non-classical monocytes were stimulated with R848 as primary DCs were found to not respond to stimulation with MPLA/IFNγ (data not shown; (45)). Interestingly, platelet releasate significantly decreased TNF-α production by myeloid cDC2 and a trend for IL-12p40 inhibition was observed (**Figure 3A**), whereas cytokine production by slan+ non-classical monocytes was not affected (**Figure 3B**). Unfortunately, IL-10 production could not be detected for any of the primary DC subsets tested (*data not shown*). These findings confirm that the platelet-mediated effects found on moDC cytokine production could partly be validated in a subset of primary human blood DCs, namely myeloid cDC2s.

Platelets and Platelet Releasate Inhibit T Cell Activation and Skewing of Naïve T Cells Toward an IFNγ+ Th1 Phenotype by moDCs

Above we have shown that platelets and platelet releasate affect pro-inflammatory cytokine production by DCs, but the effect on

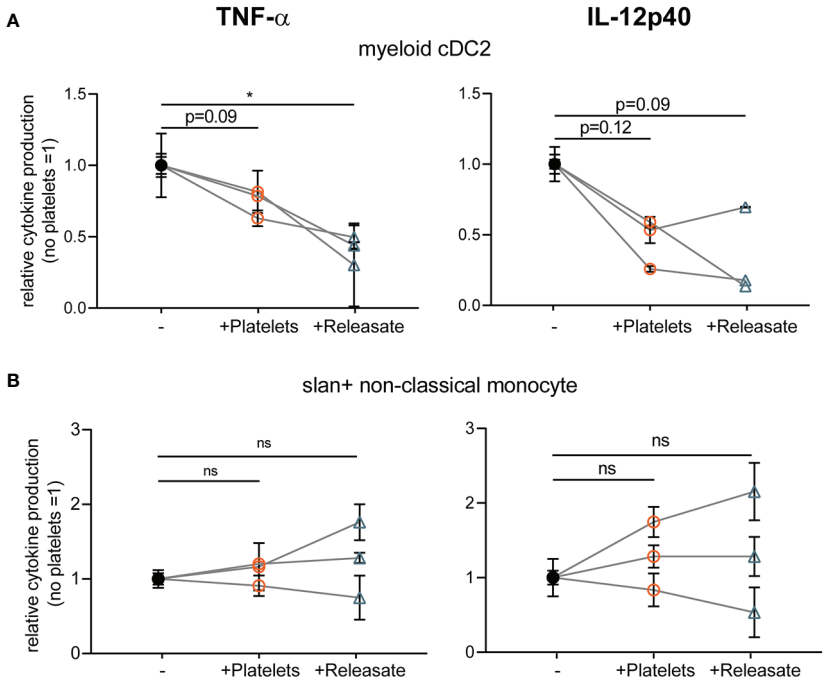

FIGURE 3 | Platelet releasate affects myeloid conventional DC2 TNFα production. Primary human blood **(A)** myeloid CD1c+ conventional DC2 and **(B)** slan+ non-classical monocytes isolated from buffy coats were **(A, B)** stimulated with R848 in absence or presence of platelets or platelet releasate (centrifuged 4000 × *g* 10') ((equivalent) platelet: dendritic cells DC ratio 50:1). After 24 h, supernatant was harvested and production of TNF-α (left; no platelets myeloid cDC2 141-364 pg/ml mean 284.7 pg/ml; slanDC 959-10100 pg/ml mean 4,306.5 pg/ml) and IL-12p40 (right; no platelets myeloid cDC2 111-335 pg/ml mean 226 pg/ml; slanDC 930-1530 pg/ml mean 1,238.3 pg/ml) was determined by ELISA (*n*=3 donors; three independent experiments). Differences in relative cytokine production (mean ± SEM) were determined using repeated measures one-way ANOVA with Tukey post testing. *p ≤ 0.05.

subsequent T cell responses remains largely unresolved. To investigate the effect of platelets on DC-mediated T cell stimulation, moDCs were loaded with tetanus toxoid (TT) and subsequently stimulated with MPLA/IFNγ in presence of platelets. MoDCs stimulated in presence of platelets induced less TT-specific autologous CD4+ and CD8+ T cell proliferation (**Figure 4A** and **Supplementary Figure S5A**). A similar decrease in the ability of moDCs to induce allogeneic CD4+ but not CD8+ proliferation under influence of platelets or platelet releasate was found (**Figure 4B** and **Supplementary Figures S5B, C**).

Another interesting aspect of DC biology is their ability to skew naïve T cells toward a specific T helper phenotype upon the initiation of an immune response. MoDCs were cultured with MPLA/IFNγin presence of whole platelets and platelet releasate. In a subsequent co-culture with naïve CD4+ CD45RA+ T cells, moDCs stimulated in presence of platelets or platelet releasate induced less allogeneic proliferation of naïve T cells (**Figure 4B**, left panel, gating strategy in **Supplementary Figure S6A**). Additionally, divided T cells (CFSEdim) displayed decreased IFNγ production compared to control co-cultures where moDCs were stimulated in the absence of platelets or platelet releasate (**Figures 4B**, middle panel, and **4C**). Furthermore, the divided T cells produced less TNFα compared to control co-cultures where moDCs were stimulated in the absence of platelets but not platelet releasate (**Figures 4B**, right panel, and **4C**). No significant production of IL-10 was detected in any of the DC-T cell co-cultures with or without platelet releasate (*data not shown*).

To determine whether effects on T cell skewing are dependent on the type of stimulation, cultures were performed with moDCs stimulated with TNFα, IL-1β; and PGE_2. We observed an increase in moDC anti-inflammatory IL-10 production when stimulated in presence of platelet releasate (**Supplementary Figure S6B**). Simultaneously, we observed a decrease in IL-6 production (**Supplementary Figure S6B**; TNFα could not be analyzed as it was present in the stimulation cocktail) and also a decreased ability to induce naïve T cell proliferation as measured by CFSE dilution by flow cytometry (**Supplementary Figure S6C**, left panel). No effect was found on the IFNγproduction of these naïve T cells compared to controls (**Supplementary Figure S6C**, right panel). All in all, platelets and platelet releasate can decrease the ability of moDCs to induce both memory and naïve T cell proliferation. Additionally, the ability of MPLA/IFNγstimulated moDCs to induce IFNγ+ Th1 responses was reduced when stimulated in presence of platelets or platelet releasate.

DISCUSSION

The mechanisms underlying TRIM are hard to investigate, but the role platelets themselves may play in this immune modulatory phenomenon after transfusion is increasingly being acknowledged

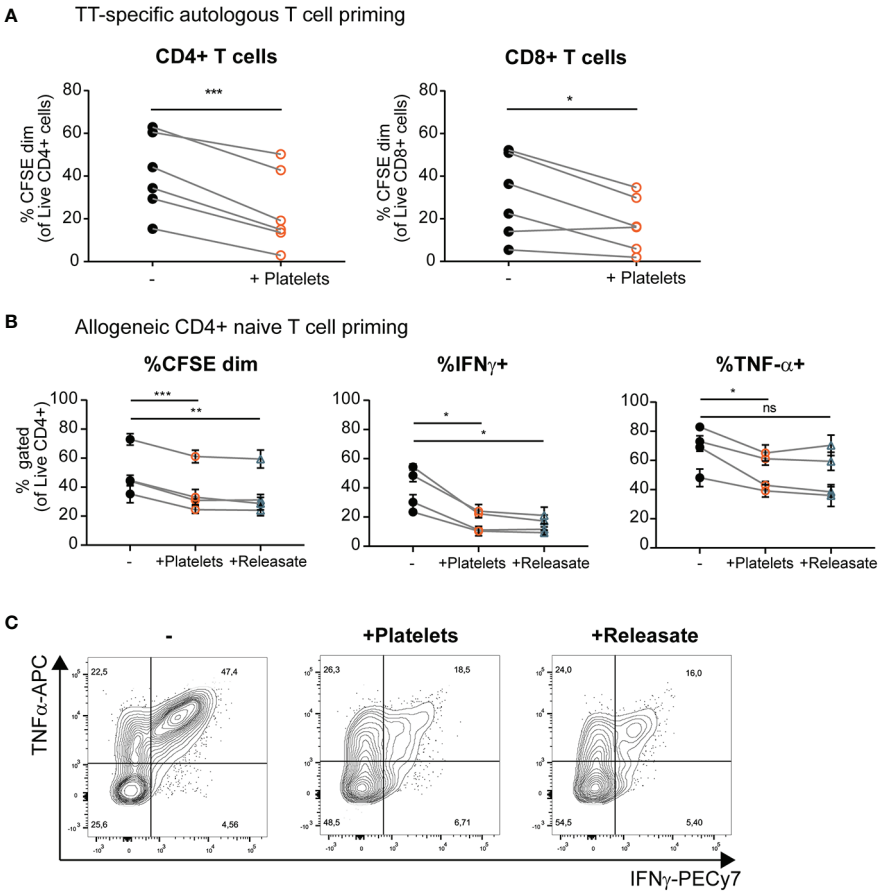

FIGURE 4 | Platelets and platelet releasate inhibit T cell activation and skewing of naïve T cells toward an IFNγ+ Th1 phenotype by monocyte-derived dendritic cells (moDCs). **(A)** After 1 h of pre-incubation with tetanus toxoid (TT), moDCs were stimulated with monophosporyl lipid A (MPLA)/IFNγ in absence or presence of whole platelets (platelet: dendritic cells DC ratio 40:1). After 48 h, DCs were harvested and incubated 1:10 with CFSE-labeled autologous lymphocytes. After 8 days, T cell proliferation was determined using flow cytometry (*n*=6 donors; six independent experiments) **(B, C)** moDCs were stimulated with MPLA/IFNγ in absence or presence of whole platelets or platelet releasate (centrifuged 4000 x *g* 10')((equivalent) platelet:DC ratio 50:1). After 48 h, DCs were harvested and incubated 1:10 with CFSE labeled allogeneic naïve CD4+ CD45RA+ T cells. After 10 days, T cell proliferation and intracellular cytokine production was determined by flow cytometry (*n*=4 donors; two independent experiments). **(C)** Representative plots of intracellular TNFα and IFNγ production by naïve CD4+ CD45RA+ T cells stimulated as described above. **(A)** Differences in proliferation were determined using paired t-tests. **(B)** Differences in proliferation and cytokine production (mean ± SEM) were determined by repeated measures one-way ANOVA with Tukey post testing. *p ≤ 0.05, **p ≤ 0.01, ***p ≤ 0.001.

(12, 31). Mechanisms of immune suppression as a result of TRIM are worth elucidating as these might be both beneficial (e.g. decreased graft rejection) or detrimental (e.g. recurrence resected malignancies) for the patient (14, 15, 18). However, much is still unclear about platelet-mediated immune modulation on DCs and whether platelets also affect subsequent ability of DCs to prime naïve and re-activate memory T cells. Here we show that a soluble factor secreted by platelets affects both moDC and primary myeloid CD1c+ conventional DC2 cytokine production under different stimulation conditions. Furthermore, these platelet-modulated moDCs are less capable to induce T cell proliferation and to skew naïve T cells toward a Th1 IFNγ$^+$ phenotype.

Activation of transfused platelets could be induced by the so-called platelet storage lesion (53) or after transfusion by vascular damage in the recipient, which is frequently observed in hemato-oncological patients (7). Our observation of activated platelets decreasing pro-inflammatory responses at a potential physiological site of tissue damage makes sense when considering that here platelet-mediated immune suppression could favor wound healing over an excessive inflammatory response. In the setting of TRIM however, interaction of activated platelets with DCs might also occur in absence of tissue injury. This is an important mechanism to consider especially in thrombopenic and immune-compromised hemato-oncological patients whom are the primary recipients of platelet transfusions (7). Within the vasculature, transfused activated platelets might come across blood DCs (53–55) or encounter APCs while passing through the white and red pulp of the spleen (56).

Previous studies have reported contrasting results on the effect of platelets on DC activation. Platelets have generally

been found to increase activation of DCs in absence of an additional stimulus (36, 39–42), while in presence of TLR-4 stimulus (i.e. LPS) platelets suppress DCs pro-inflammatory capacity or even induce an anti-inflammatory phenotype (33, 34, 37, 38, 43). In line, here platelets are shown to decrease pro-inflammatory cytokine production by DCs after stimulation with various TLR-dependent as well as TLR-independent agonists, implicating a more generic effect. Hagihara and colleagues described previously that moDCs activated with LPS in presence of platelets showed increased IL-10 production (33). Here, in agreement with a general immune suppressive effect, we found an increased IL-10 production for R848/IFNγ- and IL-1β/TNFα/PGE_2- stimulated moDCs in the presence of platelets.

Despite the profound effect of platelet-derived mediators on moDC cytokine production, the effect on costimulatory marker expression was limited. Previous studies have shown varying effects of platelets on co-stimulatory marker expression by DCs (33–36, 38, 43). We have previously observed that inhibition of cytokine production by moDCs is not always linked to reduced co-stimulatory marker expression (57). To gain more insight in the mechanism behind reduced cytokine expression with limited effects on co-stimulatory marker expression, it is important to investigate at which level of the DC activation signaling cascade platelets or platelet-derived factors interfere. Irrespectively, we have shown that moDCs stimulated in presence of platelets showed decreased ability to activate a TT-specific memory response as well as induce proliferation and Th1 IFNγ+ skewing of naïve T cells in an allogeneic setting.

A number of studies have also reported on direct effects of platelets on T cell proliferation and cytokine production (29, 51, 58). Despite extensive washing, complex formation between platelets and DCs might occur during DC stimulation (13, 41). However, our experiments using platelet releasate where platelet-derived factors were washed away before co-culture of DCs and T cells show very comparable effects on T cell proliferation and cytokine production. This demonstrates that the effects of platelets on T cell proliferation and cytokine production are highly likely to be mediated through a direct effect of platelets on DC effector function.

Interestingly, experiments performed with platelet releasate showed that the platelet-mediated effects on DC cytokine production and T cell priming capacity are primarily mediated by soluble factors and are not mediated by microvesicles. We are the first to show that the platelet-mediated effects on DC cytokine production are not mediated by microvesicles. Microvesicles were previously shown to affect HLA II and CD80 expression as well as phagocytic capacity of immature moDCs differentiated in the presence of microparticles shed by stored platelets (38), and were shown to inhibit human plasmacytoid DC pro-inflammatory cytokine production (59).

The immune modulatory factor(s) secreted by platelets that affect DC function remain(s) to be identified. Platelets are capable of secreting a wide range of mediators that could influence DC biology (12, 30). For example, TGF-β is activated and expressed by platelets and is known to alter DC effector functions by directing toward a tolerance-inducing phenotype (46–49). Here we show for the first time that platelet-derived TGF-β is unlikely to be involved in platelet-induced inhibition of DC. Next to TGF-β, platelets are able to express and secrete (soluble) CD40L, but as this molecule usually induces DC maturation and upregulation of cytokine production (40, 60, 61) (s)CD40L is an unlikely mediator of the results described here. For CXCL4 (platelet factor 4) contrasting literature exists on its effects on DC function, with reports documenting anti-inflammatory effects (62) as well as potentiated response to TLR ligands upon culture of moDCs in presence of CXCL4 (63, 64). In addition, multiple factors could act together to mediate suppression of pro-inflammatory cytokine production by moDC.

Further research is warranted to elucidate which platelet-derived factors affect DC activation. We propose for upcoming studies to first validate whether the platelet-derived factor is (partly) of a proteinaceous nature, or whether e.g. platelet metabolites are responsible for the observed effects. An unbiased approach using liquid chromatography, potentially in combination with mass spectrometry (as described in (29)) would be interesting to identify the responsible platelet-derived factor(s) involved in the inhibition of DC effector functions.

Platelet-mediated inhibition was not only found for moDC but also observed for myeloid conventional DC2's isolated from the blood, in line with previous research using platelet concentrates (36, 37). However, as these studies were performed in a whole blood culture, indirect effects on DCs *via* other cells could not be excluded. Here we show that platelet-derived soluble mediators inhibit pro-inflammatory cytokine production of purified myeloid cDC2, thus proving a direct effect of platelet (releasate) on primary DCs. As myeloid cDC2s have an extensive array of PRRs and a widespread tissue distribution, platelet-mediated inhibition could affect immunity against a wide range of pathogens (32). Interestingly, cytokine production of slan+ non-classical monocytes was not affected, which may be explained by their intrinsic capacity of higher production of IL-12 and TNFα compared to myeloid cDCs (65, 66).

In summary, we have shown that platelets reduce pro-inflammatory cytokine production of both moDCs and primary myeloid CD1c+ conventional DC2s. This inhibition is mediated by a soluble factor, and was observed in the presence of a range of both TLR-dependent as well as TLR-independent stimuli. Moreover, moDCs stimulated in the presence of platelets show a decreased ability to induce (antigen-specific) T cell proliferation as well as naïve T cell skewing toward a Th1 $IFN\gamma^+$ phenotype. Together, these data show that platelets can influence the adaptive T cell response by inhibition of DC activation, with potential implications in platelet transfusions.

DATA AVAILABILITY STATEMENT

The raw data supporting the conclusions of this article will be made available by the authors, without undue reservation.

ETHICS STATEMENT

The studies involving human participants were reviewed and approved by the Ethical Advisory Council of Sanquin Blood Supply Foundation and are in accordance with the declaration of Helsinki and Dutch regulations. The patients/participants provided their written informed consent to participate in this study.

AUTHOR CONTRIBUTIONS

AS and JS conceptualized and designed the study, acquired and interpreted data, wrote and revised the manuscript. DS and GS acquired data. JZ, SH, and AB conceptualized and designed the study, interpreted data and critically revised the manuscript. All authors contributed to the article and approved the submitted version.

FUNDING

This work was supported by Sanquin Blood Supply Foundation (grant PPOC 17-44).

ACKNOWLEDGMENTS

We thank the central facility at Sanquin for help with operation of the ELUTRA system and isolation of primary DCs.

SUPPLEMENTARY MATERIAL

The Supplementary Material for this article can be found online at: https://www.frontiersin.org/articles/10.3389/fimmu.2021.631285/full#supplementary-material

REFERENCES

1. Stroncek D, Rebulla P. Platelet transfusions. *Lancet* (2017) 370:1391–401. doi: 10.1007/978-3-319-47462-5_94
2. Cameron B, Rock G, Olberg B, Neurath D. Evaluation of platelet transfusion triggers in a tertiary-care hospital. *Transfusion* (2007) 47:206–11. doi: 10.1111/j.1537-2995.2007.01090.x
3. Charlton A, Wallis J, Robertson J, Watson D, Iqbal A, Tinegate H. Where did platelets go in 2012? A survey of platelet transfusion practice in the North of England. *Transfus Med* (2014) 24:213–8. doi: 10.1111/tme.12126
4. Greeno E, McCullough J, Weisdorf D. Platelet utilization and the transfusion trigger: A prospective analysis. *Transfusion* (2007) 47:201–5. doi: 10.1111/j.1537-2995.2007.01089.x
5. Mayr WR. Blood transfusion in Europe-The White Book 2005: The patchwork of transfusion medicine in Europe. *Transfus Clin Biol* (2005) 12:357–8. doi: 10.1016/j.tracli.2005.10.006
6. Estcourt L, Stanworth S, Doree C, Hopewell S, Murphy MF, Tinmouth A, et al. Prophylactic platelet transfusion for prevention of bleeding in patients with haematological disorders after chemotherapy and stem cell transplantation. *Cochrane Database Syst Rev* (2012) 5:CD004269. doi: 10.1002/14651858.CD004269.pub3
7. Wandt H, Schäfer-Eckart K, Greinacher A. Platelet transfusion in hematology, oncology and surgery. *Dtsch Arztebl Int* (2014) 111:809–15. doi: 10.3238/arztebl.2014.0809
8. Katus MC, Szczepiorkowski ZM, Dumont LJ, Dunbar NM. Safety of platelet transfusion: Past, present and future. *Vox Sang* (2014) 107:103–13. doi: 10.1111/vox.12146
9. Eder AF, Moroff G. Platelet storage and adverse transfusion outcomes: Old platelets? *Transfusion* (2010) 50:2288–91. doi: 10.1111/j.1537-2995.2010.02901.x
10. Semple JW, Rebetz J, Kapur R. Transfusion-Associated Circulatory Overload and Transfusion-Related Acute Lung Injury. *Blood Rev* (2019) 33:767–79. doi: 10.1016/j.hoc.2019.05.003
11. Muszynski JA, Spinella PC, Cholette JM, Acker JP, Hall MW, Juffermans NP, et al. Transfusion-related immunomodulation: review of the literature and implications for pediatric critical illness. *Transfusion* (2017) 57:195–206. doi: 10.1111/trf.13855
12. Sut C, Tariket S, Aubron C, Aloui C, Hamzeh-Cognasse H, Berthelot P, et al. The non-hemostatic aspects of transfused platelets. *Front Med* (2018) 5:42. doi: 10.3389/fmed.2018.00042
13. Saris A, Peyron I, van der Meer PF, Stuge TB, Zwaginga JJ, van Ham SM, et al. Storage-induced platelet apoptosis is a potential risk factor for alloimmunization upon platelet transfusion. *Front Immunol* (2018) 9:1251. doi: 10.3389/fimmu.2018.01251
14. Blumberg N, Heal JM. Effects of transfusion on immune function. Cancer recurrence and infection. *Arch Pathol Lab Med* (1994) 118:371–9.
15. Heiss MM, Mempel W, Delanoff C, Jauch KW, Gabka C, Mempel M, et al. Blood transfusion-modulated tumor recurrence: first results of a randomized study of autologous versus allogeneic blood transfusion in colorectal cancer surgery. *J Clin Oncol* (1994) 12:1859–67. doi: 10.1200/JCO.1994.12.9.1859
16. Jensen LS, Kissmeyer-Nielsen P, Wolff B, Qvist N. Randomised comparison of leucocyte-depleted versus buffy-coat-poor blood transfusion and complications after colorectal surgery. *Lancet (London England)* (1996) 348:841–5. doi: 10.1016/S0140-6736(96)06168-5
17. Vamvakas EC, Blajchman MA. Transfusion-related immunomodulation (TRIM): An update. *Blood Rev* (2007) 21:327–48. doi: 10.1016/j.blre.2007.07.003
18. Aslam R, Speck ER, Kim M, Freedman J, Semple JW. Transfusion-related immunomodulation by platelets is dependent on their expression of MHC Class I molecules and is independent of white cells. *Transfusion* (2008) 48:1778–86. doi: 10.1111/j.1537-2995.2008.01791.x
19. Geiger TL. Transfusion-associated immune modulation: a reason to TRIM platelet transfusions? *Transfusion* (2008) 48:1772–3. doi: 10.1111/j.1537-2995.2008.01860.x
20. Nelson KA, Aldea GS, Warner P, Latchman Y, Gunasekera D, Tamir A, et al. Transfusion-related immunomodulation: gamma irradiation alters the effects of leukoreduction on alloimmunization. *Transfusion* (2019) 59:3396–404. doi: 10.1111/trf.15555
21. Frojmovic MM, Milton JG. Human platelet size, shape, and related functions in health and disease. *Physiol Rev* (1982) 62:185–261. doi: 10.1152/physrev.1982.62.1.185
22. Blair P, Flaumenhaft R. Platelet α–granules: Basic biology and clinical correlates. *Blood Rev* (2009) 23:177–89. doi: 10.1016/j.blre.2009.04.001.Platelet
23. Cognasse F, Nguyen KA, Damien P, McNicol A, Pozzetto B, Hamzeh-Cognasse H, et al. The inflammatory role of platelets via their TLRs and Siglec receptors. *Front Immunol* (2015) 6:83. doi: 10.3389/fimmu.2015.00083
24. Semple JW, Italiano JE, Freedman J. Platelets and the immune continuum. *Nat Rev Immunol* (2011) 11:264–74. doi: 10.1038/nri2956
25. Duerschmied D, Bode C, Ahrens I. Immune functions of platelets. *Thromb Haemost* (2014) 112:678–91. doi: 10.1160/TH14-02-0146
26. Koupenova M, Corkrey HA, Vitseva O, Manni G, Pang CJ, Clancy L, et al. The role of platelets in mediating a response to human influenza infection. *Nat Commun* (2019) 10:1780. doi: 10.1038/s41467-019-09607-x
27. Elzey BD, Tian J, Jensen RJ, Swanson AK, Lees JR, Lentz SR, et al. Platelet-mediated modulation of adaptive immunity: a communication link between innate and adaptive immune compartments. *Immunity* (2003) 28:555–60. doi: 10.1016/j.smim.2016.10.008

28. Elzey BD, Grant JF, Sinn HW, Nieswandt B, Waldschmidt TJ, Ratliff TL. Cooperation between platelet-derived CD154 and CD4+ T cells for enhanced germinal center formation. *J Leukoc Biol* (2005) 78:80–4. doi: 10.1189/jlb.1104669
29. Rachidi S, Metelli A, Riesenberg B, Wu BX, Nelson MH, Wallace C, et al. Platelets subvert T cell immunity against cancer via GARP-TGF axis. *Sci Immunol* (2017) 2:7911. doi: 10.1126/sciimmunol.aai7911
30. Kapur R, Zufferey A, Boilard E, Semple JW. Nouvelle Cuisine: Platelets Served with Inflammation. *J Immunol* (2015) 194:5579–87. doi: 10.4049/jimmunol.1500259
31. Stolla M, Refaai MA, Heal JM, Spinelli SL, Garraud O, Phipps RP, et al. Platelet transfusion - The new immunology of an old therapy. *Front Immunol* (2015) 6:28. doi: 10.3389/fimmu.2015.00028
32. Collin M, Bigley V. Human dendritic cell subsets: an update. *Immunology* (2018) 154:3–20. doi: 10.1111/imm.12888
33. Hagihara M, Higuchi A, Tamura N, Ueda Y, Hirabayashi K, Ikeda Y, et al. Platelets, after Exposure to a High Shear Stress, Induce IL-10-Producing, Mature Dendritic Cells In Vitro. *J Immunol* (2004) 172:5297–303. doi: 10.4049/jimmunol.172.9.5297
34. Kissel K, Berber S, Nockher A, Santoso S, Bein G, Hackstein H. Human platelets target dendritic cell differentiation and production of proinflammatory cytokines. *Transfusion* (2006) 46:818–27. doi: 10.1111/j.1537-2995.2006.00802.x
35. Singh MV, Suwunnakorn S, Simpson SR, Weber EA, Singh VB, Kalinski P, et al. Monocytes complexed to platelets differentiate into functionally deficient dendritic cells. *J Leukoc Biol* (2020) 2020:1–14. doi: 10.1002/JLB.3A0620-460RR
36. Ki KK, Faddy HM, Flower RL, Dean MM. Platelet concentrates modulate myeloid dendritic cell immune responses. *Platelets* (2018) 29:373–82. doi: 10.1080/09537104.2017.1306045
37. Perros AJ, Christensen AM, Flower RL, Dean MM. Soluble Mediators in Platelet Concentrates Modulate Dendritic Cell Inflammatory Responses in an Experimental Model of Transfusion. *J Interf Cytokine Res* (2015) 35:821–30. doi: 10.1089/jir.2015.0029
38. Sadallah S, Eken C, Martin PJ, Schifferli JA. Microparticles (Ectosomes) Shed by Stored Human Platelets Downregulate Macrophages and Modify the Development of Dendritic Cells. *J Immunol* (2011) 186:6543–52. doi: 10.4049/jimmunol.1002788
39. Ki KK, Johnson L, Faddy HM, Flower RL, Marks DC, Dean MM. Immunomodulatory effect of cryopreserved platelets: altered BDCA3+ dendritic cell maturation and activation in vitro. *Transfusion* (2017) 57:2878–87. doi: 10.1111/trf.14320
40. Czapiga M, Kirk AD, Lekstrom-Himes J. Platelets deliver costimulatory signals to antigen-presenting cells: A potential bridge between injury and immune activation. *Exp Hematol* (2004) 32:135–9. doi: 10.1016/j.exphem.2003.11.004
41. Hamzeh-cognasse H, Cognasse F, Palle S, Chavarin P, Olivier T, Delézay O, et al. Direct contact of platelets and their released products exert different effects on human dendritic cell maturation. *BMC Immunol* (2008) 15:1471–2172. doi: 10.1186/1471-2172-9-54
42. Nguyen XF, Müller-Berghaus J, Kälsch T, Schadendorf D, Borggrefe M, Klüter H. Differentiation of monocyte-derived dendritic cells under the influence of platelets. *Cytotherapy* (2008) 10:720–9. doi: 10.1080/14653240802378912
43. Tešić N, Pekle Simonič I, Roškar K, Rožman P, Švajger U. Dendritic Cells Generated in the Presence of Platelet Lysate Have a Reduced Type 1 Polarization Capacity. *Immunol Invest* (2019) 0139:215–31. doi: 10.1080/08820139.2019.1624768
44. ten Brinke A, Karsten ML, Dieker MC, Zwaginga JJ, van Ham SM. The clinical grade maturation cocktail monophosphoryl lipid A plus IFNγ generates monocyte-derived dendritic cells with the capacity to migrate and induce Th1 polarization. *Vaccine* (2007) 25:7145–52. doi: 10.1016/j.vaccine.2007.07.031
45. Zaal A, Dieker M, Oudenampsen M, Turksma AW, Lissenberg-Thunnissen SN, Wouters D, et al. Anaphylatoxin C5a regulates 6-Sulfo-LacNAc dendritic cell function in human through crosstalk with toll-like receptor-induced CREB signaling. *Front Immunol* (2017) 8:818. doi: 10.3389/fimmu.2017.00818
46. Blakytny R, Ludlow A, Martin GEM, Ireland G, Lund LR, Ferguson MWJ, et al. Latent TGF-beta1 activation by platelets. *J Cell Physiol* (2004) 199:67–76. doi: 10.1002/jcp.10454
47. Esebanmen GE, Langridge WHR. The role of TGF-beta signaling in dendritic cell tolerance. *Immunol Res* (2017) 65:987–94. doi: 10.1007/s12026-017-8944-9
48. Travis MA, Sheppard D. TGF-β Activation and Function in Immunity. *Annu Rev Immunol* (2014) 32:51–82. doi: 10.1146/annurev-immunol-032713-120257
49. Strobl H, Knapp W. TGF-β1 regulation of dendritic cells. *Microbes Infect* (1999) 1:1283–90. doi: 10.1016/S1286-4579(99)00256-7
50. Ramalingam R, Larmonier CB, Thurston RD, Midura-Kiela MT, Zheng SG, Ghishan FK, et al. Dendritic Cell-Specific Disruption of TGF-β Receptor II Leads to Altered Regulatory T Cell Phenotype and Spontaneous Multiorgan Autoimmunity. *J Immunol* (2012) 189:3878–93. doi: 10.4049/jimmunol.1201029
51. Riesenberg BP, Ansa-Addo EA, Gutierrez J, Timmers CD, Liu B, Li Z. Cutting Edge: Targeting Thrombocytes to Rewire Anticancer Immunity in the Tumor Microenvironment and Potentiate Efficacy of PD-1 Blockade. *J Immunol* (2019) 203:1105–10. doi: 10.4049/jimmunol.1900594
52. Calzetti F, Tamassia N, Micheletti A, Finotti G, Bianchetto-Aguilera F, Cassatella MA. Human dendritic cell subset 4 (DC4) correlates to a subset of CD14dim/–CD16++ monocytes. *J Allergy Clin Immunol* (2018) 141:2276–2279.e3. doi: 10.1016/j.jaci.2017.12.988
53. Ng MSY, Tung J-P, Fraser JF. Platelet Storage Lesions: What More Do We Know Now? *Transfus Med Rev* (2018) 32:144–54. doi: 10.1016/j.tmrv.2018.04.001
54. Langer HF, Daub K, Braun G, Schönberger T, May AE, Schaller M, et al. Platelets recruit human dendritic cells via Mac-1/JAM-C interaction and modulate dendritic cell function in vitro. *Arterioscler Thromb Vasc Biol* (2007) 27:1463–70. doi: 10.1161/ATVBAHA.107.141515
55. Maître B, Mangin PH, Eckly A, Heim V, Cazenave JP, Lanza F, et al. Immature myeloid dendritic cells capture and remove activated platelets from preformed aggregates. *J Thromb Haemost* (2010) 8:2262–72. doi: 10.1111/j.1538-7836.2010.03983.x
56. Villadangos JA, Heath WR. Life cycle, migration and antigen presenting functions of spleen and lymph node dendritic cells: limitations of the Langerhans cells paradigm. *Semin Immunol* (2005) 17:262–72. doi: 10.1016/j.smim.2005.05.015
57. Kolanowski STHM, Dieker MC, Lissenberg-thunnissen SN, Van Schijndel GMW, Van Ham SM. TLR4-mediated pro-inflammatory dendritic cell differentiation in humans requires the combined action of MyD88 and TRIF. *Innate Immun* (2013) 0:1–8. doi: 10.1177/1753425913498626
58. Zimmer N, Krebs FK, Zimmer S, Mitzel-rink H, Kumm EJ, Jurk K, et al. Platelet-Derived GARP Induces Peripheral Regulatory T Cells — Potential Impact on T Cell Suppression in Patients with. *Cancers (Basel)* (2020) 12:3653. doi: 10.3390/cancers12123653
59. Ceroi A, Delettre FA, Marotel C, Gauthier T, Asgarova A, Biichlé S, et al. The anti-inflammatory effects of platelet-derived microparticles in human plasmacytoid dendritic cells involve liver X receptor activation. *Haematologica* (2016) 101:72–6. doi: 10.3324/haematol.2015.135459
60. Sprague DL, Elzey BD, Crist SA, Waldschmidt TJ, Jensen RJ, Ratliff TL. Platelet-mediated modulation of adaptive immunity: Unique delivery of CD154 signal by platelet-derived membrane vesicles. *Blood* (2008) 111:5028–36. doi: 10.1182/blood-2007-06-097410
61. Nishat S, Wuescher LM, Worth RG. Platelets enhance dendritic cell responses against Staphylococcus aureus through CD40-CD40L. *Infect Immun* (2018) 86:00186–18. doi: 10.1128/IAI.00186-18
62. Xia C-Q, Kao K-J. Effect of CXC chemokine platelet factor 4 on differentiation and function of monocyte-derived dendritic cells. *Int Immunol* (2003) 15:1007–15. doi: 10.1093/intimm/dxg100
63. Silva-Cardoso SC, Tao W, Malvar Fernandez B, Boes M, Radstake TRDJ, Pandit A. CXCL4 suppresses tolerogenic immune signature of monocyte-derived dendritic cells. *Eur J Immunol* (2020) 50:1–9. doi: 10.1002/eji.201948341
64. Silva-Cardoso SC, Affandi AJ, Spel L, Cossu M, van Roon JAG, Boes M, et al. CXCL4 Exposure Potentiates TLR-Driven Polarization of Human Monocyte-Derived Dendritic Cells and Increases Stimulation of T Cells. *J Immunol* (2017) 199:253–62. doi: 10.4049/jimmunol.1602020
65. Ahmad F, Döbel T, Schmitz M, Schäkel K. Current Concepts on 6-sulfo LacNAc Expressing Monocytes (slanMo). *Front Immunol* (2019) 10:948. doi: 10.3389/fimmu.2019.00948

66. Baran W, Oehrl S, Ahmad F, Döbel T, Alt C, Buske-Kirschbaum A, et al. Phenotype, Function, and Mobilization of 6-Sulfo LacNAc-Expressing Monocytes in Atopic Dermatitis. *Front Immunol* (2018) 9:1352:1352. doi: 10.3389/fimmu.2018.01352

Conflict of Interest: The authors declare that the research was conducted in the absence of any commercial or financial relationships that could be construed as a potential conflict of interest.

frontiers in Immunology

ORIGINAL RESEARCH
published: 11 November 2021
doi: 10.3389/fimmu.2021.772859

Platelet-Mediated NET Release Amplifies Coagulopathy and Drives Lung Pathology During Severe Influenza Infection

Seok-Joo Kim[1†], Agostina Carestia[1†], Braedon McDonald[2], Amanda Z. Zucoloto[1], Heidi Grosjean[1], Rachelle P. Davis[1], Madison Turk[1], Victor Naumenko[1], Silvio Antoniak[3], Nigel Mackman[4], Mohamed Sarjoon Abdul-Cader[5], Mohamed Faizal Abdul-Careem[5], Morley D. Hollenberg[6] and Craig N. Jenne[1]*

[1] Department of Microbiology, Immunology, and Infectious Diseases, University of Calgary, Calgary, AB, Canada, [2] Department of Critical Care Medicine, University of Calgary, Calgary, AB, Canada, [3] UNC Blood Research Center, Department of Pathology and Laboratory Medicine, University of North Carolina at Chapel Hill, Chapel Hill, NC, United States, [4] UNC Blood Research Center, Department of Medicine, University of North Carolina at Chapel Hill, Chapel Hill, NC, United States, [5] Faculty of Veterinary Medicine, University of Calgary, Calgary, AB, Canada, [6] Department of Physiology and Pharmacology, University of Calgary, Calgary, AB, Canada

OPEN ACCESS

Edited by:
Fabrice Cognasse, INSERM U1059 SAnté INgéniérie BIOlogie (INSERM), France

Reviewed by:
Coen Maas, University Medical Center Utrecht, Netherlands
Jan Rossaint, University of Münster, Germany

***Correspondence:**
Craig N. Jenne
cnjenne@ucalgary.ca

[†]These authors have contributed equally to this work and share first authorship

Specialty section:
This article was submitted to Inflammation, a section of the journal Frontiers in Immunology

Received: 08 September 2021
Accepted: 26 October 2021
Published: 11 November 2021

Citation:
Kim S-J, Carestia A, McDonald B, Zucoloto AZ, Grosjean H, Davis RP, Turk M, Naumenko V, Antoniak S, Mackman N, Abdul-Cader MS, Abdul-Careem MF, Hollenberg MD and Jenne CN (2021) Platelet-Mediated NET Release Amplifies Coagulopathy and Drives Lung Pathology During Severe Influenza Infection. Front. Immunol. 12:772859. doi: 10.3389/fimmu.2021.772859

The influenza A virus (IAV) causes a respiratory tract infection with approximately 10% of the population infected by the virus each year. Severe IAV infection is characterized by excessive inflammation and tissue pathology in the lungs. Platelet and neutrophil recruitment to the lung are involved in the pathogenesis of IAV, but the specific mechanisms involved have not been clarified. Using confocal intravital microscopy in a mouse model of IAV infection, we observed profound neutrophil recruitment, platelet aggregation, neutrophil extracellular trap (NET) production and thrombin activation within the lung microvasculature *in vivo*. Importantly, deficiency or antagonism of the protease-activated receptor 4 (PAR4) reduced platelet aggregation, NET production, and neutrophil recruitment. Critically, inhibition of thrombin or PAR4 protected mice from virus-induced lung tissue damage and edema. Together, these data imply thrombin-stimulated platelets play a critical role in the activation/recruitment of neutrophils, NET release and directly contribute to IAV pathogenesis in the lung.

Keywords: influenza A virus, platelets, PAR4, thrombin, neutrophils, NETs, intravital microscopy (IVM)

INTRODUCTION

Influenza is a common respiratory tract infection and a leading cause of death from infectious disease in United States (1). Influenza A virus (IAV) caused 50-100 million deaths during pandemic of 1918-1919, and continues to infect 10-20% of the population each year (2). Although adaptive immunity is essential for IAV clearance, innate immune cells also play key roles in viral control and IAV pathogenesis (3, 4). Critically, an overly robust innate immune response can lead to enhanced tissue damage, predisposing the patient to secondary infections (5, 6). Thus, though important for

pathogen clearance, innate immunity also has the capacity to cause collateral damage and subsequent organ dysfunction if not properly regulated.

Much of the host inflammatory response is mediated by neutrophils, cells that are rapidly recruited to the lung in response to infection (7–9), representing one of the first, non-resident, immune responders against pathogens (10). Neutrophils mediate host-defense against a wide variety of invading microorganisms, possessing a broad arsenal of defense strategies, including release of neutrophil extracellular traps (NETs); highly charged mixtures of decondensed DNA, nuclear, and granular proteins. These structures entrap and kill pathogens and can neutralize viral particles (11).

During IAV infection, neutrophils have been shown to limit viral replication and disease progression (12, 13). However, this local increase in neutrophil recruitment may not be entirely beneficial as it can also inflict damage, exacerbating pulmonary inflammation through excessive NET release (14, 15). Platelets also play a significant role in host defense to infection by expressing immune receptors and immune effectors upon activation (16). During inflammation, platelets recognize, sequester and kill pathogens directly (17, 18), and regulate immune cell recruitment and activation (19). Platelet-neutrophil interaction is often required for cellular recruitment to infection sites, and studies have demonstrated that this interaction is crucial for NET release (20).

Further linking infection and platelets, IAV infection leads to increased tissue factor expression, thrombin generation and activation of the coagulation cascade (21). Importantly, dysregulation of coagulation has been associated with increased morbidity and mortality in other viral lung infections. Early data from the COVID-19 pandemic has indicated evidence of coagulopathy in the most severely affected patients and this systemic activation of coagulation is associated with end-organ damage and subsequent death (22–24). These observations highlight the need to understand the interplay between infection, inflammation, and coagulation.

Here, using high-resolution confocal intravital microscopy (IVM), we demonstrate that collaboration between thrombin, platelets, and NETs leads to enhanced inflammation and tissue damage during IAV infection. Using a fluorescent enzyme substrate and a PAR4 inhibitor, we demonstrate that thrombin, *via* platelet activation, is a principal driver of IAV-mediated lung pathogenesis.

MATERIALS AND METHODS

Mice and Viruses

C57Bl/6 mice were purchased from Jackson Laboratories (Bar Harbor, ME, USA). CD41-/- (CD41YFP/YFP, yellow fluorescent protein [YFP] sequence knocked into the CD41 locus) mice were on a C57BL/6 background and were provided by Dr. K. McNagny (University of British Columbia). PAR4-/- mice on the C57Bl/6 background were generated as previously described (25). All mice were 7-10 weeks old and maintained in a specific pathogen-free environment at the University of Calgary. Influenza A virus strain A/PR/8/34 (PR8, H1N1) was grown in 10-day embryonated hen's eggs by standard procedures and titrated on Madin-Darby canine kidney (MDCK) cells as described (26). All experimental animal protocols were approved by the University of Calgary Animal Care Committee in compliance with guidelines from the Canadian Council for Animal Care (Protocol AC18-0050).

Infection and Treatment of Mice

Under isoflurane anesthesia, mice were challenged with intranasal (i.n.) PR8 infection (250 PFU unless otherwise indicated). Mice were weighed daily and assessed for visual signs of clinical disease. Animals that lost 25% of their original weight were removed from the study and euthanized. At day 1, day 3 or day 5 post-infection, IVM was conducted.

In vivo blockade of CD18 was achieved by intravenous (i.v.) administration of 100 μg of anti-CD18 (clone GAME-46, eBioscience, San Diego, CA, USA) 1 h prior to IAV infection. For *in vivo* PAR4 inhibition, 20 mg/kg of an antagonist peptide, TcY-NH2 (Tocris Bioscience, Bristol, UK) dissolved in 25 mM sterile HEPES, was administered intraperitoneally (i.p.) 20 min prior to IAV infection. Thrombin inhibitor, argatroban (Sigma; 10 mg/kg), was dissolved in DMSO and 100 μl weas delivered i.p. once 30 min before IAV infection or daily starting at day 3 of infection. DNase I (Roche; 2000 international units) was resuspended in water as per manufacturer instructions and delivered i.v. immediately before IAV infection and once a day for 4 days.

Preparation of the Mouse Lung for Intravital Microscope

For microscopic visualization, we used a modification of the methodology proposed by Looney et al. (27). In brief, mice were anesthetized with ketamine (200 μg/kg; Bayer Animal Health, Toronto, Canada) and xylaxine (10 mg/kg; Bimeda-MTC, Cambridge, Canada) i.p. and the jugular vein was cannulated to permit the injection of fluorescently labeled antibodies and for the maintenance of anesthetic. A tracheotomy was performed and PE90 tubing was inserted into the incision site and secured with a silk suture. Following i.t. catheterization, mice were mechanically ventilated at 150 breaths/min with 120 μl of tidal volume using an Inspira ASV (Harvard Apparatus, Holliston, MA, USA). Mice were placed in the right lateral decubitus position, and the lung left lobe was exposed through removal of the overlying skin, fat, and sections of two to three anterior ribs. A thoracic suction window attached to a micromanipulator on the microscope stage was then placed into position and 20–25 mm Hg of suction was applied (Amvex Corporation, Richmond Hill, Canada) to gently immobilize the lung. The water-immersion objective (HC FLUOTAR L 25x/0.95 W VISIR) of resonant-scanning confocal microscope (TCS-SP8, Leica Microsystems, Concord, Canada) was lowered into place over the thoracic suction window. This microscope platform is equipped with multiple excitation lasers (405 nm, 488 nm, 552 nm, 647 nm), a tunable digital emission filter and 5 independent

detectors [2 photomultiplier tubes (PMT), 3 hybrid HyD SP GaAsP detectors (HyD)] allowing for simultaneous imaging of up to 5 independent channels (Davis et al., 2020). Typical microscope settings were: for the 405 nm excitation laser (33.8% power), emission filter scanned from 410 to 468 nm (detector PMT1, gain 814.4V); for the 488 nm excitation laser (28% power), emission filter scanned from 501 to 544 nm (detector HyD2,gain 18.8%) and from 571 to 586 (detector HyD4, gain 35%); and for the 638 nm excitation laser (24.9% power), emission filter scanned from 656 to 696 nm (detector HyD5, gain 16.5%).

Antibodies and Fluorescent Probes

For IVM, Brilliant Violet 421-conjugated anti-Ly6G (neutrophils; clone 1A8, BD Biosciences, San Diego, CA, USA, 1.6 μg), AlexaFluor 647- or PE-conjugated anti-CD49b (platelets; clone HMα2, BioLegend, San Diego, CA, USA, 1.6 μg), PE-conjugated anti-CD31 (endothelium; clone 390, Biolegend, 0.8 μg), goat anti-mouse histone H2Ax (clone M20, Santa Cruz Biotechnology, USA, 2 μg) was conjugated to AlexaFluor 555 and goat–anti-mouse neutrophil elastase (M18, 2 μg) was conjugated to AlexaFluor 647 using a labelling kit as per the manufacturer's instructions (Life technologies, Carlsbad, CA, USA). Quantities and clones of antibodies used to label neutrophils and platelets have been previously optimized and demonstrated to have minimal impact on cellular recruitment and or clearance through mechanisms such as antibody-dependent cellular cytotoxicity (28, 29). Thrombin was visualized with 5-FAM/QXL® 520 FRET substrate (SensoLyte® 520 Thrombin Activity Assay Kit, AnaSpec, Inc., Fremont, CA, USA). FITC- or AF647-albumin was used to delineate the vasculature.

Analysis of Resonant-Scanning Confocal Microscope-Acquired Images

In most experiments, anti-CD31 or albumin as a contrast agent was used to landmark lung structures and set imaging depth. Total numbers of neutrophils were counted for of 3-6 FOV per animal and averaged. Quantification of NETs, platelet aggregation and thrombin activity involved measurement of the total area of staining for each marker per FOV in a minimum of 3 FOV per animal. Detail analysis parameters were as described previously (30, 31). The number of platelet aggregates ≥10, 25, 50, or 100 μm^2 were counted using the Analyze Particles function within ImageJ, as previously described (28).

Immunohistochemistry

Infected mice were euthanized with CO_2, lungs removed and immediately frozen in optimal cutting temperature (OCT) media. OCT-embedded frozen tissues were sectioned (7 μm), fixed in PFA 4%, blocked with PBS containing 1% donkey serum and 3% BSA, permeabilized with PBS/Triton 0.01% and stained with fluorescently-conjugated antibodies.

Bronchoalveolar Lavage Fluid (BALF) and Lung Edema

Following euthanasia, a catheter was inserted into the trachea. BALF was collected by five washes of 1 mL of PBS containing 5mM EDTA and total cell numbers was determined using a hemocytometer. Lung edema was measured in separate animals. Lungs were removed, weighed, dried for 72 h at 65°C, and then reweighed in order to obtain the wet-to-dry tissue weight ratio as previously described (32).

Myeloperoxidase (MPO) Activity

Lungs were homogenized in detergent (0.5% hexadecyltrimethylammonium bromide buffer), and supernatant was reacted with hydrogen peroxide and a hydrogen donor, O-dianisidine dihydrochloride. Reaction was measured over time *via* a colored compound development using a spectrophotometer to determine MPO content (450 nm, 25°C; SpectraMax Plus 384, Molecular Devices, Sunnyvale, CA, USA).

Flow Cytometry Analysis

Lung tissues were harvested and minced with scissors in an ice-cold HEPES solution and then were digested with collagenase D (2 mg/mL) and DNase (80 U/ml) for 30 min in 37°C. After the digestion, tissues were passed through a 70-μm filter and washed with HEPES supplemented with 2% FBS. Following centrifugation, erythrocytes were lysed with hypotonic buffer and the remaining leukocytes were washed in FACS buffer (PBS +5% fetal bovine serum+0.5 mM EDTA). Cells were blocked with an FcR-blocking antibody (clone 2.4g2) and stained for neutrophils (Ly6G), platelets (CD41), and markers of neutrophil activation (CD11b, clone M1/70 and PSGL-1, clone 2PH1) for 30 min on ice. The cells were washed and analyzed using an Attune NxT flowcytometer (Thermo Fisher Scientific).

Quantification of Extracellular DNA

Complexes of DNA bound to histones were measured in plasma and BALF using commercially available cell death detection ELISAPLUS kit according to the manufacturer's instructions. The calibration curve was constructed using a standard of nucleosomal DNA of a known concentration.

Platelet Counts

Platelets were counted manually using a hemocytometer.

Viral Load Assessment

MDCK cells were cultured in DMEM (10% FBS,1% Penicillin-Streptomycin) until confluent, seeded in 12-well plates and incubated at 37°C and 5% CO2 for 24 hours to generate a monolayer. Lungs were harvested 5 days post-infection, homogenized and used to produce ten-fold serial dilutions in PBS. MDCK monolayers were infected with 50μL of each dilution (1h at 37°C, 5% CO2) followed by addition of agar overlay. Plates were incubated (37°C, 5% CO2 48 h), washed and plaques visualized by staining with crystal violet for 15 minutes. Plaque-forming units (PFUs)/mL were calculated and converted into a log10 scale.

Statistical Analysis

All results are presented as means ± SEM. Overall significance was examined by one-way analysis of variance with post-hoc Bonferroni test (for parametric data) or a Kruskal-Wallis with

post-hoc Dunn's test (for nonparametric data). Differences between the groups were considered statistically significant at a $P < 0.05$.

RESULTS

IAV Induces Platelet Aggregation, Neutrophil Recruitment, and Inflammation in the Lung

Previous reports indicated activation and aggregation of platelets within the lung vasculature worsen the severity of lung injury during viral infection (33–35). Moreover, platelets potentiate leukocyte recruitment to sites of infection (36) and neutrophils interact with damaged endothelium in areas rich in platelet aggregates (37). Direct interaction between platelets and neutrophils results in further neutrophil recruitment and activation (38). To better understand these dynamic cell-cell interactions within the intact lung, we utilized IVM (**Supplemental Figure 1**) to study a mouse model of severe IAV infection. Mice were challenged with 250 PFU IAV A/PR/8/34 (H1N1) i.n. and studied 5 days post-infection. This model of IAV infection results in all animals reaching the humane weight-loss threshold of 25% by day 6-7 post-infection. Although some impact on cell mobility may be expected following surgery to visualize and stabilize the lung, using IVM, we observed a marked increase in platelet accumulation and the formation of large platelet aggregates within the lung vasculature following IAV infection as compared to control animals (**Figure 1Ai**). Quantification of aggregates demonstrated a significant increase in both small (10 and 25 μm^2) and large platelet aggregates (50 and 100 μm^2) following IAV infection (**Figure 1Aii**). Moreover, IAV infected mice have significantly fewer circulating platelets (**Figure 1B**). Additionally, IAV induced profound neutrophil recruitment to the lung (**Figure 1C** and **Supplemental Video 1**). These IVM findings were confirmed by flow cytometry and by the detection of elevated MPO levels in the lungs of IAV infected animals (**Figures 1D, E**). Analysis of BALF showed IAV increased the number of cells within the bronchoalveolar space (**Figure 1F**). Finally, IAV induced a significant increase in wet-to-dry weight ratios of the lung (**Figure 1G**), a validated measure of overall tissue fluids (32). These results show IAV infection induces a rapid platelet and neutrophil recruitment to the lungs and subsequent pulmonary edema.

Platelets recruited to the infected lung were observed interacting with adherent neutrophils (**Figure 1H**) forming large, dynamic aggregates (**Supplemental Video 2**). By introducing a fluorescent contrast agent (labeled albumin) into circulation, we demonstrated that these aggregates are in the intravascular space (**Supplemental Figure 2**). These observed neutrophil-platelet interactions were confirmed by flow cytometry (**Figure 1I**). Additionally, severe IAV infection results in significant animal weight loss over the course of infection (**Figure 1J**), demonstrating this model of IAV infection induces significant disease and inflammation in the lung that is reflective of reports following severe IAV infection of patients (13, 14). Considering that the number of pulmonary vessels can differ depending on the depth of the observation region, neutrophil counts and platelet aggregates were analyzed by vessel area, and similar results were obtained (**Supplemental Figure 3**).

Neutrophil Accumulation and Formation of Neutrophil-Platelet Aggregates Are Mediated by Integrins

Blockade of adhesion molecules, such as CD18 (β2 integrin), dramatically reduces platelet recruitment to the inflamed liver (28). Moreover, CD18 has been implicated in the binding of platelets to neutrophils (20), and this binding subsequently triggers neutrophil activation and migration (39). The integrin CD41/CD61 (GPIIb/IIIa), which is found solely on platelets, is responsible for the formation of fibrinogen bridges among platelets, facilitating platelet cohesion, aggregation, and subsequent thrombus growth (40, 41).

Based on these studies, we interrogated the role of these integrins in neutrophil and platelet accumulation in the lungs following viral challenge. A significant reduction in neutrophil recruitment and platelet aggregation in the lung microvasculature was observed following IAV infection in mice pretreated with an anti-CD18 blocking antibody (**Figures 2A–C**, **Supplemental Video 3**), a finding that was confirmed by flow cytometric analysis of the lung (**Supplemental Figure 4A**). Analysis of cellular behavior demonstrated that IAV infected mice have increased neutrophil diameter and decreased roundness, key markers of cellular activation (**Supplemental Figures 4B, C**). These results were confirmed by an elevated expression of CD11b, but interestingly not PSGL-1, by neutrophils isolated from the blood, lung and BALF (**Supplemental Figure 4D**). Although blockade of CD18 reduced overall neutrophil recruitment, no impact on cellular diameter (lengthening of the neutrophil) or cellular roundness (more pseudopod formation; **Supplemental Figures 4B, C**) was observed. Moreover, the increased neutrophil crawling observed following IAV infection was diminished by CD18 blockade (**Supplemental Figure 4E**) indicating CD18 was required for neutrophil motility but not for neutrophil activation. Targeting platelet-expressed integrins, CD41-deficient mice had less platelet accumulation in the lung after IAV infection than did wild-type mice (**Figure 2C**). Interestingly, we also observed reduced neutrophil recruitment to the lung in CD41-deficient mice following IAV infection (**Figure 2B**).

Although neutrophil recruitment often precedes platelet aggregation (28, 30), other studies have demonstrated a role for platelets in facilitating neutrophil recruitment to various vascular beds (42, 43). The phenotype observed in the CD41-deficient animals suggested a significant proportion of neutrophil recruitment to the lung following viral challenge is mediated by platelets. Moreover, CD41-deficiency also reduced both neutrophil activation and crawling (**Supplemental Figures 4B, C, E**) suggesting platelet aggregation was not only critical for neutrophil recruitment but also played a role in cellular activation and motility. Concomitant with this reduced cellular

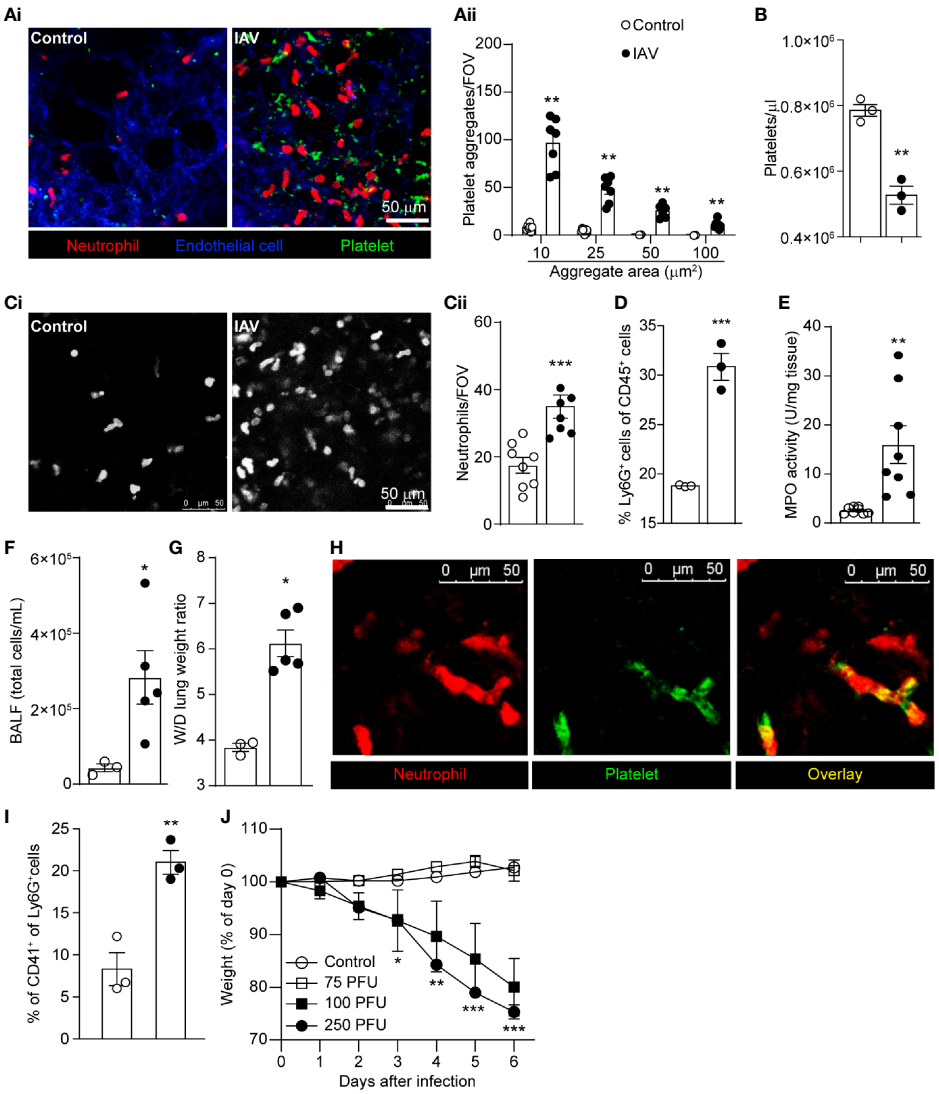

FIGURE 1 | Intranasal IAV Infection of Mice Results in Platelet Aggregation, Neutrophil Recruitment, and Lung Edema. **(Ai)** Intravital visualization of platelet and neutrophils following administration of PBS or infection with IAV in the lung vasculature (neutrophils, red; platelets, green; endothelium, blue). **(Aii)** Quantification of platelet aggregates of the indicated sizes in PBS-treated mice or IAV-challenged mice. Values are shown as mean ± SEM, n=8 per group. **(B)** Peripheral blood platelet counts in control and IAV-infected mice. **(Ci)** Imaging (neutrophils, white) and **(Cii)** quantification of neutrophil recruitment within the lung in PBS-treated mice or IAV-challenged mice. Values are shown as mean ± SEM, n=6-8 per group. **(D)** Flow cytometric quantification of the percentage of neutrophils ($Ly6G^+$ cells) in the lung. MPO activity **(E)**, BALF cell counts **(F)** and lung wet-to-dry tissue weight ratios **(G)** following IAV infection. Values are shown as mean ± SEM, n=3-8 per group. **(H)** Co-localization of neutrophil and platelet aggregates within the lung vasculature of a IAV infected animal (neutrophils, red; platelets, green). **(I)** Flow cytometric quantification of the percentage of neutrophils ($Ly6G^+$ cells) that are interacting with platelets ($CD41^+$) in the lung **(J)** Animal weight measurements following infection with indicated inoculums of IAV. *p < 0.05, **p < 0.01, ***p < 0.001 compared to the control group.

recruitment, an attenuation of weight loss after IAV infection was observed in the presence of CD18-blockade or CD41-deficiency (**Figure 2D**). This potential linkage between platelet integrins and neutrophil recruitment led us to investigate if platelet recruitment to the lung precedes neutrophil accumulation in severe IAV infection. Assessment of early cell recruitment (24h post-infection) reveals a clear and significant accumulation of platelets (**Figures 2E, F**) prior to observed increases in neutrophil numbers (**Figures 2E, G**). Furthermore, IVM and MPO assays revealed that neutrophil recruitment starts after 3 days of infection (**Figures 2G, H**). Importantly, this early role for platelets was only evident during severe IAV infection; infection with a lower inoculum of virus (25 PFU) failed to induce platelet accumulation in advance of neutrophil recruitment (**Supplemental Figure 5**).

IAV Infection Induces the Release of NETs Within the Lung Vasculature

Neutrophil-platelet interactions drive NET production in response to several viral pathogens (14, 30, 44, 45). IVM

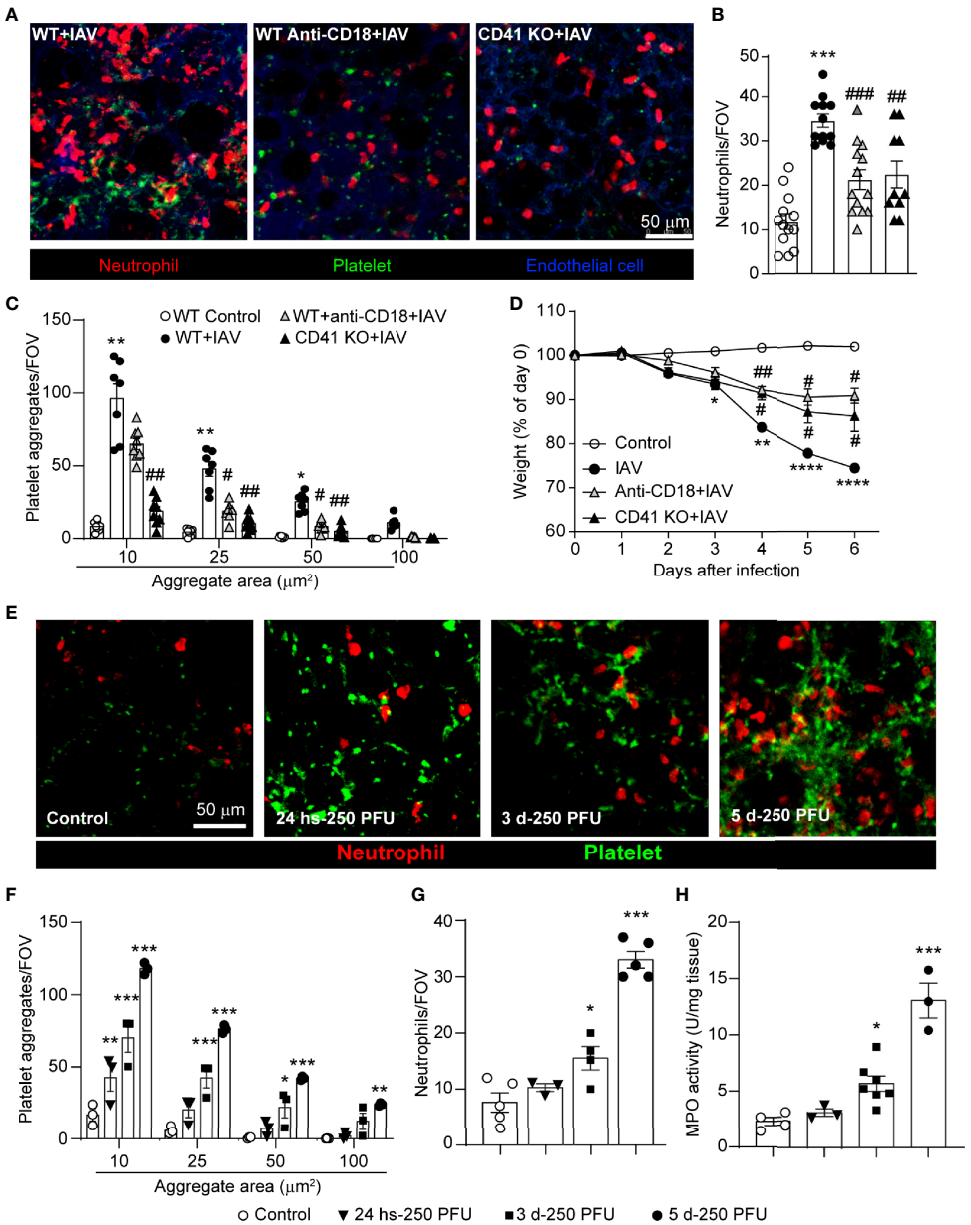

FIGURE 2 | Dynamics of Virus-Induced Neutrophil Recruitment and Platelet Accumulation in the Lungs. **(A)** Intravital visualization of neutrophils and platelet aggregation in the lung vasculature 5d-post IAV-infection in animals with anti-CD18 blocking antibody (WT Anti-CD18+IAV) or CD41 deficiency (CD41 KO+IAV) (neutrophils, red; platelets, green; endothelium, blue). Quantification of neutrophils **(B)** and platelets **(C)** within the lung as measured by IVM. Values are the mean number of neutrophils per field of view (FOV) ± SEM, n=3-5 per group. **(D)** Animal weight measurements following infection with or without integrin blockade/deficiency. Values are shown as the mean of weights normalized to day 0 ± SEM, n=3-5 per group. **(E)** IVM of neutrophil recruitment and platelet aggregation in control, 24h-post IAV infection and 3d and 5d-post IAV infection (neutrophils, red; platelets, green). **(F)** Quantification of platelet aggregates of indicated sizes **(F)** and neutrophils **(G)** at indicated times post IAV infection. **(H)** MPO activity at indicated times post IAV infection. Values are the mean number of aggregates per field of view (FOV) ± SEM, n=3-5 per group. *p < 0.05, **p < 0.01, ***p < 0.001 ****p < 0.0001 compared to the control group; $^{\#}$p < 0.05, $^{\#\#}$p < 0.01, $^{\#\#\#}$p < 0.001 compared to the IAV-infected group.

analysis identified a significant increase in extracellular histone H2Ax in the lung following IAV infection (**Figure 3A**). Analysis of plasma and BALF by ELISA confirmed the presence of elevated extracellular histone levels following IAV infection (**Supplementary Figures 6A, B**). Blockade of CD18, or deficiency in CD41, significantly inhibited extracellular histone deposition in the lung (**Figure 3A**), demonstrating a role for platelet-neutrophil interaction in the release of extracellular DNA structures in response to IAV infection. As extracellular histone may correspond to both NETs and other extracellular

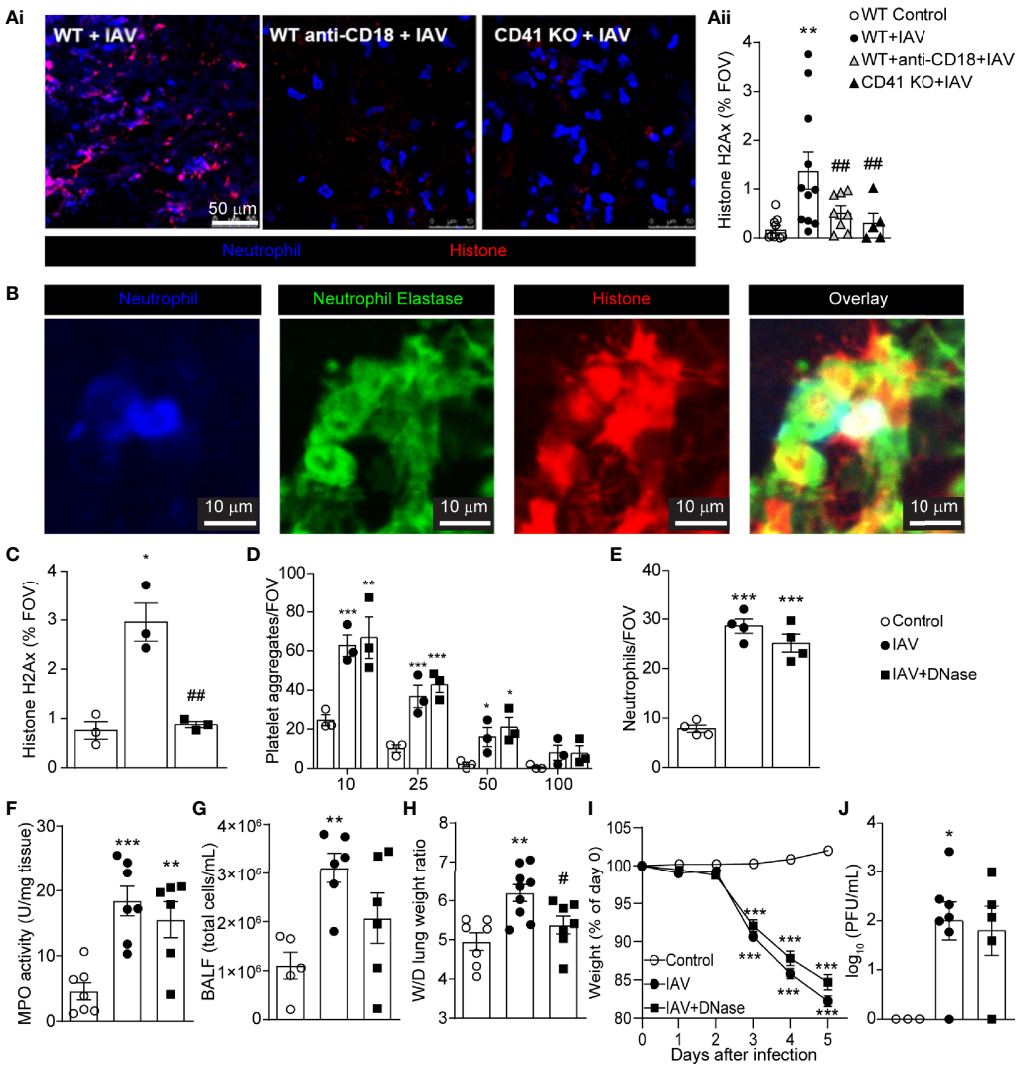

FIGURE 3 | IAV Infection Induces the Release of NETs within the Lung Vasculature. **(Ai)** IVM imaging of NETs in IAV-infected animals pretreated with anti-CD18 blocking antibody or animals deficient for CD41 (neutrophils, blue; extracellular histone, red). **(Aii)** Quantification of the area of staining of extracellular histone. Values represent staining area as a % of the FOV and are presented as the mean+/- SEM. n=5-9 per group **(B)** Representative IVM imaging of the lung vasculature 5d post-IAV infection (neutrophils, blue; neutrophil elastase, green; extracellular histone, red). Quantification of histone H2Ax **(C),** platelet aggregates of indicated sizes **(D)** and neutrophils **(E)** measured by IVM in mice treated with DNase. Quantification of lung MPO activity **(F)**, total BALF cellularity **(G)**, and lung wet-to-dry tissue weight ratios **(H)** following IAV infection of control and DNase-treated animals. Animal body mass **(I)** and lung viral loads **(J)** following IAV infection of control and DNase-treated animals. Values represent the mean +/- SEM. n = 5-9 per group. *p < 0.05, **p < 0.01, ***p < 0.001 compared to the control group. #p < 0.05, ##p < 0.01 compared to the IAV-infected group.

structures (e.g. DNA released from cell lysis), we sought to confirm if histone staining corresponded to NETs in the lung vasculature following IAV infection. Immunostaining of IAV-infected lungs reveals extensive colocalization of staining of extracellular histone and NE (**Figure 3B**), markers that when found together are hallmarks of NETs. Moreover, quantification of extracellular NE staining by IVM confirmed a significant increase in this marker within the lungs following IAV infection (**Supplementary Figure 6C**).

NETs, if produced in an uncontrolled fashion can cause damage to the vasculature and associated tissues. To determine if NET production contributed to IAV-mediated lung pathology, mice were treated with DNase, an enzyme that cleaves and clears NETs and extracellular DNA structures (**Figure 3C**) but leaves recruited neutrophils and platelets unaltered. Breakdown of NETs and/or extracellular DNA did not affect total platelet aggregates (**Figure 3D**) or neutrophil recruitment to the lung, as measured by IVM (**Figure 3E**) and MPO activity (**Figure 3F**). Removal of NETs and/or extracellular DNA did reduce BALF cellularity (**Figure 3G**) and led to a significant decrease in the wet-to-dry weight ratio of lung tissue (**Figure 3H**), suggesting NETs and/or extracellular DNA contribute to localized lung

damage. Despite this reduction in localize lung pathology, DNase treatment did not prevent animal weight loss or impact viral clearance (**Figures 3I, J**), a finding that is in agreement with an earlier study in PAD4-deficient mice (46). These results indicate that clearance of NETs and/or extracellular DNA does not change the overall outcome for the animal.

Thrombin Mediates Platelet Aggregation and NET Release

It has been shown that NETs potentiate thrombin generation and drive intravascular coagulation in liver after S. aureus infection (31). To determine if a similar process occurs in the lung following IAV infection, we utilized a quenched-fluorescence peptide substrate to visualize thrombin activity within the living animal (31). Robust intravascular thrombin activity was observed within the lung microvasculature of IAV-infected mice (**Figure 4Ai**). To confirm thrombin specificity of the peptide probe, mice were given argatroban (a thrombin inhibitor), which demonstrated significant attenuation of fluorescence intensity (**Figure 4Aii**). Although inhibition of probe activation by argatroban does not completely rule out the possibility of another protease, this observation is strongly suggestive of a role for thrombin in the host-response to IAV infection. Interestingly, pretreatment of mice with argatroban significantly reduced neutrophil recruitment, platelet aggregation and NET formation 5 days after IAV infection (**Figures 4B–D**). Cell recruitment was confirmed by measuring the cellularity of the BALF and quantifying lung MPO activity (**Figures 4E, F**). Furthermore, pretreatment with argatroban also reduced wet-to-dry weight ratios and weight loss induced by IAV (**Figures 4G, H**). Some mice were treated with vehicle, DMSO, and no effect on weight loss, MPO activity or wet-to-dry weight ratios was observed (**Supplemental Figure 7**). Importantly, inhibition of thrombin did not exacerbate infection as the viral load recovered from the lungs 5 days post-infection was not changed (**Figure 4I**). These results demonstrate thrombin activation precedes NET generation in IAV-infected lungs and potentiates platelet aggregation, neutrophil recruitment, NET production, and tissue pathology in IAV-infected lungs but does not appear to play a role in viral control. Interestingly, argatroban had no effect if administered as a therapy at the time of neutrophil recruitment and NET generation (at day 3 and 4 of infection [**Supplemental Figure 8**]).

PAR4 Contributes IAV-Induced Inflammatory Lung Tissue Damage

PAR4 is the primary thrombin receptor on mouse platelets and plays an essential role in platelet activation. Immuno-histochemistry on lung sections demonstrated an apparent increase in NET and/or extracellular DNA release (**Figure 5A**; diffuse, intravascular histone staining; arrowhead) and increased numbers of platelet aggregates in wild-type animals following IAV infection. Analysis of lungs from PAR4-deficient animals demonstrated increased staining for histone, likely reflecting the increased number of cells (and by extension nuclei) recruited to the IAV-infected lung, a reduction in diffuse NET-like staining was observed (histone remains as a punctate, nuclear stain; full arrow). As this staining was conducted on tissue sections obtained from frozen samples, we were unable to determine specifically the levels of extracellular versus intracellular (nuclear) histone but the difference in appearance (diffuse verses punctate) prompted us to investigate the possibility that PAR4 activation was needed for the production of NETs. To further explore the role of PAR4 in platelet aggregation and subsequent neutrophil activity, we administered a PAR4 peptide antagonist (trans-cinnamoyl-YPGKF-NH2 [TcY-NH2]) (47) prior to IAV infection. Pretreatment with PAR4 antagonist significantly attenuated intravascular thrombin formation following IAV infection (**Figure 5B**) indicating platelet activation, through PAR4, results in a positive feedback loop, augmenting thrombin production. In addition, pretreatment with PAR4 antagonist significantly reduced neutrophil recruitment, platelet aggregation and platelet-neutrophil interactions 5 days after IAV infection (**Figures 5C–E**, **Supplemental Video 4**). Inhibition of thrombin, or antagonism of PAR4 also reduced overall neutrophil activation and crawling (**Supplemental Figure 9**). In accordance with reduced neutrophil recruitment and platelet aggregation, NET release was also significantly diminished after PAR4 inhibitor treatment (**Figure 5F**) and PAR4 inhibition prior to IAV infection resulted in a significant reduction in MPO activity in the lung and BALF cellularity (**Figures 5G, H**).

PAR4 has been implicated in immune-mediated tissue damage, and it has been reported that PAR4 inhibition offers cytoprotection in sepsis and other inflammatory diseases (48, 49). Whereas IAV infection results in reproducible weight loss in mice, PAR4 antagonist-pretreatment significantly reduces weight loss after IAV infection (**Figure 5I**). Moreover, pretreatment with PAR4 inhibitor resulted in a reduced wet-to-dry weight ratio of lung tissue (**Figure 5J**) illustrating a role for PAR4 in lung pathology following severe IAV infection. Importantly, as observed with the inhibition of thrombin, antagonism of PAR4 had no impact on viral loads suggesting this pathway is not directly involved in pathogen clearance within the context of severe IAV infection (**Figure 5K**). These results suggest PAR4 is involved in IAV-induced inflammatory responses. Additionally, inhibition of PAR4 not only attenuates the amplification of this inflammatory response, but also limits the early steps of virus-induced pathology and prevents tissue damage in severe IAV infection.

DISCUSSION

Several studies have indicated an excessive inflammatory response to IAV infection is detrimental, worsening the severity of influenza pneumonia at multiple levels (14, 50). Uncontrolled inflammation is mediated by various cell lineages and the combination of multiple cytokines and other inflammatory mediators such as bioactive lipids. Platelets are important source of inflammatory mediators which can be rapidly released upon activation. Importantly, not only do

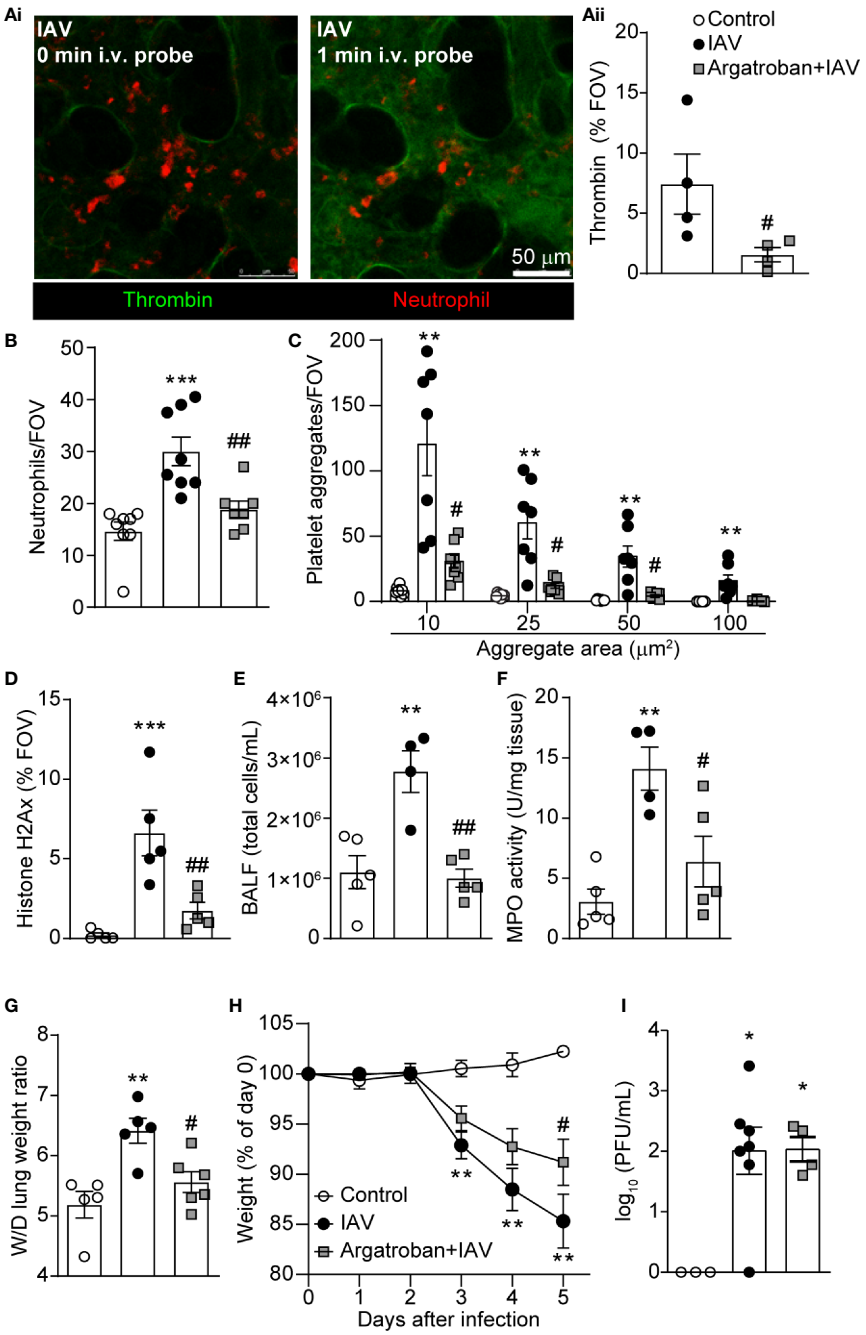

FIGURE 4 | Thrombin Mediates Platelet Aggregation and NET Release within the Lung Vasculature during IAV Infection. **(Ai)** Representative IVM images of thrombin probe cleavage in the mouse lung 5d-post IAV-infection at the time of probe infusion (0 min, left) and 1 min after probe infusion (right; neutrophils, red; thrombin activity, green). **(Aii)** Quantification of thrombin activity measured as a % of the FOV labelled by the fluorescent substrate in IAV-infected control and argatroban-pretreated animals. Quantification of neutrophils **(B)**, platelet aggregation **(C)**, extracellular histone **(D)**, BALF cellularity **(E)**, lung MPO activity **(F)**, lung wet-to-dry tissue weight ratios **(G)**, animal body mass **(H)** and viral loads **(I)** in IAV-infected control and argatroban-pretreated mice. Values represent the mean +/- SEM. n=4-8 per group. $^{*}p < 0.05$, $^{**}p < 0.01$, $^{***}p < 0.001$ compared to the control group. $^{\#}p < 0.05$, $^{\#\#}p < 0.01$ compared to the IAV-infected group.

platelets release cytokines and chemokines, but they also directly interact with inflammatory leukocytes and potentiate the effector responses of these cells (51). Furthermore, there is clear evidence of platelet activation in the blood of critically ill influenza patients (52), and platelets have been suggested to play an active role in development of pathogenesis during IAV infections (33). In animal models of IAV infection, H1N1 promotes platelet activation through the formation of immune

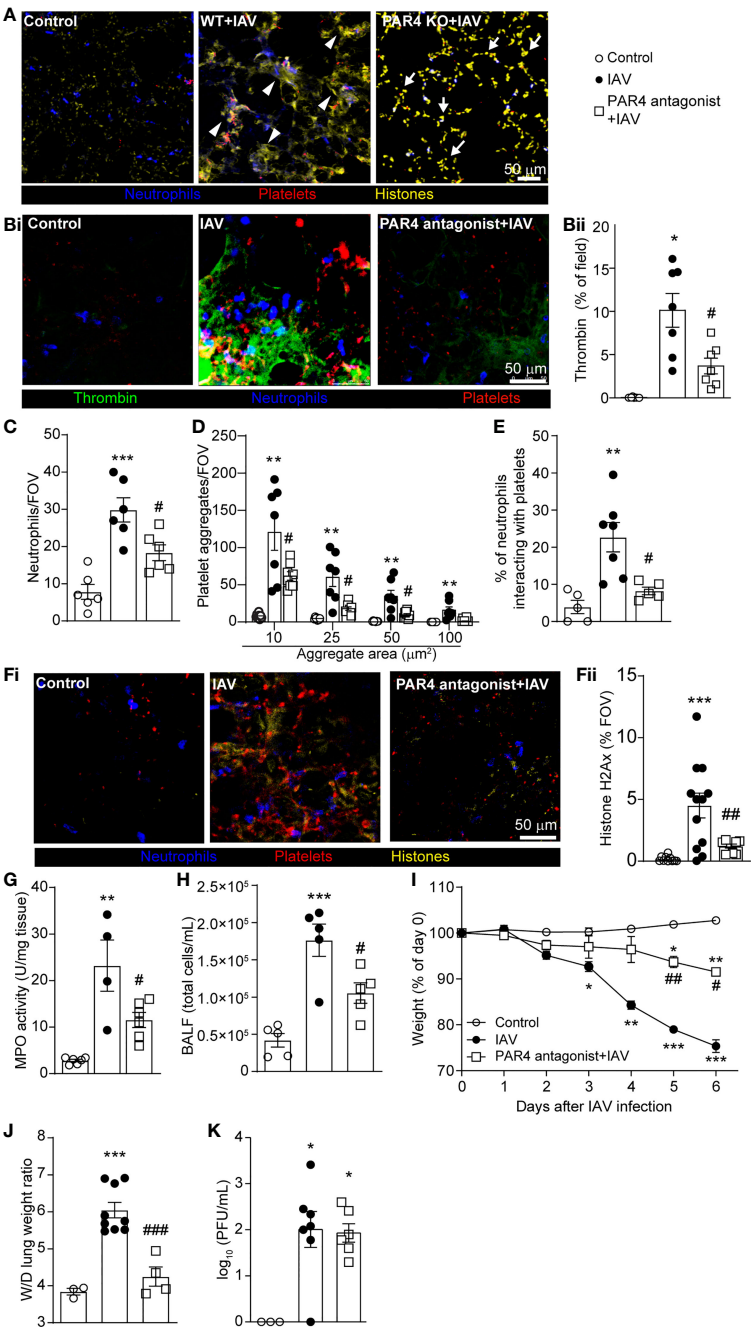

FIGURE 5 | PAR4 Drives IAV-Induced Inflammation and Subsequent Tissue Damage. **(A)** Representative immunostaining of WT lung tissue uninfected control and WT and PAR4 KO ($PAR4^{-/-}$) mice 5d after IAV infection (neutrophils, blue; histone, yellow; platelets, red). Arrowheads denote diffuse, intravascular histone staining (NETs), and full arrows indicate punctate, nuclear histone stain. **(Bi)** Representative IVM image of lungs of control (uninfected) and 5d post IAV infection of control and PAR4 antagonist ($TcY\text{-}NH_2$)-pretreated mice demonstrating intravascular thrombin activity (neutrophils, blue; platelets, red; thrombin activity, green). **(Bii)** Quantification of thrombin activity measured as a % of the FOV labelled by the fluorescent substrate in uninfected control, IAV-infected control and PAR4 antagonist pretreated animals. Quantification of neutrophils **(C)**, platelet aggregation **(D)**, platelet-neutrophil interactions expressed as a % of neutrophils contacting platelets **(E)** in IAV-infected control and PAR4 inhibitor ($TcY\text{-}NH_2$) pretreated mice. **(Fi)** Representative IVM image of lungs of control (uninfected) and 5d post IAV infection of control and PAR4 antagonist ($TcY\text{-}NH_2$)-pretreated mice demonstrating histone staining (neutrophils, blue; histone, yellow; platelets, red). Quantification of extracellular histone **(Fii)**, lung MPO activity **(G)**, BALF cellularity **(H)**, animal body mass **(I)**, lung wet-to-dry tissue weight ratios **(J)**, and viral loads **(K)** in IAV-infected control and PAR4 inhibitor ($TcY\text{-}NH_2$) pretreated mice. Values represent the mean +/- SEM. n = 4-12 per group. $^{*}p < 0.05$, $^{**}p < 0.01$, $^{***}p < 0.001$ compared to the control group. $^{\#}p < 0.05$, $^{\#\#}p < 0.01$, $^{\#\#\#}p < 0.001$ compared to the IAV-infected group.

complexes and thrombin generation (53). Considering the broad inflammatory role of activated platelets, including their direct release of microvesicles and indirect interaction with other inflammatory cells, platelet activation may represent a key contributor to the excessive inflammation frequently observed following viral infection. Using IVM, we directly visualized platelet recruitment, activation, and behavior within intact lung tissue during severe IAV infection.

Platelet-neutrophil interaction is a crucial process that drives immune responses during various models of inflammatory disease (54, 55). McDonald et al. (20) demonstrated that blocking platelet-neutrophil interactions improved sepsis-induced acute liver injury Moreover, it is known that platelets drive NET production (20, 56), facilitate neutrophil recruitment, and platelet-endothelial cell interactions drive lung injury during IAV infection (33, 34); however, the specific mechanisms involved in these interactions, and their role in IAV pathology have not yet been elucidated. In our study, we provide evidence that, within the context of severe IAV infection, platelet recruitment to, and aggregation within the lung vasculature precedes activation and recruitment of neutrophils. Large platelet aggregates form in lung vasculature within the first 24h following infection and subsequently neutrophils are recruited, co-localizing with aggregated platelets. These platelet-neutrophil interactions appear critical for the progression of lung pathology following IAV infection. Inhibition of platelet aggregation (CD41-deficient mice) or platelet-neutrophil interactions (CD18 blocking antibodies), prevents NET formation and subsequent lung tissue damage. Our findings demonstrate a requirement for platelet aggregation on adherent neutrophils for the generation of NETs, an effector mechanism that, when produced in excess, causes tissue injury (14). However, these findings must be balanced with the previous evidence that NETs released during infection can trap and inactivate viruses, potentially contributing to pathogen clearance *in vivo* (30, 57). Interestingly neither inhibition of NET formation (CD18 blockade/CD41 deficiency), nor removal of NETs from the vasculature (DNase), impacted viral clearance suggesting that within the context of severe IAV infection, NETs do more harm than good.

Following IAV infection, thrombin activates platelets, promoting both coagulation and the release of inflammatory microparticles from platelets (53). We hypothesized that an early thrombin signal generated shortly after severe IAV infection represents an inflammatory "spark" that bridges coagulation and inflammation, potentiating platelet-mediated inflammatory responses. Recent studies have pushed platelets into the forefront of IAV research, demonstrating that platelets amplify the host inflammatory response to IAV infection (33, 53, 58, 59). Importantly, using a mix of *in vitro* human and *in vivo* mouse studies, these previous studies confirmed that platelets can directly bind IAV virions and can initiate signaling through innate pattern recognition receptors (PRRs). These studies clearly illustrate the role platelets play in the host response to influenza and highlight innate immune receptors expressed by platelets.

It is important to note that PRRs are not the only means by which platelets can respond to an inflammatory signal. Through experiments that directly inhibit thrombin (argatroban), we identified a central role for thrombin in platelet activation and the initiation of inflammation in the lung following IAV infection. Not only was platelet aggregation and NET generation reduced in argatroban-pretreated animals, but a significant decrease in neutrophil recruitment and pathology was also observed following IAV infection in argatroban-treated animals demonstrating a requirement for thrombin-mediated signaling in the initiation of the host inflammatory response following severe viral infection.

NETs, and their components (DNA, histone proteins, neutrophil proteases) are one of the primary driving forces in the initiation of thrombosis and inhibition of fibrinolysis; hallmarks of disseminated intravascular coagulation (18, 60). These findings suggest a vicious cycle of NET release, microvascular thrombosis, thrombin-induced platelet activation which then precipitates further platelet aggregation, amplifying inflammation and tissue damage. Our data indicate that thrombin generation, within the context of IAV infection, precedes NET release and may represent a potential target in the mitigation of lung inflammation following viral infection.

PARs are receptors that facilitate thrombin-mediated signal transduction. Importantly, PAR1 and PAR4 are reported to be involved in development of IAV pathogenesis (33, 61–63). As mouse platelets do not express PAR1, thrombin-mediated platelet activation occurs through PAR4 (64, 65). Here, we demonstrate that inhibition of PAR4 drastically attenuates the formation of platelet aggregates, platelet-neutrophil aggregates, and reduces neutrophil recruitment following IAV infection. In addition, we show PAR4 inhibition attenuates subsequent thrombin generation and tissue pathology. In contrast, recent work by Tatsumi et al. (35) demonstrated that a global deficiency of PAR4 worsens disease in the context of mild to moderate IAV infection suggesting PAR4 may be protective during influenza infection. To reconcile our findings with these previous observations, we treated animals with a PAR4 antagonist followed by infection with a lower titer of IAV. Surprisingly, whereas PAR4 inhibition was protective when animals were challenged with a high viral load, inhibition of PAR4 in the context of a less severe infection worsened disease (**Supplemental Figure 10**), directly confirming the results of Tatsumi et al. It may be the case, that in the presence of low viral load, PAR4 signaling on non-platelets is required to increase the sensitivity of PRRs; however, in the case of higher viral loads, PRR sensitivity is no longer an issue and instead, PAR4 signaling, and activation of platelets becomes pathogenic. This creates an interesting dichotomy whereby the same receptor is both protective and pathogenic depending on the viral load, leading to potential problems with pursuing the PAR4-pathway as a therapeutic target for the treatment of IAV infection. Moreover, proteases released from neutrophils also have the ability to activate PARs, potentially bypassing the effect of anti-thrombin drugs and exacerbating the effect of the inflammatory milieu (66–68). These findings highlight the need for a better overall understanding of the overlapping inflammatory pathways at play in the lung before we can safely attempt to modulate thrombin generation or PAR activation in an effort to treat IAV infections.

Current approaches to treating IAV infection, focused on targeting specific viral proteins, have several disadvantages, including the rapid development of resistant/escape viral variants. Based on this very real limitation, drugs regulating the host inflammatory response to IAV infection might prove to be a more appealing target for future therapeutics. Treatment strategies that limit neutrophil recruitment, reduce NET production, or enhance NET clearance may effectively reduce lung pathology, although there is a risk that such treatments may also reduce the efficacy of the host immune response. Given the central role platelets play in the initiation and amplification of the host inflammatory response, thrombocytes represent an interesting potential target in the treatment of viral lung infections. Importantly, many clinically approved drugs that modulate platelet activation are already in use, making the development of potential therapeutic strategies a realistic possibility. Our results highlight dynamic and coordinated innate immune responses within lung vasculature during IAV infection. We demonstrate that modulating platelet activation, and their interactions with other immune cells, may protect lungs from IAV-induced pathogenesis in an experimental model of viral infection. Furthermore, we also provided insight on infection-induced thrombin, with evidence suggesting thrombin is a key molecule linking coagulation and inflammation, both of which are crucial axes in the immunopathology, and resolution, of IAV infection.

DATA AVAILABILITY STATEMENT

The raw data supporting the conclusions of this article will be made available by the authors, without undue reservation.

ETHICS STATEMENT

The animal study was reviewed and approved by University of Calgary Animal Care Committee.

AUTHOR CONTRIBUTIONS

S-JK and AC designed and performed experiments, analyzed data, and prepared figures. HG, AZZ, RD, MT, and VN performed experiments and analyzed data. SA performed experiments and contributed reagents/materials/analysis tools. NM and MFA-C contributed reagents/materials/analysis tools. MSA-C performed experiments, analyzed data and contributed reagents/materials/analysis tools. MDH designed experiments and contributed reagents/materials/analysis tools. CNJ designed experiments and together with S-JK and BM wrote the paper. All authors contributed to the article and approved the submitted version.

FUNDING

This research was supported by Basic Science Research Program through the National Research Foundation of Korea (NRF) funded by the Ministry of Education (2014R1A6A3A03058770) and through grants from the Heart and Stroke Foundation of Canada (HSFC), the Natural Sciences and Engineering Research Council of Canada (NSERC), the University of Calgary URGC, the Lung Association of Alberta & NWT, the Canadian Foundation for Innovation, Alberta Innovates and Advanced Education. CJ is supported by the Canada Research Chairs program.

ACKNOWLEDGMENTS

The authors thank Mandy Tse for excellent technical assistance.

SUPPLEMENTARY MATERIAL

The Supplementary Material for this article can be found online at: https://www.frontiersin.org/articles/10.3389/fimmu.2021.772859/full#supplementary-material

REFERENCES

1. Hamilton BE, Minino AM, Martin JA, Kochanek KD, Strobino DM, Guyer B. Annual Summary of Vital Statistics: 2005. *Pediatrics* (2007) 119:345–60. doi: 10.1542/peds.2006-3226
2. Schanzer DL, Langley JM, Tam TWS. Co-Morbidities Associated With Influenza-Attributed Mortality, 1994–2000, Canada. *Vaccine* (2008) 26:4697–703. doi: 10.1016/j.vaccine.2008.06.087
3. Biondo C, Lentini G, Beninati C, Teti G. The Dual Role of Innate Immunity During Influenza. *BioMed J* (2019) 42(1):8–18. doi: 10.1016/j.bj.2018.12.009
4. Tripathi S, White MR, Hartshorn KL. The Amazing Innate Immune Response to Influenza a Virus Infection. *Innate Immun* (2015) 21(1):73–98. doi: 10.1177/1753425913508992
5. Manna S, Baindara P, Mandal SM. Molecular Pathogenesis of Secondary Bacterial Infection Associated to Viral Infections Including SARS-CoV-2. *J Infect Public Health* (2020) 13(13):1397–404. doi: 10.1016/j.jiph.2020.07.003
6. Sharma-Chawla N, Sender V, Kershaw O, Gruber AD, Volckmar J, Henriques-Normark B, et al. Influenza a Virus Infection Predisposes Hosts to Secondary Infection With Different Streptococcus Pneumoniae Serotypes With Similar Outcome But Serotype-Specific Manifestation. *Infect Immun* (2016) 84(12):3445–57. doi: 10.1128/IAI.00422-16
7. Bordon J, Aliberti S, Fernandez-Botran R, Uriarte SM, Rane MJ, Duvvuri P, et al. Understanding the Roles of Cytokines and Neutrophil Activity and Neutrophil Apoptosis in the Protective *Versus* Deleterious Inflammatory Response in Pneumonia. *Int J Infect Dis* (2013) 17:e76–83. doi: 10.1016/j.ijid.2012.06.006
8. Geerdink RJ, Pillay J, Meyaard L, Bont L. Neutrophils in Respiratory Syncytial Virus Infection: A Target for Asthma Prevention. *J Allergy Clin Immunol* (2015) 136:838–47. doi: 10.1016/j.jaci.2015.06.034
9. Tsai KS, Grayson MH. Pulmonary Defense Mechanisms Against Pneumonia and Sepsis. *Curr Opin Pulm Med* (2008) 14:260–5. doi: 10.1097/MCP.0b013e3282f76457
10. Kolaczkowska E, Kubes P. Neutrophil Recruitment and Function in Health and Inflammation. *Nat Rev Immunol* (2013) 13:159–75. doi: 10.1038/nri3399
11. Brinkmann V, Reichard U, Goosmann C, Fauler B, Uhlemann Y, Weiss DS, et al. Neutrophil Extracellular Traps Kill Bacteria. *Science* (2004) 303:1532–5. doi: 10.1126/science.1092385
12. Garcia CC, Weston-Davies W, Russo RC, Tavares LP, Rachid MA, Alves-Filho JC, et al. Complement C5 Activation During Influenza a Infection in Mice Contributes to Neutrophil Recruitment and Lung Injury. *PloS One* (2013) 8:e64443. doi: 10.1371/journal.pone.0064443
13. Perrone LA, Plowden JK, García-Sastre A, Katz JM, Tumpey TM, Garcia-Sastre A, et al. H5N1 and 1918 Pandemic Influenza Virus Infection Results in

Early and Excessive Infiltration of Macrophages and Neutrophils in the Lungs of Mice. *PLoSPathog* (2008) 4:e1000115. doi: 10.1371/journal.ppat.1000115
14. Narasaraju T, Yang E, Samy RP, Ng HH, Poh WP, Liew A-AA, et al. Excessive Neutrophils and Neutrophil Extracellular Traps Contribute to Acute Lung Injury of Influenza Pneumonitis. *AmJPathol* (2011) 179:199–210. doi: 10.1016/j.ajpath.2011.03.013
15. Short KR, Kroeze EJBV, Fouchier RAM, Kuiken T. Pathogenesis of Influenza-Induced Acute Respiratory Distress Syndrome. *Lancet Infect Dis* (2014) 14:57–69. doi: 10.1016/S1473-3099(13)70286-X
16. Semple JW, Freedman J. Platelets and Innate Immunity. *Cell MolLife Sci* (2010) 67:499–511. doi: 10.1007/s00018-009-0205-1
17. McMorran BJ, Marshall VM, de Graaf C, Drysdale KE, Shabbar M, Smyth GK, et al. Platelets Kill Intraerythrocytic Malarial Parasites and Mediate Survival to Infection. *Science (80-)* (2009) 323:797–800. doi: 10.1126/science.1166296
18. Semple JW, Italiano JE, Freedman J, Italiano JE, Freedman J. Platelets and the Immune Continuum. *Nat Rev Immunol* (2011) 11:264–74. doi: 10.1038/nri2956
19. Von Hundelshausen P, Koenen RR, Weber C, Von Hundelshausen P, Koenen RR, Weber C. Platelet-Mediated Enhancement of Leukocyte Adhesion. *Microcirculation* (2009) 16:84–96. doi: 10.1080/10739680802564787
20. McDonald B, Urrutia R, Yipp BG, Jenne CN, Kubes P. Intravascular Neutrophil Extracellular Traps Capture Bacteria From the Bloodstream During Sepsis. *Cell Host Microbe* (2012) 12:324–33. doi: 10.1016/j.chom.2012.06.011
21. Antoniak S, Tatsumi K, Hisada Y, Milner JJ, Neidich SD, Shaver CM, et al. Tissue Factor Deficiency Increases Alveolar Hemorrhage and Death in Influenza a Virus-Infected Mice. *J Thromb Haemost* (2016) 14:1238–48. doi: 10.1111/jth.13307
22. Bilaloglu S, Aphinyanaphongs Y, Jones S, Iturrate E, Hochman J, Berger JS. Thrombosis in Hospitalized Patients With COVID-19 in a New York City Health System. *JAMA - J Am Med Assoc* (2020) 324(8):799–801. doi: 10.1001/jama.2020.13372
23. Klok FA, Kruip MJHA, van der Meer NJM, Arbous MS, Gommers DAMPJ, Kant KM, et al. Incidence of Thrombotic Complications in Critically Ill ICU Patients With COVID-19. *Thromb Res* (2020) 191:145–7. doi: 10.1016/j.thromres.2020.04.013
24. MacKman N, Antoniak S, Wolberg AS, Kasthuri R, Key NS. Coagulation Abnormalities and Thrombosis in Patients Infected With SARS-CoV-2 and Other Pandemic Viruses. *Arterioscler Thromb Vasc Biol* (2020) 40(9):2033–44. doi: 10.1161/ATVBAHA.120.314514
25. Sambrano GR, Weiss EJ, Zheng Y-WW, Huang W, Coughlin SR. Role of Thrombin Signalling in Platelets in Haemostasis and Thrombosis. *Nature* (2001) 413:74–8. doi: 10.1038/35092573
26. Anders EM, Hartley CA, Reading PC, Ezekowitz RA. Complement-Dependent Neutralization of Influenza Virus by a Serum Mannose-Binding Lectin. *JGenVirol* (1994) 75(Pt 3):615–22. doi: 10.1099/0022-1317-75-3-615
27. Looney MR, Thornton EE, Sen D, Lamm WJ, Glenny RW, Krummel MF. Stabilized Imaging of Immune Surveillance in the Mouse Lung. *NatMethods* (2011) 8:91–6. doi: 10.1038/nmeth.1543
28. Jenne CN, Wong CHY, Petri B, Kubes P. The Use of Spinning-Disk Confocal Microscopy for the Intravital Analysis of Platelet Dynamics in Response to Systemic and Local Inflammation. *PLoSOne* (2011) 6:e25109. doi: 10.1371/journal.pone.0025109
29. Yipp BG, Kubes P. Antibodies Against Neutrophil LY6G do Not Inhibit Leukocyte Recruitment in Mice *in Vivo*. *Blood* (2013) 121:241–2. doi: 10.1182/BLOOD-2012-09-454348
30. Jenne CN, Wong CHY, Zemp FJ, McDonald B, Rahman MM, Forsyth PA, et al. Neutrophils Recruited to Sites of Infection Protect From Virus Challenge by Releasing Neutrophil Extracellular Traps. *Cell Host Microbe* (2013) 13:169–80. doi: 10.1016/j.chom.2013.01.005
31. McDonald B, Davis RP, Kim SJ, Tse M, Esmon CT, Kolaczkowska E, et al. Platelets and Neutrophil Extracellular Traps Collaborate to Promote Intravascular Coagulation During Sepsis in Mice. *Blood* (2017) 129:1357–67. doi: 10.1182/blood-2016-09-741298
32. Wong CH, Jenne CN, Lee WY, Leger C, Kubes P. Functional Innervation of Hepatic Inkt Cells is Immunosuppressive Following Stroke. *Science* (2011) 334:101–5. doi: 10.1126/science.1210301
33. Le VB, Schneider JG, Boergeling Y, Berri F, Ducatez M, Guerin J-LL, et al. Platelet Activation and Aggregation Promote Lung Inflammation and Influenza Virus Pathogenesis. *Am J Respir Crit Care Med* (2015) 191:804–19. doi: 10.1164/rccm.201406-1031OC
34. Sugiyama MG, Gamage A, Zyla R, Armstrong SM, Advani S, Advani A, et al. Influenza Virus Infection Induces Platelet-Endothelial Adhesion Which Contributes to Lung Injury. *J Virol* (2016) 90:1812–23. doi: 10.1128/JVI.02599-15
35. Tatsumi K, Schmedes CM, Houston ER, Butler E, Mackman N, Antoniak S. Protease-Activated Receptor 4 Protects Mice From Coxsackievirus B3 and H1N1 Influenza a Virus Infection. *Cell Immunol* (2019) 344:1039–49. doi: 10.1016/j.cellimm.2019.103949
36. Asaduzzaman M, Lavasani S, Rahman M, Zhang S, Braun OÖO, Jeppsson B, et al. Platelets Support Pulmonary Recruitment of Neutrophils in Abdominal Sepsis. *Crit Care Med* (2009) 37:1389–96. doi: 10.1097/CCM.0b013e31819ceb71
37. Zarbock A, Singbartl K, Ley K. Complete Reversal of Acid-Induced Acute Lung Injury by Blocking of Platelet-Neutrophil Aggregation. *J Clin Invest* (2006) 116:3211–9. doi: 10.1172/JCI29499
38. Zarbock A, Polanowska-Grabowska RK, Ley K. Platelet-Neutrophil-Interactions: Linking Hemostasis and Inflammation. *Blood Rev* (2007) 21:99–111. doi: 10.1016/j.blre.2006.06.001
39. Kornerup KN, Salmon GP, Pitchford SC, Liu WL, Page CP. Circulating Platelet-Neutrophil Complexes are Important for Subsequent Neutrophil Activation and Migration. *J Appl Physiol* (2010) 109:758–67. doi: 10.1152/japplphysiol.01086.2009
40. Bombeli T, Schwartz BR, Harlan JM. Adhesion of Activated Platelets to Endothelial Cells: Evidence for a Gpiibiiia-Dependent Bridging Mechanism and Novel Roles for Endothelial Intercellular Adhesion Molecule 1 (ICAM-1), Alphavbeta3 Integrin, and Gpibalpha. *JExpMed* (1998) 187:329–39. doi: 10.1084/jem.187.3.329
41. Dubois C, Meyer Reigner SC, Steiner B, Riederer MA. Thrombin Binding to Gpibα Induces Integrin αiibβ3 Dependent Platelet Adhesion to Fibrin in *Ex Vivo* Flowing Whole Blood. *Thromb Haemost* (2004) 91:233–7. doi: 10.1160/TH03-03-0126
42. Carvalho-Tavares J, Hickey MJ, Hutchison J, Michaud J, Sutcliffe IT, Kubes P. A Role for Platelets and Endothelial Selectins in Tumor Necrosis Factor-Alpha-Induced Leukocyte Recruitment in the Brain Microvasculature. *CircRes* (2000) 87:1141–8. doi: 10.1161/01.RES.87.12.1141
43. Slaba I, Wang J, Kolaczkowska E, McDonald B, Lee WY, Kubes P. Imaging the Dynamic Platelet-Neutrophil Response in Sterile Liver Injury and Repair in Mice. *Hepatology* (2015) 62:1593–605. doi: 10.1002/hep.28003
44. Funchal GA, Jaeger N, Czepielewski RS, Machado MS, Muraro SP, Stein RT, et al. Respiratory Syncytial Virus Fusion Protein Promotes TLR-4–Dependent Neutrophil Extracellular Trap Formation by Human Neutrophils. *PloS One* (2015) 10:e0124082. doi: 10.1371/journal.pone.0124082
45. Raftery MJ, Lalwani P, Krautkrmer E, Peters T, Scharffetter-Kochanek K, Kruger R, et al. Beta2 Integrin Mediates Hantavirus-Induced Release of Neutrophil Extracellular Traps. *J Exp Med* (2014) 211:1485–97. doi: 10.1084/jem.20131092
46. Hemmers S, Teijaro JR, Arandjelovic S, Mowen KA. PAD4-Mediated Neutrophil Extracellular Trap Formation is Not Required for Immunity Against Influenza Infection. *PloS One* (2011) 6:e22043. doi: 10.1371/journal.pone.0022043
47. Hollenberg MD, Saifeddine M. Proteinase-Activated Receptor 4 (PAR4): Activation and Inhibition of Rat Platelet Aggregation by PAR4-Derived Peptides. *Can J Physiol Pharmacol* (2001) 79:439–42. doi: 10.1139/y01-013
48. Kolpakov MA, Rafiq K, Guo X, Hooshdaran B, Wang T, Vlasenko L, et al. Protease-Activated Receptor 4 Deficiency Offers Cardioprotection After Acute Ischemia Reperfusion Injury. *J Mol Cell Cardiol* (2016) 90:21–9. doi: 10.1016/j.yjmcc.2015.11.030
49. Slofstra SH, Bijlsma MF, Groot AP, Reitsma PH, Lindhout T, ten Cate H, et al. Protease-Activated Receptor-4 Inhibition Protects From Multiorgan Failure in a Murine Model of Systemic Inflammation. *Blood* (2007) 110:3176–82. doi: 10.1182/blood-2007-02-075440
50. Berri F, Le VB, Jandrot-Perrus M, Lina B, Riteau B, Lê VB, et al. Switch From Protective to Adverse Inflammation During Influenza: Viral Determinants and Hemostasis are Caught as Culprits. *Cell Mol Life Sci* (2014) 71:885–98. doi: 10.1007/s00018-013-1479-x
51. Kirschenbaum LA, Adler D, Astiz ME, Barua RS, Saha D, Rackow EC. Mechanisms of Platelet-Neutrophil Interactions and Effects on Cell

Filtration in Septic Shock. *Shock* (2002) 17:508–12. doi: 10.1097/00024382-200206000-00012
52. Rondina MT, Brewster B, Grissom CK, Zimmerman G a, Kastendieck DH, Harris ES, et al. In Civo Platelet Activation in Critically Ill Patients With Primary 2009 Influenza a (H1N1). *Chest* (2012) 141:1490–5. doi: 10.1378/chest.11-2860
53. Boilard E, Pare G, Rousseau M, Cloutier N, Dubuc I, Levesque T, et al. Influenza Virus H1N1 Activates Platelets Through Fc RIIA Signaling and Thrombin Generation. *Blood* (2014) 123:2854–63. doi: 10.1182/blood-2013-07-515536
54. Kral JB, Schrottmaier WC, Salzmann M, Assinger A. Platelet Interaction With Innate Immune Cells. *Transfus Med Hemotherapy* (2016) 43:78–88. doi: 10.1159/000444807
55. Li J, Kim K, Barazia A, Tseng A, Cho J. Platelet-Neutrophil Interactions Under Thromboinflammatory Conditions. *Cell Mol Life Sci* (2015) 72:2627–43. doi: 10.1007/s00018-015-1845-y
56. Carestia A, Kaufman T, Rivadeneyra L, Landoni VI, Pozner RG, Negrotto S, et al. Mediators and Molecular Pathways Involved in the Regulation of Neutrophil Extracellular Trap Formation Mediated by Activated Platelets. *JLeukocBiol* (2016) 99:153–62. doi: 10.1189/jlb.3A0415-161R
57. Saitoh T, Komano J, Saitoh Y, Misawa T, Takahama M, Kozaki T, et al. Neutrophil Extracellular Traps Mediate a Host Defense Response to Human Immunodeficiency Virus-1. *Cell Host Microbe* (2012) 12:109–16. doi: 10.1016/j.chom.2012.05.015
58. Koupenova M, Corkrey HA, Vitseva O, Manni G, Pang CJ, Clancy L, et al. The Role of Platelets in Mediating a Response to Human Influenza Infection. *Nat Commun* (2019) 10:1780. doi: 10.1038/s41467-019-09607-x
59. Zhang HH, Yu WY, Li L, Wu F, Chen Q, Yang Y, et al. Protective Effects of Diketopiperazines From Moslae Herba Against Influenza a Virus-Induced Pulmonary Inflammation *via* Inhibition of Viral Replication and Platelets Aggregation. *J Ethnopharmacol* (2018) 215:156–66. doi: 10.1016/j.jep.2018.01.005
60. Fuchs TA, Bhandari AA, Wagner DD. Histones Induce Rapid and Profound Thrombocytopenia in Mice. *Blood* (2011) 118:3708–14. doi: 10.1182/blood-2011-01-332676
61. Antoniak S, Owens APIII, Baunacke M, Williams JC, Lee RD, Weithauser A, et al. PAR-1 Contributes to the Innate Immune Response During Viral Infection. *J Clin Invest* (2013) 123:1310–22. doi: 10.1172/JCI66125
62. Khoufache K, Berri F, Nacken W, Vogel AB, Delenne M, Camerer E, et al. PAR1 Contributes to Influenza a Virus Pathogenicity in Mice. *J Clin Invest* (2013) 123:206–14. doi: 10.1172/JCI61667
63. Lan RS, Stewart GA, Goldie RG, Henry PJ. Altered Expression and *In Vivo* Lung Function of Protease-Activated Receptors During Influenza a Virus Infection in Mice. *Am J Physiol Lung Cell Mol Physiol* (2004) 286:L388–98. doi: 10.1152/ajplung.00286.2003
64. Coughlin SR. Protease-Activated Receptors in Hemostasis, Thrombosis and Vascular Biology. *J Thromb Haemost* (2005) 3:1800–14. doi: 10.1111/j.1538-7836.2005.01377.x
65. Coughlin SR. Thrombin Signalling and Protease-Activated Receptors. *Nature* (2000) 407:258–64. doi: 10.1038/35025229
66. Mihara K, Ramachandran R, Renaux B, Saifeddine M, Hollenberg MD. Neutrophil Elastase and Proteinase-3 Trigger G Protein-Biased Signaling Through Proteinase-Activated Receptor-1 (PAR1). *J Biol Chem* (2013) 288:32979–90. doi: 10.1074/jbc.M113.483123
67. Ramachandran R, Mihara K, Chung H, Renaux B, Lau CS, Muruve DA, et al. Neutrophil Elastase Acts as a Biased Agonist for Proteinase-Activated Receptor-2 (PAR2). *JBiolChem* (2011) 286:24638–48. doi: 10.1074/jbc.M110.201988
68. Sambrano GR, Huang W, Faruqi T, Mahrus S, Craik C, Coughlin SR. Cathepsin G Activates Protease-Activated Receptor-4 in Human Platelets. *J Biol Chem* (2000) 275:6819–23. doi: 10.1074/jbc.275.10.6819

Conflict of Interest: The authors declare that the research was conducted in the absence of any commercial or financial relationships that could be construed as a potential conflict of interest.

Publisher's Note: All claims expressed in this article are solely those of the authors and do not necessarily represent those of their affiliated organizations, or those of the publisher, the editors and the reviewers. Any product that may be evaluated in this article, or claim that may be made by its manufacturer, is not guaranteed or endorsed by the publisher.

frontiers | Frontiers in Immunology

ORIGINAL RESEARCH
published: 04 April 2022
doi: 10.3389/fimmu.2022.865386

Platelet-Depletion of Whole Blood Reveals That Platelets Potentiate the Release of IL-8 From Leukocytes Into Plasma in a Thrombin-Dependent Manner

Huy Quang Quach[1*†], *Christina Johnson*[1†], *Karin Ekholt*[1], *Rakibul Islam*[1], *Tom Eirik Mollnes*[1,2,3] *and Per H. Nilsson*[1,4]

[1] Department of Immunology, Oslo University Hospital Rikshospitalet, University of Oslo, Oslo, Norway, [2] Research Laboratory, Nordland Hospital, K.G Jebsen Center TREC, University of Tromsø, Bodø, Norway, [3] Centre of Molecular Inflammation Research, Department of Cancer Research and Molecular Medicine, Norwegian University of Science and Technology, Trondheim, Norway, [4] Department of Chemistry and Biomedicine, Linnaeus Centre for Biomaterials Chemistry, Linnaeus University, Kalmar, Sweden

OPEN ACCESS

Edited by:
Alok Agrawal,
East Tennessee State University, United States

Reviewed by:
Qizhen Shi,
Medical College of Wisconsin, United States
Udai P. Singh,
University of Tennessee Health Science Center (UTHSC), United States

***Correspondence:**
Huy Quang Quach
huy.q.quach@gmail.com

[†]*These authors have contributed equally to this work*

Specialty section:
This article was submitted to Molecular Innate Immunity, a section of the journal Frontiers in Immunology

Received: *29 January 2022*
Accepted: *14 March 2022*
Published: *04 April 2022*

Citation:
Quach HQ, Johnson C, Ekholt K, Islam R, Mollnes TE and Nilsson PH (2022) Platelet-Depletion of Whole Blood Reveals That Platelets Potentiate the Release of IL-8 From Leukocytes Into Plasma in a Thrombin-Dependent Manner. Front. Immunol. 13:865386. doi: 10.3389/fimmu.2022.865386

Objective: In a recent study, we found an elevated level of interleukin 8 (IL-8) in response to bacterial incubation in thrombin-sufficient human whole blood anticoagulated by the fibrin polymerization blocking peptide GPRP. Whether thrombin directly activated leukocytes or mediated the release *via* thrombin-dependent activation of platelets remains unresolved. Herein, we addressed the role of thrombin and platelets in IL-8 release.

Methods: We separated platelets from whole blood using a combination of 0.7% (w/v) citrate and GPRP for attenuating the hemostatic response during the separation of platelets. Cytokine responses were compared in whole blood and platelet-depleted blood upon *Escherichia coli* incubation. Cytokine responses were also profiled with and without reconstitution of either platelets or the supernatant from activated platelets.

Results: Platelets were not activated during the separation process but responded to stimuli upon re-calcification. Plasma levels of IL-1β, IL-1Ra, IL-6, IL-8, IP-10, MIP-1α, and MIP-1β were significantly reduced in platelet-depleted blood compared to whole blood, but recovered in the presence of platelets, or with the supernatant of activated platelets. The leukocyte fraction and platelets were each found to contribute to the elevation of IL-8 at around 5 ng/ml; however, if combined, the release of IL-8 increased to 26 ng/ml. This process was dependent on thrombin since the levels of IL-8 remained at 5 ng/ml in whole blood if thrombin was blocked. Intracellular staining revealed that monocytes were the main source for IL-8 expression.

Conclusion: Our findings suggest that the release of IL-8 is mediated by the leukocytes, mainly monocytes, but potentiated *via* thrombin-dependent activation of platelets.

Keywords: platelets, IL-8, acute inflammation, human whole blood, thrombin, cytokines

INTRODUCTION

Platelets are vital for hemostasis and inflammation (1, 2). Conceptually, primary hemostasis is the act of platelet adhesion and aggregation to seal vascular injury by forming a platelet plug (1, 2), while the processes of platelet activation and granule secretion modulate coagulation as well as inflammatory responses (3–6). To study platelets as modulators of inflammation, there is a need to silence platelet functions in whole blood and compare the responses in whole blood with and without platelet contribution. This can be achieved by attenuating platelet activation or separating platelets from whole blood. The advantage of the latter approach is that platelets can be reconstituted back to the same whole blood at later stages after being stored in an inert milieu. However, separating platelets from whole blood needs to be performed delicately without activating the platelets or affecting other blood components to preserve mutual interactions between all blood constituents. Many current methods to purify platelets are suboptimal since they employ inhibitors like citrate in high concentrations or ethylenediamine tetra-acetic acid (EDTA), all of which can alter or even damage platelet functions and influence downstream inflammatory processes (4, 7–9). Citrate is one of the most commonly used anticoagulants (10). While citrate does not interact with proteins *per se*, it does lower the physiological concentration of Ca^{2+} ions (11), inhibiting catalytic activities of proteases requiring Ca^{2+}, e.g., the conversion of prothrombin to thrombin by factor (F) Xa in blood coagulation (7). Thrombin is a potent activator of platelets *via* protease-activated receptors (PAR) 1 and 4, a pathway that is inhibited in citrated whole blood (12). Platelet function has also been attenuated in citrate-anticoagulated whole blood in response to activators other than thrombin (13); thus, re-calcification is required to activate isolated platelets for the downstream study of platelet function (10).

The advantage of using a whole blood model for acute inflammation studies is that blood cells and protein cascades can mutually interact in their physiological environments (14). We have extensively investigated innate immunity activation in whole blood anticoagulated with the thrombin inhibitor lepirudin (15), blocking the last step before fibrinogen is activated and keeping all other inflammatory systems, including the complement system, open to mutually interact. Still, however, the limitation of this model is that thrombin is blocked. Recently, we have characterized an *ex vivo* whole blood model using the fibrin polymerization blocking peptide Gly-Pro-Arg-Pro (GPRP) as the anticoagulant (16). Since GPRP exerts its effect downstream of thrombin generation in the coagulation cascade, it allows the study of the crosstalk between coagulation and complement from the node of thrombin (14). The thrombotic response is the primary determinant separating these two *ex vivo* whole blood models; the lepirudin-based model exhibits no active thrombin and low level of platelet activation while thrombin is fully active in the GPRP-based model, allowing platelet activation.

The release of inflammatory cytokines is a cornerstone of the cellular inflammatory responses to pathogenic stimuli (17). Interleukin (IL)-8 represents a vital chemoattractant for leukocyte recruitment (18, 19). It is secreted by various cells, including monocytes, macrophages, and endothelial cells. We and others have previously shown that plasma levels of IL-8 increased in response to complement activation (20). Further on, we recently found that IL-8 release was potentiated in the presence of thrombin (Johnson et al., *submitted manuscript*). However, whether thrombin activates IL-8-producing cells directly or *via* platelet activation remains unclear. Thus, the aim of the present study was to investigate the contribution of platelets in the release of IL-8 to plasma in a whole blood environment by using the advantage of the GPRP-based whole blood model supplemented with a low amount of citrate for gentle separation of platelets.

MATERIALS AND METHODS

Materials

Lepirudin (Refludan®) was obtained from Celgene (Uxbridge, United Kingdom). GPRP peptide (Pefabloc® FG or Pefa-6003) was purchased from Pentapharm (Basel, Switzerland). Trisodium citrate was isolated from BD Vacutainer citrate blood sampling tubes (BD, Plymouth, United Kingdom). Heat-inactivated *Escherichia coli* (*E. coli*, strain LE392, catalog no. ATCC 33572) was from American Type Culture Collection (ATCC, Manassas, VA). Thrombin-antithrombin (TAT) ELISA kit (catalog no. OWMG15) was purchased from Siemens Healthcare Diagnostics Products GmbH (Marburg, Germany) while β-thromboglobulin (βTG) ELISA kit (catalog no. 00950) was obtained from Diagnostica Stago, Inc. (Parsippany, NJ).

Blood Collection

Blood from healthy human donors was obtained by forearm venipuncture using a 21-gauge needle. Informed written consent was obtained from all blood donors. The whole blood (4.5 ml) was collected in polypropylene tubes containing 0.5 ml of either one of the following solutions: i) 0.7% (w/v) citrate, ii) 3.2% (w/v) citrate, iii) the thrombin inhibitor lepirudin (50 μg/ml, final concentration) supplemented with 0.7% (w/v) citrate, or iv) GPRP (8 mg/ml, final concentration) supplemented with 0.7% (w/v) citrate. The volume ratio of blood to anticoagulant was kept at 9:1. An aliquot (100 μl) of whole blood was used for blood cell counting immediately after collection using CELL-DYN Emerald 22 hematology analyzer (Abbott, IL). Experiments with the blood of each donor were performed in triplicates.

Platelet Isolation and Depletion From Human Whole Blood

The anticoagulated whole blood was centrifugated at 180×*g* for 15 minutes at 25°C without the brake applied. The liquid phase in upper layer, i.e., the platelet-rich plasma (PRP) layer, was gently transferred to 1.5 ml conical polypropylene tubes without disturbing the buffy layer. Tempered (25°C) modified

Dulbecco's phosphate-buffered saline without Ca^{2+} and Mg^{2+} (PBS, Sigma-Aldrich, MO) was added to the residual blood to compensate for the volume of the PRP removed. An aliquot (100 µl) of the residual blood was taken for cell counting. The blood underwent three washing cycles, each by centrifugation at 180×*g* for 15 minutes followed by platelet removal, to further reduce the number of residual platelets. After each step of washing, the blood volume was regained by adding PBS. An aliquot (100 µl) of the remaining blood was taken for cell counting after each step.

The separated PRP was centrifugated at 2000×*g* for 15 minutes at 25°C; the 2/3 top portion of the centrifugated PRP (i.e., platelet-poor plasma) was transferred back to the residual platelet-depleted blood after the last step of washing. The platelet containing portion of the PRP, i.e., the 1/3 bottom, was isolated as the platelet suspension. All cell counts and mean platelet volume (MPV) were measured using CELL-DYN Emerald 22 hematology analyzer (Abbott).

Conditions for Preparation and Incubations

For all steps in the platelet separation from whole blood, the blood was anticoagulated with 3.2% (w/v) citrate, otherwise with either lepirudin or GPRP supplemented with 0.7% (w/v) citrate. The temperature during the preparation was kept at 25°C. Before platelet and whole blood activation, the 0.7% (w/v) citrate was reversed by the addition of 6.25 mM $CaCl_2$ (Sigma-Aldrich) and 3.2% (w/v) citrate was reversed with 25 mM $CaCl_2$. The concentration of citrate, which was sufficient to dampen the hemostatic response in GPRP whole blood, was determined by adding citrate of concentrations from 0.2% (w/v) to 3.2% (w/v) to GPRP-whole blood and analysing the expression of CD62P and CD63 on platelets after 15 minutes of incubation. All incubations for functional tests of platelets were carried out at 37°C without or with the addition of *E. coli* (10^7/ml). After incubation, 16 µl of a stop solution containing a mixture of a CTAD solution [0.08 M trisodium citrate, 11 M theophylline, 2.6 M adenosine, 0.14 M dipyridamole] and 0.14 M EDTA was added to every 100 µl of blood or plasma.

Detection of Platelet Activation by Flow Cytometry

Platelet activation was quantified by the upregulation of their surface markers, CD63 and CD62P, by flow cytometry. Briefly, after separation from whole blood, the platelet suspension was kept at 25°C for 4 hours, followed by re-calcification and incubation with *E. coli* for 15 minutes at 37°C. Then, platelets were stained for 30 minutes in the dark at 4°C with an antibody mixture containing platelet CD42a-FITC (catalog no. 348083, BD Biosciences, San Jose, CA), CD63-PE-Cy7 (catalog no. 25-0639-42, Invitrogen, Carlsbad, CA), and CD62P-PE (catalog no. 555524, BD Biosciences). After staining, the solution was centrifuged at 250×*g*, 4°C for 5 minutes. The supernatant was discarded and the pellet was resuspended and fixed in PBS containing 0.1% paraformaldehyde (PFA) and 0.1% bovine serum albumin (PBSA) and stored at 4°C until analysis with flow cytometer Attune NxT Acoustic Focusing Cytometer (Thermo Fisher Scientific) within 24 hours from sampling. Platelets were gated as CD42a+ population (**Supplementary Figure 1**) while CD63 and CD62P were used as platelet activation measures. Flow data analysis was performed with FlowJo software version 10 (Ashland, OR).

Detection of Thrombin and Platelet Activation Markers in Plasma

Thrombin activation was characterized by the quantification of TAT-complexes in plasma, and platelet activation was determined by the level of plasma βTG. Briefly, 200 µl of whole blood or platelet-depleted blood was re-calcified and incubated with or without *E. coli* (10^7/ml). PBS was added to the control for volume adjustment. The blood was incubated in a rolling incubator at 37°C for 15 minutes before 32 µl of the stop solution was added. Plasma was collected after centrifugation at 3000×*g*, 4°C for 20 minutes, and stored at -80°C for further analyses.

Scanning Electron Microscopy Image of Platelets

Platelets in the platelet suspension were spun down at 250×*g* at room temperature for 15 minutes. Platelets were allowed to adhere onto Nunc™ Lab-Tek™ II CC2 chamber slide (Thermo Scientific™, catalog no. 154941). The samples then were fixed in 2% glutaraldehyde, dehydrated through an ethanol series and critical point drying (Polaron E3 Critical Point Drier, Polaron Equipment Ltd, United Kingdom). Next, the samples were sputter-coated with a 30 nm-thick layer of platinum in Polaron E5100 sputter coater before being viewed under a scanning electron microscope (SEM) GeminiSEM 300 (Carl Zeiss Microscopy GmbH, Germany).

Activation of Monocytes and Granulocytes

Platelet-depleted blood (40 µl) was incubated with *E. coli* (10^7/ml) in a rolling incubator at 37°C for 15 minutes. After adding 6.4 µl of the stop solution, the leukocytes were stained with antibodies: CD45-Pacific Orange (catalog no. MHCD4530, Invitrogen™), CD14-PerCP (catalog no. 340585, BD Biosciences), CD15-V450 (catalog no. 48-0158-42, Invitrogen™), CD11b-APC/Fire 750 (catalog no. 101262, BioLegend, San Diego, CA), and CD35-Alexa Fluor 647 (catalog no. 1981978, Invitrogen™) for 15 minutes at 4°C. After lysing the red blood cells with fixative-free lysis buffer (Invitrogen™, catalog no. HYL250), the solution was centrifuged at 250×*g*, 4°C for 5 minutes. After centrifugation, the supernatant was discarded and the pellet was resuspended in PBSA. The expression of the abovementioned markers was analysed with Attune NxT Acoustic Focusing Cytometer (Thermo Fisher Scientific). Granulocytes were gated as CD15+ population (**Supplementary Figure 2**), while monocytes were gated as CD15- and CD14+ population (**Supplementary Figure 3**). The activation of granulocytes and monocytes was evaluated by the

expression levels of CD11b and CD35 on their surfaces. Flow data analysis was performed with FlowJo version 10.

Intracellular Detection of IL-8

GPRP-anticoagulated whole blood was immediately supplemented with monensin (GolgiStop™, BD Biosciences, San Jose, CA) at 2 µM final concentration and incubated with bacteria for 2 hours. Then, EDTA was added at a 10 mM final concentration. For each test, 25 µl (for monocyte and granulocyte analyses) or 100 µl (for platelet analyses) of whole blood was lysed and fixed utilising the Cytofix/Cytoperm kit containing GolgiStop™ from BD Biosciences (San Jose, CA). Flow cytometry was performed on a Novocyte Flow Cytometer (ACEA Biosciences Inc., San Diego, CA, USA). Single cells were gated utilizing the forward scatter-area (FSC-A) versus the forward scatter-height (FSC-H) dot plot. Granulocytes were identified in a side scatter (SSC)/CD15 dot plot using anti-CD15 BV605 (BD Biosciences). Monocytes were identified in a SSC/CD14 dot plot from the CD15 negative population using anti-CD14 FITC (BD Biosciences). Platelets were analysed in a separate set-up and gated in a SSC/CD42a dot plot using anti-CD42a FITC (BD Biosciences). Here, monocytes were detected using an anti-CD14 V500 antibody (BD Biosciences). Expression of intracellular IL-8 was detected using anti-IL-8 BV421 (clone G265-8, BD Biosciences and expressed as MFI.

Cytokine Profiling

To study the role of platelets in the inflammatory response, whole blood was collected with GPRP supplemented with 0.7% (w/v) citrate. One part was kept as whole blood, and the other part was processed according to the protocol above, i.e., prepared as platelet suspension as one part and blood containing plasma and all cells except platelets as a second part. Half of the platelet-plasma suspension was re-calcified and incubated for 15 minutes at 37°C to activate the platelets. The activated platelet-plasma suspension was centrifuged for 15 minutes at 3000×*g*, 25°C to remove platelets by hard pellet formation. From the processed blood fractions, the following conditions were prepared: i) whole blood, ii) platelet-depleted blood, iii) platelet-depleted blood with the addition of platelet-plasma suspension, iv) platelet-depleted blood with the addition of plasma after platelet activation, and v) platelet suspension. All components were re-calcified and incubated with *E. coli* (10^7/ml) in a rolling incubator at 37°C for 4 hours. Plasma was prepared by centrifugation at 3000×*g*, 4°C for 20 minutes and stored at -80°C until analysis with multiplex technology by MAGPIX Luminex (Bio-Rad Laboratories, Hercules, CA) according to the manufacturer's protocols. A panel of ten inflammatory cytokines and chemokines (IL-1β, IL-1Ra, IL-6, IL-8, IFN-γ, IP-10, MCP-1, MIP-1α, MIP-1β, and TNF) were analysed.

Statistical Analysis

Statistical comparisons were calculated using GraphPad Prism 9 (GraphPad Software, CA). Tests employed were paired Kruskal–Wallis one-way analysis of variance. A p-value <0.05 was considered statistically significant. All data are presented as mean ± standard deviation (SD).

Ethics Statement

This study was designed and performed according to the ethical guidelines from the declaration of Helsinki. Informed written consent was obtained from the blood donors. The study was approved by the ethical committee of the Norwegian Regional Health Authority, ethical permit REK#S-04114, 2010/934.

RESULTS

Platelet Separation From Whole Blood

A low amount of citrate was used to initially stabilize platelet function and its concentration was titrated into GPRP-anticoagulated blood with platelet expression of CD63 and CD62P as the activation read-outs. The expression level of CD63 and CD62P initially decreased in response to the concentration of citrate supplemented (**Supplementary Figure 4**), and 0.7% (w/v) citrate was the optimal concentration in supplementation in GPRP-anticoagulated blood for the expression lowest of CD63 and CD62P (**Supplementary Figure 4**). Meanwhile, there was no difference in the intensities of CD63 and CD62P in lepirudin-anticoagulated blood without and with 0.7% (w/v) citrate supplemented (**Supplementary Figures 5A, B**). To re-calcify, 6.25 mM $CaCl_2$ was required to compensate the Ca^{2+} chelated by 0.7% (w/v) citrate, and 25 mM $CaCl_2$ for 3.2% (w/v) citrate.

Platelet counts and mean platelet volumes (MPV) in blood anticoagulated with 0.7% (w/v) citrate were similar to those in blood anticoagulated with 3.2% citrate (w/v) and either lepirudin or GPRP supplemented with 0.7% (w/v) citrate (**Supplementary Figures 5C, D**). However, blood anticoagulated with only 0.7% citrate clotted within 10 minutes after blood sampling; hence, data from this blood sample condition could not be further collected. Platelets in 0.7% (w/v) citrated blood transformed their morphologies into early dendritic shapes (**Supplementary Figures 5E, F**), signalling early stage of platelet activation (21). No blood clot was formed with 3.2% (w/v) citrate, a condition used in routine haematological laboratories worldwide and included as control in this study. Neither was any clot formed in 0.7% (w/v) citrate supplemented in either lepirudin or GPRP blood sampling conditions. We found that after one centrifugation, 71.1 ± 2.7% of platelets remained in 3.2% citrated blood after removing the PRP layer (**Figure 1A**). These numbers in lepirudin- and GPRP-anticoagulated blood were 84.9 ± 13.3% and 31.7 ± 29.4%, respectively (**Figure 1A**).

Three more washing steps were applied by repeated centrifugation and the number of platelets remaining in the residual blood reduced after each step (**Figure 1A**). At the end (4^{th} centrifugation) of the washing process, 6.1 ± 0.6% and 3.7 ± 1.8% of platelets remained in lepirudin- and GPRP-anticoagulated blood, respectively, while this number in 3.2% citrated blood was 7.0 ± 1.3%. Throughout the process, MPV remained at <10 fl throughout the successive washing steps (**Figure 1B**). In addition, the cell counts of other blood cells, i.e., white and red blood cells, remained mainly unchanged (**Supplementary Figure 6**).

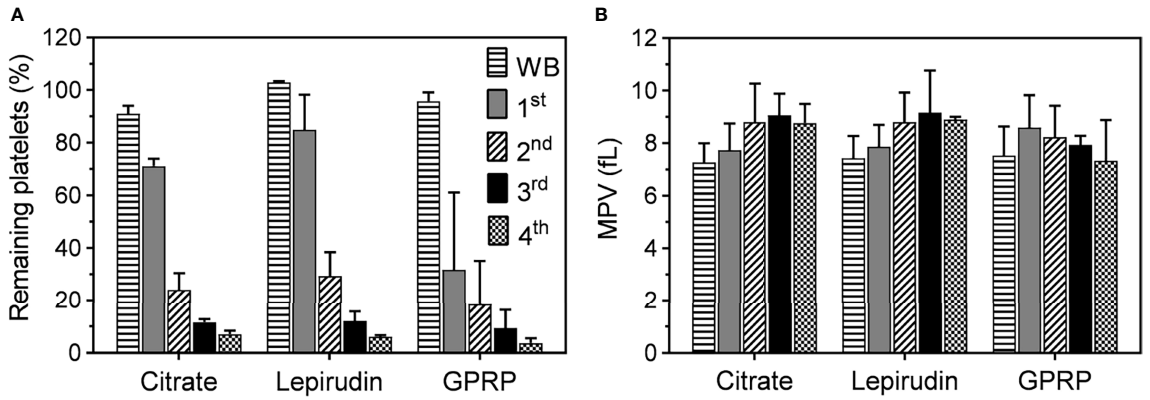

FIGURE 1 | Platelet counts and mean platelet volume (MPV) during the platelet separation process. **(A)** The number of platelets in whole blood immediately after collection (WB) and after the first (1st), second (2nd), third (3rd), and fourth (4th) centrifugation. Blood was collected in tubes containing either lepirudin or GPRP, supplemented with 0.7% (w/v) citrate, (labelled in the graphs as "Lepirudin" and "GPRP") or 3.2% (w/v) citrate only (labelled as "Citrate"), with blood to anticoagulant ratio 9:1. Data are presented as the normalized mean percentage of platelet number ± standard deviation (SD) for each donor (n = 9). **(B)** Mean platelet volume (MPV), as an indicator of platelet integrity, remained at <10 fl throughout the whole purification process. Data are presented as mean of MPV ± standard deviation (SD). Blood from each donor (n = 9) was analysed in triplicates.

Activation of Platelets

In addition to measuring MPV of platelets as an indicator of platelet activation (**Figure 1B**), we further characterized the expression of platelet activation markers on the platelet surface. Both CD63 and CD62P markers from dense and alpha granules, respectively, were detected at background levels immediately after blood collection and remained almost unchanged after preparing the PRP suspension until 4 hours after blood sampling (**Figures 2A, B**), implying minimal activation of the platelets (22). Equally important, platelets retained their functions in response to *E. coli*. Upon re-calcification, incubation with *E. coli* for 15 minutes at 37°C induced a substantial expression of both CD63 and CD62P on platelets in PRP suspension from both citrate 3.2% (w/v) and GPRP (**Figures 2A, B**). In contrast, platelets prepared from lepirudin-anticoagulated blood only expressed background levels of CD63 and CD62P when incubated with *E. coli* (**Figures 2A, B**).

Upon activation, platelets undergo morphological changes and enhance the expression of surface markers like CD63 and CD62P and release alpha granule-stored βTG (23). In 3.2% (w/v) citrate and in GPRP-anticoagulated blood, βTG was detected at ~1000 UI/ml after re-calcification and incubation at 37°C for 15 minutes (**Figure 2C**). After platelet depletion, the level of βTG in 3.2% (w/v) citrate and GPRP-anticoagulated blood dropped to 10 - 15% of the corresponding platelet-intact whole blood (**Figure 2C**). A virtually identical pattern was observed with TAT, which was detected at levels up to 6 μg/ml before platelet removal and decreased to 0.2 μg/ml after platelet depletion (**Figure 2D**). In contrast, βTG and TAT were detected at background levels in lepirudin-anticoagulated blood both before and after platelet depletion (**Figures 2C, D**). The activation of platelets in blood was confirmed under SEM (**Figures 2E–G**). Platelets isolated from 3.2% (w/v) citrate-, lepirudin-, and GPRP-anticoagulated blood were activated under thrombin stimulation, as evidenced by their wide-spreading (**Figures 2E–G**), indicating that platelets retained their functions during the separation process (21).

Activation of Granulocytes and Monocytes

Granulocytes and monocytes play an important role in the acute inflammatory response (24, 25). We characterized the activation of these cells in blood before and after platelet separation. The expression level of the activation marker CD11b on both granulocytes and monocytes in all anticoagulants was low immediately after blood sampling and remained unchanged after the blood underwent successive washing steps (**Figures 3A, B**). To confirm that the protocol did not interfere with cell functions, the activation of these cells was evaluated in platelet-depleted blood. *E. coli* at 10^7/ml induced a 5-fold increase in CD11b expression, which was comparable to the activation levels in whole blood incubated with *E. coli* after collection without centrifugation (**Figures 3A, B**).

Complement receptor 1 or CD35, with C3b as the main ligand, is expressed on the surface of both monocytes and granulocytes, and an up-regulation of CD35 is indicative of the activation status of these cells (26). Similar to CD11b, we found that the expression of CD35 was not affected by the platelet separation protocol and responded to *E. coli* incubation (**Figures 3C, D**).

Plasma Cytokine Release

Having shown that our protocol effectively removed platelets from whole blood (**Figure 1**), while not activating platelets (**Figure 2**), granulocytes and monocytes (**Figure 3**), we further profiled the release of ten inflammatory cytokines and chemokines in platelet-depleted blood in response to *E. coli*, including IL-1β, IL-1Ra, IL-6, IL-8, IFN-γ, IP-10, MCP-1, MIP-1α, MIP-1β, and TNF. This panel was selected basing on its elevation in response to *E. coli* in whole blood after a 4-hour

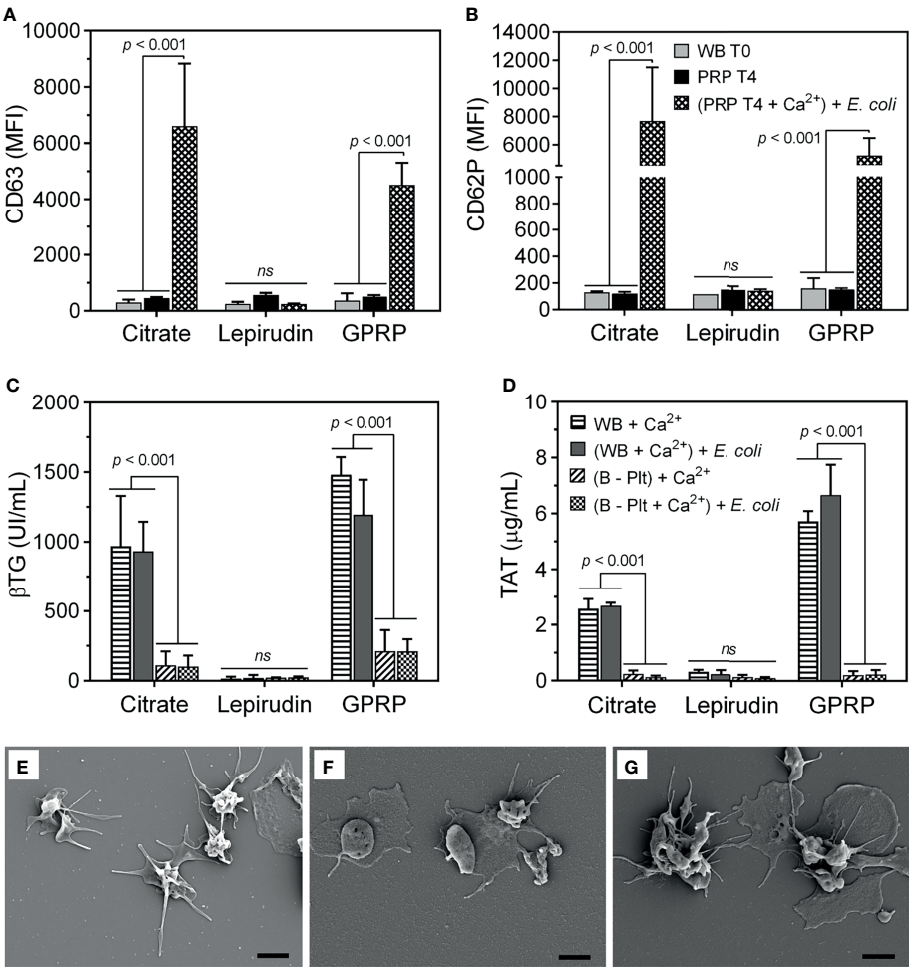

FIGURE 2 | Evaluation of platelet activation during the platelet separation process. The activation of platelets was evaluated by the expression of **(A)** CD63 and **(B)** CD62P on the platelet surface using flow cytometry. The expression of CD63 and CD62P was measured in whole blood immediately after collection (indicated as "WB T0") and in platelet-rich plasma (PRP) 4 hours after platelet isolation (indicated as "PRP T4"). In addition, 4 hours after platelet separation, platelet activation was induced by incubation with *E. coli* (10^7/ml, indicated as "(PRP T4 + Ca^{2+}) + *E. coli*" after re-calcification. Data are presented as mean of median fluorescence intensity (MFI) ± standard deviation (SD) (n = 9). **(A, B)** have the same annotation as shown in **(B)**. In addition, platelet activation was evaluated by its soluble activation marker **(C)** β-thromboglobulin (βTG) and thrombin generation by **(D)** thrombin-antithrombin complex (TAT) in plasma from whole blood after blood sampling (WB + Ca^{2+}) and whole blood after platelet-depletion [(B - Plt) + Ca^{2+}], or after incubation with *E. coli* for 15 minutes, indicated as "(WB + Ca^{2+}) + *E. coli*" and "(B - Plt + Ca^{2+}) + *E. coli*", respectively. Data are represented as mean ± standard deviation (SD) (n = 6). **(C, D)** have the same annotation as shown in **(D)**. Platelet activation was further evaluated with scanning electron microscopy, as presented in an image representative of 6-9 samples collected **(E–G)**. Platelets were collected in plasma-rich plasma (PRP) from whole blood anticoagulated with 3.2% (w/v) citrate **(E)**, lepirudin (50 µg/ml) supplemented with 0.7% (w/v) citrate **(F)**, and GPRP (8 mg/ml) supplemented with 0.7% (w/v) citrate **(G)**. Thrombin was used as a platelet activator. The scale bar at the lower right represents 2 µm. ns, non significant.

incubation. Remarkable reductions were observed in the release of seven cytokines in platelet-depleted blood as compared to whole blood, including IL-8 (**Figure 4A**), IL-1β, IL-1Ra, IL-6, IP-10, MIP-1α, and MIP-1β (**Supplementary Figures 7A–F**). Meanwhile, there was no apparent difference in the release of IFN-γ, MCP-1, and TNF before and after platelet removal (**Supplementary Figures 7G–J**).

IL-8 levels were elevated in GPRP-whole blood in response to *E. coli* and decreased to background level in platelet-depleted blood (**Figure 4A**). However, IL-8 levels in GPRP-anticoagulated blood were resurgent in platelet-depleted blood upon the addition of either the platelet-plasma suspension or only the supernatant from activated platelets (**Figure 4A**). This result indicated that the increased IL-8, which we previously characterized to be dependent on thrombin, was mediated *via* the activation of platelets.

We investigated the role of platelets in the upregulation of IL-8 by measuring plasma levels of IL-8 in PRP, in platelet-depleted blood, and in GPRP-whole blood upon *E. coli* incubation. Interestingly, plasma IL-8 was detected at 4.19 ng/ml in PRP prepared from GPRP anticoagulated blood (**Figure 4B**). Lepirudin was also included here as control and the IL-8-level

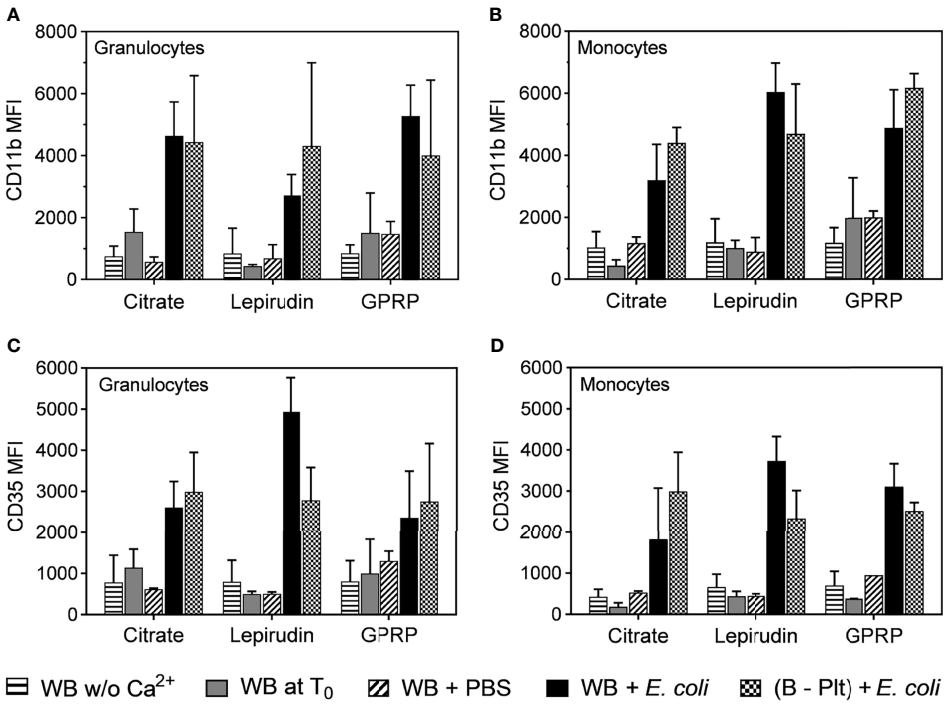

FIGURE 3 | Activation of granulocytes and monocytes during the platelet depletion process. The activation of granulocytes **(A, C)** and monocytes **(B, D)** were evaluated by the surface expression levels of CD11b **(A, B)** and CD35 **(C, D)** by flow cytometry. The activation of these cells was measured in whole blood immediately after collection without re-calcification (indicated as "WB w/o Ca^{2+}") or whole blood with Ca^{2+} added at T0 (WB at T0). In addition, the activation of granulocytes and monocytes in Ca^{2+} supplemented whole blood was incubated with PBS (WB + PBS) or *E. coli* (WB + *E. coli*). After platelet removal, these cells were activated with *E. coli* ((B – Plt) + *E. coli*). All incubations were carried out for 15 minutes after the addition of Ca^{2+}. Data are presented as mean of median fluorescence intensity (MFI) ± standard deviation (SD) (n = 9).

was detected at 0.22 ng/ml in PRP from lepirudin-anticoagulated blood. Plasma IL-8 was also detected at 5.81 and 5.36 ng/ml in platelet-depleted blood anticoagulated with lepirudin and GPRP, respectively (**Figure 4B**). Notably, IL-8 level increased up to 26.36 ng/ml in whole blood anticoagulated with GPRP (**Figure 4B**).

The activation of platelets was confirmed by a significant increase of platelet-derived growth factor (PDGF) in PRP and whole blood prepared with GPRP (**Figure 4C**) (27). The levels of PDGF were not significantly different between PRP and whole blood prepared with GPRP (**Figure 4C**). In contrast, in platelet-removed blood, PDGF was detected at background levels and there was no difference in PDGF levels between lepirudin- and GPRP-blood (**Figure 4C**).

We further investigated which leukocyte population was the main source of IL-8. Intracellular cytokine staining showed that IL-8 was mainly generated by monocytes (**Figure 4D**). As such, monocytes alone attributed to an average IL-8 intensity of 3485 MFI, which was comparable to that of platelets (3502 MFI) (**Figure 4D**). However, the intensity of IL-8 increased over 17 folds, to 59690 MFI when monocytes were found in conjugation with platelets (**Figure 4D**). Meanwhile, IL-8 in granulocytes was detected at 6417 MFI and increased 1.3 folds to an intensity of 8397 MFI together with platelets (**Figure 4D**).

DISCUSSION

We have recently characterized the four-amino acid peptide GPRP for the anticoagulation of human whole blood for up to 8 hours at 37°C (16). In this whole blood model, we found that βTG and TAT were instantly generated in the anticoagulated blood during the process of blood sampling. This was dependent on instant activations of the coagulation system and platelets in the blood from contact with the surfaces of the needle, the sampling tube and the contact with air. Thus, in this study, we exploited citrate at low concentration (0.7%, w/v) supplemented in GPRP for controlling the instant thrombin activation. With citrate, we could gently separate platelets from whole blood and study the contribution of platelets in the inflammatory response to *E. coli*. We chose to combine citrate with GPRP since the citrate-dependent chelation of Ca^{2+} ions is reversible (10), and with GPRP, we blocked the coagulation cascade without interfering with thrombin. Altogether, this approach offered a holistic system to study thromboinflammation in an *ex vivo* blood model.

The addition of citrate to GPRP-whole blood prevented the instant platelet activation in a manner dependent on citrate concentration and 0.7% citrate (w/v) was selected for further experiments (**Supplementary Figure 4**). The parallel result was observed in lepirudin-anticoagulated blood supplemented with

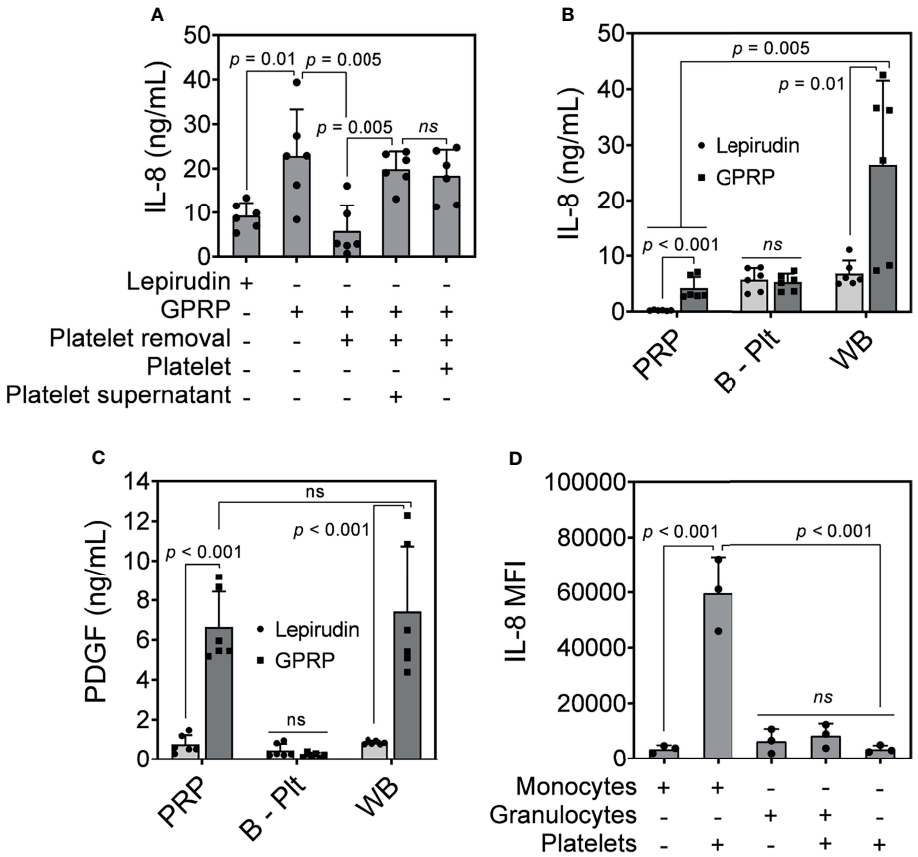

FIGURE 4 | IL-8 release in response to *E. coli*. **(A)** IL-8 was measured in GPRP-anticoagulated blood after incubation with *E. coli* (10^7/ml) for 4 hours after the addition of Ca^{2+}. The IL-8 levels were compared in whole blood, in platelet-depleted blood ("Platelet removal"), in platelet-plasma reconstituted ("Platelet"), and in reconstituted plasma supernatant from activated platelets ("Platelet supernatant"). **(B)** IL-8 and **(C)** PDGF measured in activated platelet-rich plasma (PRP), in platelet-depleted blood (B - Plt) and in whole blood (WB), all anticoagulated with either GPRP or lepirudin. Data are presented as mean ± standard deviation (SD) (n = 6). **(D)** Detection of intracellular IL-8 by flow cytometry in GPRP-anticoagulated blood. Data are presented as mean of median fluorescence intensity (MFI) ± standard deviation (SD) from 3 blood donors with each dot representing average MFI of two replicates from each donor. ns, non significant.

0.7% citrate (w/v) (**Supplementary Figure 5**), reflecting the nature of this *ex vivo* blood model. As such, thrombin, as a potent platelet activator and a key component in the coagulation cascade, is blocked in lepirudin-anticoagulated blood (15), and consequently, the addition of citrate did not affect platelet activation. Although 0.7% (w/v) citrate was sufficient to stabilize platelets initially in GPRP-whole blood, it did not completely prevent blood from clotting by itself.

The high percentage of platelets remaining in whole blood after the first centrifugation indicated that one round of 15 minutes centrifugation at 180×*g* was not sufficient to remove all platelets from whole blood. The remaining platelets may exert their effects, leading to an inaccurate conclusion unnoticedly and necessitating a method to completely remove platelets from whole blood. After three successive washing steps, platelets were successfully removed with only <4% of platelets remaining in GPRP-blood supplemented with 0.7% citrate (w/v) (**Figure 1A**). As an indicator of platelet activation, MPV remained at <10 fl (**Figure 1B**), which was within the acceptable range of 7.2 to 11.7 fl (28), implying that platelet integrity was kept intact throughout the washing process (22).

A major concern during the separation of platelets is that platelet activation may be induced unintentionally. In addition to acceptable MPV (**Figure 1B**), background levels of both CD63 and CD62P suggested low activation levels of platelets, if any, from blood sampling up to 4 hours of storing platelets in PRP (**Figures 2A, B**). Upon incubation with *E. coli*, separated platelets from 3.2% (w/v) citrate and GPRP supplemented with 0.7% (w/v) citrate blood activated normally as evidenced in significant increases of CD63 and CD62P (**Figures 2A, B**) and their well-spread morphologies in SEM images (**Figures 2E–G**) (29). These responses suggested that platelets retained their functions during the separation process. Background levels of βTG and TAT detected in blood after platelet removal when incubated with *E. coli* confirmed a minimal residual number of platelets (**Figures 2C, D**), which was consistent with the low platelet counts in platelet-depleted blood observed earlier (**Figure 1A**). Platelets prepared from thrombin inhibitor

lepirudin-anticoagulated blood only expressed background levels of CD63 and CD62P even in incubation with *E. coli* (**Figures 2A, B**), confirming the role of thrombin as a crucial platelet activator (12). Taken together, these results suggested that the whole separation process did not induce detectable activation of the platelets, and the separated platelets retained their functions by responding to stimuli.

Our method of platelet removal from whole blood was based on repeated centrifugations, which may induce activation of other circulating cells in the blood, especially granulocytes and monocytes, which are critically involved in the acute inflammatory response (24, 25). CD11b/CD18 (complement receptor 3, CR3) is involved in cellular adhesion and migration, and is the most important complement phagocytosis receptor using iC3b as a ligand (30). CD11b is rapidly increased during leukocyte activation; hence, a low expression of CD11b observed in both granulocytes and monocytes correlated with a low level of activation of these cells (**Figures 3A, B**). Similarly, low expression of CD35 or complement receptor 1, with C3b as its main ligand, suggested a low activation status of granulocytes and monocytes (**Figures 3C, D**) (26). However, the expression of both CD11b and CD35 in platelet-removed blood increased up to the levels of those in whole blood in response to *E. coli* incubation, confirming these cells were functional after the platelet removal process (**Figure 3**).

Among the seven cytokines that were platelet-dependent (**Figure 4A** and **Supplementary Figures 7A–F**), IL-1β is crucially dependent on inflammasome activation; IL-6 are typical of early pro-inflammatory mediators; IL-10 and IL-1Ra are typically anti-inflammatory; whereas IL-8, MIP-1α, and MIP-1β are highly potent chemokines. Interestingly, the levels of these cytokines were resurgent by adding back to platelet-removed blood either separated platelets or the supernatant of activated platelets. This resurgence implied that the activation of platelets serves as a trigger for the release of these cytokines in whole blood upon *E. coli* incubation.

Also shown as platelet-dependent cytokine (**Figure 4A**), IL-8 was detected at 4.1 ± 1.9 ng/ml in the PRP portion of GPRP-anticoagulated blood and at 0.2 ± 0.1 ng/ml in the PRP portion of lepirudin-anticoagulated blood (**Figure 4B**), suggesting that platelets released IL-8 in a thrombin-dependent manner. Higher than background levels of IL-8 detected in platelet-removed blood indicated that IL-8 was also released or stored by other cells and this IL-8 source was not dependent on platelets (**Figure 4B**). However, IL-8 detected in GPRP-whole blood was significantly higher than those in the PRP portion of GPRP-blood and lepirudin-whole blood, meaning that platelets potentiated the release of IL-8 from leukocytes. Both platelets and leukocytes can independently release IL-8 into plasma, but for the leukocytes to produce and release IL-8 at higher levels, it needs the potentiation from platelets. The activation of platelets was confirmed with a significant increase of PDGF in both the PRP portion and whole blood anticoagulated with GPRP compared to lepirudin (**Figure 4C**). The elevation of IL-8 in monocytes, but not granulocytes, when incubated with platelets further revealed monocytes as a main source of IL-8. Combined with the resurgence of IL-8 in platelet-removed blood with the addition of either platelets or the supernatant from activated platelets (**Figure 4A**) and intracellularly detected IL-8 (**Figure 4D**), these results supported monocytic origin of the IL-8 release; however, this increase was triggered in response to activated platelets.

In conclusion, we present here an approach to separate and, in parallel, deplete platelets from human whole blood using GPRP in combination with low levels of citrate as an anticoagulant. This method removed 96% of the platelets in whole blood, mitigating their effects in the inflammatory response in whole blood. This method showed remarkably low background activity during the process, and with platelets not undergoing methodological activation. We unravelled the essential role of platelets in potentiating bacterial-induced IL-8 release from monocytes in human whole blood.

DATA AVAILABILITY STATEMENT

The original contributions presented in the study are included in the article/**Supplementary Material**. Further inquiries can be directed to the corresponding author.

ETHICS STATEMENT

This study was designed and performed according to the ethical guidelines from the declaration of Helsinki. Informed written consent was obtained from the blood donors. The study was approved by the ethical committee of the Norwegian Regional Health Authority, ethical permit REK#S-04114, 2010/934. The patients/participants provided their written informed consent to participate in this study.

AUTHOR CONTRIBUTIONS

HQ conceived of the presented idea. HQ, CJ, KE, and RI carried out the experiments. HQ wrote the manuscript with support from CJ, TM, and PN. TM and PN supervised the project. All authors contributed to the article and approved the submitted version.

FUNDING

This study was financially supported by The Norwegian Research Council (Project No. 274332), The Swedish Research Council (Project No. 2018-04087), The Norwegian Council on Cardiovascular Disease, The Odd Fellow Foundation, The Simon Fougner Hartmann Family Fund, and The Crafoord Foundation (20190890 and 20210961).

SUPPLEMENTARY MATERIAL

The Supplementary Material for this article can be found online at: https://www.frontiersin.org/articles/10.3389/fimmu.2022.865386/full#supplementary-material

REFERENCES

1. Weyrich A, Lindemann S, Zimmerman G. The Evolving Role of Platelets in Inflammation. *J Thromb Haemostasis* (2003) 1:1897–905. doi: 10.1046/j.1538-7836.2003.00304.x
2. Thomas MR, Storey RF. The Role of Platelets in Inflammation. *Thromb Haemostasis* (2015) 114:449–58. doi: 10.1160/TH14-12-1067
3. Heemskerk JW, Bevers EM, Lindhout T. Platelet Activation and Blood Coagulation. *Thromb Haemostasis* (2002) 88:186–93. doi: 10.1055/s-0037-1613209
4. Hirsh J, O'donnell M, Weitz JI. New Anticoagulants. *Blood* (2005) 105:453–63. doi: 10.1182/blood-2003-12-4195
5. Franco AT, Corken A, Ware J. Platelets at the Interface of Thrombosis, Inflammation, and Cancer. *Blood* (2015) 126:582–8. doi: 10.1182/blood-2014-08-531582
6. Sekhon UDS, Sen Gupta A. Platelets and Platelet-Inspired Biomaterials Technologies in Wound Healing Applications. *ACS Biomaterials Sci Eng* (2017) 4:1176–92. doi: 10.1021/acsbiomaterials.7b00013
7. Furie B, Furie BC. The Molecular Basis of Blood Coagulation. *Cell* (1988) 53:505–18. doi: 10.1016/0092-8674(88)90567-3
8. Packham M, Bryant N, Guccione M, Kinlough-Rathbone R, Mustard J. Effect of the Concentration of Ca2+ in the Suspending Medium on the Responses of Human and Rabbit Platelets to Aggregating Agents. *Thromb Haemostasis* (1989) 62:968–76. doi: 10.1055/s-0038-1651037
9. Bates SM, Weitz JI. The Status of New Anticoagulants. *Br J Haematology* (2006) 134:3–19. doi: 10.1111/j.1365-2141.2006.06134.x
10. Mann KG, Whelihan M, Butenas S, Orfeo T. Citrate Anticoagulation and the Dynamics of Thrombin Generation. *J Thromb Haemostasis* (2007) 5:2055–61. doi: 10.1111/j.1538-7836.2007.02710.x
11. Adcock DM, Kressin DC, Marlar RA. Effect of 3.2% vs 3.8% Sodium Citrate Concentration on Routine Coagulation Testing. *Am J Clin Pathol* (1997) 107:105–10. doi: 10.1093/ajcp/107.1.105
12. Monroe DM, Hoffman M, Roberts HR. Platelets and Thrombin Generation. *Arteriosclerosis Thrombosis Vasc Biol* (2002) 22:1381–9. doi: 10.1161/01.atv.0000031340.68494.34
13. Wallen NH, Ladjevardi M, Albert J, Broijersen A. Influence of Different Anticoagulants on Platelet Aggregation in Whole Blood; a Comparison Between Citrate, Low Molecular Mass Heparin and Hirudin. *Thromb Res* (1997) 87:151–7. doi: 10.1016/s0049-3848(97)00114-x
14. Markiewski MM, Nilsson B, Ekdahl KN, Mollnes TE, Lambris JD. Complement and Coagulation: Strangers or Partners in Crime? *Trends Immunol* (2007) 28:184–92. doi: 10.1016/j.it.2007.02.006
15. Mollnes TE, Brekke O-L, Fung M, Fure H, Christiansen D, Bergseth G, et al. Essential Role of the C5a Receptor in E Coli–Induced Oxidative Burst and Phagocytosis Revealed by a Novel Lepirudin-Based Human Whole Blood Model of Inflammation. *Blood* (2002) 100:1869–77. doi: 10.1182/BLOOD.V100.5.1869.H81702001869_1869_1877
16. Nilsson PH, Johnson C, Quach QH, Macpherson A, Durrant O, Pischke SE, et al. A Conformational Change of Complement C5 Is Required for Thrombin-Mediated Cleavage, Revealed by a Novel *Ex Vivo* Human Whole Blood Model Preserving Full Thrombin Activity. *J Immunol* (2021) 207:1641–51. doi: 10.4049/jimmunol.2001471
17. Elenkov IJ, Iezzoni DG, Daly A, Harris AG, Chrousos GP. Cytokine Dysregulation, Inflammation and Well-Being. *Neuroimmunomodulation* (2005) 12:255–69. doi: 10.1159/000087104
18. Baggiolini M, Clark-Lewis I. Interleukin-8, a Chemotactic and Inflammatory Cytokine. *FEBS Lett* (1992) 307:97–101. doi: 10.1016/0014-5793(92)80909-Z
19. Singer M, Sansonetti PJ. IL-8 is a Key Chemokine Regulating Neutrophil Recruitment in a New Mouse Model of Shigella-Induced Colitis. *J Immunol* (2004) 173:4197–206. doi: 10.4049/jimmunol.173.6.4197
20. Berg A, Otterdal K, Patel S, Gonca M, David C, Dalen I, et al. Complement Activation Correlates With Disease Severity and Contributes to Cytokine Responses in Plasmodium Falciparum Malaria. *J Infect Dis* (2015) 212:1835–40. doi: 10.1093/infdis/jiv283
21. Thon JN, Italiano JE. "Platelets: Production, Morphology and Ultrastructure,". In: *Antiplatelet Agents*. Heidelberg: Springer (2012). p. 3–22.
22. Choudhury A, Chung I, Blann AD, Lip GY. Platelet Surface CD62P and CD63, Mean Platelet Volume, and Soluble/Platelet P-Selectin as Indexes of Platelet Function in Atrial Fibrillation: A Comparison of "Healthy Control Subjects" and "Disease Control Subjects" in Sinus Rhythm. *J Am Coll Cardiol* (2007) 49:1957–64. doi: 10.1016/j.jacc.2007.02.038
23. Kamath S, Blann A, Lip G. Platelet Activation: Assessment and Quantification. *Eur Heart J* (2001) 22:1561–71. doi: 10.1053/euhj.2000.2515
24. Shi C, Pamer EG. Monocyte Recruitment During Infection and Inflammation. *Nat Rev Immunol* (2011) 11:762. doi: 10.1038/nri3070
25. Kolaczkowska E, Kubes P. Neutrophil Recruitment and Function in Health and Inflammation. *Nat Rev Immunol* (2013) 13:159. doi: 10.1038/nri3399
26. Roozendaal R, Carroll MC. Complement Receptors CD21 and CD35 in Humoral Immunity. *Immunol Rev* (2007) 219:157–66. doi: 10.1111/j.1600-065X.2007.00556.x
27. Andrae J, Gallini R, Betsholtz C. Role of Platelet-Derived Growth Factors in Physiology and Medicine. *Genes Dev* (2008) 22:1276–312. doi: 10.1101/gad.1653708
28. Demirin H, Ozhan H, Ucgun T, Celer A, Bulur S, Cil H, et al. Normal Range of Mean Platelet Volume in Healthy Subjects: Insight From a Large Epidemiologic Study. *Thromb Res* (2011) 128:358–60. doi: 10.1016/j.thromres.2011.05.007
29. Aslan JE, Itakura A, Gertz JM, Mccarty OJ. "Platelet Shape Change and Spreading". In: *Platelets and Megakaryocytes*. New York: Springer (2012). p. 91–100.
30. Hughes B, Hollers J, Crockett-Torabi E, Smith CW. Recruitment of CD11b/CD18 to the Neutrophil Surface and Adherence-Dependent Cell Locomotion. *J Clin Invest* (1992) 90:1687–96. doi: 10.1172/JCI116041

Conflict of Interest: The authors declare that the research was conducted in the absence of any commercial or financial relationships that could be construed as a potential conflict of interest.

frontiers | Frontiers in Immunology

ORIGINAL RESEARCH
published: 04 April 2022
doi: 10.3389/fimmu.2022.806686

Nanodiamond-Induced Thrombocytopenia in Mice Involve P-Selectin-Dependent Nlrp3 Inflammasome-Mediated Platelet Aggregation, Pyroptosis and Apoptosis

*Shih-Che Hung[1], Lu-Chu Ke[2], Te-Sheng Lien[2], Hsuan-Shun Huang[3], Der-Shan Sun[1,2], Chia-Liang Cheng[4] and Hsin-Hou Chang[1,2]**

[1] Institute of Medical Sciences, Tzu-Chi University, Hualien, Taiwan, [2] Department of Molecular Biology and Human Genetics, Tzu-Chi University, Hualien, Taiwan, [3] Center for Prevention and Therapy of Gynecological Cancers, Department of Research, Buddhist Tzu Chi General Hospital, Hualien, Taiwan, [4] Department of Physics, National Dong Hwa University, Hualien, Taiwan

Nanodiamond (ND) has been developed as a carrier to conduct various *in vivo* diagnostic and therapeutic uses. Safety is one of the major considerations, while the hemocompatibility of ND is not clearly addressed. Here we found that, compared to the other sizes of ND with relatively inert properties, treatments of 50 nm ND induced stronger platelet aggregation, platelet pyroptosis, apoptosis and thrombocytopenia in mice. Blockage treatments of soluble P-selectin, reactive oxygen species (ROS), and Nlrp3 inflammasome inhibitors markedly suppressed such adverse effects, suggesting ND-induced platelet activation and pyroptosis involves surface P-selectin-mediated enhancement of mitochondrial superoxide levels and Nlrp3 inflammasome activation. In addition, challenges of NDs induced less platelet pyroptosis and displayed less thrombocytopenia in P-selectin (*Selp*$^{-/-}$), Nlrp3 (*Nlrp3*$^{-/-}$) and caspase-1 (*Casp1*$^{-/-}$) mutants, as compared to the wild type mice. Blockers of P-selectin, ROS, and Nlrp3 inflammasome pathways could be considered as antidotes for ND induced platelet activation and thrombocytopenia.

Keywords: nanodiamond induced thrombocytopenia, P-selectin, inflammasome, pyroptosis, platelet regulated cell death, apoptosis, necroptosis, ferroptosis

OPEN ACCESS

Edited by:
Fabrice Cognasse, INSERM U1059 SAnté INgéniérie BIOlogie, France

Reviewed by:
Rostyslav Bilyy, Danylo Halytsky Lviv National Medical University, Ukraine
Kerstin Jurk, Johannes Gutenberg University Mainz, Germany

***Correspondence:**
Hsin-Hou Chang
hhchang@mail.tcu.edu.tw;
hhchang@gms.tcu.edu.tw

Specialty section:
This article was submitted to Inflammation, a section of the journal Frontiers in Immunology

Received: *01 November 2021*
Accepted: *09 March 2022*
Published: *04 April 2022*

Citation:
Hung S-C, Ke L-C, Lien T-S, Huang H-S, Sun D-S, Cheng C-L and Chang H-H (2022) Nanodiamond-Induced Thrombocytopenia in Mice Involve P-Selectin-Dependent Nlrp3 Inflammasome-Mediated Platelet Aggregation, Pyroptosis and Apoptosis. Front. Immunol. 13:806686. doi: 10.3389/fimmu.2022.806686

INTRODUCTION

With reduced sizes, nanomaterials exert unique physio-chemical properties and are suitable for biomedical applications (1, 2). Among these, nanodiamond (ND) is one of the promising materials attracting researcher's attentions. With unique spectroscopic properties such as Raman, infrared, and defect-induced color centers fluorescence, ND has been demonstrated as a feasible optical probe

in biomedical usages (3–5). In addition, the excellent physical and chemical stability further enable ND as the most biocompatible nanoparticle in the carbon family (5). Early cellular studies have revealed low cytotoxicity of ND. Evidences have shown that ND exerted no toxicity to various cell types, and did not induce cellular reactive oxygen species (ROS) (6, 7). These results and later cell line investigations have concluded that ND is a low cytotoxic material (8).

Despite of these *in vitro* studies, more recent studies have suggested ND is a promising and useful material for drug delivery and bio-labeling (5, 9–11). Because of the potential biomedical applications of ND, and low hemocompatibility limits the use of nanoparticles (12, 13), the hemocompatibility analyses become essential for NDs.

The hemocompatibility of a nanomaterial could be characterized by property on the induction of platelet activation, platelet aggregation, thrombocytopenia and thrombosis after *in vivo* treatments (12, 14–18). Platelets are small anucleate multifunctional blood cells, which involve in many pathophysiological processes including coagulation, thrombosis, inflammation, and innate immunity (18–20). Inflammasomes are caspase-1 containing cytosolic multiprotein complexes, and are activated by pattern recognition receptors in responses to stimulations of pathogen-associated molecular patterns (PAMPs) and danger-associated molecular patterns (21–25). The activated caspase-1 cleaves the immature precursors and leads to the production of mature form of proinflammatory cytokine interleukin-1β (IL-1β), and pore-forming protein gasdermins (26–28). Inflammasomes play critical roles in platelet-mediated inflammation and coagulation (29–31). Expression levels of inflammasome (32) and IL-1β (33–35) in platelets could be up-regulated after stimulations by PAMPs. In addition, platelet inflammasome activation has been revealed in sepsis (36), thrombosis formation (37) and hindlimb ischemia (32) models. Despite the detailed mechanism remains to be further elucidated, activation of inflammasome by dengue virus has been associated with induction of platelet pyroptosis (38). Pyroptosis belongs to the family of regulated cell deaths (RCDs), which include additional cell death pathways such as apoptosis, necroptosis, ferroptosis and autophagy (39–41). Evidences have suggested that RCDs involve in platelet maturation, activation and aggregation (29, 42–45). However, the property of NDs on the induction of platelet cell death remains elusive.

NLR pyrin domain containing 3 (Nlrp3) inflammasome is one of the most studied inflammasomes, sensing a variety of cellular stresses and stimulus, such as ROS, toxins, pathogens, metabolites, nucleic acids, uric acid crystals and nanoparticles (46–50). Several lines of evidences have implicated that over activation of inflammasomes through different pathways in cells can lead to major types of RCDs, including pyroptosis (47), apoptosis (51, 52), necroptosis (52), ferroptosis (53) and autophagy (54, 55). For example, inflammasome activation leads to the maturation and activation of pore-forming protein gasdermins, cell membrane rupture and cell death in pyroptosis (47). Inflammasome activation also leads to apoptosis through Bid and caspase-8 pathways in gasdermin deficient cell models (51). Z-DNA binding protein 1 (ZBP1), a regulator of Nlrp3 inflammasome, was shown to induce pyroptosis, apoptosis, and necroptosis (52). Ferroptosis is associated with inflammasome activation in placental trophoblast cell model of oxidative stress (53). Overexpression of NLRP3 inflammasome components elevated autophagy, and, conversely, silencing of the NLRP3 downregulated autophagy (54). However, these results are obtained from diverse cell models. The regulation networks between inflammasome and these RCDs in a single cell type remains greatly unknown. In addition, the impact of ND treatments on the stimulation of platelet inflammasomes and RCDs remains unclear.

To analyze the hemocompatibility of ND, in this present study, we investigate ND-induced platelet changes *in vitro* and thrombocytopenia *in vivo*. The analyses data revealed that ND induces platelet aggregation is associated with P-selectin-dependent enhanced ROS-medicated activation of Nlrp3 inflammasome and subsequently platelet pyroptosis. Challenges of NDs induced less platelet cell death in P-selectin (*Selp*$^{-/-}$), Nlrp3 (*Nlrp3*$^{-/-}$) and caspase-1 (*Casp1*$^{-/-}$) null mice as compared to the wild type mice. Treatments of inhibitors against P-selectin, ROS and Nlrp3 inflammasome pathways ameliorated both ND-induced platelet activation *in vitro* and ND-induced thrombocytopenia in mice. These results collective suggested that ND-induced Nlrp3 inflammation activation is one of the initiation steps leading to the platelet activation and thrombocytopenia *in vivo*. Administrations of ND with lower doses are helpful to reduce such platelet-related adverse effect. Related regulatory pathways in ND-stimulated platelets are discussed.

MATERIALS AND METHODS

Chemicals and Nanomaterials

The chemicals used in this study were purchased from Sigma-Aldrich (St. Louis, MO, USA). To prepare the stock solutions of 10 mg/mL TiO_2 (5 and 60 nm; Nanostructured & Amorphous Materials, Katy, TX, USA), 10 mg/mL NDs (5-200 nm; Kay Diamond Products, Boca Raton, FL. USA) (56, 57), and red fluorescent NDs (50 nm; brFND-50, nitrogen-vacancy NV centers per particle > 100, FND Biotech, Taipei, Taiwan) (58, 59), the nanoparticles (NPs) were dispersed in distilled deionized water under sonication (80 W/L, 46 kHz) for 20 min. Test NP solutions were prepared immediately before use by dilution of the stock solutions with distilled deionized water and sonication (80 W/L, 46 kHz) for 20 min (60).

Experimental Mice

Wild type male C57BL/6J mice (8–12 wk old) were obtained from the National Laboratory Animal Center (Taipei, Taiwan). Gene knockout mice with a C57BL/6J background, including *Nlrp3*$^{-/-}$ and *Casp1*$^{-/-}$ (61), were kindly provided by the Centre National de Recherche Scientifique (Orléans, France) (61–63). C57BL/6J male mice (8–12 wk old) deficient in P-selectin (B6; 129S2-*Selp*^{tm1Hyn}/J) (*Selp*$^{-/-}$) (19, 64, 65) were purchased from the Jackson Laboratory (Maine, USA). All animals were maintained

in a specific-pathogen-free (SPF) facility in the Laboratory Animal Center of Tzu Chi University (Hualien, Taiwan).

Ethics Statement

Animal experiments in this study were conducted in agreement with the National (Taiwan Animal Protection Act, 2008) directive for the protection of laboratory animals. All experimental protocols for examining experimental animals were approved by the Animal Care and Use Committee of Tzu-Chi University, Hualien, Taiwan (approval ID: 108067).

Blood and Platelet Isolation and Parameter Analyses

Collected mouse blood samples were transferred into polypropylene tubes containing anticoagulant acid-citrate-dextrose solution (38 mM citric acid, 75 mM sodium citrate, and 100 mM dextrose) (64, 65). Washed platelets were prepared as previously described (19, 38). Platelet counts of mice were measured using a hematology analyzer (KX-21N; Sysmex, Kobe, Japan) (64–66).

In Vivo Analyses: The Induction and Rescue of Thrombocytopenia in Mice

Various sizes (5, 50, 100, 200 nm) of NDs, or different doses (0.3125, 0.625, 1.25 mg/kg) of 50 nm NDs were injected into mice intravenously. Platelet counts were analyzed 1, 4, 24 and 72 h later after ND treatments using a hematology analyzer (KX-21N; Sysmex). To perform rescue, regents were pretreated before administration of NDs (NAC 300 mg/kg, Sigma-Aldrich; MitoTEMPO 0.1 mg/kg, Sigma-Aldrich; OLT1177 50 mg/kg, Cayman Chemical, Ann Arbor, MI, USA; soluble recombinant P-selectin, rP-sel, 0.24 mg/kg, R&D Systems, Minneapolis, MN, USA; Z-WEHD-FMK, 7.5-750 μg/kg, R&D Systems; Z-DEVD-FMK, 6.5-65 μg/kg, R&D Systems), and then the platelet counts were then analyzed additional 1 h after ND treatments.

In Vitro Analyses: Platelet Regulated Cell Death and Mitochondrial Superoxide

Proteins (1 mg/mL), including bovine serum albumin (BSA) (Sigma-Aldrich), C-type lectin domain family 2 [CLEC2, a gift from Professor Shie-Liang Hsieh, Genomics Research Center, Academia Sinica, Taipei, Taiwan (67)], toll-like receptor 4 (TLR4; R&D Systems), rP-sel (R&D Systems), coated fluorescent silica beads (1 mg/mL, Bangs Laboratories, Fishers, IN, USA; Alex488-goat-anti-mouse antibody pre-coated before aforementioned protein coating) and red fluorescent NDs (1 mg/mL, brFND-50, FND-Biotech) were used to analyze ND protein binding. After incubation of NDs with different proteins for 1 h, the ND-protein complexes were analyzed using flow cytometer. To determine ND-induced platelet aggregation, mouse platelets (5×10^{7}/mL) were treated with NDs (30 μg/mL). After 1 h, the aggregated populations were analyzed using flow cytometry (gating in **Figure S1**). To analyze ND induced platelet cell death, washed mouse platelets from wild type and mutant (*Selp*$^{-/-}$, *Nlrp3*$^{-/-}$ and *Casp1*$^{-/-}$) mice were incubated with ND for 1 h in a shaker (20 rpm, 25°C) and then subjected to analyses by flow cytometers [Gallios, Beckman Coulter, Brea, CA, USA, and FACScalibur, BD Biosciences, San Jose, CA, USA (64, 65)] analyses after washed with PBS. Various regulated cell death (RCD) responses, including apoptosis (CaspGLOWTM Red Active Caspase-3 Staining Kit, BioVision, Milpitas, CA, USA), autophagy (Cyto-ID™ Autophagy Detection Kit, Enzo Life Sciences, Farmingdale, NY, USA), ferroptosis (C11 BODIPY 581/591, Cayman Chemical, Ann Arbor, MI, USA), necroptosis (RIP3/B-2 alexa Fluor 488, Santa Cruz Biotechnology, Santa Cruz, CA, USA), pyroptosis (Caspase-1 Assay, Green, ImmunoChemistry Technologies, MI, USA), and live/dead cell labeling (Zombie NIR Fixable Viability Kit, Biolegend, San Diego, CA, USA), were analyzed using respective cell labeling reagents (30 min in PBS). Notably, to avoid detecting those RCD signals not contributing by the ND treatments (e.g. those RCDs elicited by purification and manipulation processes), Zombie-live/dead cell labeling (30 min) should be performed immediately after ND treatments, and before the subsequent RCD signal staining (30 min); and then the RCD pattern only analyzing on dead-cell population indicating by Zombie-live/dead staining. Blockers and inhibitors were used to address the involvements of specific pathways in platelets from wild type mice (Z-WEHD-FMK, 10 μM, R&D Systems; Z-DEVD-FMK, 10 μM, R&D Systems; OLT1177, 10 μM, Cayman Chemical; NAC 150 ng/mL, Sigma-Aldrich; MitoTEMPO, 1 μM, Sigma-Aldrich; P-selectin: rP-sel, 100 ng/mL R&D Systems; 30 min pretreatments before addition of ND). To analyze the induction of mitochondrial superoxide, MitoSOX™ Red mitochondrial superoxide indicator was used (Thermo Fisher Scientific; 30 min in PBS). Carboxyfluorescein succinimidyl ester (CFSE, Sigma-Aldrich) and CellTracker Blue Dye (ThermoFisher Scientific, Waltham, MA, USA) were used to label mouse platelets for flow cytometry and microscopy analyses.

In Vitro Analyses: Confocal Microscopy Analysis on the Morphology of Platelet Aggregates

A confocal microscope (C2+, Nikon, Tokyo, Japan) was employed on the analysis of platelet aggregate morphology. Same conditions of treatment dosage for ND and cell death inhibitors were applied in the confocal microscopy as the conditions used in the platelet cell death analyses. To distinguish populations of platelets, NDs and platelet-ND aggregates, CellTracker Blue Dye (ThermoFisher Scientific) labeled mouse platelets, and red fluorescent 50 nm NDs (brFND-50, FND Biotech) were used in this experiment. The counts of platelet aggregates per field (> 400 pixels) and the total platelet aggregate area (pixels) per field were analyzed using ImageJ software (version 1.32; National Institutes of Health, USA) (38, 68).

Neutrophil Extracellular Traps Formation (NETosis)-Related Analyses

According to previously reported methods (69), neutrophils were purified from mouse blood samples using Ficoll-Paque (Ficoll-Paque Plus, 1.077 g/mL, GE Healthcare, Chicago, IL, USA) and dextran (Sigma-Aldrich) sedimentation (3% w/v) density gradient centrifugation and red blood cell lysis. A flow cytometer (Gallios, Beckman Coulter, Brea, CA, USA) and a

fluorescent anti-citrullinated histone H3 (CitH3) antibody (Abcam, Cambridge, UK) were used to investigate the neutrophil expression of NETosis marker CitH3 after treatments of supernatants from platelets or platelets plus NDs. To prepare the platelet supernatants, inhibitors (Z-WEHD-FMK, 10 μM, R&D Systems; Z-DEVD-FMK, 10 μM, R&D Systems; OLT1177, 10 μM, Cayman Chemical; NAC 150 ng/mL, Sigma-Aldrich; MitoTEMPO, 1 μM, Sigma-Aldrich; P-selectin: rP-sel, 100 ng/mL R&D Systems; 30 min pretreatments before addition of ND) were used to block ND-induced platelet activation and cell death. After treatments with or without NDs and inhibitors, platelet supernatants were harvested by centrifugation (2.5 x 10^4 g, 10 min; Benchtop Centrifuge, ThermoFisher Scientific) to remove platelets and NDs. Peptidyl arginine deiminase 4 (PAD4) inhibitor GSK484 (10μM, Sigma–Aldrich, St. Louis, MO, USA) was used to block neutrophil NETosis *in vitro* and *in vivo* as described (69).

Statistical Analyses

The means, standard deviation (SD), and statistics of the quantifiable data were calculated using Microsoft Office Excel 2003, SigmaPlot 10, and SPSS 17, respectively. Unless specified, the significance of the data was examined using one-way ANOVA, followed by the *post hoc* Bonferroni-corrected *t* test. A probability of type 1 error ($\alpha = 0.05$) was recognized as the threshold for statistical significance.

RESULTS

Different Sizes of NDs Induced Different Levels of Platelet-Count Suppression in Mice

To investigate how ND sizes influence the blood cell counts, various sizes (5 nm, 50 nm, 100 nm and 200 nm; **Figures 1A–C**) of NDs were intravenously injected into mice. Here we found that, compared to red blood cell and white blood cell counts, platelet counts displayed more divergence outcomes when treated with different sizes of NDs (**Figures 1A** vs. **B, C**), in which the 50 nm ND induced more severe thrombocytopenia as compared to nanoscaled titanium dioxide (TiO_2; 5 nm and 60 nm), and the other sizes of ND (**Figure 1A**, 50 nm ND vs. 5 nm, 100 nm, and 200 nm groups). Different doses (0.3, 0.6, 1.25 mg/kg) of 50 nm NDs were further injected into the mice to evaluate the dosage effect. Analysis data revealed that only treatments with low dose (0.3 mg/kg) did not displayed obvious effects, while treatments with doses higher than 0.6 mg/kg (0.625 and 1.25 mg/kg) of 50 nm ND caused markedly lower platelet counts in mice (**Figure 1D**).

Pyroptosis and Apoptosis Are Two Major Cell Death Pathways of Platelets Treated With 50 nm NDs

Evidences have suggested that platelet activation and aggregation involve RCD processes of platelets (42–45). However, whether

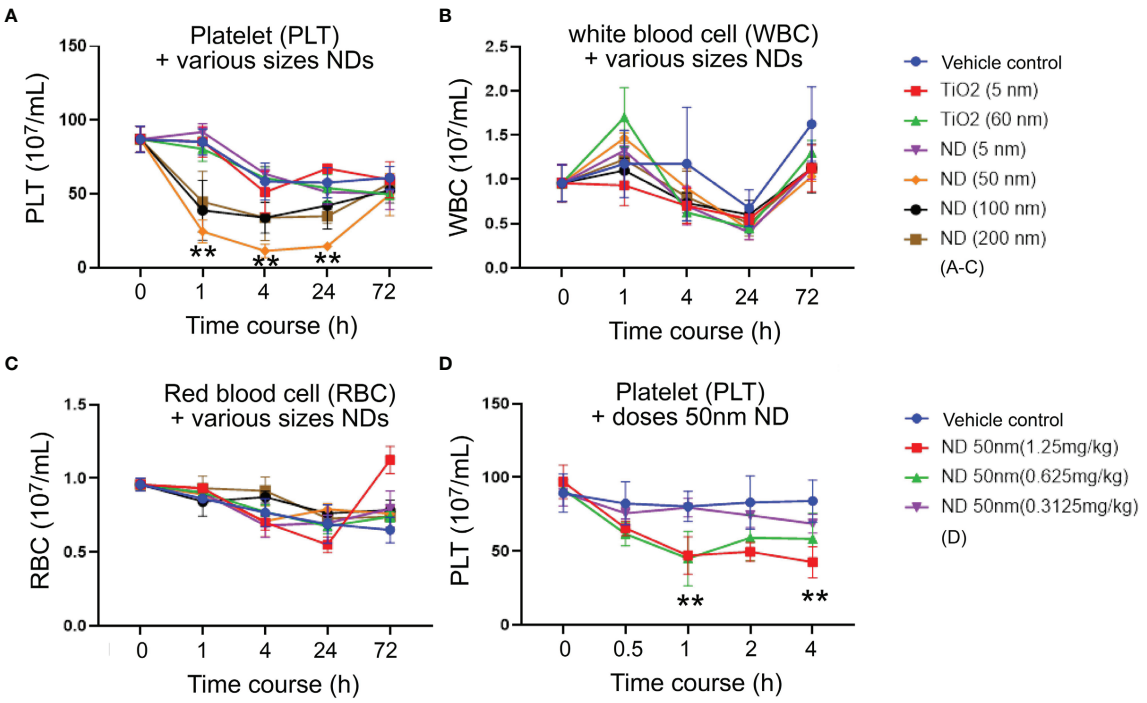

FIGURE 1 | ND-induced thrombocytopenia in mice. **(A)** Platelet (PLT) counts, **(B)** white blood cell (WBC) counts, **(C)** red blood cell (RBC) counts, of wild type C57Bl/6J mice challenged by TiO_2 (5 and 60 nm; 1.25 mg/kg) and various sizes of ND (5-200 nm; 1.25 mg/kg) nanoparticles. **(D)** Platelet counts of wild type C57Bl/6J mice challenged by various doses (0.625-1.25 mg/kg) of 50 nm ND nanoparticles. n = 6 (three experiments with two mice per group). $^{**}P < 0.01$, vs. 0 h groups.

platelet RCDs also involve in ND-induced platelet aggregation and thrombocytopenia is not clearly addressed. In addition, according to our previous findings, one cell-death inducer may trigger multiple RCDs in a specific cell type, such as platelet (38). The compositions of multiple RCDs are identified and described as cell-type-specific RCD patterns (CTS-RCDPs) (38, 62, 69). Accordingly, we would like to investigate 50 nm ND-induced RCD and CTS-RCDP in platelets. Those most described RCD pathways (40), which include pyroptosis, necroptosis, ferroptosis, apoptosis, and autophagy, were analyzed using flow cytometry approach following previously described methods (38, 62, 69). We found that 50 nm NDs induced platelet cell death levels are associated with platelet aggregation levels in a dose-dependent manner (**Figure 2A**, aggregation levels, gating in **Figure S1**; **Figure 2B**, dead cell populations). Flow cytometry analyses of CTS-RCDP revealed that treatments with 50 nm NDs induced considerable higher levels of pyroptosis and apoptosis as compared to the other analyzed RCDs in platelet death cell population (**Figure 2B**, dead cell population; **Figure 2C**, 30 and 1250 μg/mL ND groups, indicated ND-induced platelet CTS-RCDP; gating and calculation of CTS-RCDP in **Figure S2**).

Inhibitors Against P-Selectin, Nlrp3 Inflammasome Pathways Suppressed ND-Induced Platelet Aggregation, and Cell Death *In Vitro*

To investigate potential therapeutic interventions through suppression of pyroptosis and apoptosis, ROS inhibitors (N-acetyl-l-cysteine [NAC], mitochondria-targeted antioxidant MitoTEMPO (62, 70)), Nlrp3 inhibitor OLT1177, inflammasome/caspase1 inhibitor Z-WEHD-FMK (38, 62, 69), caspase-3 inhibitor Z-DEVD-FMK (71), were used in the following experiments. Our parallel experiments revealed that P-selectin, an adhesion receptor expressing on the surfaces of activated platelets and endothelial cells, displayed markedly higher ND-binding property as compared to various control proteins, including known pattern recognition receptors of platelets, such as toll-like receptor 4 (TLR4) and C-type lectin domain family 2 (CLEC2) (**Figure S3**). Consistently, platelets from wild type ($Selp^{+/+}$) mice displayed relatively higher ND-binding property as compared to the P-selectin-deficient platelets from the $Selp^{-/-}$ mutant mice (**Figure S4**). In addition, when compared to BSA, soluble recombinant P-selectin (rP-sel) treatments drastically suppressed 50 nm NDs induced platelet cell death as compared to the BSA-treated controls (**Figure S5**). Accordingly, here we used rP-sel as additional platelet cell death inhibitor in the following experiments. Analyses results revealed that treatments of rP-sel, NAC, MitoTEMPO, OLT1177, Z-WEHD-FMK and Z-DEVD-FMK markedly reduced ND-induced platelet total cell death (**Figure 3A**). By dividing total death cell population (**Figure 3A**, dead-cell population) into respective RCD cell populations (**Figures 3B–G**; **Figure S6**, specific RCD inducers induced platelet cell death, positive controls of RCD analyses), we found that inhibitors rP-sel, NAC, MitoTEMPO, OLT1177, Z-WEHD-FMK and Z-DEVD-FMK suppressed RCDs, including pyroptosis, apoptosis, necroptosis, autophagy, except ferroptosis (**Figures 3C, D, F, G**). To investigate whether the platelet aggregation is associated with the induction and reversal of platelet cell death, the morphology of ND-induced platelet aggregation was further analyzed using confocal microscopy under conditions with or without the inhibitor treatments. In agreement with the cell death analyses, NDs are able to induce platelet aggregation, and such platelet aggregates are markedly suppressed by treatments of cell death inhibitors, which include rP-sel, NAC, MitoTEMPO, OLT1177, Z-WEHD-FMK and Z-DEVD-FMK (**Figures 4A–I**, example images; **Figures 4J, K**, quantitative results; video S1, an example 3D structure of ND-platelet aggregates). These results suggested that ND-induced platelet aggregation is associated with ND-induced cell death.

ND Induced Less Pyroptosis and Apoptosis in Platelets From $Selp^{-/-}$, $Nlrp3^{-/-}$ and $Casp1^{-/-}$ Mutants, as Compared to the Same Treatments to Platelets From Wild Type Mice

To further verify whether platelet P-selectin and Nlrp3 inflammasome (Nlrp3 and caspase 1) pathways indeed involve

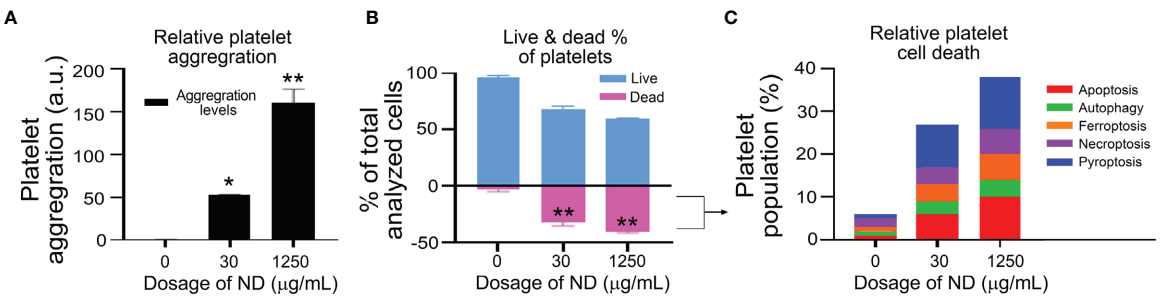

FIGURE 2 | ND-induced platelet cell death and aggregation *in vitro*. **(A, B)** Treatments of 50 nm NDs induced dose-dependent (0, 30, 1250 μg/mL) platelet aggregation **(A)** and cell death **(B)**, as measured by flow cytometry (**A**, gating in **Figure S1**), and Zombie NIR live/dead analysis kit **(B)**, respectively. **(C)** We observed the ND treatments induced multiple regulated cell death pathways (RCDs) in the dead cell population of mouse platelets. n = 6 (3 experiments with 2 samples per group). *P < 0.05, **P < 0.01, vs. vehicle control (0 μg/mL) groups.

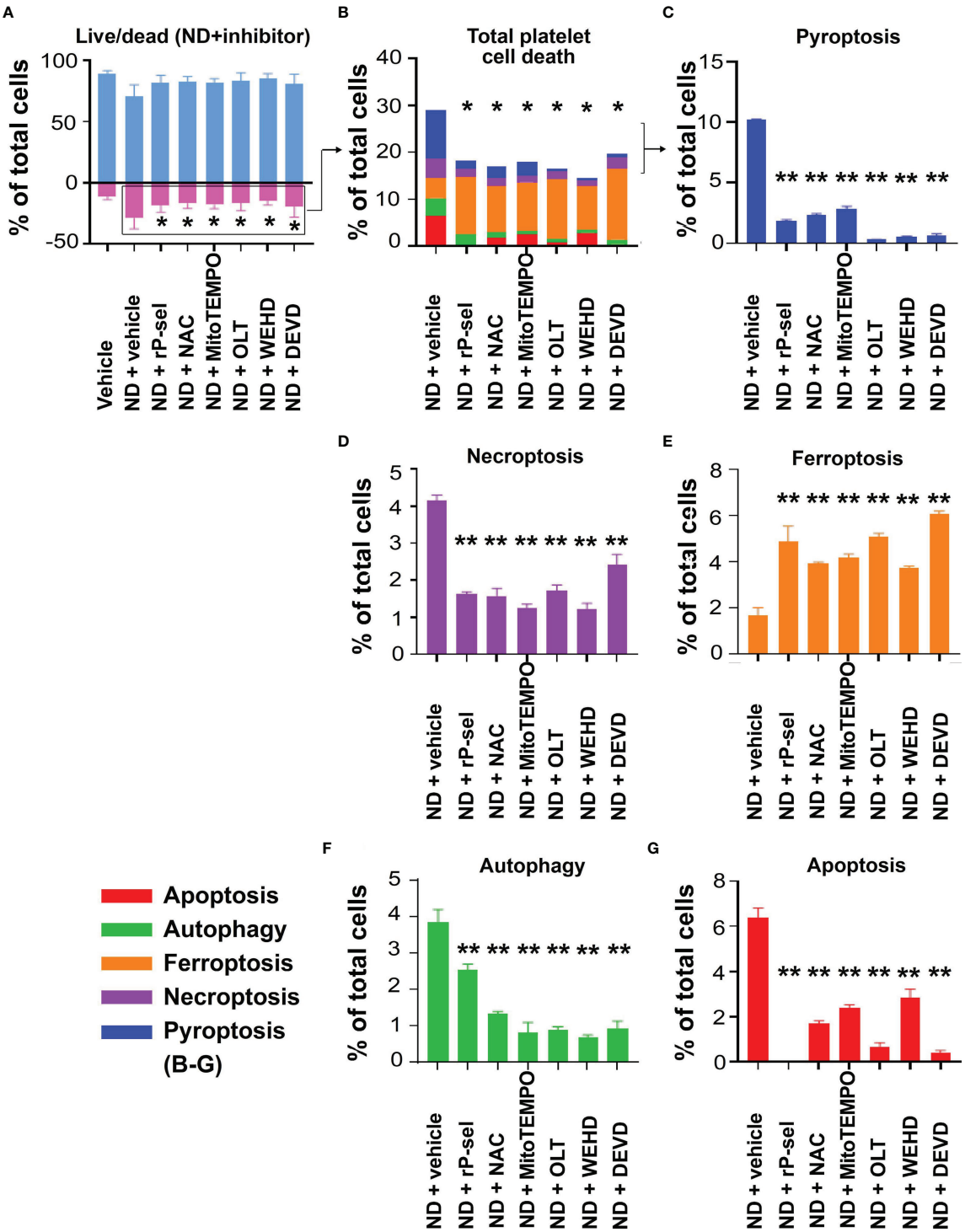

FIGURE 3 | P-selectin, Nlrp3, caspase-1 and caspase-3 inhibitors protect platelets from ND-induced pyroptosis and apoptosis. Treatments with competitive P-selectin inhibitor rP-sel (100 ng/mL), ROS inhibitor NAC (150 μg/mL), mitochondria-targeted antioxidant MitoTEMPO (10 μMu;), Nlrp3 inhibitor OLT1177 (OLT, 10 μM), caspase 1 inhibitor Z-WEHD-FMK (WEHD, 10 μM) and caspase 3 inhibitor Z-DEVD-FMK (DEVD, 10 μM) rescued ND-induced platelet cell death **(A, B)**. By dividing total cell death **(B)** into respective RCDs **(C–G)**, we found that pyroptosis and apoptosis are the top 2 RCDs induced by ND challenges. Additional treatments with rP-sel, NAC, MitoTEMPO, OLT1177, Z-WEHD-FMK and Z-DEVD-FMK, all markedly rescued ND-induced platelet pyroptosis **(C)**, apoptosis **(G)**, necroptosis **(D)** and autophagy **(F)** levels. Despite overall platelet survival rate increased after the inhibitor treatments, the ferroptosis levels exacerbated **(E)**. n = 6 (3 experiments with 2 samples per group), $^{*}P < 0.05$, $^{**}P < 0.01$, vs. vehicle groups.

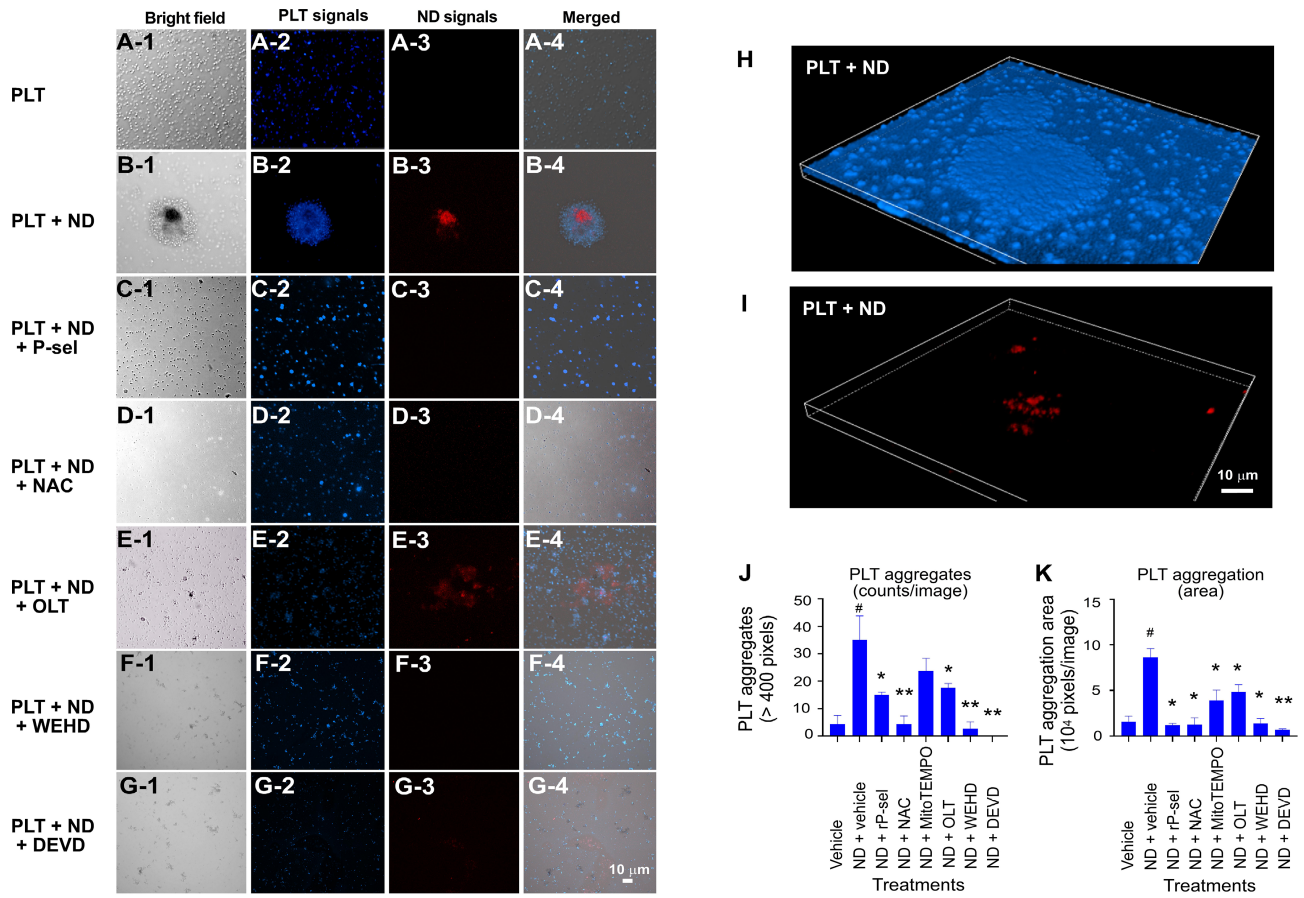

FIGURE 4 | Confocal microscopy analyses on the morphology of ND-induced platelet aggregates. **(A–I)** Example images of platelet (PLT) aggregates that were induced by treatments of ND, with or without additional treatments of inhibitors (rP-sel, NAC, OLT1177, Z-WEHD-FMK and Z-DEVD-FMK) were shown. CellTracker Blue Dye labeled mouse platelets, and red fluorescent 50 nm NDs (NV center > 100 per particle, FND Biotech) were employed in this experiment. **(J, K)** Quantitative analyses revealed that ND treatments markedly enhanced the platelet aggregate counts (those > 400 pixels) **(J)**, and area **(K)**. All tested inhibitors (rP-sel, NAC, MitoTEMPO, OLT1177, Z-WEHD-FMK and Z-DEVD-FMK) suppressed ND-induced aggregation **(K**, area; and **J**, counts; except MitoTEMPO**)**. n = 6 (2 experiments with 3 mice per group). $^{\#}P < 0.05$ vs. vehicle groups. $^{*}P < 0.05$, $^{**}P < 0.01$, vs. ND + vehicle groups. Example images of 3D morphology of ND-induced platelet aggregate are highlighted **(H, I**; similar result referred to **Supplementary Video S1**). Scale bars: **(A–G)**, 10 μm (G-4); **(H, I)**, 10 μm **(I)**.

in ND induced platelet cell death, live/dead and CTS-RCDP status were analyzed using platelets from *Selp*$^{-/-}$, *Nlrp3*$^{-/-}$ and *Casp1*$^{-/-}$ mutants. In agreement with the inhibitor experiments, 50 nm ND induced less pyroptosis and apoptosis levels in platelets from *Selp*$^{-/-}$, *Nlrp3*$^{-/-}$ and *Casp1*$^{-/-}$ mutants, as compared to the same treatments to platelets from wild type mice (**Figure 5**). These results suggested that P-selectin and Nlrp3 inflammasome pathways indeed involve in ND-induced pyroptosis and apoptosis.

Inhibitors Against P-Selectin, ROS and Nlrp3 Inflammasome Pathways Suppressed Platelet Aggregation and Mitochondria Superoxide Burden *In Vitro*

Because Nlrp3 inflammasome-mediated pyroptosis is a major RCD involved in 50 nm ND-induced platelet defects, we further investigated whether the suppression of platelet Nlrp3 inflammasome through inhibitor treatments is sufficient to ameliorate 50 nm ND-induced abnormal platelet activation. Here we found that 50 nm ND-induced platelet aggregation, and increased mitochondrial superoxide levels (**Figure 6**). Superoxide is a powerful cell-damaging ROS, which is produced in mitochondria by electrons leaking from the electron transfer system (72, 73). Upregulated mitochondrial superoxide indicated increased levels of cellular oxidative stress and mitochondrial burden (72, 73). Consistent with the platelet cell death analyses (**Figure 3**), ND treatments with additional P-selectin (rP-sel), Nlrp3 inflammasome (OLT1177 and Z-WEHD-FMK), apoptosis (Z-DEVD-FMK), and ROS [NAC; and MitoTEMPO, a mitochondria targeted antioxidant (62, 70)] inhibitors treatments, ameliorated such ND-induced platelet aggregation and mitochondria superoxide levels (**Figure 6**).

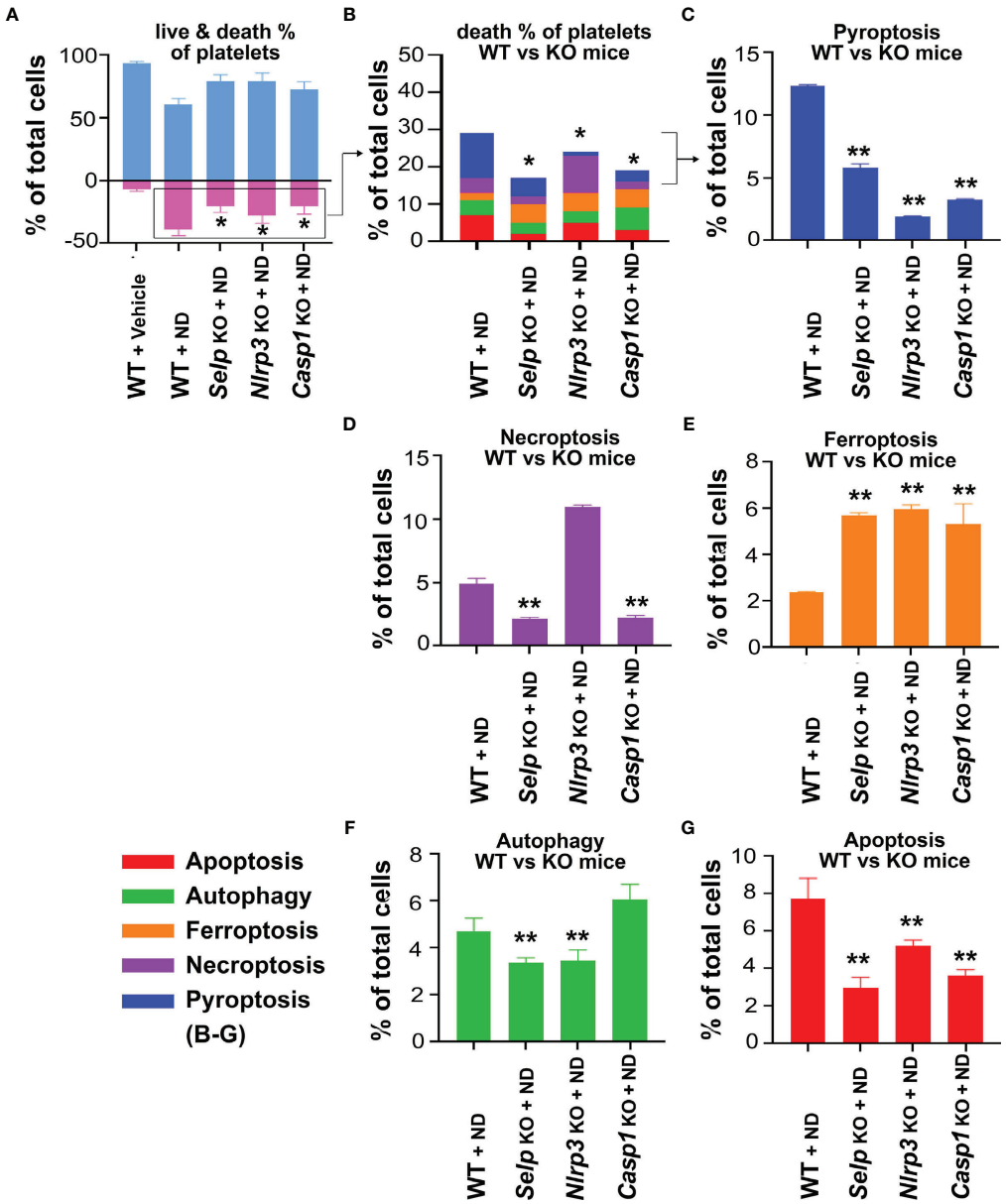

FIGURE 5 | P-selectin, Nlrp3 and caspase-1 deficiencies protect platelets from ND-induced pyroptosis and apoptosis. **(A, B)** Compared with wild type (WT) controls, P-selectin (*Selp*$^{-/-}$), Nlrp3 (*Nlrp3*$^{-/-}$) and caspase 1 (*Casp1*$^{-/-}$) deficient platelets displayed less cell death levels in response to ND treatments. **(C–G)** Consistent with the cell death analysis, platelets from P-selectin (*Selp*$^{-/-}$), Nlrp3 (*Nlrp3*$^{-/-}$) and caspase 1 (*Casp1*$^{-/-}$) deficient mice displayed less pyroptosis and apoptosis, the 2 major RCDs, levels in response to ND challenges. n = 6 (2 experiments with 3 mice per group), *$P < 0.05$, **$P < 0.01$, vs. WT groups.

Inhibitors Against P-Selectin, ROS, Nlrp3 Inflammasome Pathways Suppressed Platelet Aggregation, Pyroptosis and Apoptosis *In Vivo*

In vivo mouse experiments further revealed that, in agreement with the *in vitro* analyses, treatments with P-selectin (rP-sel), Nlrp3 inflammasome (OLT1177 and Z-WEHD-FMK), apoptosis (Z-DEVD-FMK), and ROS (NAC and MitoTEMPO) inhibitors markedly ameliorated ND-induced thrombocytopenia (**Figure 7A**), and platelet pyroptosis (**Figure 7B**, except Z-DEVD-FMK) and apoptosis (**Figure 7C**) levels in C57BL/6J mice. These results suggested that 50 nm ND induces platelet aggregation and platelet cell death, involve P-selectin, and Nlrp3 inflammasome mediated enhancement of mitochondrial oxidative stress, pyroptosis and apoptosis.

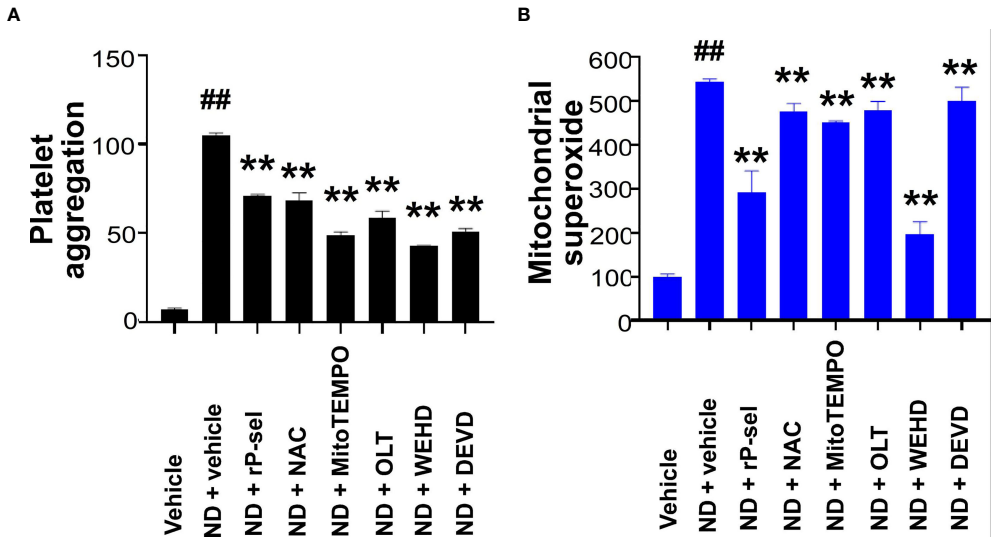

FIGURE 6 | P-selectin, Nlrp3, caspase-1 and ROS inhibitors protect platelets from ND-induced activation. ND-induced platelet activation, including **(A)** platelet aggregation, and **(B)** mitochondrial superoxide levels, could be suppressed with the treatments with P-selectin, ROS inhibitors, Nlrp3, caspase-1 and caspse-3 inhibitors [rP-sel (100 ng/mL), OLT1177 (OLT, 10 μM), Z-WEHD-FMK (WEHD, 10 μM), Z-DEVD-FMK (DEVD, 10 μM), NAC (150 μg/mL), and MitoTEMPO (1 μM)], respectively **(A, B)**. **(A)** ND + vehicle groups were normalized to 100%; **(B)** vehicle groups were normalized to 100%. n = 6 (2 experiments with 3 mice per group), $^{\#\#}P < 0.05$, vs. respective vehicle groups; $^{**}P < 0.01$, vs. respective ND + vehicle groups.

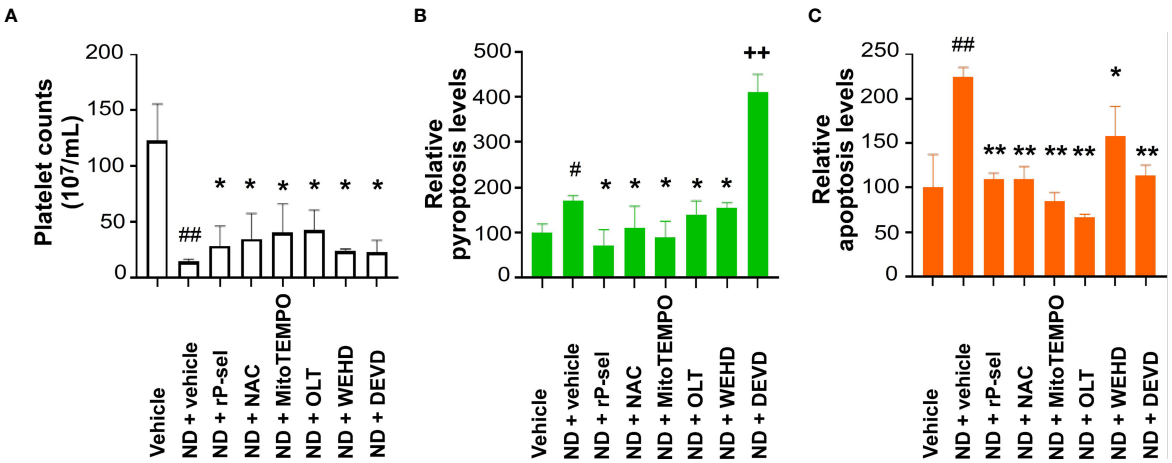

FIGURE 7 | Treatments of P-selectin, ROS, Nlrp3, caspase-1, and caspase-3 inhibitors ameliorate ND-induced thrombocytopenia in mice. Treatments with P-selectin, ROS, Nlrp3, caspase-1, and caspase-3 inhibitors [rP-sel (0.24 mg/mL), OLT1177 (OLT, 50 mg/kg), NAC (300 mg/kg), and MitoTEMPO (0.1 mg/kg), Z-WEHD-FMK (ZWEHD, 750 μg/kg), Z-DEVD-FMK (DEVD, 6.5 μg/kg)], ameliorated ND (50 nm; 1.25 mg/kg)-induced thrombocytopenia **(A)**, and platelet pyroptosis **(B)** and apoptosis **(C)** levels in C57BL/6J mice. **(B, C)** Vehicle groups were normalized to 100%. n = 6, (2 experiments with 3 mice per group). $^{\#}P < 0.05$, $^{\#\#}P < 0.01$, vs. respective vehicle groups; $^{*}P < 0.05$, $^{**}P < 0.01$ significantly lower, vs. respective ND + vehicle groups; $^{++}P < 0.01$ significantly higher, vs. ND + vehicle groups.

Inhibitors Against P-Selectin, ROS, Nlrp3 Inflammasome and Caspase-3 Pathways Suppressed ND-Induced Platelet-Enhanced Neutrophil Extracellular Trap Formation

Flow cytometry analyses were employed to further investigate whether ND-induced platelet cell death involves in ND-induced NETosis. In agreement with previous reports (74–76), we found that ND-treatments directly induced mouse neutrophil NETosis (**Figures 8A–F** gatings; **Figure 8G** quantitative results). Intriguingly, after stimulation and removal of NDs, the supernatants form ND-activated platelets (PLT+ND sup) also induced comparable levels of NETosis (**Figure 8G**, ND groups vs. PLT+ND sup groups). In addition, the capability of the

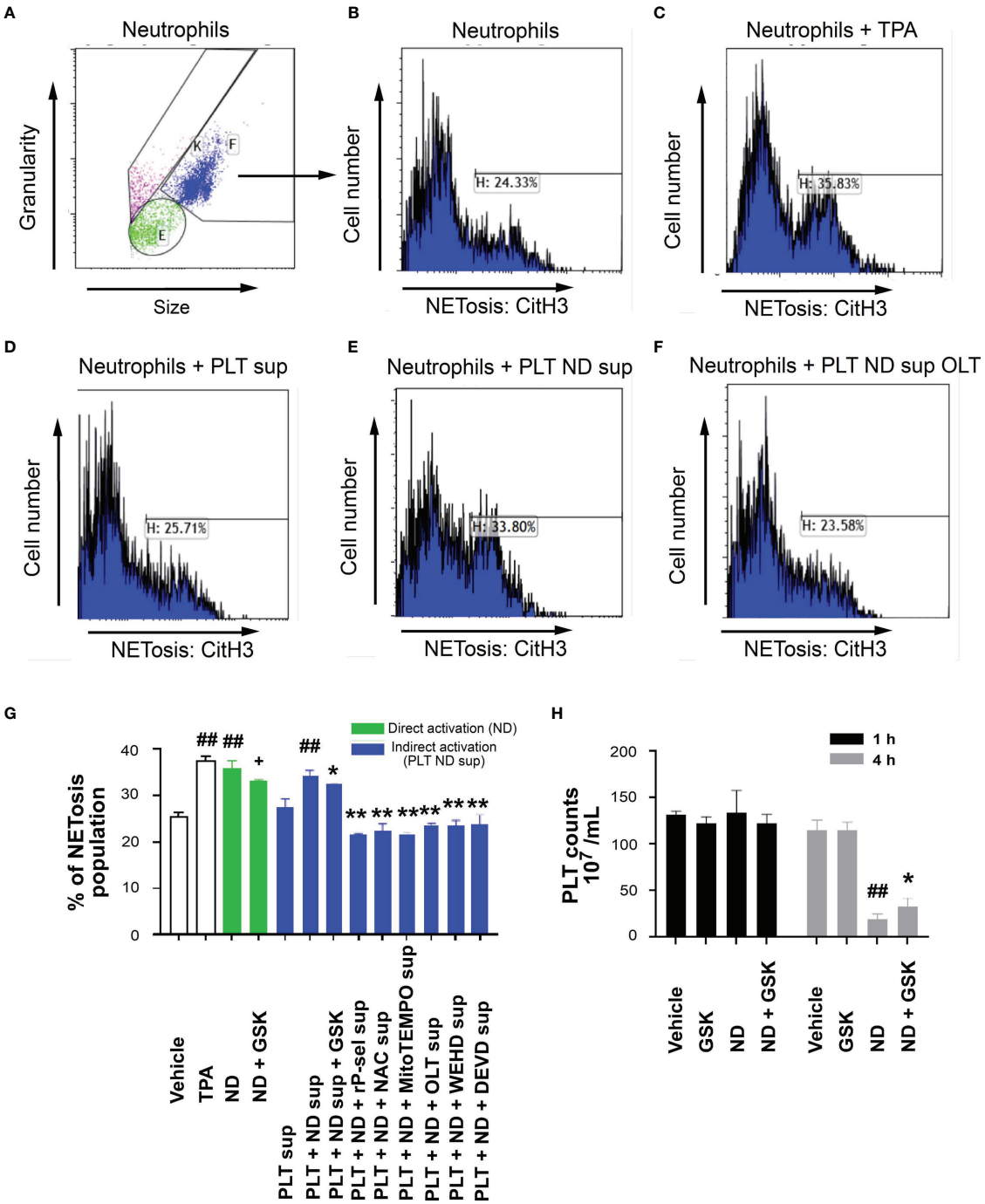

FIGURE 8 | Reversal of ND-induced thrombocytopenia through suppression of NETosis in mice. Flow cytometry gating of NETosis (citrullinated histone H3, CitH3 staining) levels of mouse neutrophils treated with vehicle **(A, B)**, 12-O-tetradecanoylphorbol-13-acetate **(C**, TPA, a positive control NETosis inducer; 2 nM**)**, and supernatants from 50 nm NDs (30 μg/mL) activated (30 min) wild mice platelets (2×10^6) (PLT ND sup) **(E)** with or without additional inhibitor **(F**, OLT**)** pretreatments (30 min), as compared to the NETosis induced by none-activated platelet supernatants **(D**, PLT sup**)**. **(G)** The quantified results indicated that ND can induce NET formation directly (green columns). ND treatments can also enhance NETosis indirectly through soluble factors released from ND-activated platelets **(G**, PLT+ND sup**)**, and such this "PLT+ND sup"-induced NETosis could be suppressed by treatments of additional inhibitors such as GSK484, rP-sel, NAC, MitoTEMPO, OLT1177, Z-WEHD-FMK and Z-DEVE-FMK **(G**, blue columns**)**. **(H)** Treatments NETosis inhibitor GSK484 ameliorated ND-induced thrombocytopenia. **(G, H)** $^{\#\#}P < 0.01$ vs. vehicle groups. **(G)** $^{+}P < 0.05$, vs. ND groups; $^{*}P < 0.05$, $^{**}P < 0.01$, vs. "PLT + ND sup" groups. **(H)** $^{*}P < 0.05$, vs. ND groups. n = 6 (2 experiments with 3 mice per group).

PLT+ND sup to induce NETosis could be suppressed by treatments of platelet cell death inhibitors, including rP-sel, NAC, MitoTEMPO, OLT1177, Z-WEHD-FMK and Z-DEVD-FMK, during ND stimulation (**Figure 8G**). This suggests that, in addition to direct stimulation of neutrophils, ND can also induce NETosis indirectly through induction of platelet activations. Platelet counts of ND-challenges of mice, with or without NETosis inhibitor GSK484 treatments, were further evaluated to investigate whether NETosis might involve in ND-induced thrombocytopenia. Data revealed that GSK484 treatments markedly rescued ND-induced low platelet counts (**Figure 8H**). These results suggested that there is a feedforward regulation between platelets and neutrophils: ND-activated platelets release soluble factors induced NETosis, and NETosis further exacerbate ND-induced thrombocytopenia.

DISCUSSION

Hemocompatibility of blood-contacting nanomaterials is one of the most important criteria for their successful *in vivo* applicability (12, 17, 18). Among coagulation cascades, platelet activation and aggregation play central roles in determining the hemocompatibility of nanomaterials (18). As more *in vivo* applications of ND have been reported (5, 9–11), in this present study, we analyzed the impact of ND treatments on the stimulation of platelet aggregation and cell death. Analyses results revealed that among the various sizes (5-200 nm) of detonation NDs, with unknown reasons, treatments of 50 nm NDs induced highest level of platelet aggregation and thrombocytopenia, *in vitro* and *in vivo*. Complex factors may affect the hemocompatibility of nanomaterials *in vivo*, such as nanomaterial interaction and activation with respective types of blood cells and coagulation cascades (12, 13, 17). Thus, the mechanism of how 50 nm NDs displayed highest hemocompatibility-associated adverse effects is worthy of further investigated. In addition, here we found that NDs induce platelet cell death dependent aggregation, because pyroptosis and apoptosis inhibitors block the platelet aggregation *in vitro* and thrombocytopenic responses *in vivo*. These results suggested that suppression of platelet pyroptosis and apoptosis could be a useful method to manage the hemocompatibility-associated adverse effects of ND.

Our previous findings have shown that a single domain of dengue virus protein (envelope protein domain III; DENV-EIII) can elicit various types of RCDs in different cell types including platelets (38, 62, 69). With more complexed compositions, ND surfaces were reported to have evenly distributed high levels of phenols, pyrones, and sulfonic acid groups, as compared to hydroxyl and epoxide groups that are present only on some areas of the surfaces (77). Therefore, it is reasonable that ND can induce various RCDs in platelets. It is yet unclear why single reagent, such as ND and dengue virus envelope protein (38), can induce different types of RCDs in platelets. Cell death pathways have long been considered to regulate in independently; while it is currently clear that pyroptosis, necroptosis, and apoptosis are tightly connected and can cross-regulate each other (78). For example, in the absence of gasdermin D, activation of pyroptosis inducer caspase-1 redirects cell fate toward caspase-3-dependent apoptosis in macrophages (79). Necroptosis effector protein receptor-interacting serine/threonine-protein kinase 3 (RIPK3) promotes cell death and NLRP3 inflammasome activation in the absence of mixed lineage kinase domain-like pseudokinase (MLKL) (80). These evidences collectively suggested that pyroptosis, necroptosis, and apoptosis cross-regulate each other. Here we found that treatments of Nlrp3 inhibitor OLT1177 not only suppressed ND-induced pyroptosis, but also apoptosis, necroptosis and autophagy levels are also suppressed (**Figure 3**). This is in agreement with our finding that treatments of Nlrp3 inhibitor OLT1177 suppressed of DENV-EIII-induced pyroptosis, necroptosis, and apoptosis in mouse platelets (38). Because the RCD pathways cross-regulate to each other, the CTS-RCDP could be served as a molecular-regulation fingerprint to identify the coordinated regulation of RCDs. For example, despite the detailed mechanism remains to be further studied, it seems that there are alternative RCDs, when one particular RCD is blocked. For instance, when the apoptosis (caspase-3) is blocked, pyroptosis levels are increased in the platelets (**Figures 7B, C**, ND + DEVD groups). When pyroptosis and apoptosis are blocked, ferroptosis levels are increased in the platelets (**Figures 3**, **5**, ferroptosis groups). These results suggested that RCDs are regulated in a coordinated manner. Here we identified pyroptosis and apoptosis as the top 2 ND-induced RCDs in platelets. ND-induced adverse effects, such as platelet aggregation and thrombocytopenia, may be therefore rescued through suppression of inflammasome activation and the cell death pathways. As a result, these inhibitors may be considered as antidotes for *in vivo* treated NDs. Notably, our analyses data revealed that P-selectin serves as an upstream pathway of Nlrp3 inflammasome and plays a critical role on the regulation of ND-induced platelet cell death.

P-selectin is a cell adhesion molecule expressing on the surfaces of activated endothelial cells and activated platelets. It is clear that P-selectin can function as a counter-receptor to stimulate P-selectin glycoprotein ligand-1 (PSGL-1) signaling, as interactions of PSGL-1 with immobilized P-selectin rapidly induce tyrosine phosphorylation of multiple proteins, and P-selectin-mediated adhesion enables activation outside-in signaling of β2 integrins in leukocytes (81). By contrast, the function of P-selectin in serving as a signaling receptor is less clear. We have previously shown that the binding of DENV-EIII or anti-P-selectin antibody to endothelial surface P-selectin initiate cellular inflammasome activation and pyroptosis (62). In agreement with this, here we found that blockage of ND-P-selectin interaction by addition of rP-sel markedly suppressed ND-induced platelet pyroptosis *in vitro* and *in vivo*. Moreover, compared to the wild type controls, P-selectin deficient mice displayed markedly less platelet activation and thrombocytopenia after ND injections. These results suggest that P-selectin is a ND-sensitizing pattern recognition receptor on platelets. Because P-selectin is highly expressed on the platelet surfaces during coagulation activation and various inflammatory diseases,

the pattern-recognition property enables P-selectin serving as a critical coordinator that links the inflammation (immune system) to the thrombosis (coagulation system), and vice versa. The detailed mechanism of how P-selectin initiates inflammasome activation is worthy or further investigation. As the property of a blood-contacting material to induce thrombosis and inflammation determine the hemocompatibility, P-selectin-material interaction is one of the critical properties for analyzing hemocompatibility of *in vivo* used materials.

Previous reports have indicated that nanomaterial-induced NETs are critical for the initiation of adverse effects *in vivo* (74–76, 82). At the same time, platelets are involved in NET-related abnormal inflammation and coagulation (67, 83). Consequently, NETs may also contribute to ND-induced platelet-associated adverse effects *in vivo*. Our *in vitro* analysis results indicated that, compared to the supernatant from vehicle-treated control platelets, "PLT+ND sup" induced markedly higher NETosis levels of mouse neutrophils (**Figure 8**). Treatments of Nlrp3 inflammasome inhibitor OLT1177 drastically reduced NETosis-induction property of the "PLT+ND sup" (**Figure 8**), suggesting platelet pyroptosis and apoptosis are part of the up-stream pathways of ND-induced NETosis. At the same time, because treatments of NETosis inhibitor GSK484 markedly rescued ND-induced low platelet counts in mice (**Figure 8**), this indicated that NETosis in turn exacerbated ND-induced platelet defect. These results collectively suggested that there exists a feedforward regulation between platelets and neutrophils after ND-treatments. Moreover, in addition to direct activation of platelets, NDs can also indirectly cause platelet-associated defects through inducing NETosis. The interplay between platelets and neutrophils in ND-induced abnormal platelet responses are intriguing, and worth of further investigations.

In summary, here we found that treatments of 50 nm NDs with dose of 1.25 mg/kg can lead to platelet cell death and thrombocytopenia in mice. ND induced the platelet activation, pyroptosis and apoptosis through surface P-selectin-mediated activation of mitochondrial superoxide levels and Nlrp3 inflammasome. Blockage of P-selectin and Nlrp3 inflammasome by treatments of rP-sel and Nlrp3 inflammasome inhibitors markedly suppressed the adverse effects. However, NDs were shown to trigger the formation of platelet aggregates and NETs; and NDs are not easy to be sequestered *in vivo* and excreted from the body, because of their non-biodegradable property (74–76, 82). Consequently, despite of blockers of P-selectin and Nlrp3 inflammasome pathways displayed as antidotes of ND, these adverse effects prohibit the *in vivo* use of ND before the fundamental safety problems are solved.

DATA AVAILABILITY STATEMENT

The original contributions presented in the study are included in the article/**Supplementary Material**. Further inquiries can be directed to the corresponding author.

ETHICS STATEMENT

The animal study was reviewed and approved by Prof. Kun-Ta Yang Department of Physiology, School of Medicine, Tzu Chi University, Hualien, Taiwan.

AUTHOR CONTRIBUTIONS

H-HC conceptualized and supervised this project. S-CH, L-CK, T-SL, H-SH, D-SS, and C-LC performed experiments and analysed the data. HHC wrote this manuscript. All authors contributed to the article and approved the submitted version.

FUNDING

This work was supported by research funding from Ministry of Science and Technology, Taiwan (98-2320-B-320-004MY3, 101-2320-B- 320-004-MY3, 105-2923-B-320-001-MY3, 107- 2311-B-320-002-MY3), Tzu-Chi University (TCIRP95002; TCIRP98001; TCIRP101001) and Tzu-Chi Medical Foundation (TCMMP104; TCMMP108; TCMMP110; TCAS-108-01).

ACKNOWLEDGMENTS

The authors are grateful to the helps from Experimental Animal Center, and Core Facility Center of Tzu-Chi University. The authors also want to thank Professor Shie-Liang Hsieh, Genomics Research Center, Academia Sinica, Taipei, Taiwan, for his kindly support of CLEC2 recombinant protein.

SUPPLEMENTARY MATERIAL

The Supplementary Material for this article can be found online at: https://www.frontiersin.org/articles/10.3389/fimmu.2022.806686/full#supplementary-material

REFERENCES

1. Mitchell MJ, Billingsley MM, Haley RM, Wechsler ME, Peppas NA, Langer R. Engineering Precision Nanoparticles for Drug Delivery. *Nat Rev Drug Discov* (2021) 20(2):101–24. doi: 10.1038/s41573-020-0090-8
2. Aflori M. Smart Nanomaterials for Biomedical Applications-A Review. *Nanomater (Basel)* (2021) 11(2):1–33. doi: 10.3390/nano11020396
3. Gao G, Guo Q, Zhi J. Nanodiamond-Based Theranostic Platform for Drug Delivery and Bioimaging. *Small* (2019) 15(48):e1902238. doi: 10.1002/smll.201902238
4. Terada D, Genjo T, Segawa TF, Igarashi R, Shirakawa M. Nanodiamonds for Bioapplications-Specific Targeting Strategies. *Biochim Biophys Acta Gen Subj* (2020) 1864(2):129354. doi: 10.1016/j.bbagen.2019.04.019
5. Perevedentseva E, Lin YC, Cheng CL. A Review of Recent Advances in Nanodiamond-Mediated Drug Delivery in Cancer. *Expert Opin Drug Deliv* (2021) 18(3):369–82. doi: 10.1080/17425247.2021.1832988
6. Schrand AM, Huang H, Carlson C, Schlager JJ, Omacr Sawa E, Hussain SM, et al. Are Diamond Nanoparticles Cytotoxic? *J Phys Chem B* (2007) 111(1):2–7. doi: 10.1021/jp066387v

7. Yu SJ, Kang MW, Chang HC, Chen KM, Yu YC. Bright Fluorescent Nanodiamonds: No Photobleaching and Low Cytotoxicity. *J Am Chem Soc* (2005) 127(50):17604–5. doi: 10.1021/ja0567081
8. Schrand AM, Ciftan Hens SA, Shenderova OA. Nanodiamond Particles: Properties and Perspectives for Bioapplications. *Crit Rev Solid State Mater Sci* (2009) 34(1-2):18–74. doi: 10.1080/10408430902831987
9. Tsai LW, Lin YC, Perevedentseva E, Lugovtsov A, Priezzhev A, Cheng CL. Nanodiamonds for Medical Applications: Interaction With Blood in Vitro and in Vivo. *Int J Mol Sci* (2016) 17(7):1–17. doi: 10.3390/ijms17071111
10. Chauhan S, Jain N, Nagaich U. Nanodiamonds With Powerful Ability for Drug Delivery and Biomedical Applications: Recent Updates on In Vivo Study and Patents. *J Pharm Anal* (2020) 10(1):1–12. doi: 10.1016/j.jpha.2019.09.003
11. van der Laan K, Hasani M, Zheng T, Schirhagl R. Nanodiamonds for In Vivo Applications. *Small* (2018) 14(19):e1703838. doi: 10.1002/smll.201703838
12. de la Harpe KM, Kondiah PPD, Choonara YE, Marimuthu T, du Toit LC, Pillay V. The Hemocompatibility of Nanoparticles: A Review of Cell-Nanoparticle Interactions and Hemostasis. *Cells* (2019) 8(10):1–25. doi: 10.3390/cells8101209
13. Saha AK, Zhen MS, Erogbogbo F, Ramasubramanian AK. Design Considerations and Assays for Hemocompatibility of FDA-Approved Nanoparticles. *Semin Thromb Hemost* (2020) 46(5):637–52. doi: 10.1055/s-0039-1688491
14. Ilinskaya AN, Dobrovolskaia MA. Nanoparticles and the Blood Coagulation System. Part II: Safety Concerns. *Nanomed (Lond)* (2013) 8(6):969–81. doi: 10.2217/nnm.13.49
15. Chang WK, Sun DS, Chan H, Huang PT, Wu WS, Lin CH, et al. Visible Light-Responsive Core-Shell Structured In(2)O(3)@CaIn(2)O(4) Photocatalyst With Superior Bactericidal Properties and Biocompatibility. *Nanomedicine* (2012) 8(5):609–17. doi: 10.1016/j.nano.2011.09.016
16. Narayanan P, Shen L, Curtis BR, Bourdon MA, Nolan JP, Gupta S, et al. Investigation Into the Mechanism(s) That Leads to Platelet Decreases in Cynomolgus Monkeys During Administration of ISIS 104838, a 2'-MOE-Modified Antisense Oligonucleotide. *Toxicol Sci* (2018) 164(2):613–26. doi: 10.1093/toxsci/kfy119
17. Weber M, Steinle H, Golombek S, Hann L, Schlensak C, Wendel HP, et al. Blood-Contacting Biomaterials: In Vitro Evaluation of the Hemocompatibility. *Front Bioeng Biotechnol* (2018) 6:99. doi: 10.3389/fbioe.2018.00099
18. Matus MF, Vilos C, Cisterna BA, Fuentes E, Palomo I. Nanotechnology and Primary Hemostasis: Differential Effects of Nanoparticles on Platelet Responses. *Vascul Pharmacol* (2018) 101:1–8. doi: 10.1016/j.vph.2017.11.004
19. Huang HS, Sun DS, Lien TS, Chang HH. Dendritic Cells Modulate Platelet Activity in IVIg-Mediated Amelioration of ITP in Mice. *Blood* (2010) 116 (23):5002–9. doi: 10.1182/blood-2010-03-275123
20. Huang HS, Chang HH. Platelets in Inflammation and Immune Modulations: Functions Beyond Hemostasis. *Arch Immunol Ther Exp (Warsz)* (2012) 60 (6):443–51. doi: 10.1007/s00005-012-0193-y
21. Kelley N, Jeltema D, Duan Y, He Y. The NLRP3 Inflammasome: An Overview of Mechanisms of Activation and Regulation. *Int J Mol Sci* (2019) 20(13):1–24. doi: 10.3390/ijms20133328
22. Davis BK, Wen H, Ting JP. The Inflammasome NLRs in Immunity, Inflammation, and Associated Diseases. *Annu Rev Immunol* (2011) 29:707–35. doi: 10.1146/annurev-immunol-031210-101405
23. Fusco R, Siracusa R, Genovese T, Cuzzocrea S, Di Paola R. Focus on the Role of NLRP3 Inflammasome in Diseases. *Int J Mol Sci* (2020) 21(12):1–26. doi: 10.3390/ijms21124223
24. Lamkanfi M, Dixit VM. Mechanisms and Functions of Inflammasomes. *Cell* (2014) 157(5):1013–22. doi: 10.1016/j.cell.2014.04.007
25. Sharma D, Kanneganti TD. The Cell Biology of Inflammasomes: Mechanisms of Inflammasome Activation and Regulation. *J Cell Biol* (2016) 213(6):617–29. doi: 10.1083/jcb.201602089
26. Zheng D, Liwinski T, Elinav E. Inflammasome Activation and Regulation: Toward a Better Understanding of Complex Mechanisms. *Cell Discov* (2020) 6:36. doi: 10.1038/s41421-020-0167-x
27. Gaidt MM, Hornung V. Alternative Inflammasome Activation Enables IL-1beta Release From Living Cells. *Curr Opin Immunol* (2017) 44:7–13. doi: 10.1016/j.coi.2016.10.007
28. Sun Q, Scott MJ. Caspase-1 as a Multifunctional Inflammatory Mediator: Noncytokine Maturation Roles. *J Leukoc Biol* (2016) 100(5):961–7. doi: 10.1189/jlb.3MR0516-224R
29. Margraf A, Zarbock A. Platelets in Inflammation and Resolution. *J Immunol* (2019) 203(9):2357–67. doi: 10.4049/jimmunol.1900899
30. Eisinger F, Langer HF. The Mutual Relation of Platelet Activation and Innate Immunity. *Hamostaseologie* (2018) 38(4):186–202. doi: 10.1055/s-0038-1669450
31. Hottz ED, Monteiro AP, Bozza FA, Bozza PT. Inflammasome in Platelets: Allying Coagulation and Inflamm in Infectious and Sterile Diseases? *Mediators Inflammation* (2015) 2015:435783. doi: 10.1155/2015/435783
32. Vogel S, Murthy P, Cui X, Lotze MT, Zeh HJ 3rd, Sachdev U. TLR4-Dependent Upregulation of the Platelet NLRP3 Inflammasome Promotes Platelet Aggregation in a Murine Model of Hindlimb Ischemia. *Biochem Biophys Res Commun* (2019) 508(2):614–9. doi: 10.1016/j.bbrc.2018.11.125
33. Brown GT, McIntyre TM. Lipopolysaccharide Signaling Without a Nucleus: Kinase Cascades Stimulate Platelet Shedding of Proinflammatory IL-1beta-Rich Microparticles. *J Immunol* (2011) 186(9):5489–96. doi: 10.4049/jimmunol.1001623
34. Lindemann S, Tolley ND, Dixon DA, McIntyre TM, Prescott SM, Zimmerman GA, et al. Activated Platelets Mediate Inflammatory Signaling by Regulated Interleukin 1beta Synthesis. *J Cell Biol* (2001) 154(3):485–90. doi: 10.1083/jcb.200105058
35. Denis MM, Tolley ND, Bunting M, Schwertz H, Jiang H, Lindemann S, et al. Escaping the Nuclear Confines: Signal-Dependent pre-mRNA Splicing in Anucleate Platelets. *Cell* (2005) 122(3):379–91. doi: 10.1016/j.cell.2005.06.015
36. Cornelius DC, Baik CH, Travis OK, White DL, Young CM, Austin Pierce W, et al. NLRP3 Inflammasome Activation in Platelets in Response to Sepsis. *Physiol Rep* (2019) 7(9):e14073. doi: 10.14814/phy2.14073
37. Murthy P, Durco F, Miller-Ocuin JL, Takedai T, Shankar S, Liang X, et al. The NLRP3 Inflammasome and Bruton's Tyrosine Kinase in Platelets Co-Regulate Platelet Activation, Aggregation, and In Vitro Thrombus Formation. *Biochem Biophys Res Commun* (2017) 483(1):230–6. doi: 10.1016/j.bbrc.2016.12.161
38. Lien TS, Chan H, Sun DS, Wu JC, Lin YY, Lin GL, et al. Exposure of Platelets to Dengue Virus and Envelope Protein Domain III Induces Nlrp3 Inflammasome-Dependent Platelet Cell Death and Thrombocytopenia in Mice. *Front Immunol* (2021) 12:616394. doi: 10.3389/fimmu.2021.616394
39. Tang D, Kang R, Berghe TV, Vandenabeele P, Kroemer G. The Molecular Machinery of Regulated Cell Death. *Cell Res* (2019) 29(5):347–64. doi: 10.1038/s41422-019-0164-5
40. Hu XM, Li ZX, Lin RH, Shan JQ, Yu QW, Wang RX, et al. Guidelines for Regulated Cell Death Assays: A Systematic Summary, A Categorical Comparison, A Prospective. *Front Cell Dev Biol* (2021) 9:634690. doi: 10.3389/fcell.2021.634690
41. Galluzzi L, Vitale I, Aaronson SA, Abrams JM, Adam D, Agostinis P, et al. Molecular Mechanisms of Cell Death: Recommendations of the Nomenclature Committee on Cell Death 2018. *Cell Death Differ* (2018) 25 (3):486–541. doi: 10.1038/s41418-018-0102-y
42. Goette NP, Glembotsky AC, Lev PR, Grodzielski M, Contrufo G, Pierdominici MS, et al. Platelet Apoptosis in Adult Immune Thrombocytopenia: Insights Into the Mechanism of Damage Triggered by Auto-Antibodies. *PloS One* (2016) 11(8):e0160563. doi: 10.1371/journal.pone.0160563
43. McArthur K, Chappaz S, Kile BT. Apoptosis in Megakaryocytes and Platelets: The Life and Death of a Lineage. *Blood* (2018) 131(6):605–10. doi: 10.1182/blood-2017-11-742684
44. Hua VM, Abeynaike L, Glaros E, Campbell H, Pasalic L, Hogg PJ, et al. Necrotic Platelets Provide a Procoagulant Surface During Thrombosis. *Blood* (2015) 126(26):2852–62. doi: 10.1182/blood-2015-08-663005
45. Jackson SP, Schoenwaelder SM. Procoagulant Platelets: Are They Necrotic? *Blood* (2010) 116(12):2011–8. doi: 10.1182/blood-2010-01-261669
46. Swanson KV, Deng M, Ting JP. The NLRP3 Inflammasome: Molecular Activation and Regulation to Therapeutics. *Nat Rev Immunol* (2019) 19 (8):477–89. doi: 10.1038/s41577-019-0165-0
47. Yu P, Zhang X, Liu N, Tang L, Peng C, Chen X. Pyroptosis: Mechanisms and Diseases. *Signal Transduct Target Ther* (2021) 6(1):128. doi: 10.1038/s41392-021-00507-5
48. Baron L, Gombault A, Fanny M, Villeret B, Savigny F, Guillou N, et al. The NLRP3 Inflammasome Is Activated by Nanoparticles Through ATP, ADP and Adenosine. *Cell Death Dis* (2015) 6:e1629. doi: 10.1038/cddis.2014.576

49. Yazdi AS, Guarda G, Riteau N, Drexler SK, Tardivel A, Couillin I, et al. Nanoparticles Activate the NLR Pyrin Domain Containing 3 (Nlrp3) Inflammasome and Cause Pulmonary Inflammation Through Release of IL-1alpha and IL-1beta. *Proc Natl Acad Sci USA* (2010) 107(45):19449–54. doi: 10.1073/pnas.1008155107
50. Sun B, Wang X, Ji Z, Li R, Xia T. NLRP3 Inflammasome Activation Induced by Engineered Nanomaterials. *Small* (2013) 9(9-10):1595–607. doi: 10.1002/smll.201201962
51. Tsuchiya K. Inflammasome-Associated Cell Death: Pyroptosis, Apoptosis, and Physiological Implications. *Microbiol Immunol* (2020) 64(4):252–69. doi: 10.1111/1348-0421.12771
52. Malireddi RKS, Kesavardhana S, Kanneganti TD. ZBP1 and TAK1: Master Regulators of NLRP3 Inflammasome/Pyroptosis, Apoptosis, and Necroptosis (PAN-Optosis). *Front Cell Infect Microbiol* (2019) 9:406. doi: 10.3389/fcimb.2019.00406
53. Meihe L, Shan G, Minchao K, Xiaoling W, Peng A, Xili W, et al. The Ferroptosis-NLRP1 Inflammasome: The Vicious Cycle of an Adverse Pregnancy. *Front Cell Dev Biol* (2021) 9:707959. doi: 10.3389/fcell.2021.707959
54. Biasizzo M, Kopitar-Jerala N. Interplay Between NLRP3 Inflammasome and Autophagy. *Front Immunol* (2020) 11:591803. doi: 10.3389/fimmu.2020.591803
55. Lv S, Wang H, Li X. The Role of the Interplay Between Autophagy and NLRP3 Inflammasome in Metabolic Disorders. *Front Cell Dev Biol* (2021) 9:634118. doi: 10.3389/fcell.2021.634118
56. Wu MS, Sun DS, Lin YC, Cheng CL, Hung SC, Chen PK, et al. Nanodiamonds Protect Skin From Ultraviolet B-Induced Damage in Mice. *J Nanobiotechnol* (2015) 13:35. doi: 10.1186/s12951-015-0094-4
57. Tseng PH, Sie ZL, Liu MC, Lin HS, Yang WY, Lin TY, et al. Identification of Two Novel Small Compounds That Inhibit Liver Cancer Formation in Zebrafish and Analysis of Their Conjugation to Nanodiamonds to Further Reduce Toxicity. *Adv Ther* (2019) 2(12):1900105. doi: 10.1002/adtp.201900105
58. Sow M, Steuer H, Adekanye S, Gines L, Mandal S, Gilboa B, et al. High-Throughput Nitrogen-Vacancy Center Imaging for Nanodiamond Photophysical Characterization and pH Nanosensing. *Nanoscale* (2020) 12(42):21821–31. doi: 10.1039/D0NR05931E
59. Hsiao WW, Hui YY, Tsai PC, Chang HC. Fluorescent Nanodiamond: A Versatile Tool for Long-Term Cell Tracking, Super-Resolution Imaging, and Nanoscale Temperature Sensing. *Acc Chem Res* (2016) 49(3):400–7. doi: 10.1021/acs.accounts.5b00484
60. Huang CY, Yu WS, Liu GC, Hung SC, Chang JH, Chang JC, et al. Opportunistic Gill Infection Is Associated With TiO2 Nanoparticle-Induced Mortality in Zebrafish. *PloS One* (2021) 16(7):e0247859. doi: 10.1371/journal.pone.0247859
61. Lien TS, Sun DS, Chang CM, Wu CY, Dai MS, Chan H, et al. Dengue Virus and Antiplatelet Autoantibodies Synergistically Induce Haemorrhage Through Nlrp3-Inflammasome and FcgammaRIII. *Thromb Haemost* (2015) 113(5):1060–70. doi: 10.1160/TH14-07-0637
62. Lien TS, Sun DS, Wu CY, Chang HH. Exposure to Dengue Envelope Protein Domain III Induces Nlrp3 Inflammasome-Dependent Endothelial Dysfunction and Hemorrhage in Mice. *Front Immunol* (2021) 12:617251. doi: 10.3389/fimmu.2021.617251
63. Chang YS, Ko BH, Ju JC, Chang HH, Huang SH, Lin CW. SARS Unique Domain (SUD) of Severe Acute Respiratory Syndrome Coronavirus Induces NLRP3 Inflammasome-Dependent CXCL10-Mediated Pulmonary Inflammation. *Int J Mol Sci* (2020) 21(9):1–19. doi: 10.3390/ijms21093179
64. Sun DS, Ho PH, Chang HH. Soluble P-Selectin Rescues Viper Venom-Induced Mortality Through Anti-Inflammatory Properties and PSGL-1 Pathway-Mediated Correction of Hemostasis. *Sci Rep* (2016) 6:35868. doi: 10.1038/srep35868
65. Sun DS, Chang YW, Kau JH, Huang HH, Ho PH, Tzeng YJ, et al. Soluble P-Selectin Rescues Mice From Anthrax Lethal Toxin-Induced Mortality Through PSGL-1 Pathway-Mediated Correction of Hemostasis. *Virulence* (2017) 8(7):1216–28. doi: 10.1080/21505594.2017.1282027
66. Chan H, Huang HS, Sun DS, Lee CJ, Lien TS, Chang HH. TRPM8 and RAAS-Mediated Hypertension Is Critical for Cold-Induced Immunosuppression in Mice. *Oncotarget* (2018) 9(16):12781–95. doi: 10.18632/oncotarget.24356
67. Sung PS, Huang TF, Hsieh SL. Extracellular Vesicles From CLEC2-Activated Platelets Enhance Dengue Virus-Induced Lethality via CLEC5A/Tlr2. *Nat Commun* (2019) 10(1):2402. doi: 10.1038/s41467-019-10360-4
68. Chuang DJ, Pethaperumal S, Siwakoti B, Chien HJ, Cheng CF, Hung SC, et al. Activating Transcription Factor 3 Protects Against Restraint Stress-Induced Gastrointestinal Injury in Mice. *Cells* (2021) 10(12):1–18. doi: 10.3390/cells10123530
69. Lien TS, Sun DS, Hung SC, Wu WS, Chang HH. Dengue Virus Envelope Protein Domain III Induces Nlrp3 Inflammasome-Dependent NETosis-Mediated Inflammation in Mice. *Front Immunol* (2021) 12:618577. doi: 10.3389/fimmu.2021.618577
70. Mandal JP, Shiue CN, Chen YC, Lee MC, Yang HH, Chang HH, et al. PKCdelta Mediates Mitochondrial ROS Generation and Oxidation of HSP60 to Relieve RKIP Inhibition on MAPK Pathway for HCC Progression. *Free Radic Biol Med* (2021) 163:69–87. doi: 10.1016/j.freeradbiomed.2020.12.003
71. Shiri R, Yari F, Ahmadinejad M, Vaeli S, Tabatabaei MR. The Caspase-3 Inhibitor (Peptide Z-DEVD-FMK) Affects the Survival and Function of Platelets in Platelet Concentrate During Storage. *Blood Res* (2014) 49(1):49–53. doi: 10.5045/br.2014.49.1.49
72. Indo HP, Yen HC, Nakanishi I, Matsumoto K, Tamura M, Nagano Y, et al. A Mitochondrial Superoxide Theory for Oxidative Stress Diseases and Aging. *J Clin Biochem Nutr* (2015) 56(1):1–7. doi: 10.3164/jcbn.14-42
73. Palma FR, He C, Danes JM, Paviani V, Coelho DR, Gantner BN, et al. Mitochondrial Superoxide Dismutase: What the Established, the Intriguing, and the Novel Reveal About a Key Cellular Redox Switch. *Antioxid Redox Signal* (2020) 32(10):701–14. doi: 10.1089/ars.2019.7962
74. Biermann MH, Podolska MJ, Knopf J, Reinwald C, Weidner D, Maueroder C, et al. Oxidative Burst-Dependent NETosis Is Implicated in the Resolution of Necrosis-Associated Sterile Inflammation. *Front Immunol* (2016) 7:557. doi: 10.3389/fimmu.2016.00557
75. Munoz LE, Bilyy R, Biermann MH, Kienhofer D, Maueroder C, Hahn J, et al. Nanoparticles Size-Dependently Initiate Self-Limiting NETosis-Driven Inflammation. *Proc Natl Acad Sci USA* (2016) 113(40):E5856–65. doi: 10.1073/pnas.1602230113
76. Bilyy R, Bila G, Vishchur O, Vovk V, Herrmann M. Neutrophils as Main Players of Immune Response Towards Nondegradable Nanoparticles. *Nanomater (Basel)* (2020) 10(7):1–15. doi: 10.3390/nano10071273
77. Paci JT, Man HB, Saha B, Ho D, Schatz GC. Understanding the Surfaces of Nanodiamonds. *J Phys Chem C* (2013) 117(33):17256–67. doi: 10.1021/jp404311a
78. Bertheloot D, Latz E, Franklin BS. Necroptosis, Pyroptosis and Apoptosis: An Intricate Game of Cell Death. *Cell Mol Immunol* (2021) 18(5):1106–21. doi: 10.1038/s41423-020-00630-3
79. Taabazuing CY, Okondo MC, Bachovchin DA. Pyroptosis and Apoptosis Pathways Engage in Bidirectional Crosstalk in Monocytes and Macrophages. *Cell Chem Biol* (2017) 24(4):507–514 e4. doi: 10.1016/j.chembiol.2017.03.009
80. Lawlor KE, Khan N, Mildenhall A, Gerlic M, Croker BA, D'Cruz AA, et al. RIPK3 Promotes Cell Death and NLRP3 Inflammasome Activation in the Absence of MLKL. *Nat Commun* (2015) 6:6282. doi: 10.1038/ncomms7282
81. McEver RP. Selectins: Initiators of Leucocyte Adhesion and Signalling at the Vascular Wall. *Cardiovasc Res* (2015) 107(3):331–9. doi: 10.1093/cvr/cvv154
82. Bila G, Rabets A, Bilyy R. Nano- and Microparticles and Their Role in Inflammation and Immune Response: Focus on Neutrophil Extracellular Traps. In: RS Stoika, editor. *Biomedical Nanomaterials*. Zürich: Springer (2022).
83. Greinacher A, Selleng K, Palankar R, Wesche J, Handtke S, Wolff M, et al. Insights in ChAdOx1 Ncov-19 Vaccine-Induced Immune Thrombotic Thrombocytopenia. *Blood* (2021) 138(22):2256–68. doi: 10.1182/blood.2021013231

Conflict of Interest: The authors declare that the research was conducted in the absence of any commercial or financial relationships that could be construed as a potential conflict of interest.

this article, or claim that may be made by its manufacturer, is not guaranteed or endorsed by the publisher.

frontiers | Frontiers in Immunology

TYPE Original Research
PUBLISHED 03 October 2022
DOI 10.3389/fimmu.2022.995911

OPEN ACCESS

EDITED BY
Paolo Immovilli,
Guglielmo da Saliceto Hospital, Italy

REVIEWED BY
Alina Gonzalez-Quevedo,
Instituto de Neurología y Neurocirugía, La Habana, Cuba
Yicheng Xu,
Aerospace Center Hospital, China
Chiara Terracciano,
Gugliemo da Saliceto Hospital, Italy

*CORRESPONDENCE
Xu Zhang
drzhangxu@126.com
Xiang Li
wzmulixiang@126.com

†These authors share first authorship

SPECIALTY SECTION
This article was submitted to Multiple Sclerosis and Neuroimmunology, a section of the journal Frontiers in Immunology

RECEIVED 16 July 2022
ACCEPTED 01 September 2022
PUBLISHED 03 October 2022

CITATION
Weng Y, Gao Y, Zhao M, Zeng T, Huang J, Xie H, Huang J, Chen Y, Hu X, Xu J, Zhu J, Lin S, Ke T, Li X and Zhang X (2022) The white blood cell count to mean platelet volume ratio for ischemic stroke patients after intravenous thrombolysis. *Front. Immunol.* 13:995911. doi: 10.3389/fimmu.2022.995911

The white blood cell count to mean platelet volume ratio for ischemic stroke patients after intravenous thrombolysis

Yiyun Weng[1,2†], Yufan Gao[2,3†], Mingyue Zhao[2†], Tian Zeng[2,4], Jiaqi Huang[2,4], Haobo Xie[2,4], Jiexi Huang[2,4], Yiqun Chen[2,4], Xiaoya Hu[2,3], Jiahan Xu[2,4], Jinrong Zhu[2,3], Suichai Lin[5], Tingting Ke[5], Xiang Li[2*] and Xu Zhang[2*]

[1]Department of Neurology, Shandong Provincial Qianfoshan Hospital, Cheeloo College of Medicine, Shandong University, Jinan, China, [2]Department of Neurology, The First Affiliated Hospital of Wenzhou Medical University, Wenzhou, China, [3]The Second School of Medicine, Wenzhou Medical University, Wenzhou, China, [4]The First School of Medicine, School of Information and Engineering, Wenzhou Medical University, Wenzhou, China, [5]Department of Emergency, The First Affiliated Hospital of Wenzhou Medical University, Wenzhou, China

Background and Purpose: White blood cell count to mean platelet volume ratio (WMR) is increasingly recognized as a promising biomarker. However, its predictive capability for acute ischemic stroke (AIS) patients is relatively less researched. The primary aim of this study is to explore its prognostic value in AIS patients after reperfusion regarding 3-month poor functional outcome.

Methods: A total of 549 AIS patients who had undergone vascular reperfusion procedure with complete 3-month follow-up were retrospectively recruited in this study. White blood cell count, mean platelet volume at 24 h of admission were recorded. Stroke severity had been estimated using the National Institutes of Health Stroke Scale (NIHSS) and poor outcome was defined as modified Rankin Scale (mRS) 3–6 at 3 months.

Results: AIS patients with poor functional outcome at 3 months displayed higher WMR. A positive correlation between WMR and NIHSS score was found ($r = 0.334$, $p < 0.001$). After adjusting potential confounders, WMR was still an independent risk factor for poor prognosis at 3 months (OR = 2.257, 95% CI [1.117-4.564], $p = 0.023$) in multivariate logistic regression model. Subgroup analyses further suggested a significant association between WMR and poor outcome in high baseline NIHSS (per 0.1-point increase: OR = 1.153, 95% CI [1.014-1.312], $p = 0.030$) group. Receiver operating characteristic (ROC) curves analysis was utilized to assess the predictive ability of WMR, indicating a cut-off value of 0.86. A nomogram that includes age, sex, NIHSS on admission, high WMR for predicting 1-year all-cause survival was also developed (C-index = 0.628).

Conclusions: WMR is significantly correlated with stroke severity on admission and is proved to be an important prognostic indicator for AIS outcomes,

especially in high NIHSS on admission group. Additionally, the developed nomogram that includes high WMR for predicting 1-year survival provides us with an effective visualization tool.

KEYWORDS

WMR, ischemic stroke, inflammation, intravenous thrombolysis, prognosis

Introduction

Acute ischemic stroke (AIS) is a major type of stroke that can cause high mortality and morbidity (1). As a currently accepted and recognized management by rapid vascular reperfusion within 4.5 h of stroke onset, intravenous thrombolysis has been reported to yield a powerful effect on clinical outcomes and reduce disability in AIS patients (2). However, due to the following pathophysiological process after therapy, a proportion of patients are still inclined to develop poor functional outcomes (3). Therefore, seeking an accurate and reliable prognostic indicator to distinguish AIS patients after vascular reperfusion that may have a higher risk of poor functional outcomes is of great clinical value (4).

Systemic inflammation response, in which white blood cell (WBC) plays a vital role, has been proved to be involved in the pathogenesis in ischemic stroke (5). Previous studies among AIS patients have found an association between early elevation of leukocyte and the volume of infarcted area, which has been proven to be positively correlated to poor functional outcomes (6, 7). Also, several studies have suggested that WBC on admission is correlated with greater degree of neurological impairment and unfavorable long-term outcome (8, 9).

Mean platelet volume (MPV), which reflects platelet size, can provide information of platelet function and activation (10). Hyperactive platelets play a pivotal role in thrombus formation and propagation (4), which is one of the pathological processes of AIS. In inflammatory conditions, MPV is also associated with increased percentage of large platelets (11). The predictive value of MPV in ischemic stroke has been explored and confirmed in other studies (4, 12).

As a combination of the two above-mentioned biomarkers, white blood cell count to mean platelet volume ratio (WMR) indicates to be more stable and comprehensive regarding the pathology of AIS (13). It has been recognized in other literature as a relatively new marker for prognosis in atherosclerotic diseases and myocardial infarction (14). Moreover, recent evidence suggested an association between platelet-to-white blood cell ratio (PWR), a similar index to WMR, and the National Institutes of Health Stroke Scale (NIHSS) on admission and on 7 days after admission in AIS patients (15). This previous study has also provided important information on the clinical value of the two combined biomarkers. However, the predicting value of WMR in the prognosis of AIS patients still remains less researched. Therefore, in this retrospective observatory cohort study, we sought to analyze whether WMR would be able to indicate patients at high risk for poor outcomes at 3 months after vascular reperfusion.

Materials and methods

Study population

In this retrospective study, a total of 549 AIS patients receiving intravenous thrombolysis therapy were consecutively recruited from the First Affiliated Hospital of Wenzhou Medical University from January 2019 to December 2020. The exclusion criteria were set as follows (1): with cancer; (2) with autoimmune diseases; (3) with severe hepatic failure or renal failure; (4) use of steroid or non-steroid anti-inflammatory treatment (14, 16); (5) with infections within 48h after admission.

We followed up these patients for 3 months and 1 year after AIS onset. After excluding 108 patients with missing data, there remained 441 patients. Finally, a total of 329 patients were eligible for analysis with complete 3-month follow-up. Figure 1 shows the exclusion and inclusion procedure in the form of flow chart.

The study was approved by the Ethics Committee of the First Affiliated Hospital of Wenzhou Medical University and was performed in accordance with the Declaration of Helsinki. All patients signed a written informed consent form.

Data collection

Demographic data (age, sex) and medical history (smoking, alcohol, hypertension, diabetes, atrial fibrillation, coronary artery disease and prior stroke) of patients were obtained from medical records. Serum biomarkers included WBC count, MPV collected at 24 h of admission. WMR was calculated with WBC counts divided by MPV. Stroke severity was measured by NIHSS

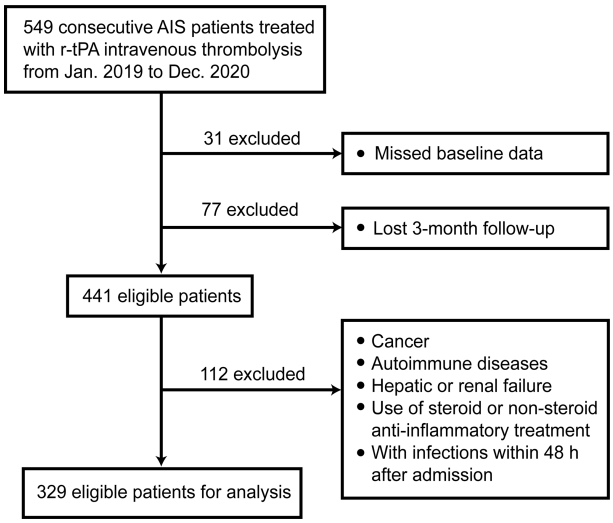

FIGURE 1
Flow chart for patient selection.

on admission and 24 h after admission. At 3 months and 1 year after the onset of AIS, the prognoses of patients were assessed using modified Rankin Scale (mRS) through telephone follow-up by two experienced clinicians.

Clinical assessment

The etiology of AIS was classified based on the Trial of Org 10,172 in Acute Stroke Treatment (TOAST) criteria: large artery atherosclerosis (LAA), small artery occlusion (SAO), cardio-embolism (CE), and others (17). Primary outcome included death or major disability at 3 months, defined as mRS score at 3-6. Secondary outcomes included poor functional outcome at 3 months defined by mRS score 2-6, early neurological improvement (ENI) defined as NIHSS score at 0-1 within 24 h after thrombolysis (18), early neurological deterioration decrease (END) defined as a decrease ≥ 4 points in the NIHSS score (19), death or major disability (mRS 3-6) at 1 year and all-cause mortality at 1 year.

Statistical analysis

We used SPSS Statistics 26.0.0.0, MedCalc Statistical Software version 18.2.1, GraphPad Prism version 9.0.0 and R version 4.1.3 for plots and statistical analyses. Data were first analyzed for normality of distribution using the Kolmogorov-Smirnov test of normality. Continuous variables with normal distribution were expressed as mean with standard deviation (mean ± SD) while continuous variables with non-normal distribution were expressed as medians and interquartile range (median, IQR). Patients were attributed into high/low WMR groups according to the cut-off value and inter-group differences were compared using Mann-Whitney U test. Participants were then divided into four groups according to WMR quartile (Q1 < 0.581, Q2 0.581-0.728, Q3 0.728-0.919, Q4 > 0.919). Differences of baseline characteristics across WMR quartile were compared using Kruskal-Wallis test. Categorical variables were presented as frequency and percentages (n, %) and differences among groups were compared through chi-squared test or Fisher's exact test.

Case distribution across quartile-based categories of WMR and mRS score at 3 months was presented using density plots. To test the correlation between WMR and NIHSS, we calculated Spearman's correlation coefficient. To account for differences in low WMR distributions across stroke subtype, and differences in mRS distribution in high and low WMR groups classified using WMR cutoff value, chi-squared test was performed.

Univariate and multivariate logistic analyses were utilized to demonstrate the association between WMR and primary outcome. The crude model, model 1, was carried out by univariate analysis. In model 2, we adjusted for covariates with a p-value < 0.1 in model 1. To further explore the potential predictive ability disparity in different subgroups, stratified analysis was undertaken. With WMR median as a node undergoing binary logistic regression, restricted cubic splines with 3 knots (at 0.6, 0.9 1.2 respectively) were also plotted to demonstrate the correlation between WMR and AIS outcomes.

Receiver operating characteristic (ROC) analysis was employed to determine the optimal cutoff value and the ability of WMR to distinguish poor functional outcomes. Multivariable

time-to-event analysis was performed using Cox proportional hazards regression models to develop a nomogram using weighted estimators corresponding to each covariate that was found statistically significant in predicting 1-year mortality using multivariate regression model. A *p*-value of less than 0.05 was considered statistically significant.

Results

Characteristics of study patients

A total of 329 AIS patients after intravenous thrombolysis were retrospectively included for analysis in this study, with a median age of 67 years and men accounting for 64.1% (211). The median NIHSS score on admission for all study patients was 6, and median WMR was 0.73. A total of 91 (27.7%) patients had poor functional outcomes at 3 months, 31 patients (9.4%) died during the 1-year follow-up. The clinical characteristics of AIS patients were displayed in Table 1. Compared with patents with a good functional outcome, those in the poor outcome group had significantly older age (median age: 72.0 vs. 65.0, $p < 0.001$), higher proportion of hypertension (71.4% vs. 50.4%, $p = 0.001$), higher proportion of atrial fibrillation (AF) (12.1% vs. 5.5%, $p = 0.039$), higher WBC count (median: 9.0 vs. 7.5, $p < 0.001$), higher WMR (median: 0.88 vs. 0.70, $p < 0.001$), higher NIHSS on admission (median: 12.0 vs. 5.0, $p < 0.001$), and at 24 h (median: 13.0 vs. 4.0, $p < 0.001$). Those with a good functional outcome were more likely to be male (71.4% vs. 45.1%, $p < 0.001$) and the small artery occlusion (SAO) subtype (24.8% vs. 4.4%, $p < 0.001$). Furthermore, smoking history (41.2% vs. 26.4%, $p = 0.013$), alcohol drinking history (38.2% vs. 25.3%, $p = 0.027$) were more prevalent in patients with a good outcome in comparison with those with a poor outcome.

As illustrated in Table 2, it was found that smoking, WBC count, MPV, NIHSS on admission and at 24 h, SAO subtype

TABLE 1 Characteristics of AIS patients with or without poor function outcomes at 90 days.

Characteristics	Total	Functional outcomes		
		mRS 0-2 (n = 238)	mRS 3-6 (n = 91)	*p*
Demographic data				
Age (years)	67.0 (57.0-75.0)	65.0 (55.0-74.0)	72.0 (62.0-80.0)	< 0.001
Sex, (male, n%)	211 (64.1)	170 (71.4)	41 (45.1)	< 0.001
Stroke risk factors, n (%)				
Smoking	122 (37.1)	98 (41.2)	24 (26.4)	0.013
Alcohol	114 (34.7)	91 (38.2)	23 (25.3)	0.027
Hypertension	185 (56.2)	120 (50.4)	65 (71.4)	0.001
Diabetes	55 (16.7)	34 (14.3)	21 (23.1)	0.056
AF	24 (7.3)	13 (5.5)	11 (12.1)	0.039
CAD	13 (4.0)	10 (4.2)	3 (3.3)	1.000
Prior stroke	31 (9.4)	19 (8.0)	12 (13.2)	0.148
Serum biomarkers				
WBC count, ($\times 10^9$/L)	7.9 (6.5-10.0)	7.5 (6.1-9.6)	9.0 (7.5-11.2)	< 0.001
MPV, (fL)	10.9 (10.2-11.5)	10.9 (10.2-11.4)	11.0 (10.1-11.8)	0.924
WMR	0.73 (0.58-0.92)	0.70 (0.56-0.86)	0.88 (0.66-1.07)	< 0.001
Clinical features				
NIHSS on admission	6.0 (3.5-11.0)	5.0 (3.0-7.0)	12.0 (9.0-17.0)	< 0.001
NIHSS at 24h	5.0 (3.0-11.0)	4.0 (2.0-6.0)	13.0 (9.0-20.0)	< 0.001
DNT	43.5 (33.2-55.1)	42.5 (32.7-52.9)	46.1 (34.9-59.6)	0.094
Stroke subtype, n				< 0.001
LAA, n (%)	136 (41.3)	93 (39.1)	43 (47.3)	
SAO, n (%)	63 (19.1)	59 (24.8)	4 (4.4)	
CE, n (%)	83 (25.2)	53 (22.3)	30 (33.0)	
Others, n (%)	47 (14.3)	33 (13.9)	14 (15.4)	
Reperfusion therapy				< 0.001
IVT, n (%)	277 (84.2)	211 (88.7)	66 (72.5)	
Bridging therapy, n (%)	52 (15.8)	27 (11.3)	25 (27.5)	

mRS, modified ranking scale; WMR, white blood cell to mean platelet volume ratio; AF, atrial fibrillation; CAD, coronary artery disease; WBC, white blood cell; MPV, mean platelet volume; NIHSS, national institute of health stroke scale; LAA, large artery atherosclerosis; SAO, small artery occlusion; CE, cardio-embolism; IVT, intravenous thrombolysis.

TABLE 2 Comparisons of baseline characteristics and outcomes between groups divided according to WMR quartile.

Characteristics	WMR				*p*
	Q1 (< 0.581)	Q2 (0.581-0.728)	Q3 (0.728-0.919)	Q4 (> 0.919)	
n	82	84	81	82	
Demographic data					
Age, (years)	68.0 (58.0-75.0)	68.0 (58.8-77.8)	67.0 (555-73.5)	63.5 (56.0-75.0)	0.367
Sex, (male, n%)	55 (67.0)	48 (57.1)	56 (69.1)	52 (63.4)	0.393
Stroke risk factors, n (%)					
Smoking	29 (35.3)	24 (28.5)	41 (50.6)	28 (34.1)	0.025
Alcohol	33 (40.2)	23 (33.3)	29 (35.8)	24 (29.2)	0.514
Hypertension	41 (50.0)	51 (60.7)	48 (59.2)	45 (54.8)	0.504
Diabetes	12 (14.6)	13 (15.4)	16 (19.7)	14 (17.0)	0.827
AF	7 (8.5)	8 (9.5)	1 (1.2)	8 (9.7)	0.066
CAD	1 (1.2)	4 (4.7)	5 (6.1)	3 (3.6)	0.413
Prior stroke	11 (13.4)	8 (9.5)	9 (11.1)	3 (3.6)	0.138
Serum biomarkers					
WBC count, ($\times 10^9$/L)	5.5 (4.6-6.2)	7.2 (6.7-7.8)	8.9 (8.2-9.7)	11.5 (10.6-13.5)	< 0.001
MPV, (fL)	11.2 (10.7-11.9)	11.1 (10.3-11.6)	10.6 (10.1-11.4)	10.5 (10.0-11.2)	< 0.001
Clinical features					
NIHSS on admission	4.0 (3.0-5.0)	6.0 (4.0-10.0)	6.0 (4.0-10.0)	10.0 (5.0-16.0)	< 0.001
NIHSS at 24h	4.0 (2.0-5.0)	6.0 (3.0-10.0)	5.0 (3.0-9.8)	9.0 (4.0-15.0)	< 0.001
DNT	44.3 (33.5-56.6)	41.1 (30.9-54.3)	47.6 (34.9-57.6)	42.8 (33.4-51.5)	0.502
Stroke subtype, n					
LAA, n (%)	29 (35.3)	30 (35.7)	39 (48.1)	38 (46.3)	0.195
SAO, n (%)	21 (25.6)	19 (22.6)	16 (19.7)	7 (8.5)	0.031
CE, n (%)	19 (23.1)	24 (28.5)	15 (18.5)	25 (30.4)	0.282
Others, n (%)	13 (15.8)	11 (13.0)	11 (13.5)	12 (14.6)	0.959
Reperfusion therapy					
IVT, n (%)	77 (93.9)	71 (84.5)	73 (90.1)	56 (68.2)	< 0.001
Bridging therapy, n (%)	5 (6.0)	13 (15.4)	8 (9.8)	26 (31.7)	< 0.001
Outcome					
mRS 3-6 at 90 days, n (%)	10 (12.1)	22 (26.1)	22 (27.1)	37 (45.1)	< 0.001
mRS 2-6 at 90 days, n (%)	19 (23.1)	33 (39.2)	29 (35.8)	48 (58.5)	< 0.001
ENI	12 (14.6)	13 (15.4)	7 (8.6)	7 (8.5)	0.375
END	3 (3.6)	7 (8.3)	7 (8.6)	10 (12.1)	0.221
mRS 3-6 at 1 year, n (%)	3 (3.6)	14 (16.6)	15 (18.5)	25 (30.4)	< 0.001
Mortality at 1 year, n (%)	0 (0)	5 (5.9)	10 (12.3)	16 (19.5)	< 0.001

WMR, white blood cell to mean platelet volume ratio; AF, atrial fibrillation; CAD, coronary artery disease; WBC, white blood cell; MPV, mean platelet volume; NIHSS, national institute of health stroke scale; DNT, door to needle time; LAA, large artery atherosclerosis; SAO, small artery occlusion; CE, cardio-embolism; IVT, intravenous thrombolysis; mRS, modified ranking scale; ENI, early neurological improvement; END, early neurological deterioration.

distribution, mRS score 3-6, 2-6, mRS 3-6 at 1 year mortality rate at 1 year differed by WMR quartile.

The correlation between WMR and clinical status

We plotted a density plot to display patient distribution cross WMR quartile. The intensity of color represented the frequency of cases. It can be observed in Figure 2A, that in general, 200 out of the total 329 cases had the outcome mRS 0-1 (60.8%). In Q1, cases with mRS score at 1 took up the highest proportion (46.3%), while in Q4, 15 cases developed a mRS score at 6 (18.3%). The case distribution across WMR quartile was statistically significant ($p < 0.001$). Correlation analysis demonstrated a significant linear trend between WMR and baseline NIHSS ($r = 0.334$, $p < 0.001$). The size of circles represented the relative weighting of mRS score at 3 months. It can be seen in Figure 2B, that patients with higher WMR showed a higher NIHSS score on admission and a higher mRS score at 3 months. We further investigated the difference in distribution of mRS score between patients in high WMR group

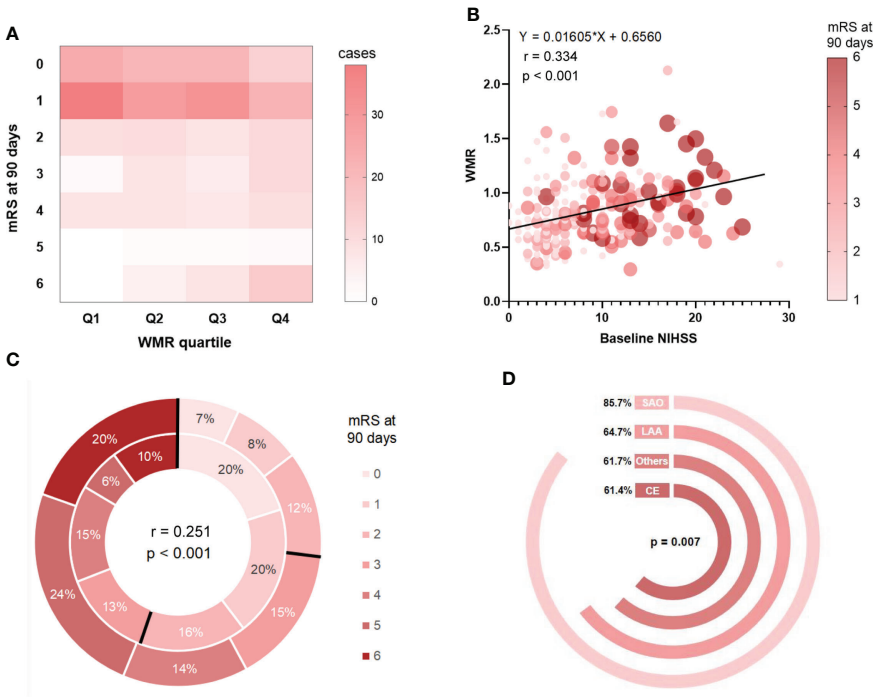

FIGURE 2
Correlation analyses between WMR and patient features and outcome. **(A)**: Case distribution across quartile-based categories of WMR and mRS score at 90 days. **(B)**: The relationships between WMR and baseline NIHSS as well as mRS at 3 months. **(C)** mRS distribution at 3 months for high WMR group v.s. low WMR group. The outer layer represented distribution of mRS score in high WMR group while the inner layer represented that in low WMR group. **(D)**: Ratio of low WMR group in different stroke subtypes.

(the outer layer of the circle) and low WMR group (the inner layer). High WMR was found to be positively related to death or major disability (mRS 3-6) (r = 0.251, $p < 0.001$), and proportion of mRS 3-6 in high WMR group was more prominent compared with that in low WMR group (Figure 2C). In addition, we plotted Figure 2D, to visually display the ratio of low WMR group in different stroke subtypes. Chi-squared test verified a significant difference in low WMR distributions across stroke subtype ($p = 0.007$), and proportion of low WMR was reported to be the largest in SAO subtype (85.7%).

Predictive value of WMR for primary outcome

As shown in model 1 conducted under the univariate regression analyses, age, smoking, alcohol, hypertension, AF, NIHSS on admission, stroke subtypes and high WMR (OR = 3.169, 95% CI [1.913-5.249], $p < 0.001$) were found significantly associated with primary outcome (mRS 3-6) at 3 months. To determine whether high WMR possessed the ability to independently indicate the prognosis for poor outcome at 3 months, multivariate logistic regression was then performed. In model 2, after adjusting for potential confounders with a p-value < 0.1 in model 1, high WMR remained to have an independent association with poor 3-month function outcome (OR = 2.257, 95% CI [1.117-4.564], $p = 0.023$) (Table 3). Univariate logistic regression model with restricted cubic splines revealed a positive association between WMR level and the odds of 3-month poor outcomes, including mRS 3-6 and mRS 2-6 (both p for linearity < 0.001, Figure 3).

In terms of the ROC analysis for the prediction of poor 3-month outcome using WMR, the cut-off value with the optimal distinguishing capacity of this indicator was 0.86 (a sensitivity of 51.6 and a specificity of 75.2). Additionally, The area under curve (AUC) was 0.662 (95% CI [0.608-0.713], $p < 0.001$) (Figure S1).

Subgroup analyses

In subgroup analyses stratified by age, sex, smoking, alcohol, hypertension, diabetes, NIHSS on admission and stroke subtype (LAA), an attenuated association between WMR and poor functional outcomes in patients with lower NIHSS score on admission was identified (Table 4). WMR per 0.1-point increase was independently associated with poor functional outcomes in age ≥ 67 (OR = 1.207, 95% CI [1.015–1.436], $p = 0.034$) and NIHSS on admission ≥ 6 (OR = 1.153, 95% CI [1.014–1.312], $p = 0.030$) groups (Table 4).

TABLE 3 Univariate and multivariate logistic regression analysis for 3-month poor outcome.

	Model 1		Model 2	
Variables	**OR (95% CI)**	***p***	**OR (95% CI)**	***p***
Age (years)	1.050 (1.027-1.073)	< 0.001	1.033 (1.002-1.064)	0.034
Sex (male, n%)	0.328 (0.199-0.541)	< 0.001	0.283 (0.121-0.661)	0.004
Vascular risk factors, n (%)				
Smoking	1.954 (1.147-3.330)	0.014	0.986 (0.385-2.526)	0.976
Alcohol	1.830 (1.066-3.141)	0.028	1.386 (0.547-3.508)	0.491
Hypertension	2.458 (1.460-4.139)	0.001	1.290 (0.628-2.652)	0.488
Diabetes	1.800 (0.980-3.306)	0.058	1.306 (0.538-3.167)	0.555
AF	2.380 (1.025-5.526)	0.044	1.203 (0.247-5.865)	0.819
CAD	0.777 (0.209-2.891)	0.707		
Prior stroke	1.751 (0.813-3.771)	0.152		
NIHSS on admission	1.267 (1.197-1.342)	< 0.001	1.213 (1.136-1.296)	< 0.001
DNT	1.012 (0.999-1.024)	0.068	1.014 (0.997-1.031)	0.102
Stroke subtype, n (%)				
LAA	1.000	0.002	1.000	0.049
SAO	0.147 (0.050-0.430)	< 0.001	0.131 (0.026-0.654)	0.013
CE	1.224 (0.689-2.177)	0.491	0.484 (0.197-1.184)	0.112
Others	0.918 (0.226-1.889)	0.815	0.892 (0.342-2.325)	0.815
High WMR	3.169 (1.913-5.249)	< 0.001	2.257 (1.117-4.564)	0.023

Model 2: adjusted for age, sex, smoking, alcohol, hypertension, diabetes, atrial fibrillation, NIHSS at admission, DNT, stroke subtype and high WMR.
OR, odd ratio; CI, confidence interval; AF, atrial fibrillation; CAD, coronary artery disease; WBC, white blood cell; MPV, mean platelet volume; WMR, white blood cell to mean platelet volume ratio; NIHSS, national institute of health stroke scale; DNT, door to needle time; LAA, large artery atherosclerosis; SAO, small artery occlusion; CE, cardio-embolism.

Predictive value of WMR for all-cause mortality

Univariate and multivariate analyses (Table S2) were performed to spot prognostic factors to build the nomogram. In the univariate analysis, age (OR = 1.092, 95% CI [1.050–1.135], $p < 0.001$), sex (OR = 0.383, 95% CI [0.176–0.836], $p = 0.016$), hypertension (OR = 3.843, 95% CI [1.502–9.833], $p = 0.005$), AF (OR = 8.064, 95% CI [2.290–28.400], $p = 0.001$), NIHSS on admission (OR = 1.260, 95% CI [1.163–1.364], $p < 0.001$) and high WMR (OR = 4.007, 95% CI [1.795–8.943], $p = 0.001$) were found to be independent risk factors for 1-year mortality. After including these factors with $p < 0.05$ into the multivariate logistic regression model, age (OR = 1.076, 95% CI [1.028–1.126], $p = 0.002$), NIHSS on admission (OR = 1.190, 95% CI [1.085–1.305], $p < 0.001$), and high WMR (OR = 3.251, 95% CI [1.145–9.227], $p = 0.027$) still remained significant. By including those, a nomogram was constructed (Figure 4) and was evaluated to possess a relatively high accuracy (C-index = 0.628). Table on the right showed the use of the nomogram with one death case as an example. For an 85-year-old patient with NIHSS score on admission at 14 and WMR at 0.72, the total

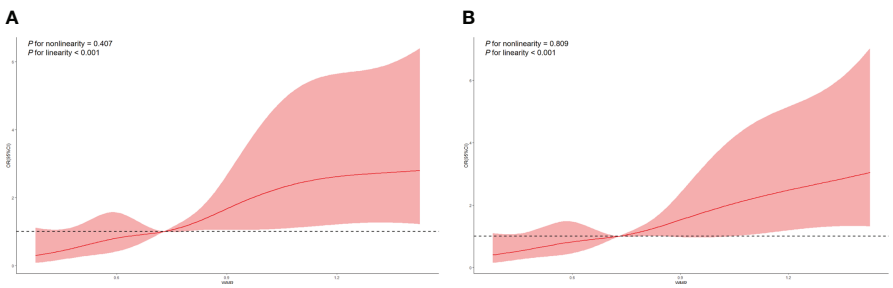

FIGURE 3
Restricted cubic spline regression analyses of WMR and poor outcomes. **(A)** mRS 3-6 at 3 months. **(B)** mRS 2-6 at 3 months.

10.3389/fimmu.2022.995911

TABLE 4 Subgroup analyses of the association between WMR and primary outcome (death or major disability).

Subgroups	Primary outcome: death or major disability (mRS 3-6)			
	N	Events (%)	WMR* OR (95% CI)	*p*
Age (≥ 67)				
Yes	173	62 (35.8)	1.207 (1.015-1.436)	0.034
No	156	29 (18.6)	0.975 (0.818-1.161)	0.773
Interaction				0.568
Sex (Male)				
Yes	211	41 (19.4)	1.059 (0.894-1.253)	0.509
No	118	50 (42.4)	1.198 (0.993-1.445)	0.059
Interaction				0.217
Smoking				
Yes	122	24 (19.7)	1.088 (0.879-1.348)	0.439
No	207	67 (32.4)	1.148 (0.980-1.346)	0.088
Interaction				0.262
Alcohol				
Yes	114	23 (20.2)	1.109 (0.918-1.339)	0.285
No	215	68 (31.6)	1.133 (0.975-1.317)	0.104
Interaction				0.554
Hypertension				
Yes	185	65 (35.1)	1.064 (0.905-1.251)	0.454
No	144	26 (18.1)	1.140 (0.885-1.467)	0.310
Interaction				0.340
Diabetes				
Yes	55	21 (38.2)	1.164 (0.671-2.020)	0.589
No	274	70 (25.5)	1.128 (0.998-1.276)	0.054
Interaction				0.654
NIHSS on admission (≥ 6)				
Yes	169	79 (46.7)	1.153 (1.014-1.312)	0.030
No	160	12 (7.5)	1.031 (0.788-1.348)	0.825
Interaction				0.036
Stroke subtype (LAA)				
Yes	136	43 (31.6)	1.079 (0.912-1.277)	0.373
No	193	48 (24.9)	1.125 (0.956-1.324)	0.158
interaction				0.639

The above model adjusted for age, sex, smoking, alcohol, hypertension, diabetes, atrial fibrillation, NIHSS at admission and stroke subtype. In each case, the model is not adjusted for the stratification variable. WMR*, per 0.1 point increase. OR, odd ratio; CI, confidence interval; mRS, modified ranking scale; AF, atrial fibrillation; NIHSS, national institute of health stroke scale; SAO, small artery occlusion; CE, cardio-embolism; OR, odd ratio; CI, confidence interval.

score (143) was calculated with corresponding scores on the nomogram and presented the 1-year survival prognosis score (< 0.1).

Discussion

This study set out to explore the association between the relatively new biomarker WMR and the functional outcomes in patients with AIS after intravenous thrombolysis therapy. Overall, our current study mainly established that (1) WMR was significantly higher in patients with poor functional outcomes; (2) There was a linear relationship between WMR and NIHSS on admission, mRS 3-6, and mRS 2-6; (3) After adjusting for potential confounders, high WMR was still significantly correlated with primary outcome; (4) WMR was independently associated with poor functional outcome in older age and high NIHSS score on admission group, and the association was attenuated in patients with lower NIHSS score on admission. (5) WMR could be utilized to predict 1-year survival with a nomogram.

Vascular reperfusion as a therapy to restore the blood supply and limit the brain damage plays an important role in the management of AIS. Currently, available types of therapy to realize the purpose of vascular reperfusion in AIS patients mainly include intravenous thrombolysis and endovascular treatment (20). However, due to the complex stroke pathobiology, these strategies

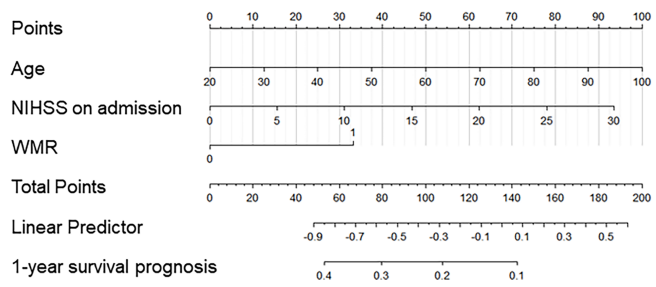

Variables	State	Score
Age	85	75
NIHSS on admission	14	44
WMR	0.72	24
Total Points	NA	143
1-year survival prognosis	NA	< 0.1

FIGURE 4
Instructions for using nomogram.

may have limited effectiveness and induce serious side effects (21). In the past few decades, blood-based biomarkers for prognosis of poor functional outcomes following reperfusion therapy in AIS patients has been an object of research (22). Therefore, it is of great importance to identify reliable and accurate biomarkers that could facilitate disease management and clinical decision making.

The impact of inflammatory processes in the progression of AIS has been widely recognized (5). Previous studies have validated that an elevated WBC count is independently associated with stroke severity on admission, poor functional outcomes at discharge, and mortality rates in AIS patients (6). Our data suggested a significantly elevated WBC count at 24 h of admission in the group with poor functional outcome, which also supported the prognostic capability of WBC count.

Platelets play a role in the formation of atherosclerosis and atherothrombosis, which is a critical process during the pathophysiology of stroke (23). They not only participate in clot formation, but are also involved in inflammatory processes (24). During the inflammatory course, the proportion of larger platelets was found to increase, probably because of a synthesis of factors that promote coagulation and inflammation, and a release of platelet stored in the spleen (11). At the same time, these platelets are fast recruited to the inflammation site where they might be activated and worn down, which can possibly account for the decrease of MPV in patients in an inflammation condition (25). Besides, ischemia-reperfusion injury (IRI) is also a prominent pathological process after reperfusion therapy in AIS patients, which may result in a consumption and sequestration of platelets, and thus be a part of the explanation (24).

WMR as a composite marker comprised of WBC count and MPV, indicates a promising value for the prognosis of cardiovascular outcomes (14). The interaction between the two single biomarkers is suggested to be related to the inflammatory response and stroke infarction development, where their counts are mutually affected (15). The elevation of WMR has been demonstrated by other study to reliably identify lower extremity artery disease (LEAD) patients at high risk for chronic limb-threatening ischemia (CLTI), and an association with the endpoint of stroke, which has not been elaborated (13). Additionally, WMR has also been researched in the prediction for patients with non-ST elevation myocardial infarction (14). Though previous research has identified an association between PWR with the severity of AIS and also divided patients according to stroke etiology, it did not examine the long-term prognostic value of the index and did not consider reperfusion therapy (15). In the current study, we explored the predictive value of WMR for different outcomes in a group of patients that all had undergone reperfusion therapy and conducted a further subgroup analysis. However, the prognostic value of WMR in AIS remains less researched. Therefore, more trials concentrating on AIS patients regarding the efficacy of WMR are supposed to be carried out in the future to validate our findings.

Our findings of the elevation in WMR might be explained by an increase in the WBC count and an decrease in the MPV in the inflammation process, which can provide indications for the disease development for AIS patients (13). Sensitivity and specificity analysis demonstrated that compared to WBC as an independent predictor, the value of sensitivity decreased but specificity for prognosis improved after adding MPV to form the WMR parameter, which reduces the probability of false positive rate (Table S1). At the same time, it can be easily calculated using the two cheap and available biomarkers from a complete blood cell count test. Thus, it can be of help for clinicians to make relatively accurate prognosis for AIS patients at an early stage.

However, it should be noted that several limitations still exist in our study. First, considering the retrospective and observational nature of this study, it was unable to determine the causality between WMR and poor functional outcomes. Second, the sample size was relatively small. Among the 549 patients who were initially enrolled under the inclusion criteria, 31 (5.6%) patients were excluded for missing baseline data and 77 (14.0) were excluded for the loss of 3 months follow-up. Partly due to the sample size, the ROC curve for the prediction of a 3-month poor outcome using WMR did not reach a high

prediction capability (AUC 0.662, sensitivity 51.6, specificity 75.2), which needs to be further researched with a larger data base. Additionally, this study was monocentric so selection bias might still exist and an external validation of the nomogram could not be conducted.

Conclusion

Our study demonstrated that there is a linear correlation between WMR and NIHSS on admission. High WMR is positively related to a poor functional outcome, and possesses a prognostic potential for AIS outcomes. The predictive capability is especially prominent in older and neurologically more severe groups. Furthermore, as an easily obtainable and cost-effective parameter, WMR can also be utilized to predict 1-year mortality.

Data availability statement

The raw data supporting the conclusions of this article will be made available by the authors, without undue reservation.

Ethics statement

The studies involving human participants were reviewed and approved by the First Affiliated Hospital of Wenzhou Medical University. The patients/participants provided their written informed consent to participate in this study.

Author contributions

XL and XZ conceptualized this work. XL and XZ supervised the study. YW, YG, MZ, TZ, JH, HX, JH, YC, XH, JX, JZ, SL, TK acquisition of data, YW, YG, MZ performed the statistical analysis and interpreted data. YW, YG, MZ prepared the manuscript. XL, XZ, YW, YG, MZ, TZ, JH, HX, JH, YC, XH, JX, JZ, SL, TK revised the manuscript. All authors approved the protocol.

Acknowledgments

We sincerely thank the participating hospitals, patients, their families and colleagues who have provided valuable suggestions for this study.

Conflict of interest

The authors declare that the research was conducted in the absence of any commercial or financial relationships that could be construed as a potential conflict of interest.

Publisher's note

Supplementary material

The Supplementary Material for this article can be found online at: https://www.frontiersin.org/articles/10.3389/fimmu.2022.995911/full#supplementary-material

References

1. Campbell BCV, Khatri P. Stroke. *Lancet* (2020) 396(10244):129–42. doi: 10.1016/S0140-6736(20)31179-X

2. Campbell BCV, De Silva DA, Macleod MR, Coutts SB, Schwamm LH, Davis SM, et al. Ischaemic stroke. *Nat Rev Dis Primers* (2019) 5(1):70. doi: 10.1038/s41572-019-0118-8

3. Orellana-Urzua S, Rojas I, Libano L, Rodrigo R. Pathophysiology of ischemic stroke: Role of oxidative stress. *Curr Pharm Design* (2020) 26(34):4246–60. doi: 10.2174/1381612826666200708133912

4. Staszewski J, Pogoda A, Data K, Walczak K, Nowocien M, Frankowska E, et al. The mean platelet volume on admission predicts unfavorable stroke outcomes in patients treated with IV thrombolysis. *Clin Interventions Aging* (2019) 14:493–503. doi: 10.2147/CIA.S195451

5. Stoll G, Nieswandt B. Thrombo-inflammation in acute ischaemic stroke - implications for treatment. *Nat Rev Neurol* (2019) 15(8):473–81. doi: 10.1038/s41582-019-0221-1

6. Furlan JC, Vergouwen MDI, Fang J, Silver FL. White blood cell count is an independent predictor of outcomes after acute ischaemic stroke. *Eur J Neurol* (2014) 21(2):215–22. doi: 10.1111/ene.12233

7. Zaidi SF, Aghaebrahim A, Urra X, Jumaa MA, Jankowitz B, Hammer M, et al. Final infarct volume is a stronger predictor of outcome than recanalization in patients with proximal middle cerebral artery occlusion treated with endovascular therapy. *Stroke* (2012) 43(12):3238–44. doi: 10.1161/STROKEAHA.112.671594

8. Lee CD, Folsom AR, Nieto FJ, Chambless LE, Shahar E, Wolfe DA. White blood cell count and incidence of coronary heart disease and ischemic stroke and mortality from cardiovascular disease in African-American and white men and women - atherosclerosis risk in communities study. *Am J Epidemiol* (2001) 154 (8):758–64. doi: 10.1093/aje/154.8.758

9. Zheng X, Zeng N, Wang A, Zhu Z, Zhong C, Xu T, et al. Prognostic value of white blood cell in acute ischemic stroke patients. *Curr Neurovascular Res* (2018) 15(2):151–7. doi: 10.2174/1567202615666180626154857

10. Gasparyan AY, Ayvazyan L, Mikhailidis DP, Kitas GD. Mean platelet volume: A link between thrombosis and inflammation? *Curr Pharm Design* (2011) 17(1):47–58. doi: 10.2174/138161211795049804

11. Schwertz H, Koster S, Kahr WHA, Michetti N, Kraemer BF, Weitz DA, et al. Anucleate platelets generate progeny. *Blood* (2010) 115(18):3801–9. doi: 10.1182/blood-2009-08-239558

12. Xie D, Xiang W, Weng Y, Li J, Xu L, Zhang X, et al. Platelet volume indices for the prognosis of acute ischemic stroke patients with intravenous thrombolysis. *Int J Neurosci* (2019) 129(4):344–9. doi: 10.1080/00207454.2018.1536054

13. Guetl K, Raggam RB, Muster V, Gressenberger P, Vujic J, Avian A, et al. The white blood cell count to mean platelet volume ratio for the prediction of chronic limb-threatening ischemia in lower extremity artery disease. *J Clin Med* (2019) 8 (10):1593. doi: 10.3390/jcm8101593

14. Sivri S, Sokmen E, Celik M, Ozbek SC, Yildirim A, Boduroglu Y. Usefulness of white blood cell count to mean platelet volume ratio in the prediction of SYNTAX score in patients with non-ST elevation myocardial infarction. *Pakistan J Med Sci* (2019) 35(3):824–9. doi: 10.12669/pjms.35.3.1017

15. Amalia L, Dalimonthe NZ. Clinical significance of platelet-to-White blood cell ratio (PWR) and national institute of health stroke scale (NIHSS) in acute ischemic stroke. *Heliyon* (2020) 6(10):e05033. doi: 10.1016/j.heliyon.2020.e05033

16. Cicek G, Acikgoz SK, Yayla C, Kundi H, Ileri M. White blood cell count to mean platelet volume ratio: A novel and promising prognostic marker for ST-segment elevation myocardial infarction. *Cardiol J* (2016) 23(3):225–35. doi: 10.5603/CJ.a2016.0001

17. Adams HPJr., Bendixen BH, Kappelle LJ, Biller J, Love BB, Gordon DL, et al. Classification of subtype of acute ischemic stroke. definitions for use in a multicenter clinical trial. TOAST. trial of org 10172 in acute stroke treatment. *Stroke* (1993) 24(1):35–41. doi: 10.1161/01.str.24.1.35

18. Wang M, Farouki Y, Hulscher F, Mine B, Bonnet T, Elens S, et al. Early neurological improvement predicts clinical outcome after thrombectomy for distal medium vessel occlusions. *Front Neurol* (2022) 13. doi: 10.3389/fneur.2022.809066

19. Saleem Y, Nogueira RG, Rodrigues GM, Kim S, Sharashidze V, Frankel M, et al. Acute neurological deterioration in Large vessel occlusions and mild symptoms managed medically. *Stroke*. (2020) 51(5):1428–34. doi: 10.1161/STROKEAHA.119.027011

20. Rha JH, Saver JL. The impact of recanalization on ischemic stroke outcome - a meta-analysis. *Stroke*. (2007) 38(3):967–73. doi: 10.1161/01.STR.0000258112.14918.24

21. Endres M, Engelhardt B, Koistinaho J, Lindvall O, Meairs S, Mohr JP, et al. Improving outcome after stroke: Overcoming the translational roadblock. *Cerebrovascular Diseases*. (2008) 25(3):268–78. doi: 10.1159/000118039

22. Montellano FA, Ungethüm K, Ramiro L, Nacu A, Hellwig S, Fluri F, et al. Role of blood-based biomarkers in ischemic stroke prognosis. *Stroke* (2021) 52 (2):543–51. doi: 10.1161/STROKEAHA.120.029232

23. Alexandru N, Andrei E, Dragan E, Georgescu A. Interaction of platelets with endothelial progenitor cells in the experimental atherosclerosis: Role of transplanted endothelial progenitor cells and platelet microparticles. *Biol Cell* (2015) 107(6):189–204. doi: 10.1111/boc.201400071

24. Burkard P, Voegtle T, Nieswandt B. Platelets in thrombo-inflammation: Concepts, mechanisms, and therapeutic strategies for ischemic stroke. *Hamostaseologie* (2020) 40(2):153–64. doi: 10.1055/a-1151-9519

25. Kamath S, Blann AD, Lip GYH. Platelet activation: assessment and quantification. *Eur Heart J* (2001) 22(17):1561–71. doi: 10.1053/euhj.2000.2515

frontiers | Frontiers in Immunology

TYPE Original Research
PUBLISHED 17 October 2022
DOI 10.3389/fimmu.2022.1016472

OPEN ACCESS

EDITED BY
Esaki M. Shankar,
Central University of Tamil Nadu, India

REVIEWED BY
Souptik Basu,
Griffith University, Australia
Huai-Sheng Chen,
Jinan University, China

*CORRESPONDENCE
Leslie Chavez-Galan
lchavezgalan@gmail.com;
lchavez_galan@iner.gob.mx

SPECIALTY SECTION
This article was submitted to Molecular Innate Immunity, a section of the journal Frontiers in Immunology

RECEIVED 11 August 2022
ACCEPTED 26 September 2022
PUBLISHED 17 October 2022

CITATION
Urbán-Solano A, Flores-Gonzalez J, Cruz-Lagunas A, Pérez-Rubio G, Buendia-Roldan I, Ramón-Luing LA and Chavez-Galan L (2022) High levels of PF4, VEGF-A, and classical monocytes correlate with the platelets count and inflammation during active tuberculosis. *Front. Immunol.* 13:1016472. doi: 10.3389/fimmu.2022.1016472

High levels of PF4, VEGF-A, and classical monocytes correlate with the platelets count and inflammation during active tuberculosis

Alexia Urbán-Solano[1], Julio Flores-Gonzalez[1], Alfredo Cruz-Lagunas[2], Gloria Pérez-Rubio[3], Ivette Buendia-Roldan[4], Lucero A. Ramón-Luing[1] and Leslie Chavez-Galan[1*]

[1]Laboratory of Integrative Immunology, Instituto Nacional de Enfermedades Respiratorias Ismael Cosío Villegas, Mexico City, Mexico, [2]Laboratory of Immunobiology and Genetic, Instituto Nacional de Enfermedades Respiratorias Ismael Cosío Villegas, Mexico City, Mexico, [3]HLA Laboratory, Instituto Nacional de Enfermedades Respiratorias Ismael Cosío Villegas, Mexico City, Mexico, [4]Translational Research Laboratory on Aging and Pulmonary Fibrosis, Instituto Nacional de Enfermedades Respiratorias Ismael Cosío Villegas, Mexico City, Mexico

Platelets play a major role in coagulation and hemostasis; evidence supports the hypothesis that they also contribute to immunological processes. Increased platelet counts have been associated with poor prognosis in tuberculosis (TB). Platelet–monocyte aggregates have been reported in patients with TB, but it is still unclear if only one monocyte subpopulation is correlated to the platelet count; moreover, the platelet–monocyte axis has not been studied during latent tuberculosis (LTB). In this study, mononuclear cells and plasma were obtained from patients diagnosed with active drug-sensitive TB (DS-TB, n = 10) and LTB (n = 10); cytokines and growth factors levels associated to platelets were evaluated, and correlations with monocyte subpopulations were performed to identify a relationship between them, as well as an association with the degree of lung damage. Our data showed that, compared to LTB, DS-TB patients had an increased frequency of platelets, monocytes, and neutrophils. Although DS-TB patients showed no significant difference in the frequency of classical and non-classical monocytes, the classical monocytes had increased CD14 intensity of expression and frequency of TLR-2+. Furthermore, the plasma levels of angiogenic factors such as vascular endothelial growth factor (VEGF-A), platelet-derived growth factor (PDGF-BB), and platelet factor-4 (PF4), and pro-inflammatory cytokines like interleukin 6 (IL-6), interleukin 1 beta (IL-1β), and interferon-γ-inducible protein 10 (IP-10) were increased in DS-TB patients. In addition, PF-4 and VEGF-A correlated positively with the frequency of classical monocytes and the platelet count. Using a principal component analysis, we identified four groups of DS-TB patients according to their levels of pro-inflammatory cytokines, angiogenic factors, and degree of lung damage. This study establishes that

there is a correlation between VEGF-A and PF4 with platelets and classical monocytes during active TB, suggesting that those cell subpopulations are the major contributors of these molecules, and together, they control the severity of lung damage by amplification of the inflammatory environment.

KEYWORDS

platelet, tuberculosis, classical monocytes, inflammation, pulmonary fibrosis

Introduction

Tuberculosis (TB) is an infectious disease caused by *Mycobacterium tuberculosis* (Mtb) and is the second leading infection killer after the current COVID-19 pandemic. The World Health Organization (WHO) estimates 10 million new TB cases in 2020 (1). After being exposed to Mtb, 5%–10% of infected individuals develop active TB (ATB), and 90% develop a TB status called latent tuberculosis (LTB), where the patient controls the infection without eliminating Mtb. Approximately 10% of LTB patients will reactivate Mtb during their life due to failures in their immune system (2, 3). During LTB, the immune response maintains Mtb in a quiescent metabolic state without evidence of abnormalities in the clinical or radiological status of the patient (4). In contrast, during ATB, the replicating Mtb triggers an important inflammatory state that induces damage to the infection site, leading to clinical and radiological manifestations (5).

Platelets are well known for their role in coagulation and hemostasis. However, current evidence supports the hypothesis that they also contribute to diverse immunological processes (6). It has been suggested that platelets drive TB immunopathology through their effect on other immune cells (7). It was recently reported that they accumulate in the lung lesions of TB patients, influencing the activation and differentiation of macrophages (8, 9).

Evidence supports the adverse effects on the immune cells by platelets during Mtb infection; for example, a high platelet count has been associated with a poor prognosis during TB because there is tissue degradation; even antiplatelet agents have been proposed as an adjunct to antibiotic treatment (10). In addition, a report suggested that platelets restricted the oxidative burst favoring disease progression; Mtb-infected and platelet-depleted mice increased cellular reactive oxygen species (ROS) levels and reduced bacterial burden (11).

Platelet factor-4 (PF4) is produced and released specifically by platelets, and it has been found to increase in TB patients, correlating with clinical and radiological severity (12). In addition, other non-specific proteins to platelets, such as platelet-derived growth factor (PDGF-BB), regulated upon activation, normal T cell expressed and presumably secreted (RANTES), macrophage inflammatory protein 1 alpha (MIP1α), transforming growth factor-beta (TGF-beta), pentraxin 3, interleukin-1-beta (IL-1β) and vascular endothelial growth factor (VEGF-A) have been found increased in plasma from TB patients (8, 9, 13).

Mtb induces the secretion of VEGF-A by infected macrophages, favoring Mtb dissemination to extrapulmonary sites through newly formed blood vessels (14). VEGF-A also regulates the expression of matrix metalloproteinases (MMPs), leading to tissue destruction. MMP expression promotes cavitations and fibrosis in the lung (15–17). Moreover, VEGF-A promotes non-vascular functions; for instance, chemotaxis of monocytes, granuloma formation, and maintaining a pro-inflammatory environment (18). The relevance of using VEGF-A inhibitors as a host-directed therapy remains to be discussed in TB treatment (19).

Platelets mediate the recruitment of monocytes and macrophages through the release of PF4, which induces the migration of C–C chemokine receptor type 1 (CCR1)-expressing cells. CCR1 promotes inflammation because it regulates the traffic of immune effector cells when binding to its ligands (20, 21); this pathway suggests a link between an inflammatory environment and PF4 (22). Currently, it is uncertain how platelet activation impacts monocyte activation and inflammation status during LTB and ATB. Therefore, understanding the dynamics between platelets and monocytes is essential to clarifying the role of the platelets in maintaining intercellular communication that regulates inflammation. Here, we measured inflammatory cytokines and angiogenic factors in the plasma of LTB and ATB patients, and correlations with platelet count and monocyte subpopulation were established.

This study suggests that platelets may promote a hyperinflammatory environment through stimulation of classical monocytes, which in turn produce cytokines and factors to favor the activation and further production of platelets, a process associated with increased severity of lung damage and probable development of pulmonary fibrosis.

10.3389/fimmu.2022.1016472

Materials and methods

Ethics statement

This study was approved by the Ethics Committee of the Instituto Nacional de Enfermedades Respiratorias Ismael Cosio Villegas (Code numbers B24-16, B07-18, and B06-22). All procedures performed in the study were conducted following the principles stipulated in the Helsinki Declaration, and all participants signed a written informed consent.

Patients

Twenty-eight patients >18-year-old with Mtb infection were enrolled during 2016–2018 at the Instituto Nacional de Enfermedades Respiratorias, Mexico City. Study populations were divided into two groups: patients with LTB (n = 13) with a positive QuantiFERON-Gold In-Tube test and a positive tuberculin skin test, and patients with ATB (n = 15) whose diagnosis was made by a clinician evaluation, positive sputum culture, and PCR Xpert MTB/RIF (Figure 1). All ATB patients had drug-sensitive tuberculosis (DS-TB). Patients with HIV infection, cancer, and those undergoing immunosuppressive or anticoagulant therapy were excluded. After the diagnosis, patients received the corresponding treatment following the international normative and a clinical follow-up. Clinical, laboratory, and radiological data were obtained from the medical records of all ATB patients.

Blood samples

Circulating blood samples were obtained at diagnosis time before the initiation of anti-TB therapy. Plasma and peripheral blood mononuclear cells (PBMCs) were recovered using BD Vacutainer tubes (BD Biosciences, San Jose, CA, USA). PBMCs were isolated by standard LymphoprepTM (Accurate Chemical-Scientific, Westbury, NY, USA) centrifugation gradient within 1 h of the blood draw and were subsequently cryopreserved. Plasma was obtained and stored at −70°C until use.

Flow cytometry analysis

PBMCs were prepared to evaluate cell surface marker expressions using monoclonal antibodies (mAbs) against CD14, CD16, human leukocyte antigen-DR (HLA-DR), integrin alpha M subunit (CD11b), toll-like receptor-2 (TLR-2), TLR-4, and L-selectin (CD62-L). All the mAbs were provided by BioLegend (San Diego, CA, USA).

The cells used for the Fluorescence Minus One (FMO) condition were stained and acquired in parallel to identify background levels of staining; dead cells were discarded using viability staining Zombie Red Dye solution (BioLegend). More details of the antibodies used can be found in Table S1. The data were acquired using a FACS Aria II flow cytometer (BD Biosciences, San Jose, CA, USA) equipped with the FACSDiva 6.1.3 software (BD Biosciences, San Jose, CA, USA). In each condition, at least 50,000 events were acquired per sample. The

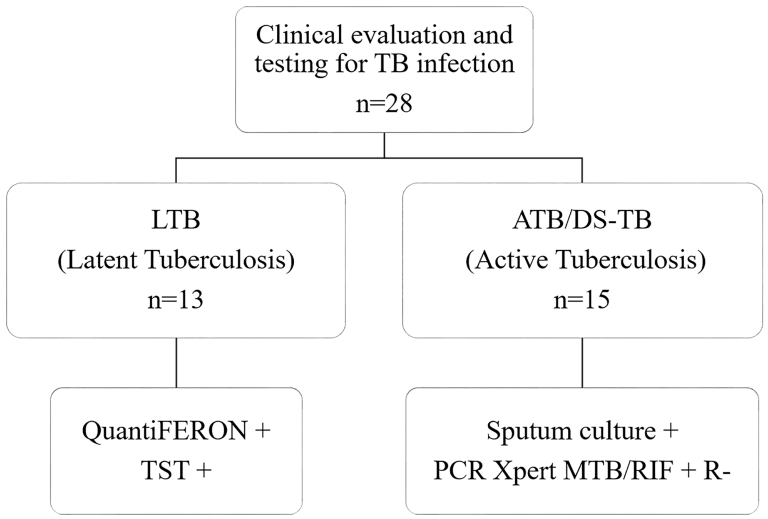

FIGURE 1
Workflow of enrolled patients. Twenty-eight subjects were recruited for this study; 13 were diagnosed with latent tuberculosis (LTB), and 15 with active drug-sensitive tuberculosis (DS-TB). TST, Tuberculin skin test; PCR Xpert MTB/RIF, Polymerase Chain Reaction Xpert *Mycobacterium Tuberculosis*/Rifampicin; R, resistant.

flow cytometry data file (FCS) was analyzed using Flow Jo (Flow Jo, LLC, Ashland, OR, USA)™ v10.6.1.

The frequency (percentage) and the mean fluorescence intensity (MFI) were obtained for all molecules. Briefly, the analysis strategy consisted of limiting the singlet cells through forward scatter (FSC-A versus FSC-H), and viability plots were selected (Zombie Red negative, Figure S1).

Soluble molecules evaluation

A Bio-plex Pro Human Cytokine Custom Panel (Bio-Rad Laboratories, Hercules, CA, USA) was used to evaluate the plasma levels of IL-6, IL-1β, interferon gamma-induced protein 10 (IP-10), PDGF-BB, and VEGF-A, following the instructions of the manufacturer. The data were acquired through a Bio-Plex 200 System and analyzed using Bio-Plex Manager 6.1 software (Bio-Rad Laboratories, Hercules, CA, USA).

Levels of platelet factor 4 (PF4/CXCL4) (R&D Systems, Minneapolis, MN, USA), monocyte chemoattractant protein-1 (MCP-1) (BioLegend, San Diego, CA, USA) and mucin 5 subtype B (MUC5B) (MyBioSource, San Diego, CA, USA) were measured in plasma using a sandwich-type Enzyme-Linked Immunosorbent Assay (ELISA) according to the instructions of the manufacturer. More details of the Bio-Plex and ELISA kits used are in Table S1. All proteins were quantified by comparison with the corresponding standard curve, and the optical density was measured using a microplate reader (Imark, Bio-Rad, Hercules, CA, USA).

Plasma from healthy donors (n = 10) was used to obtain the reference values for soluble molecule quantification (Table S2).

Statistical analysis

Data are shown as median values and interquartile ranges (IQR, 25–75). For comparisons between groups, Mann–Whitney tests were used for comparisons between groups. Spearman one-tailed correlations were performed between clinical data, soluble molecule values, and phenotypic characterization data by flow cytometry of patients with latent tuberculosis (n = 7) and active tuberculosis (n = 5). Values of p <0.05 were considered statistically significant. Statistical analysis was performed using GraphPad Prism V 9.0.2 (GraphPad Software, Inc., San Diego, CA, USA).

Principal component analysis (PCA) was performed to reduce dataset dimensionality and detect patterns of the soluble molecules measured in TB patients, using GraphPad Prism, treating each patient as one data point. We observed and related specific points that appeared in relation to the others along the two selected components to infer clusters from PCA data.

Pairwise correlations were calculated and visualized as a correlogram using R studio version 1.4.1106 with the following libraries: ggplot2, ggcorrplot, corrplot, and tidyverse. Spearman's correlation coefficient was indicated by square and heat scale; significance was indicated by *p <0.05, **p <0.01, and ***p <0.001.

Protein network analysis

We used a computational prediction using STRING (Search Tool for the Retrieval of Interacting Genes/Proteins) to construct a protein–protein interaction network, indicating functional and physical protein associations. The STRING resource is available online at https://string-db.org/. We were set to visualize only the "evidence" interactions, with a maximum of 10 interactors for the first shell and five for the second shell, and a high score (0.7) as a minimum required interaction score. STRING analysis integrates all known and predicted associations between proteins, including physical interactions and functional associations. Functional enrichments in the protein network were supported by the REVIGO analysis as a well-known classification system based on Gene Ontology. Finally, to establish a powerful visual map across these data, we performed an advanced analysis and modeling using Cytoscape V 3.9.1, selecting the first neighbors to PF4 and VEGF-A nodes and showing them in a circular layout. Ultimately, we analyzed molecules shared between nodes using a Veen and Euler diagram app.

Results

Characteristics of the study population

The demographic characteristics of LTB and DS-TB patients are summarized in Table 1. The median age was 49 years for LTB and 38 for DS-TB, and female sex was predominant for both groups. DS-TB patients had a lower BMI value than LTB [LTB 31 (23–30) vs DS-TB 21 (18–22, 31, 32), p <0.0001]. The comorbidity of diabetes mellitus type 2 was present in 40% of DS-TB patients and 8% of LTB patients. A total of 100% of DS-TB and 85% of LTB patients received the Bacillus Calmette–Guérin (BCG) vaccine during childhood.

DS-TB patient data showed important changes in the hematological parameters compared to LTB. DS-TB patients had a higher absolute count of circulating total leukocytes than LTB (p <0.05). The counts of neutrophils (p <0.001) and monocytes (p <0.001) were increased, whereas lymphocytes were decreased (p <0.001). Moreover, DS-TB displayed a higher platelet count than LTB (p <0.0001), and in line with previous reports, hemoglobin and hematocrit were lower in DS-TB than in LTB (p <0.001 for both) (Table 2).

Finally, biochemical parameters showed that compared to LTB, DS-TB patients had lower levels of albumin (p = 0.0046),

TABLE 1 Participant characteristics.

	LTB (n = 13)	DS-TB (n = 15)	*p*
Age (years)	49 (31–58)	38 (30–44)	ns
Male, n (%)	3 (23)	5 (33)	ns
Female, n (%)	10 (77)	10 (67)	ns
Body Mass Index (kg/m^2)	31 (27–34)	21 (18–24)	****
Diabetes Mellitus type 2, n (%)	1 (8)	6 (40)	ns
Arterial hypertension, n (%)	1 (8)	1 (7)	ns
Previous pulmonary disease†, n (%)	0	1 (7)	ns
Smoking, n (%)	1 (8)	3 (20)	ns
BCG vaccination, n (%)	11 (85)	15 (100)	ns

Data is represented with median and interquartile range. The statistical comparison was performed using the Mann–Whitney U Test (****p <0.0001, ns, not significant), †previous diagnosis of Chronic Obstructive Pulmonary Disease (COPD) and asthma.

total bilirubin (p = 0.0475), alanine transaminase (p = 0.0422), and creatine phosphokinase (p <0.0001) (Table 3).

In summary, DS-TB patients presented co-morbidities and lower BMI compared to LTB. Notably, the DS-TB showed high levels of platelets and immune cell subpopulations, except for lymphocytes, and a profile related to anemia.

Classical monocytes from DS-TB patients have increased intensity of expression of CD14 and CD11b

Monocytes are a precursor population to macrophages, one of the most important cell subpopulations during the immune response against Mtb (31). Having identified that DS-TB patients have an increased monocyte count compared to LTB (Table 2), the next aim was to verify if the frequencies of classical (CD14+CD16−) and non-classical (CD14+CD16+) monocytes were different between LTB and DS-TB, and this was evaluated by flow cytometry (Figure 2A).

We did not find differences in the frequency of monocyte subsets between TB patient groups (Figures 2B, left, C, left). However, the CD14 intensity of expression (reported as MFI) was increased in classical monocytes of DS-TB patients compared to the LTB group [8,889 (3,140–11,009) vs 2,817 (2,066–4,192) MFI, respectively, p = 0.0232] (Figure 2B, right), while CD16 intensity of expression was not modified on non-classical monocytes (Figure 2C right).

On both classical and non-classical monocytes, human leukocyte antigen–DR isotype (HLA-DR), integrin alpha-M (CD11b), Toll-like receptor 2 (TLR-2), and toll-like receptor 4 (TLR-4) expression were evaluated. The classical monocytes from DS-TB patients, compared with the LTB group, displayed a higher frequency of CD11b+ [95.65 (89–98) vs 81.45 (43–93), respectively, p = 0.0355] and CD11b MFI [548 (DS-TB: 379–704) vs LTB: 244 (150–371), p = 0.0115] (Figure 2D). Regarding non-classical monocytes, we did not observe differences (Figure 2E). Moreover, the classical monocytes from DS-TB, compared to LTB, had an increased frequency of TLR-2+ [100 (99.8–100) vs 99.4 (98.5–99.9), respectively, p = 0.0139] but not the TLR-2 MFI (Figure 2F). TLR2

TABLE 2 Laboratory data of hematological parameters.

	LTB	DS-TB	*p*
Leukocytes (RV 4.4–11.3 × 10^3 cells/mm^3)	7 (6–8)	8 (7–11)	*
Absolute neutrophil count (RV 1.7–7.6 × 10^3 cells/mm^3)	4 (3–5)	6 (5–8)	***
Neutrophil percentage (RV 55–62%)	59 (54–65)	70 (66–82)	**
Absolute monocyte count (RV 0.3–0.9 ×10^3 cells/mm^3)	0.4 (0.4–0.5)	0.6 (0.6–0.9)	***
Monocyte percentage (RV 4%–10%)	6 (5–8)	9 (6–11)	*
Absolute lymphocyte count (1.0–3.2 × 10^3 cells/mm^3)	2 (2–3)	1 (1–2)	*
Lymphocyte percentage (20%–40%)	31 (28–36)	18 (10–22)	***
Platelets (RV 150–400 × 10^3 cells/mm^3)	223 (198–254)	433 (317–507)	****
Hemoglobin (RV 15–18.5 g/dl)	15 (14–16)	13 (11–14)	***
Hematocrit (RV 45%–53%)	45 (43–50)	38 (34–43)	***

Data is represented with median and interquartile range. The statistical comparison was performed using Mann–Whitney U Test (*p <0.05, **p <0.01, ***p <0.001, ****p <0.0001). RV, Reference value (provided by the institutional Clinical Laboratory).

TABLE 3 Laboratory data of biochemical parameters.

	LTB	DS-TB	*p*
Glucose (RV 70–99 mg/dl)	103 (95–111)	98 (94–156)	ns
Creatinine (RV 0.8–1.3 mg/dl)	0.73 (0.6–0.9)	0.67 (0.5–0.7)	ns
Urea (RV 15 – 58 mg/dl)	21 (18–32)	22 (16–26)	ns
Blood urea nitrogen (RV 8–27 mg/dl)	10 (9–15)	10 (8–12)	ns
Uric Acid (RV 3.5–7.2 mg/dl)	5 (5–7)	5 (4–6)	ns
Total Protein (RV 6.5–8.1 g/dl)	7 (7–8)	8 (7–8)	ns
Albumin (RV 3.5–5.0 g/dl)	4 (4–4)	3 (2–4)	**
Total bilirubin (RV 0.2–1.0 mg/dl)	0.66 (0.5–1)	0.55 (0.4–0.6)	*
Aspartate transaminase (RV 12–35 U/L)	24 (20–28)	26 (18–32)	ns
Alanine transaminase (RV 9–47 U/L)	21 (15–30)	16 (12–17)	*
Lactate dehydrogenase (RV 139–205 U/L)	139 (131–171)	166 (140–233)	ns
Alkaline phosphatase (RV 40–129 U/L)	77 (68–104)	90 (75–114)	ns
Creatine phosphokinase (RV 30–223 U/L)	93 (70–136)	34 (27–44)	****
Glycated hemoglobin (RV <5.7%)	6 (5–6)	6 (6–9)	ns

Data is represented with median and interquartile range. The statistical comparison was performed using Mann–Whitney U Test (*p <0.05, **p <0.01, ****p <0.0001, ns, not significant). RV, Reference value (provided by the institutional Clinical Laboratory).

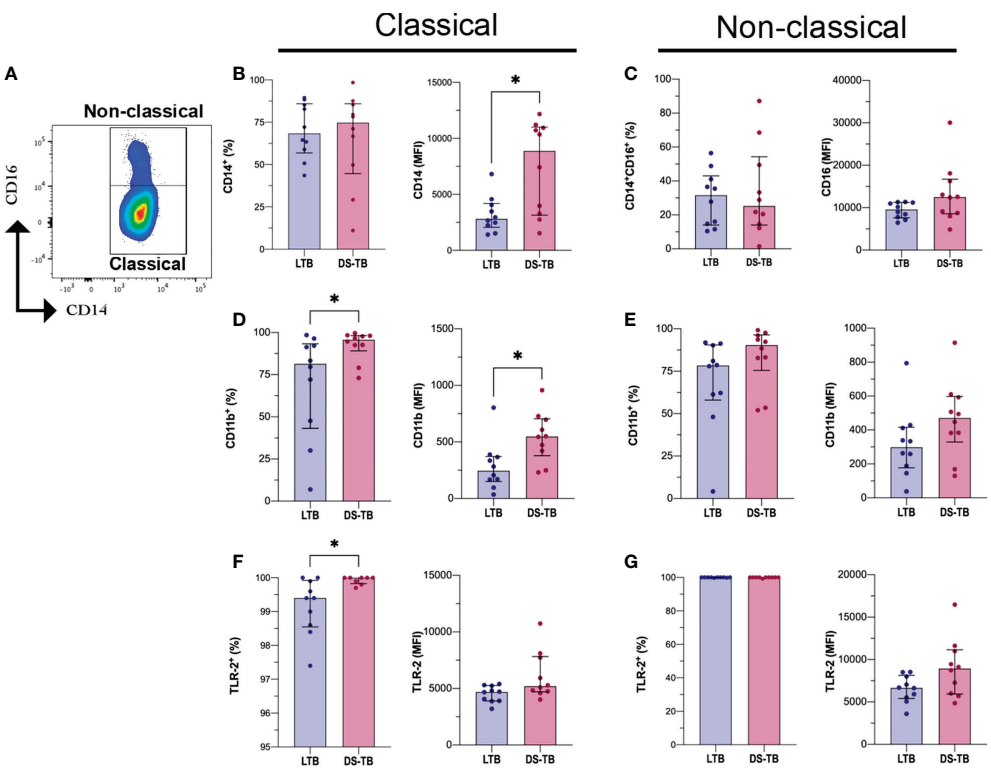

FIGURE 2
DS-TB patients have classical monocytes with CD14, CD11b and TLR-2 altered expression. **(A)** Identification of monocytes subpopulations based on CD14 and CD16 expression as Classical ($CD14^+$) and Non-classical ($CD14^+CD16^+$). **(B)** Frequency and mean fluorescent intensity (MFI) of CD14 on classical monocytes, comparison between latent and active tuberculosis patients. **(C)** Frequency and MFI of CD16 on non-classical monocytes, comparison between latent and active tuberculosis patients. Frequency and MFI of CD11b and TLR-2 on classical monocytes (**D, F**, respectively) and non-classical monocytes (**E, G**, respectively). Data are shown as median with interquartile range (IQR, 25–75). The statistical comparison was performed using Mann–Whitney U Test (*p <0.05), n = 10 for both groups.

10.3389/fimmu.2022.1016472

expression in non-classical monocytes showed no difference between groups (Figure 2G). Finally, the frequency and MFI of HLA-DR, TLR-4, and CD62L were not different between the groups (Figure S2).

These results suggest that mainly classical monocytes are affected during DS-TB compared to LTB. CD11b and TLR-2 may play a role in favoring the activation of classical monocytes, probably to maintain inter-cellular communication through cytokine production.

DS-TB patients have increased plasma levels of PF4 and VEGF-A

Because our data showed that the platelet count is increased in DS-TB patients (Table 2), plasma levels of angiogenic-related factors such as PF4, PDGF-BB, VEGF-A, and MCP-1 were evaluated to assess if platelets were activated. Higher levels of PF4 were identified in the DS-TB group than in the LTB group [LTB 2,012 (1213–2727) vs DS-TB 3,108 (2,578–3,750), $p = 0.0249$] (Figure 3A). Similar data were observed with VEGF-A [LTB 0 (0–0.55) vs DS-TB 9.64 (0–22.69), $p = 0.0067$] (Figure 3B). PDGF-BB and MCP-1 levels did not show changes (Figures 3C, D).

Thus, our results suggest that the high amounts of PF4 exhibited by DS-TB patients were delivered by activated platelets, whereas the VEGF-A levels could be produced by both platelets and monocytes.

DS-TB patients have increased levels of IL-6, IL1-β and IP-10

To evaluate the inflammatory status according to the clinical form of TB, we evaluated inflammatory cytokines in plasma of

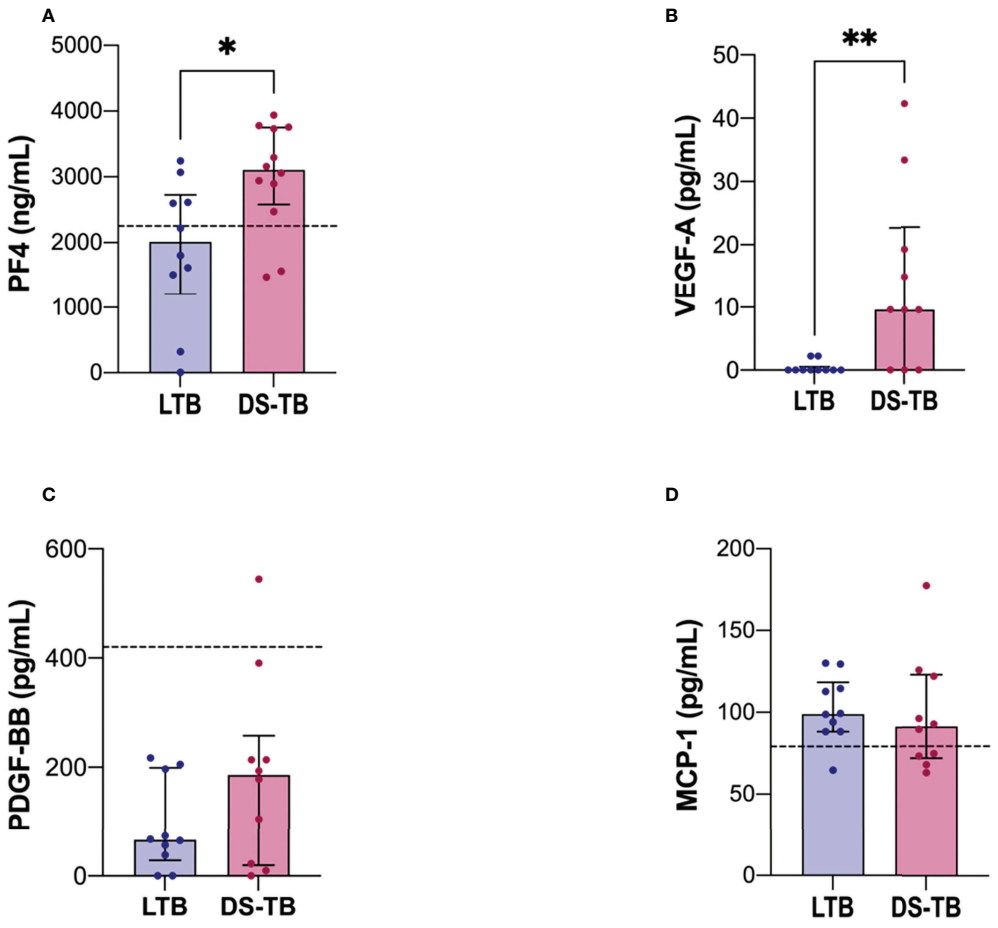

FIGURE 3
DS-TB patients have increased the soluble levels of molecules associated with a platelet activation profile. Soluble molecules evaluated in plasma: **(A)** PF4, **(B)** VEGF-A, **(C)** PDGF-BB, and **(D)** MCP-1. The black dashed lines represent the median of healthy donors (for VEGF-A, they had indetectable values, not visible). Data are shown as median with interquartile range (IQR, 25–75). The statistical comparison was performed using Mann–Whitney U Test (*p <0.05, **p <0.01), n = 10 for both groups, PF4 and MCP-1 had n = 8 for both groups. PF4, platelet factor-4; PDGF-BB, platelet-derived growth factor; VEGF-A, vascular endothelial growth factor; MCP-1, monocyte chemoattractant protein-1.

LTB and DS-TB. IL-6 levels [LTB 0.73 (0.4–1.0) vs DS-TB 15 (4–32), $p = 0.0002$] (Figure 4A), IL-1β [LTB 0.035 (0–0.14) vs DS-TB 0.465 (0.33–0.76), $p = 0.0009$) (Figure 4B) and IP-10 [LTB 282 (162–474) vs DS-TB 2,718 (1,033–5,658), $p = 0.0015$) (Figure 4C) were increased in DS-TB patients compared to LTB. These results showed that DS-TB patients display a systemic pro-inflammatory status.

DS-TB patients show strongly positive correlations between classical monocyte–platelet–platelet factors

Platelets stimulate monocyte chemotaxis, but currently, it is unclear if, specifically, only one monocyte subpopulation is related to platelets or factors delivered by platelets, such as PF4 and VEGF-A. Therefore, we performed correlograms to determine if there is a link between platelet–monocyte-inflammation.

First, we evaluated if the absolute monocyte count (AMC) correlates with the absolute neutrophil count (ANC), absolute lymphocyte count (ALC), platelet count (Plt), pro-inflammatory cytokines, and platelet factors (Figure 5). LTB showed a positive correlation between AMC and ALC (p*, rho = 0.69), VEGF-A with IL1β (p*, rho = 0.75), and PF4 with PDGF-BB (p*, rho = 0.75); LTB did not show significant correlations between platelets count and factors produced by them (Figure 5A). On the other hand, DS-TB displayed strong positive correlations with PF4 (p**, rho = 0.84), VEGF-A (p**, rho = 0.86), and PDGF-BB (p*, rho = 0.72) with total platelet count (Plt). In the same way, VEGF-A correlated positively with PDGF-BB (p**, rho = 0.83) and with PF4 (p**, rho = 0.98). IL-6 (p**, rho = 0.83), and IP-10 (p*, rho = 0.85) were positively correlated with AMC; IL-6 (p*, rho = 0.65) also showed a positive correlation with the absolute neutrophil count (ANC). On the contrary, MCP-1 (p**, rho = −0.82) had a negative correlation with ANC.

Posteriorly, we performed correlation analysis with platelets using the total and monocyte subsets data obtained by flow cytometry. LTB patients showed some positive correlations of molecules expressed on the total monocytes (TM) [VEGF-A and IL1-β (p*, rho = 0.81), HLA-DR and TLR-2 (p*, rho = 0.79); HLA-DR and IL1-β (p*, rho = 0.78); and CD62L and TLR-2 (p*, rho = 0.82)] (Figure S3A). DS-TB showed a positive correlation between TM frequency and IL-1β (p**, rho = 1) and CD14 (p*, rho = 0.9), whereas VEGF-A and PF4 correlated positively between them (p**, rho = 0.97) (Figure S3B).

LTB showed a negative correlation between the frequency of classical monocytes (CM) and TLR-2 (p**, rho = −0.96) (Figures 6A, C). DS-TB patients showed a strong positive correlation between CM and VEGF-A (p**, rho = 0.97), PF4 (p**, rho = 1) (Figure 6B), suggesting CM plays a role in inducing the secretion of these factors. Similarly, DS-TB patients had a positive correlation between CD14 MFI and IL-1β (p*, rho = 0.9), VEGF-A and PF4 (p**, rho = 0.97), and TLR-2 had a negative correlation with TLR-4 MFI (p*, rho = −1) (Figure 6B). CM from LTB did not correlate with other immune subpopulations; moreover, Plt did not correlate with TLR-2 or TLR-4 (Figure 6C). DS-TB had a positive correlation with Plt and TLR-2 (p*, rho = 0.72) (Figure 6D). It is essential to note that panels A and B had eight patients per group. In contrast, panels C and D had 10 patients per group. The discrepancy in sample size is because PF4 and MCP-1 were not measured in all patients. Although the correlograms showed slight differences in the rho value when comparing the same parameters, the behavior still had similar values and tendencies.

LTB patients had a positive correlation between non-classical monocytes (NCM) and TLR2 (p*, rho = 0.79) (Figure S4A), whereas

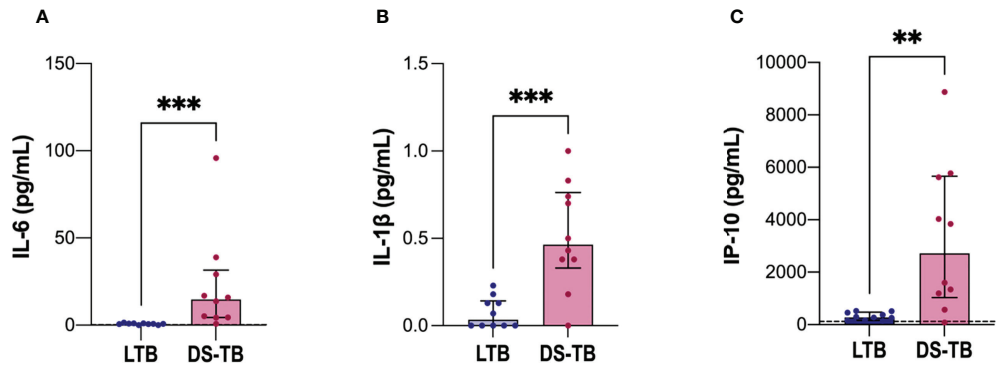

FIGURE 4
Increased soluble levels of pro-inflammatory cytokines in patients with DS-TB. Cytokines evaluated in plasma: **(A)** IL-6, **(B)** IL-1β, and **(C)** IP-10. The black dashed lines represent the median value reported of healthy donors for IP-10 (for IL-6, the median is equal to 0.22 pg/ml, and for IL-1β they had indetectable values, not visible). Data are shown as median with interquartile range (IQR, 25–75). The statistical comparison was performed using Mann–Whitney U Test (**p <0.01, ***p <0.001), n = 10 for both groups IL-6, interleukin-6; IL-1β, interleukin-1 beta; IP-10, Interferon-γ inducible protein 10.

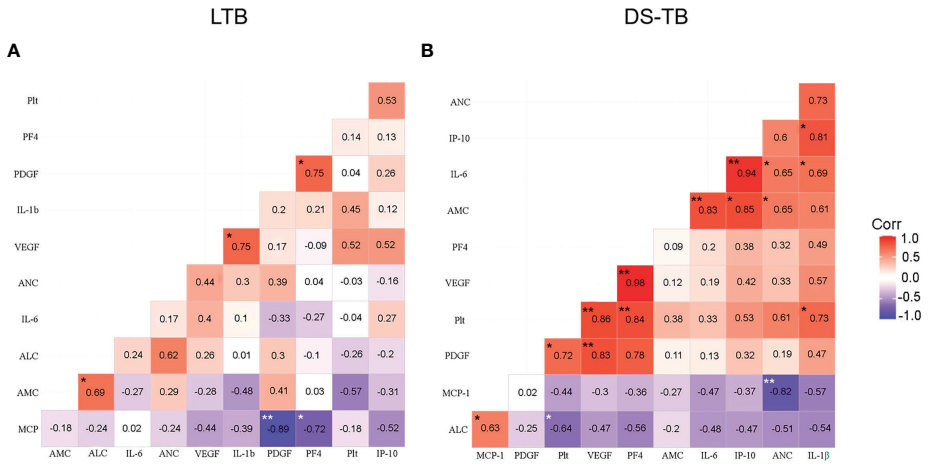

FIGURE 5
Correlation between blood cell count, platelet factors and pro-inflammatory cytokines in latent **(A)** and active **(B)** TB patients. Correlations are presented with the value of Spearman's Rho in the corresponding box. Significant correlations are represented with asterisks (*p <0.05, **p <0.01, white asterisk for negative correlation, and black asterisk for positive correlation). The red color indicates a strong positive correlation, and the blue indicates a strong negative correlation.

DS-TB subjects had a negative correlation between NCM and VEGF-A (p**, rho = −0.97), and PF4 (p**, rho = −1) (Figure S4B).

Together, these correlations showed that in DS-TB, CM, probably through TLR-2, favored the pro-inflammatory microenvironment; moreover, Plt correlated positively with TLR-2, suggesting the presence of a monocyte–TLR2–platelet-inflammation axis.

PCA reveals that DS-TB patients can be divided into four clusters

Dimension reduction by PCA was applied to LTB and DS-TB groups that were adjusted to score distance (SD) for the following variables: VEGF-A, PDGF-BB, IL-6, IP-10, PF4, IL-1β, MCP-1, and platelet count. In addition, we applied PCA to all individuals with the same parameters between groups to map differences between patients with DS-TB and LTB. The first principal component (PC1) summarized 56.86% of the variation captured by markers of systemic inflammation and angiogenic factors such as platelet count, IL-1β, and VEGF. The second principal component (PC2) summarized 19.49% of variation, and it had as its main variation IL-6, a marker of systemic inflammation (Figure 7A).

The PC score plot shows the analysis of samples from 20 patients, who had completed all the variables quantified to obtain PC1 and PC2; the LTB patients (black dot) could be easily distinguished from DS-TB (pink dot) (Figures 7B, C). On the contrary, DS-TB can be divided into IV groups according to PC1 and PC2 profiles (Figure 7B). More information on clinical and radiological data provided patient-by-patient is shown in Table 4. Group I included 2 DS-TB patients characterized by a high level of inflammatory and angiogenic factors and the presence of cavitations. Group II included three DS-TB patients, characterized by a high level of angiogenic factors but no inflammatory cytokines and lung affection with or without cavitations. Group III included three DS-TB patients, characterized by high levels of inflammatory cytokines but no angiogenic factors and destruction of lung parenchyma and cavitation. Group IV included two DS-TB patients, characterized by a low level of inflammatory and angiogenic factors (similarly to LTB); however, they showed lung affectation without cavitations.

DS-TB patients have increased MUC5B levels and lung damage

Our data suggested that patients with higher levels of pro-inflammatory cytokines and/or platelet factors also presented greater radiological severity. Mucin 5B (MUC5B) mediates the production of mucous; its overexpression leads to hyperproduction of mucus accumulated in the bronchoalveolar region and produces chronic inflammation. Moreover, it has been related to the development of idiopathic pulmonary fibrosis (IPF) (32, 33). Thus, we evaluated the MUC5B level to explore possible fibrotic lung damage in DS-TB patients.

DS-TB patients had higher MUC5B levels than LTB [LTB 131.9 (91–148) vs DS-TB 238.5 (165–365), p = 0.0427] (Figure 8), and we confirmed by chest X-ray data that MUC5B

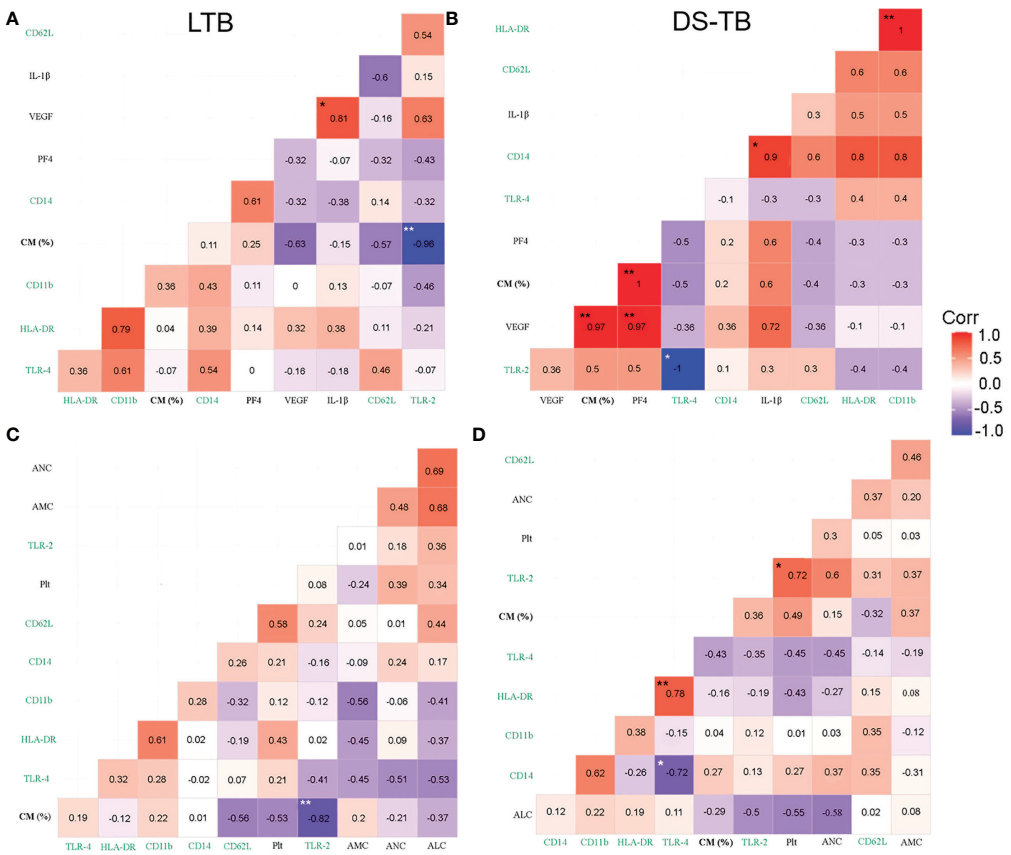

FIGURE 6
Correlation between blood cell count, platelet factors and pro-inflammatory cytokines with monocyte phenotypical characterization in TB patients. **(A, B)** Correlation between classical monocytes (CM) frequency, surface markers and plasmatic levels of soluble molecules in latent **(A)** and active **(B)** TB patients, n = 8 for both groups. **(C, D)** Correlations between CM frequency and blood cell count in latent **(C)** and active **(D)** TB patients, n = 10 for both groups. Correlations are presented with the value of Spearman's Rho in the corresponding box. Significant correlations are represented with asterisks (*p <0.05, **p <0.01, white asterisk for negative correlation, and black asterisk for positive correlation). The red color indicates a strong positive correlation, and the blue indicates a strong negative correlation. Green labels are expressed in MFI.

levels were associated with more significant pulmonary damage characterized by bigger cavitations and the destruction of pulmonary parenchyma. This result supports the hypothesis that the high presence of platelets could not benefit active TB patients; the platelet/monocyte axis probably induces high pulmonary destruction, characteristics that could be associated with a future fibrotic process.

According to STRING analysis VEGF-A mediates inflammation and angiogenesis, whereas PF4 only inflammation in DS-TB patients

A STRING analysis was performed to predict possible interactions between PF4, VEGF-A, PDGF-BB, IL-6, IP-10, IL-1β, IL-17A, MCP-1, TLR-2, TLR-4, CD11b, and other molecules involved in monocytes and platelets activation (like CCL2, MMP-1, MMP-9, CCR2, CCR1, IL-10, and S100A8) (9, 23, 34).

STRING analysis resulted in 41 nodes with an average node degree of 10.3 and a PPI enrichment p-value of less than 1.0e−16. Four main clusters were found using the MCL clustering method (similar to the results in Figure 7B). One of them was involved in inflammation (red bubbles). Two clusters were related to angiogenesis (green and blue bubbles), both mediated by VEGF-A. The last cluster was with MUC5B, which apparently had no relationship with the other evaluated molecules (Figure 9A). The findings were also supported by the REVIGO analysis (Supplementary Excel file).

We confirmed that VEGF-A is implicated in inflammation and angiogenesis (Figure 9B), whereas PF4 is related exclusively to the inflammatory process (Figure 9C) using Cytoscape analysis. This tool allowed us to predict the outcome of complex immune interactions between molecules associated

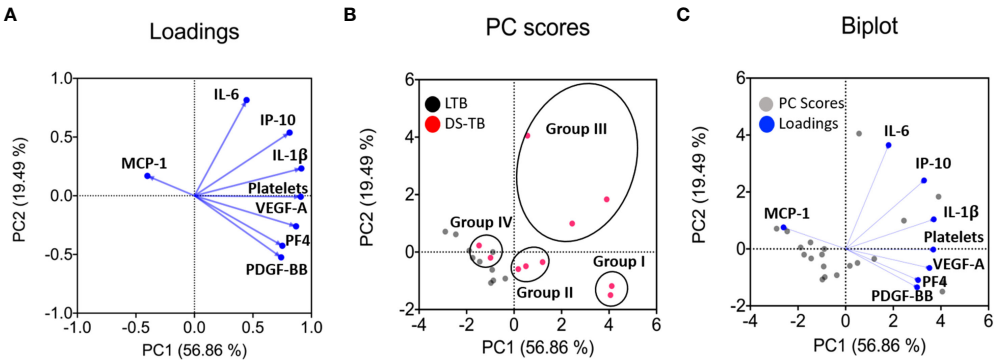

FIGURE 7
Principal component analysis (PCA) shows main dimensions of variation soluble molecules measured in patients diagnosed with TB. The PCA was constructed with eight clinical variables measurements [monocyte chemoattractant protein-1 (MCP-1), interleukin 6 (IL-6), interferon gamma-induced protein 10 (IP-10), interleukin 1 beta (IL-1β), platelets count, vascular endothelial growth factor (VEGF-A), platelet factor 4 (PF4) and platelet-derived growth factor (PDGF-BB). The correlation of each of these variables with the first two principal components is shown in a loadings plot **(A)**, demonstrating that the first principal component (PC1) was dominated by markers of systemic inflammation and angiogenic factors (platelets count, IL-1β, and VEGF-A were the most important). In contrast, the second principal component (PC2) was associated with IL-6. The PC scores plot showed that the data from 20 samples of people infected with TB were significant **(B)**. In the score plot, red and black dots represent a patient and is colored in accordance with the embedded legends. Finally, a biplot was used to show the loadings and PC scores **(C)**. These PCs explained 56.86% and 19.49% variation in the eight clinical variables measurements, respectively.

with platelets and monocytes. In addition, 32 molecules were closely associated with VEGF-A, ten were involved in PF4 networks too, and only one molecule was related exclusively to PF4 (Figure 9D).

Discussion

The role of platelets in the pathophysiology of TB has been recently explored; reports indicate that ATB patients have higher levels of platelets compared to LTB patients, and thrombocytosis is associated with greater severity and a worse prognosis for these patients (8, 24, 25). Platelets can mediate immunological mechanisms by forming aggregates with immune cells and releasing chemokines and growth factors (26).

In the context of TB, platelets mediate granuloma formation because the production of chemokines allows the recruitment of cells of the innate response such as neutrophils, monocytes, and macrophages. Moreover, platelets have the ability to induce a monocyte profile with strong collagenase activity, as well as to induce the differentiation of monocytes into multinucleated giant cells (9, 27).

In consonance with a previous report (8), we found that DS-TB patients had an elevated frequency of circulating monocytes and platelets. However, the frequency of monocytes' subpopulations (classical and non-classical) was similar between LTB and DS-TB. The classical monocytes from DS-TB patients had an altered phenotype characterized by high expression of CD11b and TLR-2. Previously, it had been reported that P-selectin mediates the interaction of platelets with monocytes (7), and that the upregulation of CD11b is related to increased circulating leukocyte-platelet aggregates (28).

Platelets can be activated by directly recognizing mycobacteria through receptors such as TLR-2 and TLR-4, relevant molecules to induce the secretion of pro-inflammatory cytokines (7, 29). In this study, we found that TLR-2 was increased on classical monocytes in DS-TB patients, and these patients also displayed elevated levels of IL-1β, IL-6, and IP-10. Consequently, a pro-inflammatory environment was favored, and this condition probably intensified platelet activation. In this regard, reports have shown that pro-inflammatory cytokines enhance platelet production by triggering megakaryocytopoiesis (30).

Although we were unable to quantify IL-17A (samples were obtained from 2016 to 2018, and this cytokine has a rapid denaturation), elevated levels of IL-17A have been reported in ATB, and reports suggest that it induces the release of platelet factors (23, 35). Using the analysis STRING, we identified that VEGF-A interacts with IL-17A. In concordance with other reports indicating a loop, IL-17A might facilitate VEGF-A-mediated angiogenesis by enhancing VEGF-A production (36, 37). Furthermore, IL-17A stimulates the production of alarmins such as S100A8/A9, which mediates lung damage during TB; this alarmin activates platelets through an interaction with TLR-4 expressed on the platelet surface (34, 38). Thus, we speculate that the IL-17A pathway may participate in the platelet–classical monocyte-inflammation axis observed in this study during DS-TB.

IL-6 was increased in DS-TB patients, and evidence suggests that this cytokine promotes thrombocytosis and regulates

10.3389/fimmu.2022.1016472

TABLE 4 Identified groups of DS-TB patients and radiological characteristics.

	# patient	Radiological characteristics		Comorbidities	Average age (years)
GROUP I. Pro-inflammatory cytokines and platelet factors elevation	1	Two caverns in RLL	100% Presence of cavitations	50% Type 2 Diabetes mellitus	41.5
	2	Caverns in LUL			
GROUP II. Platelet factors elevation but not pro-inflammatory cytokines	3	Both upper lobes with cavitated lesions	66.6% presence of cavitations. 33.3% Lung affection without cavitations.	33.3% Type 2 Diabetes mellitus	39
	4	Left apical caverns, cavern at the level of lingula, superior segment of LLL with two caverns			
	5	Right basal consolidation, reticulonodular pattern			
GROUP III. Main elevation of pro-inflammatory cytokines	6	Adenopathies, multiple cavitations. Loss of left pulmonary parenchyma.	66.6% presence of adenopathies. 100% destruction of lung parenchyma. 100% presence of cavitations.	100% Type 2 Diabetes mellitus. 33.3% Previous pulmonary disease. 33.3% Dyslipidemia. 33.3% Smoking.	44
	7	Adenopathies, multiple cavitations, destruction of right lung parenchyma			
	8	Multiple caverns. Lung parenchymal destruction in the LUL.			
GROUP IV. Low levels of platelet factors and pro-inflammatory cytokines	9	Pulmonary nodule	100% Lung affection without cavitations	None	35.5
	10	Bilateral reticular pattern, pleural thickening			

RLL, Right Lower Lobe; LUL, Left Upper Lobe; LLL, Left Lower Lobe.

thrombopoietin levels (39). Elevated PF4 levels (which are produced specifically by activated platelets) in DS-TB patients, compared to LTB, suggest that DS-TB patients have an increased presence of activated platelets, which in turn secrete factors to stimulate the inflammatory process. In consonance with another study (12), it was associated with radiological severity. Furthermore, PF4 mediates the migration of monocytes CCR1+ (22), a mechanism that could be involved during the Mtb infection to recruit monocytes and maintain the inflammatory process. Our data indicated a strong correlation between platelets, inflammatory cytokines and classical monocytes, whereas non-classical monocytes negatively correlated with platelet factors. We suggest that during DS-TB, platelets establish an inter-cellular communication with classical monocytes, probably those TLR-2+, that favors the inflammatory process and angiogenic factors that consequently lead to lung damage.

VEGF-A recently gained attention in the context of TB. On the one hand, it performs angiogenic mechanisms related to the spread of the bacteria, but on the other hand, it is also a chemokine for monocyte recruitment (14, 18). VEGF-A was increased in DS-TB patients and positively correlated with platelets and classical monocytes. The high level of VEGF-A can be attributed to the increase in monocytes and platelets, two of the main producers.

In vitro studies and murine models indicated that VEGF-A could promote platelet production by accelerating megakaryocyte maturation when interacting with its receptor, VEGFR1 (by paracrine or autocrine pathways). Platelets and monocytes can also produce this receptor (40, 41). Furthermore, VEGF-A promotes angiogenesis and regulates the expression of matrix metalloproteinases (MMP), leading to tissue destruction. Similarly, an excessive inflammatory response produces tissue damage and metalloproteinase expression, which could promote cavitation and fibrosis in the lung (15–17). Specifically, it has been described that VEGF-A can modulate the expression of MMP-1 and MMP-9, and MMP-9 can also regulate the expression of VEGF-A (15, 16, 42).

In addition, it is well known that the higher expression of extracellular MMP will lead to a higher degradation of lung tissue, and it is associated with pulmonary cavity formation in patients with ATB (17). The radiological data shown by our patients was consistent with that. The vast majority presented at least two cavitations; some had lung parenchyma destruction that had left them with sequelae of pulmonary fibrosis. The association of all these factors could explain why platelets are related to further clinical and radiological severity, the progression of the disease, and lower survival.

PF4 and VEGF-A levels have been associated with TB development. While VEGF-A can be considered a potent angiogenic mediator that favors pulmonary TB lesions, PF4 is related to the inflammatory process (8, 9, 14). We identified two clusters of TB patient groups through the PCA analysis; one group had increased, specifically, inflammatory factors, and the second group, angiogenic factors. Thus, in this study, we showed evidence that platelets are increased in DS-TB patients; moreover, these patients can be divided into groups with inflammatory or angiogenic factors, suggesting that PF4 and VEGF-A levels are determinants of the clinical status of DS-TB. Unfortunately, the bioinformatic analysis performed in our

10.3389/fimmu.2022.1016472

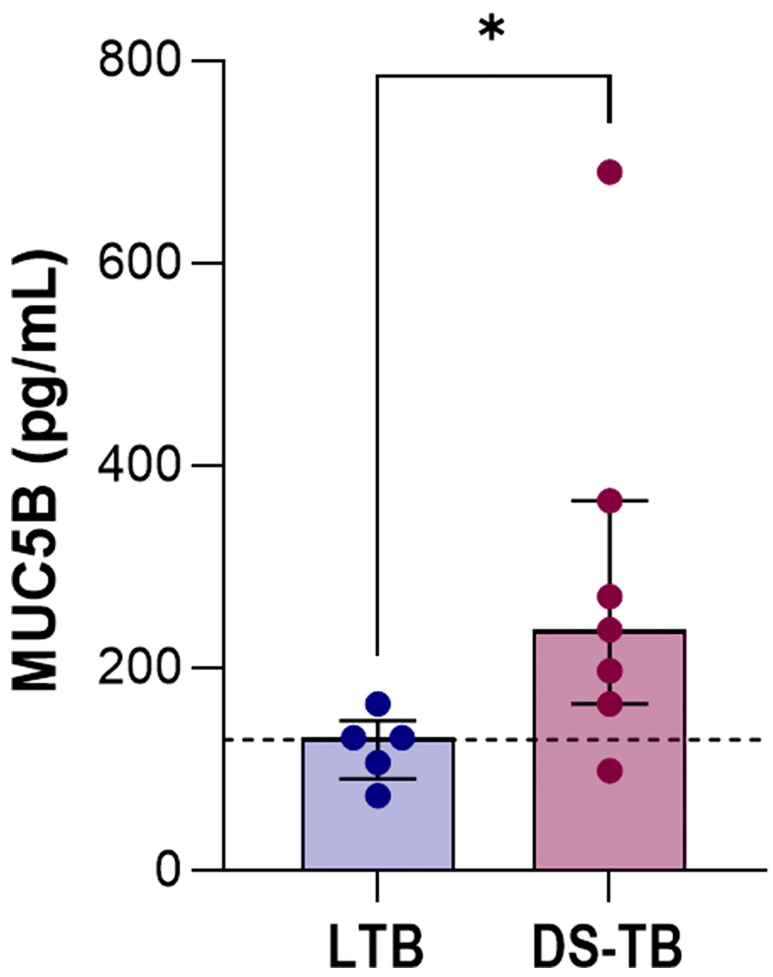

FIGURE 8
Increased levels of MUC5B in patients with active TB. Data are shown as median with interquartile range (IQR, 25–75). The black dashed lines represent the median value reported for healthy donors. The statistical comparison was performed using Mann–Whitney U Test (*p <0.05). n = 8 for both TB groups. MUC5B, mucin 5B.

study did not identify a MUC5B-dependent network, even in DS-TB patients with extensive lung damage.

Each monocyte subpopulation has a specific phenotype and well-established functions. In this study, we provided evidence that the frequency of classical monocytes TLR-2+ was increased in DS-TB. These patients had positive correlations between classical monocytes and platelets, platelet-factor, and pro-inflammatory cytokines, and this phenotype is determinant for lung damage. Another report indicated that ATB patients have an expansion of non-classical monocytes compared to a negative tuberculin test group (43); this discrepancy with our study is probably because our TB patients are exclusively drug-sensitive. At least in a mouse model (44, 45), the classical monocytes have been identified as the main subpopulation that migrates to the site of infection to differentiate into macrophages or dendritic cells. However, studies in murine models have indicated that the retention of classic monocytes in the lung predisposes to lung damage (46, 47).

In summary, our data suggest that in DS-TB, Mtb induces activation of platelets and classical monocytes, probably through TLR-2. Platelets produce high levels of PF4, and both platelets and classical monocytes could be the main contributors to VEGF-A. Moreover, classical monocytes correlated positively with high levels of IL-1β, IL-6, and IP-10. Thus, platelets and classical monocytes could establish inter-cellular communication to promote the activation in both ways (Figure 10, left). According to angiogenic factors and pro-inflammatory profile, DS-TB patients can be divided into two groups: one group displays a strong angiogenic profile, and although these patients show pulmonary affections, not all patients develop cavitary lung lesions; and the second group has

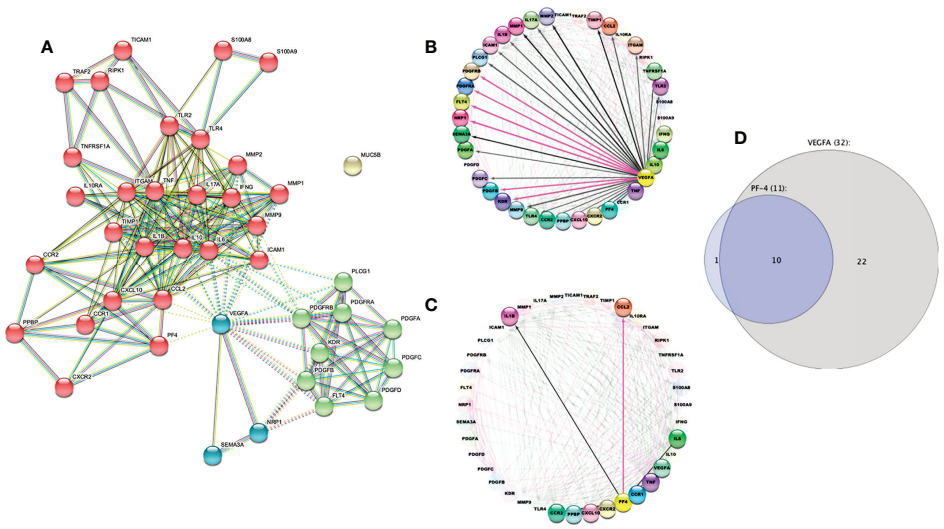

FIGURE 9
STRING protein–protein interaction diagram. **(A)** The STRING network shows protein-protein interactions. Different line colors represent the types of evidence for the association between proteins: experiments (pink line), databases (light blue line), co-expression (black line), text mining (green line) and "protein homology (violet line)." Based on the MCL clustering method (inflation parameter: 4). The solid and the dotted lines indicate connections within the same and different clusters, respectively. **(B)** The circular layout shows interactome to VEGF-A, and **(C)** shows interactome related to PF4. The black line indicates computational interaction, and the pink line indicates experimental interaction. **(D)** Venn Euler diagram showing the number of nodes in each logical grouping.

an inflammatory profile and 100% of patients show cavitation formation (Figure 10, right). All data suggest that platelets and classical monocytes (TLR-2+) during DS-TB enhance the inflammatory response, and consequently, lung damage is severe.

Thus, our study is not free of limitations. However, our study shows strong correlations, suggesting the existence of the platelet–classical monocytes–inflammation axis to mediate the lung damage during DS-TB. We did not confirm this interaction

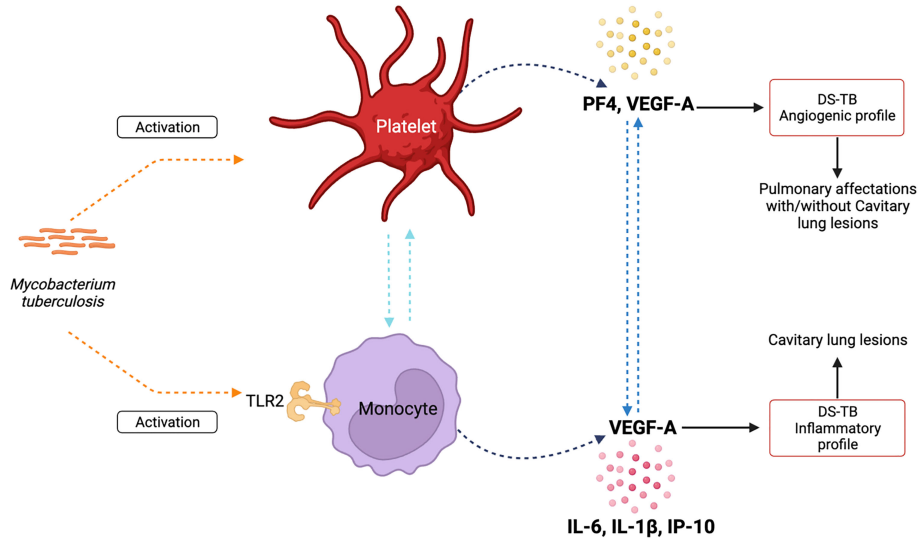

FIGURE 10
Summary of the presumptive relationship between platelet and classical monocytes to maintain an inflammatory environment and induce lung damage during active TB.

and still question whether TLR-2 is responsible for mediating the pro-inflammatory function in classical monocytes. Further, *in vitro* studies are necessary to clarify if platelets stimulate classical monocytes or if the latter is responsible for inducing the activation of platelets.

Data availability statement

The original contributions presented in the study are included in the article/Supplementary Material. Further inquiries can be directed to the corresponding author.

Ethics statement

The studies involving human participants were reviewed and approved by the Institutional Ethics and Scientific Committee. The patients/participants provided their written informed consent to participate in this study.

Author contributions

Conceptualization, LC-G. Methodology, AU-S, JF-G, and LR-L. Validation, AC-L and LR-L. Formal analysis, AU-S, JF-G, GP-R, and LC-G. Investigation, AU-S. Resources, IB-R. Data curation, JF-G and GP-R. Writing—original draft preparation, AU-S and JF-G. Writing—review and editing, LC-G. All authors have read and agreed to the published version of the manuscript.

Acknowledgments

We are grateful to the clinician staff of the Tuberculosis Clinic and Damaris Romero-Rodríguez from Flow Cytometry Core Facility, both at the Instituto Nacional de Enfermedades Respiratorias Ismael Cosio Villegas in Mexico City.

Conflict of interest

The authors declare that the research was conducted in the absence of any commercial or financial relationships that could be construed as a potential conflict of interest.

Publisher's note

All claims expressed in this article are solely those of the authors and do not necessarily represent those of their affiliated organizations, or those of the publisher, the editors and the reviewers. Any product that may be evaluated in this article, or claim that may be made by its manufacturer, is not guaranteed or endorsed by the publisher.

Supplementary material

The Supplementary Material for this article can be found online at: https://www.frontiersin.org/articles/10.3389/fimmu.2022.1016472/full#supplementary-material

References

1. Organización Mundial de la Salud (OMS). *Global tuberculosis report 2021*. Geneva: Repositorio Institucional para Compartir Información (IRIS) de la Organización Mundial de la Salud (OMS (2021). Available at: https://apps.who.int/iris/handle/10665/346387.

2. World Health Organization. *WHO consolidated guidelines on tuberculosis: module 1: Prevention: Tuberculosis Preventive treatment*. Geneva: World Health Organization (2020). Available at: https://apps.who.int/iris/handle/10665/331170 (Accessed November 24, 2021).

3. World Health Organization. *Guidelines on the management of latent tuberculosis infection*. Geneva: World Health Organization (2014). Available at: https://apps.who.int/iris/handle/10665/136471 (Accessed June 12, 2022).

4. Dutta NK, Karakousis PC. Latent tuberculosis infection: Myths, models, and molecular mechanisms. *Microbiol Mol Biol Rev* (2014) 78:343–71. doi: 10.1128/MMBR.00010-14

5. Sasindran SJ, Torrelles JB. Mycobacterium tuberculosis infection and inflammation: what is beneficial for the host and for the bacterium? *Front Microbio* (2011) 2:2. doi: 10.3389/fmicb.2011.00002

6. Ali RA, Wuescher LM, Worth RG. Platelets: essential components of the immune system. *Curr Trends Immunol* (2015) 16:65–78.

7. Kirwan DE, Chong DLW, Friedland JS. Platelet activation and the immune response to tuberculosis. *Front Immunol* (2021) 12:631696. doi: 10.3389/fimmu.2021.631696

8. La Manna MP, Orlando V, Badami GD, Tamburini B, Shekarkar Azgomi M, Lo Presti E, et al. Platelets accumulate in lung lesions of tuberculosis patients and inhibit T-cell responses and *Mycobacterium tuberculosis* replication in macrophages. *Eur J Immunol* (2022) 52:784–99. doi: 10.1002/eji.202149549

9. Fox KA, Kirwan DE, Whittington AM, Krishnan N, Robertson BD, Gilman RH, et al. Platelets regulate pulmonary inflammation and tissue destruction in tuberculosis. *Am J Respir Crit Care Med* (2018) 198:245–55. doi: 10.1164/rccm.201710-2102OC

10. Lee M-R, Lee M-C, Chang C-H, Liu C-J, Chang L-Y, Zhang J-F, et al. Use of antiplatelet agents and survival of tuberculosis patients: A population-based cohort study. *JCM* (2019) 8:923. doi: 10.3390/jcm8070923

11. Scheuermann L, Pei G, Domaszewska T, Zyla J, Oberbeck-Müller D, Bandermann S, et al. Platelets restrict the oxidative burst in phagocytes and facilitate primary progressive tuberculosis. *Am J Respir Crit Care Med* (2020) 202:730–44. doi: 10.1164/rccm.201910-2063OC

12. Büyükasik Y, Soylu B, Soylu AR, Özcebe OL, Canbakan S, Haznedaroglu LC, et al. *In vivo* platelet and T-lymphocyte activities during pulmonary tuberculosis. *Eur Respir J* (1998) 12:1375–9. doi: 10.1183/09031936.98.12061375

13. Alatas F, özkan A, Metintas M, özarslan A, Erginel S, Yildirim H. Vascular endothelial growth factor levels in active pulmonary tuberculosis. *Chest* (2004) 125:2156–9. doi: 10.1378/chest.125.6.2156

14. Polena H, Boudou F, Tilleul S, Dubois-Colas N, Lecointe C, Rakotosamimanana N, et al. Mycobacterium tuberculosis exploits the formation

of new blood vessels for its dissemination. *Sci Rep* (2016) 6:33162. doi: 10.1038/srep33162

15. Wang H, Keiser JA. Vascular endothelial growth factor upregulates the expression of matrix metalloproteinases in vascular smooth muscle cells: Role of flt-1. *Circ Res* (1998) 83:832–40. doi: 10.1161/01.RES.83.8.832

16. Lee KS, Min KH, Kim SR, Park SJ, Park HS, Jin GY, et al. Vascular endothelial growth factor modulates matrix metalloproteinase-9 expression in asthma. *Am J Respir Crit Care Med* (2006) 174:161–70. doi: 10.1164/rccm.200510-1558OC

17. Ong CWM, Elkington PT, Friedland JS. Tuberculosis, pulmonary cavitation, and matrix metalloproteinases. *Am J Respir Crit Care Med* (2014) 190:9–18. doi: 10.1164/rccm.201311-2106PP

18. Harding JS, Herbath M, Chen Y, Rayasam A, Ritter A, Csoka B, et al. VEGF-a from granuloma macrophages regulates granulomatous inflammation by a non-angiogenic pathway during mycobacterial infection. *Cell Rep* (2019) 27:2119–31.e6. doi: 10.1016/j.celrep.2019.04.072

19. Maison DP. Tuberculosis pathophysiology and anti-VEGF intervention. *J Clin Tuberculosis Other Mycobact Dis* (2022) 27:100300. doi: 10.1016/j.jctube.2022.100300

20. Gao J-L, Wynn TA, Chang Y, Lee EJ, Broxmeyer HE, Cooper S, et al. Impaired host defense, hematopoiesis, granulomatous inflammation and type 1–type 2 cytokine balance in mice lacking CC chemokine receptor 1. *J Exp Med* (1997) 185:1959–68. doi: 10.1084/jem.185.11.1959

21. Zhang P, Dairaghi DJ, Jaen JC, Powers JP. Recent advances in the discovery and development of CCR1 antagonists. In: *Annual reports in medicinal chemistry*. Annu Rep Med Chem: Elsevier (2013). p. 133–47. doi: 10.1016/B978-0-12-417150-3.00010-7

22. Fox JM, Kausar F, Day A, Osborne M, Hussain K, Mueller A, et al. CXCL4/Platelet factor 4 is an agonist of CCR1 and drives human monocyte migration. *Sci Rep* (2018) 8:9466. doi: 10.1038/s41598-018-27710-9

23. Gatsiou A, Sopova K, Tselepis A, Stellos K. Interleukin-17A triggers the release of platelet-derived factors driving vascular endothelial cells toward a pro-angiogenic state. *Cells* (2021) 10:1855. doi: 10.3390/cells10081855

24. Keller SP. Platelets worsen tuberculosis disease progression: Specific mechanism TBD. *Sci Transl Med* (2020) 12:eabc8940. doi: 10.1126/scitranslmed.abc8940

25. Rathod S, Samel DR, Kshirsagar P, Pokar M. Thrombocytosis: can it be used as a marker for tuberculosis? *Int J Res Med Sci* (2017) 5:3082. doi: 10.18203/2320-6012.ijrms20172991

26. Dib PRB, Quirino-Teixeira AC, Merij LB, Pinheiro MBM, Rozini SV, Andrade FB, et al. Innate immune receptors in platelets and platelet-leukocyte interactions. *J Leukoc Biol* (2020) 108:1157–82. doi: 10.1002/JLB.4MR0620-701R

27. Feng Y, Dorhoi A, Mollenkopf H-J, Yin H, Dong Z, Mao L, et al. Platelets direct monocyte differentiation into epithelioid-like multinucleated giant foam cells with suppressive capacity upon mycobacterial stimulation. *J Infect Dis* (2014) 210:1700–10. doi: 10.1093/infdis/jiu355

28. Patko Z, Csaszar A, Acsady G, Peter K, Schwarz M. Roles of mac-1 and glycoprotein IIb/IIIa integrins in leukocyte–platelet aggregate formation: Stabilization by mac-1 and inhibition by GpIIb/IIIa blockers. *Platelets* (2012) 23:368–75. doi: 10.3109/09537104.2011.625098

29. Portier I, Campbell RA. Role of platelets in detection and regulation of infection. *ATVB* (2020) 41:70–8. doi: 10.1161/ATVBAHA.120.314645

30. Ceresa IF, Noris P, Ambaglio C, Pecci A, Balduini CL. Thrombopoietin is not uniquely responsible for thrombocytosis in inflammatory disorders. *Platelets* (2007) 18:579–82. doi: 10.1080/09537100701593601

31. Pahari S, Kaur G, Negi S, Aqdas M, Das DK, Bashir H, et al. Reinforcing the functionality of mononuclear phagocyte system to control tuberculosis. *Front Immunol* (2018) 9:193. doi: 10.3389/fimmu.2018.00193

32. Roy MG, Livraghi-Butrico A, Fletcher AA, McElwee MM, Evans SE, Boerner RM, et al. Muc5b is required for airway defence. *Nature* (2014) 505:412–6. doi: 10.1038/nature12807

33. Yang IV, Fingerlin TE, Evans CM, Schwarz MI, Schwartz DA. MUC5B and idiopathic pulmonary fibrosis. *Ann Am Thorac Soc* (2015) 12:S193–9. doi: 10.1513/AnnalsATS.201503-110AW

34. Gopal R, Monin L, Torres D, Slight S, Mehra S, McKenna KC, et al. S100A8/A9 proteins mediate neutrophilic inflammation and lung pathology during tuberculosis. *Am J Respir Crit Care Med* (2013) 188:1137–46. doi: 10.1164/rccm.201304-0803OC

35. Pollara G, Turner CT, Rosenheim J, Chandran A, Bell LCK, Khan A, et al. Exaggerated IL-17A activity in human in vivo recall responses discriminates active tuberculosis from latent infection and cured disease. *Sci Transl Med* (2021) 13:eabg7673. doi: 10.1126/scitranslmed.abg7673

36. Takahashi H, Numasaki M, Lotze MT, Sasaki H. Interleukin-17 enhances bFGF-, HGF- and VEGF-induced growth of vascular endothelial cells. *Immunol Lett* (2005) 98:189–93. doi: 10.1016/j.imlet.2004.11.012

37. Huang Q, Duan L, Qian X, Fan J, Lv Z, Zhang X, et al. IL-17 promotes angiogenic factors IL-6, IL-8, and vegf production *via* Stat1 in lung adenocarcinoma. *Sci Rep* (2016) 6:36551. doi: 10.1038/srep36551

38. Kraakman MJ, Lee MKS, Al-Sharea A, Dragoljevic D, Barrett TJ, Montenont E, et al. Neutrophil-derived S100 calcium-binding proteins A8/A9 promote reticulated thrombocytosis and atherogenesis in diabetes. *J Clin Invest* (2017) 127:2133–47. doi: 10.1172/JCI92450

39. Kaser A, Brandacher G, Steurer W, Kaser S, Offner FA, Zoller H, et al. Interleukin-6 stimulates thrombopoiesis through thrombopoietin: role in inflammatory thrombocytosis. *Blood* (2001) 98:2720–5. doi: 10.1182/blood.V98.9.2720

40. Casella I, Feccia T, Chelucci C, Samoggia P, Castelli G, Guerriero R, et al. Autocrine-paracrine VEGF loops potentiate the maturation of megakaryocytic precursors through Flt1 receptor. *Blood* (2003) 101:1316–23. doi: 10.1182/blood-2002-07-2184

41. Pitchford SC, Lodie T, Rankin SM. VEGFR1 stimulates a CXCR4-dependent translocation of megakaryocytes to the vascular niche, enhancing platelet production in mice. *Blood* (2012) 120:2787–95. doi: 10.1182/blood-2011-09-378174

42. Hollborn M, Stathopoulos C, Steffen A, Wiedemann P, Kohen L, Bringmann A. Positive feedback regulation between MMP-9 and VEGF in human RPE cells. *Invest Ophthalmol Vis Sci* (2007) 48:4360. doi: 10.1167/iovs.06-1234

43. Castaño D, García LF, Rojas M. Increased frequency and cell death of CD16 + monocytes with mycobacterium tuberculosis infection. *Tuberculosis* (2011) 91:348–60. doi: 10.1016/j.tube.2011.04.002

44. Sampath P, Moideen K, Ranganathan UD, Bethunaickan R. Monocyte subsets: Phenotypes and function in tuberculosis infection. *Front Immunol* (2018) 9:1726. doi: 10.3389/fimmu.2018.01726

45. Balboa L, Barrios-Payan J, González-Domínguez E, Lastrucci C, Lugo-Villarino G, Mata-Espinoza D, et al. Diverging biological roles among human monocyte subsets in the context of tuberculosis infection. *Clin Sci* (2015) 129:319–30. doi: 10.1042/CS20150021

46. Chong SZ, Evrard M, Devi S, Chen J, Lim JY, See P, et al. CXCR4 identifies transitional bone marrow premonocytes that replenish the mature monocyte pool for peripheral responses. *J Exp Med* (2016) 213:2293–314. doi: 10.1084/jem.20160800

47. O'Dea KP, Wilson MR, Dokpesi JO, Wakabayashi K, Tatton L, van Rooijen N, et al. Mobilization and margination of bone marrow gr-1 ^{high} monocytes during subclinical endotoxemia predisposes the lungs toward acute injury. *J Immunol* (2009) 182:1155–66. doi: 10.4049/jimmunol.182.2.1155

frontiers | Frontiers in Immunology

TYPE Original Research
PUBLISHED 11 November 2022
DOI 10.3389/fimmu.2022.1054457

OPEN ACCESS

EDITED BY
Meganathan Kannan,
Central University of Tamil Nadu, India

REVIEWED BY
Chen Wang,
Peking University, China
Christoph Licht,
University of Toronto, Canada
Marc Hilhorst,
Academic Medical Center

*CORRESPONDENCE
Björn Tampe
bjoern.tampe@med.uni-goettingen.de

SPECIALTY SECTION
This article was submitted to Molecular Innate Immunity, a section of the journal Frontiers in Immunology

RECEIVED 26 September 2022
ACCEPTED 31 October 2022
PUBLISHED 11 November 2022

CITATION
Baier E, Tampe D, Kluge IA, Hakroush S and Tampe B (2022) Implication of platelets and complement C3 as link between innate immunity and tubulointerstitial injury in renal vasculitis with MPO-ANCA seropositivity.
Front. Immunol. 13:1054457.
doi: 10.3389/fimmu.2022.1054457

Implication of platelets and complement C3 as link between innate immunity and tubulointerstitial injury in renal vasculitis with MPO-ANCA seropositivity

Eva Baier[1], Désirée Tampe[1], Ingmar Alexander Kluge[2], Samy Hakroush[2,3] and Björn Tampe[1]*

[1]Department of Nephrology and Rheumatology, University Medical Center Göttingen, Göttingen, Germany, [2]Institute of Pathology, University Medical Center Göttingen, Göttingen, Germany, [3]SYNLAB Pathology Hannover, SYNLAB Holding Germany, Augsburg, Germany

Introduction: Antineutrophil cytoplasmic antibody (ANCA)-associated vasculitis (AAV) is a potentially life-threatening systemic small-vessel vasculitis that is characterized by pauci-immune glomerulonephritis, depicting in turn a major denominator of AAV mortality. It is well established that AAV patients feature an increased risk of developing thrombotic events, and platelets are activated in AAV patients being triggered by the alternative complement pathway. Platelets guard vessels integrity and initiate thrombus formation in response to endothelial damage, further constituting a triangular interconnection with the activation of neutrophils and the complement system. We here aimed to systematically assess the relevance of platelet counts and systemic complement system activation regarding distinct histopathological lesions in ANCA-associated renal vasculitis.

Methods: A cohort of 53 biopsy-proven cases of ANCA-associated renal vasculitis were retrospectively enrolled in a single-center observational study. Univariate and multivariate regression analysis was performed to identify parameters associated with platelet counts in ANCA-associated renal vasculitis compared to disease controls. Finally, the relevance of platelets for disease course and recovery was assessed by survival analysis.

Results: Lower platelet counts correlated with markers of kidney injury including eGFR loss ($p=0.0004$) and lower complement C3 levels ($p=0.0037$). Multivariate and subgroup analysis revealed that this association was only present in the subgroup with MPO-ANCA seropositivity (eGFR loss: $p=0.0009$, lower C3: $p=0.0032$). While lower platelet counts correlated with kidney injury in the PR3-ANCA subgroup (eGFR loss: $p=0.0272$), we did not observe an independent association with complement C3 levels ($p=0.4497$). Independent of any glomerular lesion, lower platelet counts correlated with interstitial fibrosis

10.3389/fimmu.2022.1054457

(*p=0.0313*), tubular atrophy (*p=0.0073*), and tubulitis in areas of interstitial fibrosis and tubular atrophy (*p=0.0033*). Finally, we observed significant differences with increased requirement of kidney replacement therapy (KRT) or death in the subgroup below median platelet counts (HR: 4.1, 95% CI: 1.6-10, *p=0.0047*), associated with a lower probability of discharge and prolonged hospitalization in this subgroup (HR: 0.5, 95% CI: 0.3-0.9, *p=0.0113*).

Conclusion: Based on our observation that an association between platelets and complement system activation is only observed in the MPO-ANCA subgroup, this could implicate that platelets and complement C3 link innate immunity to tubulointerstitial injury in the presence of MPO-ANCA autoantibodies.

KEYWORDS

innate immunity, platelets, complement system, complement C3, ANCA-associated renal vasculitis, MPO-ANCA, PR3-ANCA, tubulointerstitial injury

Introduction

Antineutrophil cytoplasmic antibody (ANCA)-associated vasculitis (AAV) is a potentially life-threatening systemic small-vessel vasculitis that is characterized by pauci-immune glomerulonephritis in case of kidney involvement, depicting in turn a major denominator of AAV mortality (1–4). Two principal antigens on neutrophils, namely proteinase 3 (PR3) and myeloperoxidase (MPO), provide epitopes for ANCA binding, thus promoting neutrophil activation and neutrophil extracellular traps (NETs) formation ("NETosis"), which consists of the extrusion of lattice-like chromatin fibers harboring cytokines and antimicrobial proteins that contribute to host defense under physiological conditions and promote endothelial damage and vascular inflammation culminating in necrotizing vasculitis in the context of autoimmunity (5–7). ANCA-stimulated neutrophils have been shown to induce the formation of NETs, which contain the ANCA target antigens MPO and PR3 (8). In ANCA-associated renal vasculitis, NETs are located in close proximity to neutrophil infiltrates in affected glomeruli and tubulointerstitium (8). NETs are capable to activate the classical complement pathway due to the interaction with C1q (9). Neutrophils itself contain various components of the alternative but not the classical complement pathway (10). Particularly in AAV with activated neutrophils by ANCA autoantibodies, the alternative dominates over the classical complement pathway (11). Therefore, the involvement of the alternative pathway of the complement system captures a pathophysiological key role in NETosis and more generally in AAV, which is impressively constrained by the efficacy of avacopan, a novel drug targeting the C5a receptor (12–14). As part of innate immunity, the complement system is composed of approximately more than thirty serum proteins, whose pathways are either classical-, alternative- or lectin-categorized (15, 16). Depending on different induction modes, a self-reinforcing domino-effect-like cascade is initiated that disembarks in the common formation of the so-called membrane attack complex (MAC), wherein also inhibitory regulatory mechanisms are interposed, such as factor H suppressing the activation of the alternative pathway by preventing C3b opsonization, which in turn was shown to affect NETosis (17, 18).

Being influenced by both components, complement system activation and neutrophils/NETosis, the coagulation system is another relevant pathophysiological factor acting on the injured endothelium as the primary side of inflammation (18, 19). It is well established that AAV patients feature a two- to three-fold increased risk of developing thrombotic events, and platelets are activated in AAV patients being triggered by the alternative complement pathway (20–26). Platelets guard vessels integrity and initiate thrombus formation in response to endothelial damage, further constituting a triangular interconnection with the activation of neutrophils, formation of NETs and the complement system (26–28). Although ANCA autoantibody activity is an established inducer of NETs, its presence is not always consistent with disease activity (29). Regarding additional mechanisms of neutrophil activation, recent reports suggested that platelets itself can also regulate formation of NETs in AAV (30). However, the implication of platelets regarding vasculitis manifestation and complement system activation in ANCA-associated renal vasculitis has not been described yet. Therefore, we here aimed to systematically assess the relevance of platelet counts and systemic complement system activation regarding distinct histopathological lesions in ANCA-associated renal vasculitis.

10.3389/fimmu.2022.1054457

Methods

Study population and subgroup formation

A well characterized cohort of 53 biopsy-proven cases of ANCA-associated renal vasculitis were retrospectively enrolled between 2015 till 2020 in a single-center observational study at the University Medical Center Göttingen, Göttingen, Germany (Supplementary Table 1) (31–35). In addition, 18 cases with IgA nephropathy, 20 with diabetic kidney disease, and 27 with acute interstitial nephritis were included as disease controls (Supplementary Table 2). While no formal approval was required for the use of routine clinical data, a favorable ethical opinion was granted by the local Ethics committee (no. 22/2/14 and 28/09/17). All participants provided their written informed consent for the utilization of routinely collected data for research purposes as part of their regular medical care. Medical records were used to collect data on age, sex, medication, comorbidities, laboratory findings at admission (creatinine, estimated glomerular filtration rate/eGFR, blood urea nitrogen/BUN, potassium, albumin, aspartate-amino transferase/AST, alkaline phosphatase/AP, gamma glutamyl transferase/γGT, bilirubin, complement C3 and C4), at the time of kidney biopsy (platelets, hemoglobin, white blood cells/WBC, C-reactive protein/CRP), dates of admission and discharge from hospital. The Birmingham Vasculitis Activity Score (BVAS) was assessed as previously described (36).

Renal histopathology

Renal pathologists evaluated all kidney biopsies and was blinded to clinical data analysis. Based on the current version of the Banff scoring system for renal allograft pathology, tubulointerstitial lesions were scored as previously reported: arteriolar hyalinosis (*ah*), arteritis (*v*), glomerulitis (*g*), inflammation in areas of interstitial fibrosis and tubular atrophy (*i-IFTA*), interstitial fibrosis (*ci*), interstitial inflammation (*i*), peritubular capillaritis (*ptc*), total inflammation (*ti*), tubular atrophy (*ct*), tubulitis (*t*), and tubulitis in areas of interstitial fibrosis and tubular atrophy (*t-IFTA*) (37, 38). Tubular injury lesions were systematically assessed as recently described (39). Briefly, tubular dilation, tubular necrosis, epithelial simplification, non-isometric cell vacuolization, red blood cell (RBC) and necrotic casts were scored with a range from 0 to 4 depending on the fraction of affected cortical area of renal biopsy (score 0: <1%, 1: ≥1-10%, 2: ≥10-25%, 3: ≥25-50%, 4: >50%). Moreover, all injured glomeruli (crescentic or/and necrotic) were screened for the presence of a Bowman's capsule rupture, whose extent was further quantified as previously described (40–42).

Remission induction therapy

Steroids were administered either as intravenous pulse therapy or orally with a tapering schedule. At time of platelet measurement and kidney biopsy, all patients received steroids and further remission induction therapy was initiated thereafter based on histopathological confirmation of ANCA GN. Plasma exchange (PEX) was administered during the induction period at the discretion of treating physicians. Rituximab (RTX) was administered as four intravenous doses at 375 mg/m^2 every week; RTX was not administered within 48 hours before PEX treatment. Cyclophosphamide (CYC) was administered as three intravenous doses up to 15 mg/kg every 2 weeks and every 3 weeks thereafter, adjusted for age and renal function. Combination therapy was administered as four intravenous doses at 375 mg/m^2 RTX every week and two intravenous doses at 15 mg/kg CYC every 2 weeks. On the discretion of treating physicians, choice of remission induction therapy was dependent on previous regimens and individual patients, more likely to choose RTX in younger patients with toxicity being the main reason for this choice (Supplementary Table 1) (43). Prophylaxis to prevent pneumocystis (carinii) jiroveci infection was administered according to local practice.

Statistical analysis

Normally distributed values are presented as mean ± standard deviation (SD), while non-normally distributed parameters are shown as median and interquartile range (IQR). Normal distribution was evaluated by Shapiro-Wilk testing. Categorical variables as percentages of total. Statistical comparisons were not formally powered or prespecified. Probability values (p value) below 0.05 were considered statistically significant. For normally distributed values, mean comparisons were performed with unpaired student's t-test, while estimation plots were used for data visualization. For non-normally distributed values, median comparisons were performed with the Mann-Whitney-U-test. Heatmaps reflect the mean values of Spearman's ρ in the univariate linear regression analysis, circle size represents significance level. Survival-curve analyses were performed using the Kaplan-Meier method, wherein log rank (Mantel-Cox) testing was conducted for curve comparison. Time-to-event was registered and discharge from hospital was defined as event. Results are shown as hazard ratio (HR) and 95% confidence interval (CI). For stepwise multiple linear regression, covariates were retained to significant differences in the linear regression model to avoid model over-fit. Data analyses were performed with GraphPad Prism (version 9.4 for MacOS, GraphPad Software, San Diego, California, USA) and IBM SPSS Statistics (version 28 for MacOS, IBM Corporation, Armonk, NY, USA).

Results

Lower platelet counts associate with kidney injury and lower complement C3 levels in MPO-ANCA-associated renal vasculitis

The study conduction is summarized in Supplementary Figure 1, the baseline characteristics of the total cohort are shown in Supplementary Table 1. Median (IQR) platelet counts were 300,000/µL (207,000-438,000/µL), therefore most patients were within or above the normal range (150,000-350,000/µL, Figure 1A). Univariate analysis revealed that lower platelet counts correlated with markers of kidney injury, including serum creatinine levels (ρ=-0.51, *p<0.0001*), eGFR loss (ρ=0.47, *p=0.0004*), and BUN (ρ=-0.44, *p=0.0025*, Figure 1B). Furthermore, lower platelet counts were also associated with reduced levels of serum albumin (ρ=0.59, *p=0.0020*) and complement C3 (ρ=0.46, *p=0.0037*, Figure 1B). By contrast, we observed no association between platelet counts and ANCA autoantibody levels, coagulation parameters, other markers of systemic inflammation, or parameters indicative for liver injury (Figure 1B). Multivariate analysis confirmed an independent association between platelet counts, kidney injury (eGFR loss: *p=0.0005*) and lower levels of complement C3 (*p=0.0416*) in the total cohort of ANCA-associated renal vasculitis (Table 1). Moreover, BUN itself was not the main denominator associated with lower platelet counts (*p=0.4011*, Table 1), implicating distinct mechanisms independent of uremia in ANCA-associated renal vasculitis. This association was equally detectable in the subgroup with MPO-ANCA seropositivity (eGFR loss: *p=0.0009*, lower complement C3: *p=0.0032*, Table 1). While lower platelet counts correlated with kidney injury in renal vasculitis with PR3-ANCA seropositivity (eGFR loss: *p=0.0272*), we did not observe an independent association with complement C3 levels in this subgroup (*p=0.4497*, Table 1). To validate that these findings are specific for ANCA-associated renal vasculitis, we next analyzed platelet counts, markers of kidney injury and complement levels in disease controls including IgA nephropathy, diabetic kidney disease, and acute interstitial nephritis (Supplementary Table 2). We did not observe any significant association between platelet counts and serum creatinine levels (ρ=-0.23, *p>0.05*), eGFR (ρ=0.24, *p>0.05*), complement C3 (ρ=0.07, *p>0.05*) or C4 (ρ=0.06, *p>0.05*, Supplementary Figure 2). In summary, lower platelet counts associated with kidney injury in

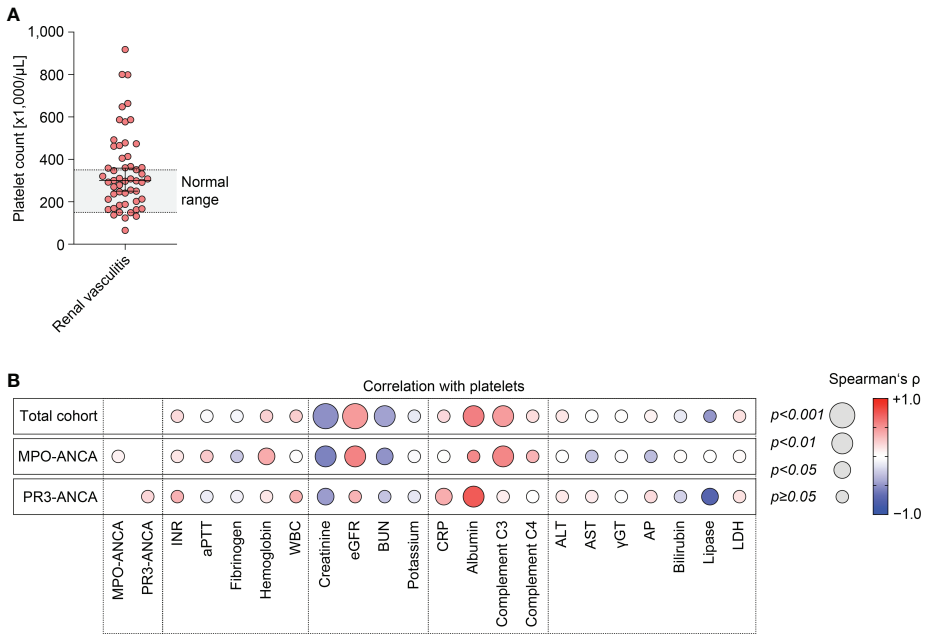

FIGURE 1
Lower platelet counts associate with kidney injury and lower complement C3 levels in ANCA-associated renal vasculitis. **(A)** Distribution of platelet counts in the total cohort of ANCA-associated renal vasculitis (normal range: 150,000-350,000/µL). **(B)** Correlations between platelet counts and laboratory parameters in ANCA-associated renal vasculitis are shown by heatmap reflecting mean values of Spearman's ρ, circle size represents significance level. ALT, alanine aminotransferase; ANCA, antineutrophil cytoplasmic antibody; AP, alkaline phosphatase; aPTT, activated partial thromboplastin time; AST, aspartate amino transferase; BUN, blood urea nitrogen; CRP, C-reactive protein; eGFR, estimated glomerular filtration rate (CKD-EPI); INR, international normalized ratio; LDH, lactate dehydrogenase; MPO, myeloperoxidase; PR3, proteinase 3; WBC, white blood cells; γGT, gamma glutamyl transferase.

10.3389/fimmu.2022.1054457

TABLE 1 Stepwise multiple linear regression analyses with platelet counts as the dependent variable.

Total cohort	β	p value
Creatinine – mg/dL	-0.0107	*0.9645*
eGFR – mL/min/1.73 m^2	0.6405	*0.0005*
BUN – mg/dL	-0.1567	*0.4011*
Albumin – g/dL	0.1056	*0.5109*
Complement C3 – g/L	0.3276	*0.0416*
MPO-ANCA		
eGFR – mL/min/1.73 m^2	0.6784	*0.0009*
Albumin – g/dL	-0.0597	*0.7791*
Complement C3 – g/L	0.5375	*0.0032*
PR3-ANCA		
eGFR – mL/min/1.73 m^2	0.7247	*0.0272*
Albumin – g/dL	0.2595	*0.4013*
Complement C3 – g/L	0.2443	*0.4497*

ANCA, antineutrophil cytoplasmic antibody; BUN, blood urea nitrogen; eGFR, estimated glomerular filtration rate (CKD-EPI); MPO, myeloperoxidase; PR3, proteinase 3.

ANCA-associated renal vasculitis. Furthermore, lower platelet counts were independently correlated with lower complement C3 levels specifically in patients with MPO-ANCA seropositivity that was not confirmed in the PR3-ANCA subgroup. Finally, there was no association with unspecific markers of systemic inflammation in ANCA-associated renal vasculitis.

Lower platelet counts associate specifically with tubulointerstitial injury in ANCA-associated renal vasculitis

Because we have observed an association between lower platelet counts and laboratory markers of kidney injury, we next analyzed the association between platelet counts and histopathological lesions in ANCA-associated renal vasculitis. Interestingly, there was no association between platelet counts and any glomerular lesion in ANCA-associated renal vasculitis (Figure 2). By contrast, lower platelet counts correlated with interstitial fibrosis (*ci*, *p=0.0313*), tubular atrophy (*ct*, *p=0.0073*), and tubulitis in areas of interstitial fibrosis and tubular atrophy (*t-IFTA*, *p=0.0033*, Figure 2). Detailed morphological analysis of tubular injury indicated that lower platelet counts correlated specifically with tubular dilatation in renal vasculitis with MPO-ANCA seropositivity (*p=0.0347*), while an association with cellular casts was observed in the PR3-ANCA subgroup (*p=0.0352*, Figure 2). By contrast, we did not observe any association with inflammatory lesions including intrarenal immune cell infiltration (Figure 2). In summary, lower platelet counts correlated specifically with tubulointerstitial injury in ANCA-associated renal vasculitis. Moreover, we again observed differences between ANCA subtypes regarding distinct tubular injury patterns.

Disease course and recovery in ANCA-associated renal vasculitis differs according to platelet counts

Finally, we performed cohort dichotomization by using median platelet counts (300,000/µL) to separate groups for survival-curve analyses using the Kaplan-Meier method and log-rank testing (Figure 3A). As previously observed, group separation resulted in significant differences were again observed for markers of kidney injury, including serum creatinine levels (*p=0.0007*), eGFR (*p=0.0029*), and BUN (*p=0.0061*), and complement C3 levels (*p=0.0313*, Table 2). This also correlated with disease course reflected by significant differences in requirement of kidney replacement therapy (KRT) or death in the subgroup below median platelet counts (HR: 4.1, 95% CI: 1.6-10, *p=0.0047*, Figure 3B). Furthermore, we observed a lower probability of discharge with prolonged hospitalization

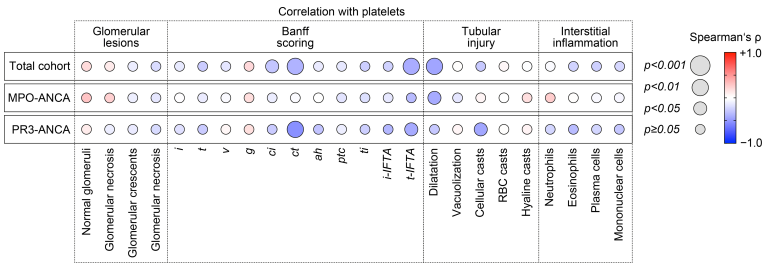

FIGURE 2
Lower platelet counts associate specifically with tubulointerstitial injury in ANCA-associated renal vasculitis. Correlations between platelet counts and histopathological lesions in ANCA-associated renal vasculitis are shown by heatmap reflecting mean values of Spearman's ρ, circle size represents significance level. *ah*, arteriolar hyalinosis; ANCA, antineutrophil cytoplasmic antibody; *ci*, interstitial fibrosis; *ct*, tubular atrophy; *g*, glomerulitis; *i*, interstitial inflammation; *i-IFTA*, inflammation in areas of interstitial fibrosis and tubular atrophy; MPO, myeloperoxidase; PR3, proteinase 3; *ptc*, peritubular capillaritis; RBC, red blood cell; *t*, tubulitis; *ti*, total inflammation; *t-IFTA*, tubulitis in areas of interstitial fibrosis and tubular atrophy; *v*, intimal arteritis.

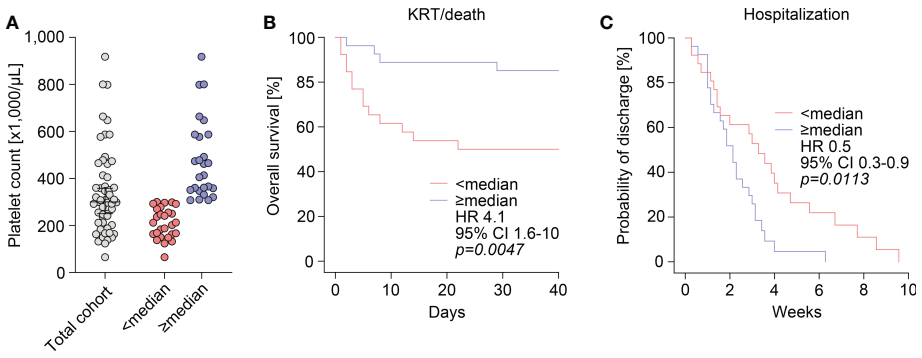

FIGURE 3
Disease course and recovery in ANCA-associated renal vasculitis differs according to platelet counts. **(A)** The scatter dot plots show platelet counts with median ± IQR, group separation was performed according to median platelet count (300,000/µL). **(B)** Overall survival (KRT/death) within 40 days after admission according to group separation by median platelet count (300,000/µL). Comparison of survival curves was performed with log rank (Mantel-Cox) testing. **(C)** Probability of discharge from hospital after admission according to group separation by median platelet count (300,000/µL). Comparison of survival curves was performed with log rank (Mantel-Cox) testing. ANCA, antineutrophil cytoplasmic antibody; CI, confidence interval; HR, hazard ratio; IQR, interquartile range; KRT, kidney replacement therapy.

TABLE 2 Group separation by median platelet count (300,000/µL).

Clinical data	<median	≥median	p value
Age – years	65 (54.5-76)	65 (54-74)	*0.4930*
Female sex – no. (%)	9 (34.6)	14 (51.9)	*0.2056*
MPO-/PR3-ANCA – no./no. (%/%)	16/10 (61.5/38.5)	10/17 (37/63)	*0.0745*
BVAS – points	17 ± 4.4	18.6 ± 3.9	*0.1725*
Serum parameters			
Platelets – x1,000/µL	207 (159.8-258.8)	414 (347-587)	*<0.0001*
INR –ratio	1 (1-1.2)	1.1 (1-1.3)	*0.5208*
aPTT – seconds	28 (26-31.5)	28 (26.75-32)	*0.7177*
Fibrinogen – mg/dL	388 ± 155.4	390.1 ± 232.7	*0.9805*
Hemoglobin – g/dL	9.3 (8.15-10.8)	10.2 (9.2-12.2)	*0.1106*
WBC – x1,000/µL	9.88 (6.74-14.1)	12.4 (9.86-15.5)	*0.0672*
Creatinine – mg/dL	3.62 (2.11-5.01)	1.42 (0.77-2.91)	*0.0007*
eGFR – mL/min/1.73 m^2	16.25 (9.03-27.4)	48.4 (24-98.4)	*0.0029*
BUN – mg/dL	53 (36.5-77.5)	29 (19.5-44)	*0.0061*
Potassium – mmol/L	4.3 (4.15-4.7)	4.3 (4-4.43)	*0.3401*
CRP – mg/L	60.4 (6.55-113.2)	63.8 (26.2-109.5)	*0.4037*
Albumin – g/dL	2.08 ± 0.6	2.76 ± 0.5	*0.0110*
Complement C3 – g/L	1.12 ± 0.3	1.35 ± 0.28	*0.0313*
Complement C4 – g/L	0.25 ± 0.1	0.25 ± 0.08	*0.8862*
ALT – U/L	13.5 (10-25.5)	19 (8-47)	*0.8525*
AST – U/L	25 (15-28.5)	21 (18.75-34)	*0.9856*
γGT – U/L	54 (17-77.75)	34 (20-107)	*0.9955*
AP – U/L	86.5 (71-106.5)	90 (70-126.5)	*0.4653*
Bilirubin – mg/dL	0.4 (0.3-0.55)	0.3 (0.3-0.73)	*0.8660*
Lipase – U/L	46 (25.5-70.5)	24 (19.5-30.5)	*0.0563*
LDH – U/L	265.5 (210.3-301.5)	288.5 (241.5-326.8)	*0.2901*

Mean ± SD are shown for normally distributed values, group comparisons were performed with unpaired student's t-test. Median (IQR) for non-normally distributed values, group comparisons were performed with Mann-Whitney-U-test. Categorical variables are presented as frequency and percentage, non-parametric between-group-comparisons were performed with Pearson's Chi-square test.

ALT, alanine aminotransferase; ANCA, antineutrophil cytoplasmic antibody; AP, alkaline phosphatase; aPTT, activated partial thromboplastin time; AST, aspartate amino transferase; BUN, blood urea nitrogen; BVAS, Birmingham Vasculitis Activity Score; CRP, C-reactive protein; eGFR, estimated glomerular filtration rate (CKD-EPI); INR, international normalized ratio; IQR, interquartile range; LDH, lactate dehydrogenase; MPO, myeloperoxidase; no., number; PR3, proteinase 3; SD, standard deviation; WBC, white blood cells; γGT, gamma glutamyl transferase.

in this subgroup (HR: 0.5, 95% CI: 0.3-0.9, *p=0.0113*, Figure 3C), indicating disease course and recovery in ANCA-associated renal vasculitis differed according to platelet counts.

Discussion

Innate immunity refers to non-specific recognition of exogenous or endogenous components, leading to an activation of the immune system, and resulting in clearance of these molecules. Megakaryocyte-derived platelets are a key component of the blood, playing a critical role in immune responses by secretion of active mediators. The ability of enucleated platelets to crosstalk with immune cells contributing to innate immune responses is attributed to the expression of membrane proteins, storage granules, and a variety of megakaryocyte-derived molecules. Platelets are a key component of innate immunity that trap immunogenic molecules by necessitating the process of clotting, preventing them from being accessible and to disseminate. Moreover, it is also well established that the platelets are the primary mediators of hemostasis and thrombosis. Therefore, it is increasingly recognized that a hypercoagulable state is persistently active in patients with ANCA-associated renal vasculitis, and studies investigating the impact of tailored anticoagulation are needed to reduce the burden of thromboembolism (24).

We here observed that most patients with active ANCA-associated renal vasculitis had platelet counts within or above the normal range. This is in line with previous reports that platelet counts were significantly higher in patients in active disease stage compared with those in remission (44). Within our cohort of active ANCA-associated renal vasculitis, we observed an association between lower platelet counts and kidney injury, disease course and recovery in ANCA-associated renal vasculitis. These results implicate that platelets in active ANCA-associated renal vasculitis result from a reactive increase, and that a consumptive decrease may indicate accelerated kidney injury. Interestingly, this concept is confirmatory to previous reports that hypercoagulability contributes to kidney injury in vascular diseases, including ANCA-associated renal vasculitis (45–48). In addition, we here observed that lower platelet counts associated specifically with tubulointerstitial injury in ANCA-associated renal vasculitis independent of any glomerular lesion. In this context, experimental studies have already shown that platelets are main contributors to microvascular injury and rarefaction of tubulointerstitial capillaries (49). In ANCA-associated renal vasculitis, the occurrence of tubulointerstitial injury independent of glomerular lesions has already been described (50–53). Our observations might indicate that the tubulointerstitial compartment is particularly susceptible to a hypercoagulable state mediated by platelets. The concept that loss of kidney function is more affected by tubulointerstitial rather than glomerular injury has been described more than 50 years ago in glomerulonephritis (54). In response to tubular damage, different cell death modes (namely apoptosis, necroptosis, and ferroptosis) feature different degrees of immunogenicity, wherein the two latter-mentioned constitute different pathways that are implied in acute kidney injury (AKI), transition from AKI to CKD, sepsis-associated AKI, but also autoimmune vasculitis affecting the kidneys (55).

Moreover, lower platelet counts associated with complement system activation reflected by lower serum C3 levels in ANCA-associated renal vasculitis. Complement system activation with reduced complement C3 levels and intrarenal complement deposits are important denominators of poor outcome in ANCA-associated renal vasculitis (56–60). Our observation that an association between platelets, kidney injury and complement C3 is not present in disease controls (IgA nephropathy, diabetic kidney disease, and acute interstitial nephritis) and specifically observed in the MPO-ANCA subgroup implicates distinct pathomechanisms dependent on seropositivity for MPO-ANCA or PR3-ANCA. This is especially relevant since two complement system inhibitors are currently in clinical development for AAV. Thus, our results may contribute to a more personalized treatment approach of AAV depending on the ANCA serotype and the relevance of complement system activation.

Finally, we here provide evidence that platelets and complement system activation is especially relevant in the subgroup with MPO-ANCA seropositivity. Detailed morphological analysis of tubular injury indicated that lower platelet counts correlated specifically with tubular dilatation in renal vasculitis with MPO-ANCA seropositivity, while an association with cellular casts was observed in the PR3-ANCA subgroup. Although tubular dilatation and cellular casts are both observed in injured kidneys indicating tubular injury and cell death, the association with either ANCA subtype again could also implicate distinct pathomechanisms of tubulointerstitial injury dependent on seropositivity for MPO-ANCA or PR3-ANCA (61, 62). Regarding potential mechanisms, it has been suggested that MPO can directly interact and induce priming of platelets that can contribute to the development of vascular inflammation (63). Therefore, binding of MPO-ANCA autoantibodies could further aggravate platelet activation and vascular injury. These results require confirmation but may contribute to a personalized treatment approach of AAV.

Our study has several limitations, such as the small patient number and the retrospective study design. Furthermore, our observations are associative and do not proof causality requiring mechanistic studies that also include platelet activation and function. Nevertheless, we provide a clinically approached link between platelets, complement system activation and tubulointerstitial injury patterns specifically in MPO-ANCA-associated renal vasculitis, thus broadening our current pathophysiological understanding.

Conclusion

Based on our observation that an association between platelets and complement system activation is only observed in the MPO-ANCA subgroup, this could implicate that platelets and complement C3 link innate immunity to tubulointerstitial injury in the presence of MPO-ANCA autoantibodies. These results require confirmation but may contribute to a personalized treatment approach of AAV.

Data availability statement

The original contributions presented in the study are included in the article/Supplementary Material. Further inquiries can be directed to the corresponding author.

Ethics statement

The studies involving human participants were reviewed and approved by the local Ethics committee (no. 22/2/14 and 28/09/17). The patients/participants provided their written informed consent to participate in this study.

Author contributions

BT conceived the study and edited the manuscript. EB collected and analyzed data, and wrote the first draft. DT collected and analyzed data, IK and SH evaluated kidney biopsies. All authors contributed to the article and approved the submitted version.

Funding

This study was supported by the Else-Kröner research program entitled "*molecular therapy and prediction of gastrointestinal malignancies*", grant number 7-67-1840876. We also acknowledge support by the Open Access Publication Funds of the Göttingen University. The funders had no role in the design of the study; in the collection, analyses, or interpretation of data; in the writing of the manuscript, or in the decision to publish the results.

Conflict of interest

Author SH was employed by company SYNLAB Pathology Hannover, SYNLAB Holding Germany.

The remaining authors declare that the research was conducted in the absence of any commercial or financial relationships that could be construed as a potential conflict of interest.

Publisher's note

Supplementary material

The Supplementary Material for this article can be found online at: https://www.frontiersin.org/articles/10.3389/fimmu.2022.1054457/full#supplementary-material

References

1. Jennette JC, Nachman PH. Anca glomerulonephritis and vasculitis. *Clin J Am Soc Nephrol* (2017) 12(10):1680–91. doi: 10.2215/CJN.02500317

2. Lee T, Gasim A, Derebail VK, Chung Y, McGregor JG, Lionaki S, et al. Predictors of treatment outcomes in anca-associated vasculitis with severe kidney failure. *Clin J Am Soc Nephrol* (2014) 9(5):905–13. doi: 10.2215/CJN.08290813

3. Jennette JC, Wilkman AS, Falk RJ. Anti-neutrophil cytoplasmic autoantibody-associated glomerulonephritis and vasculitis. *Am J Pathol* (1989) 135(5):921–30.

4. Flossmann O, Berden A, de Groot K, Hagen C, Harper L, Heijl C, et al. Long-term patient survival in anca-associated vasculitis. *Ann Rheum Dis* (2011) 70 (3):488–94. doi: 10.1136/ard.2010.137778

5. Lee KH, Kronbichler A, Park DD, Park Y, Moon H, Kim H, et al. Neutrophil extracellular traps (Nets) in autoimmune diseases: A comprehensive review. *Autoimmun Rev* (2017) 16(11):1160–73. doi: 10.1016/j.autrev.2017.09.012

6. Berthelot JM, Le Goff B, Neel A, Maugars Y, Hamidou M. Netosis: At the crossroads of rheumatoid arthritis, lupus, and vasculitis. *Joint Bone Spine* (2017) 84 (3):255–62. doi: 10.1016/j.jbspin.2016.05.013

7. Frangou E, Vassilopoulos D, Boletis J, Boumpas DT. An emerging role of neutrophils and netosis in chronic inflammation and fibrosis in systemic lupus erythematosus (Sle) and anca-associated vasculitides (Aav): Implications for the pathogenesis and treatment. *Autoimmun Rev* (2019) 18(8):751–60. doi: 10.1016/j.autrev.2019.06.011

8. Kessenbrock K, Krumbholz M, Schonermarck U, Back W, Gross WL, Werb Z, et al. Netting neutrophils in autoimmune small-vessel vasculitis. *Nat Med* (2009) 15(6):623–5. doi: 10.1038/nm.1959

9. Leffler J, Martin M, Gullstrand B, Tyden H, Lood C, Truedsson L, et al. Neutrophil extracellular traps that are not degraded in systemic lupus erythematosus activate complement exacerbating the disease. *J Immunol* (2012) 188(7):3522–31. doi: 10.4049/jimmunol.1102404

10. Chen M, Daha MR, Kallenberg CG. The complement system in systemic autoimmune disease. *J Autoimmun* (2010) 34(3):J276–86. doi: 10.1016/j.jaut.2009.11.014

11. Van Timmeren MM, Chen M, Heeringa P. Review article: Pathogenic role of complement activation in anti-neutrophil cytoplasmic auto-Antibody-Associated vasculitis. *Nephrol (Carlton)* (2009) 14(1):16–25. doi: 10.1111/j.1440-1797.2009.01086.x

12. Jayne D. Complement inhibition in anca vasculitis. *Nephrol Ther* (2019) 15 (6):409–12. doi: 10.1016/j.nephro.2019.04.001

13. Andrighetto S, Leventhal J, Zaza G, Cravedi P. Complement and complement targeting therapies in glomerular diseases. *Int J Mol Sci* (2019) 20 (24):6336. doi: 10.3390/ijms20246336

14. Chen M, Jayne DRW, Zhao MH. Complement in anca-associated vasculitis: Mechanisms and implications for management. *Nat Rev Nephrol* (2017) 13(6):359–67. doi: 10.1038/nrneph.2017.37

15. Merle NS, Church SE, Fremeaux-Bacchi V, Roumenina LT. Complement system part I - molecular mechanisms of activation and regulation. *Front Immunol* (2015) 6:262. doi: 10.3389/fimmu.2015.00262

16. Merle NS, Noe R, Halbwachs-Mecarelli L, Fremeaux-Bacchi V, Roumenina LT. Complement system part ii: Role in immunity. *Front Immunol* (2015) 6:257. doi: 10.3389/fimmu.2015.00257

17. Moore SR, Menon SS, Cortes C, Ferreira VP. Hijacking factor h for complement immune evasion. *Front Immunol* (2021) 12:602277. doi: 10.3389/fimmu.2021.602277

18. de Bont CM, Boelens WC, Pruijn GJM. Netosis, complement, and coagulation: A triangular relationship. *Cell Mol Immunol* (2019) 16(1):19–27. doi: 10.1038/s41423-018-0024-0

19. Maugeri N, Rovere-Querini P, Baldini M, Sabbadini MG, Manfredi AA. Translational mini-review series on immunology of vascular disease: Mechanisms of vascular inflammation and remodelling in systemic vasculitis. *Clin Exp Immunol* (2009) 156(3):395–404. doi: 10.1111/j.1365-2249.2009.03921.x

20. Miao D, Li DY, Chen M, Zhao MH. Platelets are activated in anca-associated vasculitis *Via* thrombin-pars pathway and can activate the alternative complement pathway. *Arthritis Res Ther* (2017) 19(1):252. doi: 10.1186/s13075-017-1458-y

21. Nygaard L, Polcwiartek C, Nelveg-Kristensen KE, Carlson N, Kristensen S, Torp-Pedersen C, et al. Long-term cardiovascular outcomes and temporal trends in patients diagnosed with anca-associated vasculitis: A Danish nationwide registry study. *Rheumatol (Oxford)* (2022). doi: 10.1093/rheumatology/keac386

22. Kronbichler A, Leierer J, Leierer G, Mayer G, Casian A, Hoglund P, et al. Clinical associations with venous thromboembolism in anti-neutrophil cytoplasm antibody-associated vasculitides. *Rheumatol (Oxford)* (2017) 56(5):704–8. doi: 10.1093/rheumatology/kew465

23. Kronbichler A, Leierer J, Shin JI, Merkel PA, Spiera R, Seo P, et al. Association of pulmonary hemorrhage, positive proteinase 3, and urinary red blood cell casts with venous thromboembolism in antineutrophil cytoplasmic antibody-associated vasculitis. *Arthritis Rheumatol* (2019) 71(11):1888–93. doi: 10.1002/art.41017

24. Kronbichler A, Leierer J, Gauckler P, Shin JI. Comorbidities in anca-associated vasculitis. *Rheumatol (Oxford)* (2020) 59(Suppl 3):iii79–83. doi: 10.1093/rheumatology/kez617

25. Moiseev S, Kronbichler A, Makarov E, Bulanov N, Crnogorac M, Direskeneli H, et al. Association of venous thromboembolic events with skin, pulmonary and kidney involvement in anca-associated vasculitis: A multinational study. *Rheumatol (Oxford)* (2021) 60(10):4654–61. doi: 10.1093/rheumatology/keab071

26. Misra DP, Thomas KN, Gasparyan AY, Zimba O. Mechanisms of thrombosis in anca-associated vasculitis. *Clin Rheumatol* (2021) 40(12):4807–15. doi: 10.1007/s10067-021-05790-9

27. Hamad OA, Back J, Nilsson PH, Nilsson B, Ekdahl KN. Platelets, complement, and contact activation: Partners in inflammation and thrombosis. *Adv Exp Med Biol* (2012) 946:185–205. doi: 10.1007/978-1-4614-0106-3_11

28. Mezger M, Nording H, Sauter R, Graf T, Heim C, von Bubnoff N, et al. Platelets and immune responses during thromboinflammation. *Front Immunol* (2019) 10:1731. doi: 10.3389/fimmu.2019.01731

29. Kraaij T, Kamerling SWA, van Dam LS, Bakker JA, Bajema IM, Page T, et al. Excessive neutrophil extracellular trap formation in anca-associated vasculitis is independent of anca. *Kidney Int* (2018) 94(1):139–49. doi: 10.1016/j.kint.2018.01.013

30. Matsumoto K, Yasuoka H, Yoshimoto K, Suzuki K, Takeuchi T. Platelet Cxcl4 mediates neutrophil extracellular traps formation in anca-associated vasculitis. *Sci Rep* (2021) 11(1):222. doi: 10.1038/s41598-020-80685-4

31. Hakroush S, Kluge IA, Strobel P, Korsten P, Tampe D, Tampe B. Systematic histological scoring reveals more prominent interstitial inflammation in myeloperoxidase-anca compared to proteinase 3-anca glomerulonephritis. *J Clin Med* (2021) 10(6):1231. doi: 10.3390/jcm10061231

32. Hakroush S, Tampe D, Korsten P, Strobel P, Tampe B. Complement components C3 and C4 indicate vasculitis manifestations to distinct renal compartments in anca-associated glomerulonephritis. *Int J Mol Sci* (2021) 22 (12):6588. doi: 10.3390/ijms22126588

33. Tampe D, Strobel P, Korsten P, Hakroush S, Tampe B. Consideration of therapeutic plasma exchange in association with inflammatory lesions in anca-associated glomerulonephritis: A real-world retrospective study from a single center. *Front Immunol* (2021) 12:645483. doi: 10.3389/fimmu.2021.645483

34. Tampe D, Korsten P, Strobel P, Hakroush S, Tampe B. Comprehensive analysis of sex differences at disease manifestation in anca-associated glomerulonephritis. *Front Immunol* (2021) 12:736638. doi: 10.3389/fimmu.2021.736638

35. Hakroush S, Tampe D, Strobel P, Korsten P, Tampe B. Comparative histological subtyping of immune cell infiltrates in mpo-anca and Pr3-anca glomerulonephritis. *Front Immunol* (2021) 12:737708. doi: 10.3389/fimmu.2021.737708

36. Mukhtyar C, Lee R, Brown D, Carruthers D, Dasgupta B, Dubey S, et al. Modification and validation of the Birmingham vasculitis activity score (Version 3). *Ann Rheum Dis* (2009) 68(12):1827–32. doi: 10.1136/ard.2008.101279

37. Roufosse C, Simmonds N, Clahsen-van Groningen M, Haas M, Henriksen KJ, Horsfield C, et al. A 2018 reference guide to the banff classification of renal allograft pathology. *Transplantation* (2018) 102(11):1795–814. doi: 10.1097/TP.0000000000002366

38. Loupy A, Haas M, Roufosse C, Naesens M, Adam B, Afrouzian M, et al. The banff 2019 kidney meeting report (I): Updates on and clarification of criteria for T cell- and antibody-mediated rejection. *Am J Transplant* (2020) 20(9):2318–31. doi: 10.1111/ajt.15898

39. Hakroush S, Tampe D, Korsten P, Strobel P, Tampe B. Systematic scoring of tubular injury patterns reveals interplay between distinct tubular and glomerular lesions in anca-associated glomerulonephritis. *J Clin Med* (2021) 10(12):2682. doi: 10.3390/jcm10122682

40. Hakroush S, Tampe D, Korsten P, Strobel P, Tampe B. Bowman's capsule rupture links glomerular damage to tubulointerstitial inflammation in anca-associated glomerulonephritis. *Clin Exp Rheumatol* (2021) 39 Suppl 129(2):27–31. doi: 10.55563/clinexprheumatol/7eol6d

41. Hakroush S, Tampe B. Neutrophils associate with bowman's capsule rupture specifically in Pr3-anca glomerulonephritis. *J Nephrol* (2022) 35 (4):1177–83. doi: 10.1007/s40620-021-01208-6

42. Hakroush S, Tampe B. Correspondence on 'Bowman's capsule rupture on renal biopsy improves the outcome prediction of anca-associated glomerulonephritis classifications'. *Ann Rheum Dis* (2021). doi: 10.1136/annrheumdis-2021-219970

43. Forbess LJ, Griffin KW, Spiera RF. Practice patterns of anca-associated vasculitis: Exploring differences among subspecialties at a single academic medical centre. *Clin Exp Rheumatol* (2014) 32(3 Suppl 82):S48–50.

44. Ma TT, Huang YM, Wang C, Zhao MH, Chen M. Coagulation and fibrinolysis index profile in patients with anca-associated vasculitis. *PLoS One* (2014) 9(5):e97843. doi: 10.1371/journal.pone.0097843

45. Sebastian JK, Voetsch B, Stone JH, Romay-Penabad Z, Lo GH, Allen NB, et al. The frequency of anticardiolipin antibodies and genetic mutations associated with hypercoagulability among patients with wegener's granulomatosis with and without history of a thrombotic event. *J Rheumatol* (2007) 34(12):2446–50.

46. Berden AE, Nolan SL, Morris HL, Bertina RM, Erasmus DD, Hagen EC, et al. Anti-plasminogen antibodies compromise fibrinolysis and associate with renal histology in anca-associated vasculitis. *J Am Soc Nephrol* (2010) 21(12):2169–79. doi: 10.1681/ASN.2010030274

47. Hertig A, Rondeau E. Role of the Coagulation/Fibrinolysis system in fibrin-associated glomerular injury. *J Am Soc Nephrol* (2004) 15(4):844–53. doi: 10.1097/01.asn.0000115400.52705.83

48. Kumar SV, Kulkarni OP, Mulay SR, Darisipudi MN, Romoli S, Thomasova D, et al. Neutrophil extracellular trap-related extracellular histones cause vascular necrosis in severe gn. *J Am Soc Nephrol* (2015) 26(10):2399–413. doi: 10.1681/ASN.2014070673

49. Schwarzenberger C, Sradnick J, Lerea KM, Goligorsky MS, Nieswandt B, Hugo CP, et al. Platelets are relevant mediators of renal injury induced by primary endothelial lesions. *Am J Physiol Renal Physiol* (2015) 308(11):F1238–46. doi: 10.1152/ajprenal.00535.2014

50. Plafkin C, Zhong W, Singh T. Anca vasculitis presenting with acute interstitial nephritis without glomerular involvement. *Clin Nephrol Case Stud* (2019) 7:46–50. doi: 10.5414/CNCS109805

51. Kasahara H, Hiroyuki N, Shinohara M, Koike T. Ap-vas 2012 case report: An atypical case of microscopic polyangiitis presenting with acute tubulointerstitial nephritis without glomerular change. *CEN Case Rep* (2014) 3(1):1–4. doi: 10.1007/s13730-013-0103-0

52. Nakabayashi K, Sumiishi A, Sano K, Fujioka Y, Yamada A, Karube M, et al. Tubulointerstitial nephritis without glomerular lesions in three patients with myeloperoxidase-Anca-Associated vasculitis. *Clin Exp Nephrol* (2009) 13(6):605–13. doi: 10.1007/s10157-009-0200-8

53. Morimoto K, Kanzaki G, Niikura T, Koike K, Matsuo N, Maruyama Y, et al. Acute tubulointerstitial nephritis associated with antineutrophil cytoplasmic antibody following cimetidine treatment: A case report. *BMC Nephrol* (2021) 22 (1):294. doi: 10.1186/s12882-021-02502-y

54. Risdon RA, Sloper JC, De Wardener HE. Relationship between renal function and histological changes found in renal-biopsy specimens from patients with persistent glomerular nephritis. *Lancet* (1968) 2(7564):363–6. doi: 10.1016/s0140-6736(68)90589-8

55. Maremonti F, Meyer C, Linkermann A. Mechanisms and models of kidney tubular necrosis and nephron loss. *J Am Soc Nephrol* (2022) 33(3):472–86. doi: 10.1681/ASN.2021101293

56. Augusto JF, Langs V, Demiselle J, Lavigne C, Brilland B, Duveau A, et al. Low serum complement C3 levels at diagnosis of renal anca-associated vasculitis is associated with poor prognosis. *PLoS One* (2016) 11(7):e0158871. doi: 10.1371/journal.pone.0158871

57. Lionaki S, Marinaki S, Liapis G, Kalaitzakis E, Fragkioudaki S, Kalogeropoulos P, et al. Hypocomplementemia at diagnosis of pauci-immune glomerulonephritis is associated with advanced histopathological activity index and high probability of treatment resistance. *Kidney Int Rep* (2021) 6(9):2425–35. doi: 10.1016/j.ekir.2021.05.043

58. Tampe D, Baier E, Hakroush S, Tampe B. Low serum levels of complement C3c at diagnosis indicate poor outcome in antineutrophil cytoplasmic antibody-associated glomerulonephritis. *Kidney Int Rep* (2022) 7(3):660–1. doi: 10.1016/j.ekir.2021.12.038

59. Tampe D, Baier E, Hakroush S, Tampe B. Comparative analysis of complement C3 and C4 serum levels for outcome prediction in anca-associated renal vasculitis. *J Nephrol* (2022). doi: 10.1007/s40620-022-01414-w

60. Hakroush S, Tampe D, Baier E, Kluge IA, Strobel P, Tampe B. Intrarenal synthesis of complement C3 localized to distinct vascular compartments in anca-associated renal vasculitis. *J Autoimmun* (2022) 133:102924. doi: 10.1016/j.jaut.2022.102924

61. Lusco MA, Fogo AB, Najafian B, Alpers CE. Ajkd atlas of renal pathology: Tubular atrophy. *Am J Kidney Dis* (2016) 67(6):e33–4. doi: 10.1053/j.ajkd.2016.04.007

62. Fogo AB, Lusco MA, Najafian B, Alpers CE. Ajkd atlas of renal pathology: Ischemic acute tubular injury. *Am J Kidney Dis* (2016) 67(5):e25. doi: 10.1053/j.ajkd.2016.03.003

63. Kolarova H, Klinke A, Kremserova S, Adam M, Pekarova M, Baldus S, et al. Myeloperoxidase induces the priming of platelets. *Free Radic Biol Med* (2013) 61:357–69. doi: 10.1016/j.freeradbiomed.2013.04.014

frontiers | Frontiers in Immunology

TYPE Original Research
PUBLISHED 27 June 2023
DOI 10.3389/fimmu.2023.1207631

OPEN ACCESS

EDITED BY
Esaki M. Shankar,
Central University of Tamil Nadu, India

REVIEWED BY
Erika M Palmieri,
National Cancer Institute at Frederick (NIH), United States
Vladimir M Pisarev,
Federal Research and Clinical Center of Intensive Care Medicine and Rehabilitation, Russia

*CORRESPONDENCE
Gilles A. Robichaud
gilles.robichaud@umoncton.ca

RECEIVED 17 April 2023
ACCEPTED 30 May 2023
PUBLISHED 27 June 2023

CITATION
Gharib E, Veilleux V, Boudreau LH, Pichaud N and Robichaud GA (2023) Platelet-derived microparticles provoke chronic lymphocytic leukemia malignancy through metabolic reprogramming. *Front. Immunol.* 14:1207631. doi: 10.3389/fimmu.2023.1207631

Platelet-derived microparticles provoke chronic lymphocytic leukemia malignancy through metabolic reprogramming

Ehsan Gharib[1,2,3], Vanessa Veilleux[1,2,3], Luc H. Boudreau[1,3], Nicolas Pichaud[1,3] and Gilles A. Robichaud[1,2,3]*

[1]Department of Chemistry and Biochemistry, Université de Moncton, Moncton, NB, Canada, [2]Atlantic Cancer Research Institute, Moncton, NB, Canada, [3]New Brunswick Center for Precision Medicine, Moncton, NB, Canada

Background: It is well established that inflammation and platelets promote multiple processes of cancer malignancy. Recently, platelets have received attention for their role in carcinogenesis through the production of microvesicles or platelet-derived microparticles (PMPs), which transfer their biological content to cancer cells. We have previously characterized a new subpopulation of these microparticles (termed mito-microparticles), which package functional mitochondria. The potential of mitochondria transfer to cancer cells is particularly impactful as many aspects of mitochondrial biology (i.e., cell growth, apoptosis inhibition, and drug resistance) coincide with cancer hallmarks and disease progression. These metabolic aspects are particularly notable in chronic lymphocytic leukemia (CLL), which is characterized by a relentless accumulation of proliferating, immunologically dysfunctional, mature B-lymphocytes that fail to undergo apoptosis. The present study aimed to investigate the role of PMPs on CLL metabolic plasticity leading to cancer cell phenotypic changes.

Methods: CLL cell lines were co-incubated with different concentrations of human PMPs, and their impact on cell proliferation, mitochondrial DNA copy number, OCR level, ATP production, and ROS content was evaluated. Essential genes involved in metabolic-reprogramming were identified using the bioinformatics tools, examined between patients with early and advanced CLL stages, and then validated in PMP-recipient CLLs. Finally, the impact of the induced metabolic reprogramming on CLLs' growth, survival, mobility, and invasiveness was tested against anti-cancer drugs Cytarabine, Venetoclax, and Plumbagin.

Results: The data demonstrated the potency of PMPs in inducing tumoral growth and invasiveness in CLLs through mitochondrial internalization and OXPHOS stimulation which was in line with metabolic shift reported in CLL patients from

early to advanced stages. This metabolic rewiring also improved CLL cells' resistance to Cytarabine, Venetoclax, and Plumbagin chemo drugs.

Conclusion: Altogether, these findings depict a new platelet-mediated pathway of cancer pathogenesis. We also highlight the impact of PMPs in CLL metabolic reprogramming and disease progression.

KEYWORDS

platelets, microvesicles, leukemia, microparticles, extracellular vesicles, mitochondria

Introduction

Chronic lymphocytic leukemia (CLL) is the most prevalent adult blood cancer in western societies and consists of almost 7% of non-Hodgkin lymphomas (NHL) cases worldwide. CLL is defined by uncontrollable proliferation of monoclonal lymphocytes, eventually resulting in a growing number of low or nonfunctional B-cells. Generally, CLL affects older adults (median age = 70) where approximately 80% of diagnosed cases sustain a five-year survival incidence. Although CLL and its prognosis are classified by several genetic factors (i.e., ZAP-70 mutation (1), immunoglobulin variable region heavy chain (IGHv) status (2), and β2 microglobulin levels (3)), CLL is not associated with a specific cytogenetic or molecular defect. In addition, while available treatments generally induce remission, most patients recidivate due to chemoresistance (4). Consequently, CLL still remains an incurable disease today.

In addition to genetic lesions, several pathogenic mechanisms have been shown to be key regulators of CLL disease, such as cancer cell interactions with its microenvironment to induce cell adaptability during disease progression. This environmental adaptation is conveyed through cancer cell metabolic reprogramming, which cumulates to promote cell survival, proliferation, and immune escape (4–6). This metabolic plasticity is particularly vital for CLL cells residing in different compartments such as bone marrow, spleen, lymph nodes, and peripheral blood, which reflect its pathological features (i.e., marrow infiltration, splenomegaly lymphadenopathy and lymphocytosis respectively) with the disease (7). Previous studies have reported that aerobic glycolysis is the dominant metabolic pathway during the early stages of CLL disease in which it efficiently supports cell growth by rapid ATP production and enhanced tissue disruption (8). However, the metabolic status of CLL is altered upon entering the bloodstream by an increase of mitochondrial content and subsequent activation of oxidative phosphorylation (OXPHOS) to evade immune assault (5, 9, 10). These changes also result in abundant reactive oxygen species (ROS) production, leading to chronic oxidative stress and metastasis stimulation (8, 11). Although metabolic plasticity is a well characterized hallmark of cancer progression, the exact mechanisms and cues involved in metabolic remodeling during cancer pathogenesis have not been fully elucidated to this day. Nonetheless, mitochondrial mass and function have been intimately linked to CLL disease progression (11–15).

Inflammation is another critical component of cancer malignancy (16) where platelets are particularly active in these events (17–19). Platelets are generated from megakaryocytes found in the bone marrow and are released in the bloodstream where they represent the most abundant blood cell type after erythrocytes (20). More recently, platelets have garnered attention for their role in cancer through the production of platelet-derived microparticles (PMPs). Upon activation, platelets shed and release extracellular vesicles in the extracellular milieu known as microparticles (also termed microvesicles, 0.1 –1 μm) (21). Moreover, PMPs and their packaged bioactive content (i.e., RNAs, transcription factors, inflammatory enzymes, etc.) are horizontally transferred into recipient target cells upon vesicle internalization (22, 23). It has been shown that the PMPs can cargo more than 600 proteins involved in cellular process (26%), regulation (22%), interaction with cells and organisms (9%), metabolic process (8%), response to stimulus and developmental process (6%), localization (5%), immunosystem process (4%), and reproduction (2%) (24). Meanwhile, the cytoplasm section had the most significant number of proteins (20%), followed by the plasma membrane (14%), other intracellular organelles (11%), nucleus (10%), cytoskeleton (9%), mitochondria (6%), extracellular and macromolecular complex (5%), endoplasmic reticulum (4%), endosome (3%), and cell surface (1%) (24). More than half of the identified proteins like STXBP2 and SH3BGRL had binding activity (48%), catalytic activity (29%) like PP2B and Catalase, enzyme regulator activity (5%), structural molecular activity (5%), molecular transducer activity, and antioxidant activity (2%).

Microparticles represent physiological vehicles of bioactive material for intercellular communication (25, 26). Given that PMPs constitute 70-90% of all circulating microparticles (27, 28), they have also been associated with numerous diseases including multiple sclerosis (29, 30), arthritis (31, 32), atherosclerosis (33, 34), and cancer (35, 36). The exact mechanism by which PMPs stimulate gene transcription for metabolic genes has not been fully understood yet, there are several proposed mechanisms such as (37–42): *i*) epigenetic modifications in which PMPs can transfer microRNAs (miRNAs) to recipient cells to regulate gene expression and modify the epigenetic landscape of the recipient cells through DNA methylation and histone modifications, thereby stimulating or inhibiting gene transcription; *ii*) signaling pathways activated by PMPs including PI3K-Akt and MAPK, which activate transcription

factors (ex: nuclear factor kappa B (NF-κB)) that bind gene promoters to activate transcription; *iii*) transcription factor transfer through PMP cargo, which regulate recipient cell gene transcription (37–42). Yet, further research is needed to fully understand the mechanisms by which PMPs modulate gene transcription and how these processes contribute to cellular metabolism.

We have previously identified and reported a novel subpopulation of PMPs which retains functional mitochondria (25, 32). Although the internalization of mitoMPs leads to a net increase of total intracellular mitochondrial mass in recipient cells, the net phenotypic outcome in permissive cells remains to be investigated[33]. This phenomenon is of particular interest in cancer as many facets of mitochondrial physiology, beyond ATP production, support cancer processes such as proliferation, redox homeostasis, invasion, drug resistance, and apoptosis resistance (43–47). Given the predominant role of mitochondria in cancer processes, we therefore set out to investigate whether and how a gain in additional mitochondrial mass (and mitochondrial function) supplied by PMPs, would provide CLL cells with a significant biological benefit leading to disease progression. In this study, we demonstrate a new aspect in the complex communication network between CLL cells and blood platelets as a source of foreign mitochondrial supply for cancer cells. We found that CLL cell acquisition of PMP-sourced mitochondria leads to a positive impact in cancer metabolism. Specifically, co-cultures of CLL with PMPs elicited metabolic reprogramming resulting in increased levels of oxygen consumption rates (OCR), ATP levels, and production of ROS. CLL cells treated with PMPs are also characterized by enhanced proliferation, mobility, invasiveness, and anticancer drug resistance. Our study thus characterizes new leukemic cell interactions with its microenvironment enabling cancer cell metabolic reprogramming and enhanced malignant features. These findings also identify new platelets mechanisms supporting cancer malignancy, which concomitantly provide new avenues for the development of anticancer strategies.

Material and methods

Cell culture and treatments

Human leukemic cell lines CII (#ACC 773), MEC-1 (ACC 497), and the megakaryocytic Set2 cell line (#ACC 608) were purchased from the Leibniz Institute DSMZ-German Collection of Microorganisms and Cell Culture (DSMZ Braunschweig, Germany). The cells were grown and maintained in RPMI 1640 media (ThermoFisher Scientific, Burlington, ON, Canada) supplemented with 10% fetal bovine serum/FBS (Wisent Bioproducts, St-Bruno, QC, Canada), FBS) at 37°C under 5% CO_2 in a humified incubator. Set2 cells were grown in RPMI 1640 medium supplemented with 20% fetal bovine serum. Culturing of cells was performed at a medium density of 2-5 x 10^5 cells/mL for CII and 0.5-2.0 x 10^6 cells/mL for MEC-1 and split at an appropriate ratio of 1:2 every 40 hrs. Cell treatments for phenotypic analyses included anticancer drug compounds Cytarabine, Venetoclax, and Plumbagin (Sigma-Aldrich) at the indicated concentrations for the indicated time points. To evaluate PMP internalization levels into cells, co-cultures were performed with cells labeled with anti-human CD19-FITC antibody (BioLegend, San Diego, CA, USA) and MitoTracker® Deep Red (MTDR, ThermoFisher Scientific)-labeled PMPs followed by cell cytometry using the 644 nm EX for MTDR and 488 nm EX for CD19 detection.

Isolation of platelets and platelet-derived microparticles

This study was conducted in accordance with the guidelines of the Declaration of Helsinki of 1975 (revised 2013, https://www.wma.net/what-we-do/medical-ethics/declaration-of-helsinki/). Institutional Review Board Statement and approval for studies involving human samples have been granted from both the Vitalité Health Network (project: CER7-3-17 Ver. 5) and the Université de Moncton (NB, Canada) (project: 1516-002) research ethics boards. Peripheral blood was obtained from consenting healthy volunteers (three men and seven women, aged 22-37). Healthy donors selected did not have any known autoimmune diseases and did not previously receive any preoperative chemotherapy and/or radiotherapy.

Patient samples consisted of 200 mL of whole peripheral blood, collected from cubital vein using a 21-gauge needle and Vacutainer tubes (ThermoFisher Scientific) containing the anticoagulant acid citrate dextrose (ACD; 0.085 mM sodium citrate, 0.0702 mM citric acid, 0.111 mM dextrose, pH 4.5). The platelets-rich plasma (PRP) layer was separated from the erythrocytes and other cell types by centrifugation at room temperature for 10 min at 265 x *g*. The PRP was transferred to a new tube where ACD (1:5 of the initial PRP volume) and ethylenediaminetetraacetic acid (EDTA, 10 mM, pH 8.0) were added, and the mixture was subsequently centrifuged at 400 x *g* for 2 minutes at room temperature. The supernatant was collected into a new tube and centrifuged at 1,300 x *g* for 10 minutes at room temperature. The harvested pellets were gently suspended in 200 µL Tyrode buffer (134 mM NaCl, 2.9 mM KCl, 0.34 mM Na_2HPO_4, 12 mM $NaHCO_3$, 20 mM HEPES, 1 mM $MgCl_2$, 5 mM glucose, and 0.5 mg/mL bovine serum albumin (BSA), pH 6.5) and then transferred in 25% volume of initial PRP of Tyrode solution (pH 7.4). Platelet count was performed with a hemocytometer slide under a Nikon TMS inverted phase-contrast microscope equipped with a Coolpix 5000 high-resolution digital camera (Nikon Corp, Melville, NY, USA). PMP production was initiated by incubating platelets (3 x 10^8 cells/mL) with thrombin (0.1 U/mL, Sigma-Aldrich, Oakville, ON, Canada) and 5 mM $CaCl_2$ overnight at room temperature. The next day, EDTA (10 mM) was added to stop the reaction and remaining platelets were isolated by centrifugation at 500 x *g* for 10 min. The supernatant was collected and centrifuged at 17,800 x *g* for 90 min at room temperature. Pelleted PMPs were then resuspended in phosphate-buffered solution (PBS, Sigma-Aldrich).

PMP quantification were performed by platelet fluorescence labeling with either 100 nM MTDR (mitochondria staining) with 2 µM PKH67 (Sigma-Aldrich) (cell membrane staining), or anti-CD41-FITC (BioLegend) (membrane staining), followed by an incubation for 15 min at 37°C. The labeling process was stopped by adding 10 mM EDTA and subsequent centrifugation at 1,300 x *g* for 10 min. The pellet, containing labelled PMPs, was resuspended in Tyrode buffer and characterized by flow cytometry (Attune NxT Flow Cytometer, ThermoFisher Scientific) using the 644 nm excitation (EX) and 665 nm emission (EM) for MTDR and 490/502 nm for PKH67. All solutions were filtered with a 0.2 µm filter before use. All experiments were performed with freshly isolated PMPs and were never frozen to ensure the functional integrity of mitochondria, unless otherwise indicated.

Mitochondrial isolation and transfections

Mitochondrial isolation was performed using a PIERCE Mitochondria Isolation Kit (ThermoFisher Scientific) according to the manufacturer's instructions. A total of 2×10^7 cells were pelleted by centrifuging at 850 × *g* for 2 min and subsequently treated with 800 µL of Mitochondria Isolation Reagent A, vortexed and kept for 2 min on ice. The samples were then mixed with 10 µL of Mitochondria Isolation Reagent B and chilled for 5 min. At the end of incubation, cells received 800 µL of Mitochondria Isolation Reagent C and centrifuged at 700 × *g* for 10 min at 4°C. The supernatant was then collected and centrifuged at 12,000 × *g* for 15 min at 4°C. The obtained pellet was mixed with 500 µL of Mitochondria Isolation Reagent C and centrifuged again at 12,000 × *g* for 5 min. The purified mitochondria were kept on ice before downstream handling.

Upon isolation, mitochondria were labeled with MTDR and quantified using flow cytometry. Purified mitochondria were then mixed with PBS and co-cultured with cells labeled with DAPI and MitoTracker™ Green FM (MTG, ThermoFisher Scientific) at 10 mitochondria per cell (10:1), and 100 mitochondria per cell (100:1) ratios as previously instructed (48, 49). Following a 24- and 48-hour incubation, cell media was replaced with fresh RPMI-1640 supplemented with 10% FBS. Cells were monitored using an Olympus FV1000 confocal fluorescence microscope at 600x magnification (UPLAN 60x oil, 1.35NA, Olympus) with appropriate excitation laser and filters. Confocal microscopy fluorescence was then confirmed by flow cytometry where gating events were based on CD19 expression and MTDR-labeled mitochondria internalization.

Cell proliferation assays

Cell viability was measured by the Cell Titer Blue assay (Promega, Madison, WI, USA) based on the manufacturer's guidelines. Briefly, cells were seeded in a 96-wells plate at a density of 5 x 10^3 cells/well and treated with PMPs (10 PMP/cell) for the indicated time points. Thereafter, 20 µL of Cell Titer Blue substrate was added to each well and incubation under standard cell culture conditions for 1 hour. The plate was read with a Synergy H1 Hybrid Multi-Mode Microplate Reader (Agilent, Santa Clara, CA, USA) at Ex/Em: 560/590 nm *via* Gen5 data analysis software (Version 2.01).

Cell-cycle analysis

Cell-cycle progression was evaluated with a propidium iodide (PI) solution (MilliporeSigma, Burlington, Massachusetts, USA). Briefly, 5 x 10^6 cells were collected by centrifugation at 300 x *g* for 5 min, washed in 1 mL PBS buffer containing 2% FBS, and resuspended in 5 mL chilled 70% ethanol dropwise and kept at 4° C. After a 24-hour incubation, fixed cells were centrifuged at 850 x *g* for 10 min, PBS-washed, and resuspended in a staining mixture of 1 mL PI staining solution + 50 µL RNase A (New England Biolabs, Whitby, Ontario, Canada) at 4°C overnight. Samples were then analyzed by flow cytometry at Ex/Em: 536/617 nm using the FlowJo software (Version 10.7, Tree Star, Inc., Ashland, OR., USA).

Apoptosis assays

Apoptosis was measured using the FITC Annexin-V Apoptosis Detection Kit with PI (BioLegend). In accordance with the manufacturer's protocol, 100 µL of PBS-washed cell samples were diluted in Annexin-V Binding Buffer at a final concentration of 1×10^7 cells/mL and subsequently treated with 5 µL of FITC Annexin-V + 10 µL of PI solution for 15 min at room temperature in the dark. After incubation, 400 µL of Annexin-V Binding Buffer was added to each sample and then analyzed by flow cytometry.

Oxygen consumption rate analysis

Cellular oxygen consumption was measured using high-resolution respirometry (Oxygraph-2k, Oroboros Instruments, Innsbruck, Austria) as previously described (50). Briefly, oxygen calibration was performed at 37°C with a continuous stirring speed of 750 rpm prior to measurements of mitochondrial OCR using 2.5 x 10^6 cells mixed with 2 mL of complete media. Evaluation of physiological ROUTINE respiration was determined as the basal state of cellular oxygen consumption (i.e., with endogenous substrates). The non-phosphorylating resting state (LEAK respiration) was obtained after injection of oligomycin (Omy; 2.5 µM) to inhibit ATP synthase. The uncoupled respiratory capacity (electron transport system capacity; ETS) was determined as the maximal capacity of the mitochondrial ETS and was measured by adding sequential injections of carbonyl cyanide m-chlorophenyl hydrazone (CCCP; 0.5 µM steps) until no further increase in OCR was detected. Residual oxygen consumption (ROX) was subsequently obtained with injections of rotenone (ROT; 0.5 µM) to inhibit complex I and antimycin A (AmA; 2.5 µM) to inhibit complex III

(50, 51). All inhibitors were purchased from Sigma-Aldrich. OCRs were corrected with ROX values and analyzed using DatLab software 7.2 (Oroboros Instruments).

ATP analysis

Cellular ATP levels were determined by an ATP determination kit (ThermoFisher Scientific) according to manufacturer's instructions. Briefly, 1 x 10^4 cells were seeded in 96-well plates with fresh media supplemented with 10% FBS for 1 hour. For glycolytic ATP, cells were treated for 15 min at 37°C with ROT (0.5 µM) and AmA (2.5 µM) to inhibit mitochondrial complexes I and III, respectively. Content of the wells was then collected by centrifugation at 500 x *g* for 5 min at 4°C, PBS-washed, and centrifuged again. Cells were lysed in 1% Triton for 10 min at room temperature and centrifuged for 5 min at 500 x *g*. Then, 10 µL of each cell lysate were transferred to another 96-well plate and diluted with 90 µL of the kit's Luciferine-Luciferase reaction reagent loaded withing the injector of a Synergy H1 Hybrid Multi-Mode Microplate Reader (Agilent). Luminescence was obtained with 1 sec integration times and analyzed with the Gen5 data analysis software (Agilent).

ROS assessment

The CellROX® Green Flow Cytometry Assay Kit (ThermoFisher Scientific) and the MitoSOX™ Red mitochondrial superoxide indicator (ThermoFisher Scientific) were used for intracellular ROS and mitochondrial superoxide determination, respectively. To this point, 5 x 10^5 cells/well were added to 24-well plates and treated with PMPs as described previously. N-acetylcysteine (NAC) and Tert-butyl hydroperoxide (TBHP) were used as negative and positive controls, respectively. Following co-culturing conditions, cells were PBS-washed three times and kept in 1 mL of media containing one of the following ROS inducers: *i*) 6 µM AmA + 5 µM ROT; *ii*) phorbol 12-myristate 13-acetate (PMA, 80 ng) for 15 min; or *iii*) mixture of AmA + ROT + PMA for 30 min. Then, each well received 1 µM/mL CellROX green reagent for 45 min along with 5 µM SYTOX Red Dead Cell Stain (1µl/mL) for 15 min. The samples were then analyzed by flow cytometry at Ex/Em: 508/525 nm (CellROX green) and 640/658 nm (SYTOX Red Dead Cell Stain). As for the evaluation of mitochondrial superoxide, 1 x 10^5 cells/mL from each experimental group were mixed with 5 µM MitoSOX™ reagent working solution and kept from the light for 10 min at 37°C. The samples were then analyzed by flow cytometry at Ex/Em: 510/580 nm.

Real-time PCR

Total RNA was extracted from the cell samples using TRIzol® reagent (ThermoFisher Scientific) and treated with DNase-I for 1 hour (Sigma-Aldrich). The integrity of RNA samples was estimated using a Nanodrop ND-1000 spectrophotometer (Nanodrop Technologies Wilmington, DE, USA). First-strand cDNA was synthesized with the SuperScript III Reverse Transcriptase (ThermoFisher Scientific) based on the manufacturer's recommendations.

Real-time PCR analysis of target genes was carried out on a CFX Connect™ Real-Time System (Bio-Rad Laboratories, Hercules, CA, USA) with the PerfeCta SYBR Green Supermix kit (Quanta Biosciences, Beverly, CA, USA). Reaction mixtures were incubated at 95°C for 5 min, followed by 39 cycles consisting of 94°C for 15 sec, 52°C for 30 sec, and 72°C for 30 sec. Amplifications were analyzed with the Bio-Rad CFX Maestro software (Bio-Rad Laboratories) and normalized to human 18S rRNA using the $2^{-\Delta\Delta CT}$ formula (52). Primers are shown in Table 1.

Evaluation of mitochondrial DNA copy number

Mitochondrial DNA (mtDNA) copy number per diploid nuclear genome was determined by relative quantitative PCR (qPCR) as previously described (53). Total DNA from 5 x 10^6 cells was extracted from cells using the gMAX DNA Mini Kit (IBI Scientific, Peosta, IA, USA) following manufacturer's instruction. DNA was evaluated for the expression levels of mt-tRNA (Leu) and normalized to 18S rRNA using the $2^{-\Delta\Delta CT}$ formula, where $\Delta Ct = (Ct_{nucDNA} - Ct_{mtDNA})$ (52). Data was obtained using qPCR on a CFX Connect Real-Time PCR instrument (Bio-Rad) using the PerfeCTa® SYBR® Green SuperMix (Quantabio, Beverly, MA, USA) following the protocol: 95°C for 5 min along with 94°C for 15 sec, 52°C for 30 sec, and 72°C for 30 sec (x 39 cycles). Primer sequences used for mt-tRNA Leu analysis are presented in Table 1.

Cell migration and invasion assays

To investigate the mobility and invasion of CLL cells, a total of 5 × 10^5 cells/group was FBS-starved for 24 hours before the assay, mixed with 100 µL of media containing 2% FBS on the next day, and added to the insert chambers of a 24-well ThinCerts cell culture plate (8.0 µm pore size, ThermoFisher Scientific). For the cell invasion assay, a layer of Matrigel® (0.5 mg/mL, Corning, Manassas, VA, USA) was added into the top transwell insert compartment to mimic the extracellular matrix. The lower plate wells were then filled with 750 µL of media containing 10% FBS. Following a 24-hour incubation at 37°C, non-migrating/non-invasive cells were removed and migrated/invaded CLLs were collected, stained with CD41 antibody for 15 min at 37°C, PBS washed and read with the flow cytometer.

Bioinformatics analysis

Cytoscape version 3.8.1 (54) was used for network illustration. The interaction between genes was predicted by the plugin BisoGenet (55). It works by integrating the gene expression data

TABLE 1 Primer sequences.

Gene	Forward (5′→3′)	Reverse (5′→3′)
HIF1-A	CTCTGATCATCTGACCAAAACTCA	CAACCCAGACATATCCACCTC
ACSL1	GTGAAAGCAACAGAGAATACAGTC	TCCATGACACAGCATTACACA
ACSL3	ATCTGTTTCTGCTGTCCTGTT	AACTAATGGTGCTCCCACTC
ACSL4	TCATGTGCTAGAACTGACAGC	GTACAGTCTCCTTTGCTTCCTT
ACACA	CTGCCCACATCTCATCCAAA	GTACATCGCTGACACTAGCTAC
ACLY	AGGACAGGAGCTCATCTACG	GTCACCATCAGACACATCTCA
ASPH	CATCTGTAGCTGTCGTTTGGT	CCACATCAAAATCTCCATCACC
FASN	TTTGATGCCTCCTTCTTCGG	CGGAGTGAATCTGGGTTGATG
FH	AGGTCTGGGAGAATTGATCTTG	TCCGACAGTGACAGCAAC
FTO	TCTTGACTGCCATCCTTGC	CCGACATTCTGGCTTCTGAT
IDH	ACTATGATGGTGACGTGCAG	CTGCTTCTACTGTCTTGCCA
MCL1	CATTAGCAGAAAGTATCACAGACG	ACATTCCTGATGCCACCTT
MKI67	CGCCTGGTTACTATCAAAAGGA	GAAGCTGGATACGGATGTCA
MLYC	CTGCTGCGATCTTTTATTCCATC	CCAGGTATAGGTGACAGACTTG
PDP1	GGAAGAATCGTTTGGTCTCCT	CCATAGATCCTGCTCAGTTCAC
PRKAA1	AAGATCGGCCACTACATTCTG	ACAGCTACTTTATGCCCAGTC
SDHB	CAAGATTAAGAATGAAGTTGACTCTACT	AGAGTGTTGCCTCCATTGATG
TFAM	GCGCTCCCCCTTCAGTTTTG	GTTTTTGCATCTGGGTTCTGAGC
NRF1	GATGCTTCAGAATTGCCAACC	GTCATCTCACCTCCCTGTAAC
18S rRNA	GTAACCCGTTGAACCCCATT	GTCATCTCACCTCCCTGTAAC
mt-tRNA Leu	CACCCAAGAACAGGGTTTGT	TGGCCATGGGTATGTTGTTA

with protein-protein interaction (PPI) data to create a comprehensive view of the interactions between genes and proteins in a given biological system using several different layout algorithms including force-directed, hierarchical, and circular layouts. CentiScaPe (Version 2.2) was applied for network topology. The list of genes involved in cancer metabolism was achieved from the DisGeNET tool (Version 7.0), a Bioinformatics tool for integrating and analyzing disorder-related genes in humans (56). DisGeNET uses databases like Comparative Toxicogenomics Database (CTD) (57), Genetic Association Database (GAD) (58), Mouse Genome Database (MGD) (59), and Online Mendelian Inheritance in Man (OMIM) (60) to identify human disease-related genes; and subsequently sorted them based on the number of sources, type of organism, and supported publications in the literature.

Expression analysis of target genes in human CLL samples was carried out using the public data sets GSE58211 (N = 287) and GSE40571 (N = 155) available on NCBI Gene Expression Omnibus (GEO, http://www.ncbi.nlm.nih.gov/geo/, accessed December 2021). Robust multi-array average (RMA) was used to remove the local biases and normalize the intensity expression of raw microarray samples to achieve the gene expression values. Hclust R-function performed hierarchical cluster analysis in R statistical environment to sort the normalized data. Identification of differentially expressed genes (DEGs) in sample files was carried out by linear models for microarray data (LIMMA) package. Annotation of genes was performed through the EnrichR server (http://amp.pharm.mssm.edu/EnrichR, accessed January 2022). The values were reported as significant if $p < 0.05$.

Statistical analysis

Statistical analyses were performed with the SPSS software (Version 26, IBM Corporation). The normalization and homogeneity of variances of obtained data were done with the Shapiro-Wilk and Levene's tests, respectively. Pairwise comparisons were made using an unpaired two-tailed Student t test. One/two-way analysis of variance (ANOVA) and Tukey's multiple comparison tests were applied to find the statistically significant differences between multiple experimental groups as appropriate. The Pearson chi-square test was used to evaluate the distribution between categorical variables. The data are presented as the mean ± SEM (Standard Error of Mean) and deemed significant if $p < 0.05$.

10.3389/fimmu.2023.1207631

Results

Platelet-derived microparticles interact with CLL cells

We and others have previously established PMP interaction and internalization into various types of recipient cancer cells (25, 61). To evaluate the potential PMP-mediated phenotypic regulation of leukemic cells, we first set out to validate the interaction of PMPs with CLL cell models using fluorescence-based approaches. Human leukemic cell lines (CII and MEC-1) were co-incubated with PMPs labeled with MitoTracker Deep Red (MTDR) at a ratio of 1:10 and 1:100 (cell:PMP) for 24 hours and examined for recipient cell acquired fluorescence transferred from labeled PMPs. Flow cytometry analysis demonstrated that both CLL cell lines acquired MTDR fluorescence indicating that CII and MEC-1 models acquire PMP-derived mitochondria (Figure 1A). Cell fluorescence from MTDR-labeled PMPs increased with cell/PMP ratios where nearly 100% of cells were positive for PMP-derived mitochondria at a 1:100 (cell/PMP) ratio after only 24 hours.

To further distinguish PMP internalization from outer cell surface interactions with target cells, we conducted fluorescence microcopy to depict intracellular compartmentalization of PMP-derived fluorescence. To do so, CII and MEC-1 cells were first

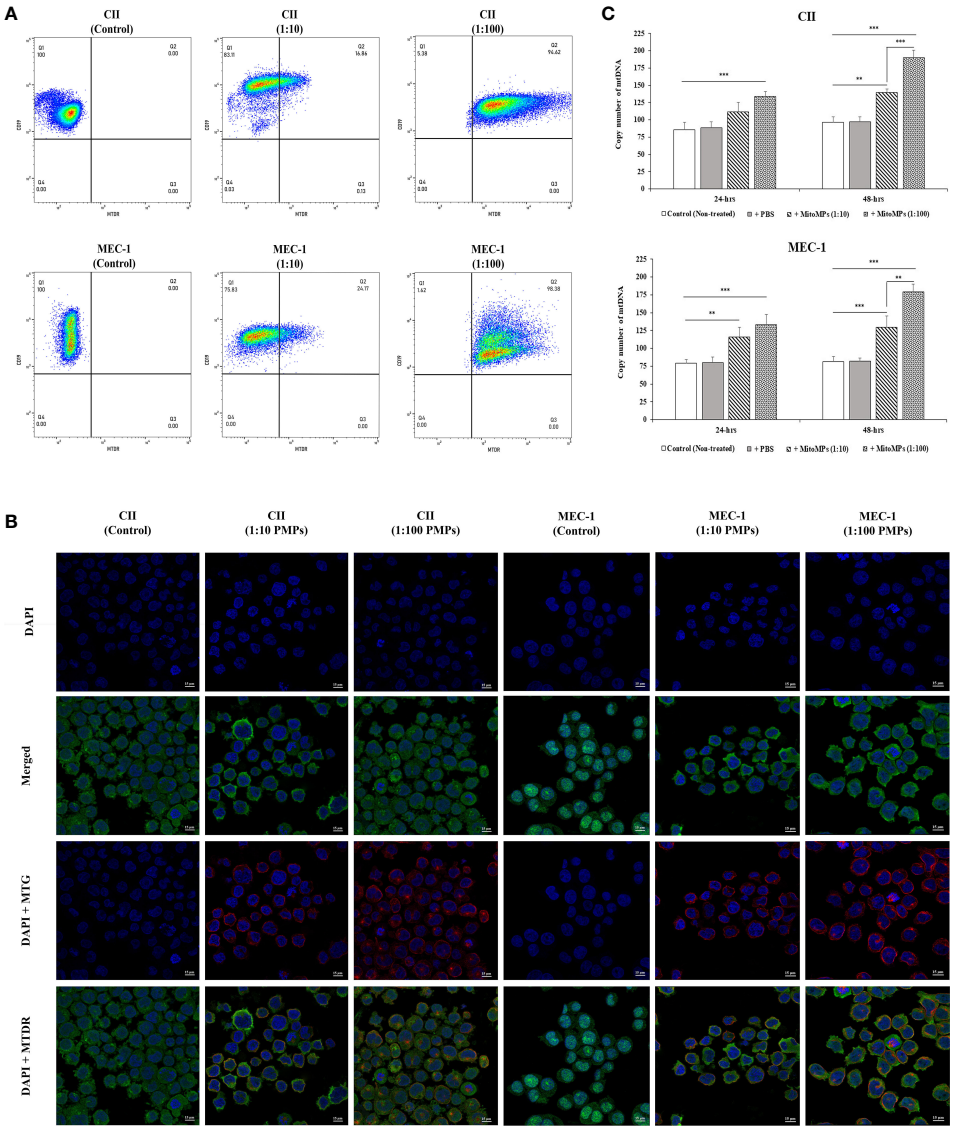

FIGURE 1
Interaction analysis of platelet-derived microparticles and CLL cells. **(A)** Flow cytometry was conducted for the characterization of CLL cell lines labeled with anti-human CD19 antibody either untreated (control) or co-incubated with platelet-derived microparticles (PMPs) labeled with MitoTracker Deep Red (MTDR). Co-incubations of CII (upper panels) or MEC-1 cells (lower panels) with PMPs were performed at 1:10 and 1:100 (cell/PMP) ratios for 48 hours. **(B)** CLL co-incubations (48 hours) with PMPs (1:10 and 1:100) were also photographed by fluorescence microscopy. CLL cell lines were labeled with DAPI and MitoTracker™ Green FM (MTG), whereas PMPs were labeled with MTDR. **(C)** Relative mitochondrial DNA copy number was obtained from cell/PMP co-cultures for 24 and 48 hours using Real-time PCR on leucine tRNA (mtDNA-tRNA-Leu) normalized with nuclear DNA copy number. Each value is the mean ± SEM of six separate experiments. The asterisk (*) indicates significant differences where $^{**}p < 0.01$, and $^{***}p < 0.001$.

stained with MitoTracker™ Green FM (MTG) and then co-incubated with MTDR-labeled PMPs at a ratio of 1:10 and 1:100 (cell: PMP) for 24 hours. Fluorescence microscopy confirmed that exogenous MTDR-labeled mitochondria provided by PMPs was transferred to CII and MEC-1 intracellular compartments. Interestingly, exogenous MTDR-labeled mitochondria also co-localized with the sub-compartmentalized region of native MTG-labeled mitochondria (Figure 1B).

To further validate horizontal transfer of platelet-derived mitochondria *via* PMPs, we performed qPCR analysis on mt-tRNA (Leu) as a mitochondrial DNA (mtDNA) or copy number indicator in CLL models co-incubated with PMPs. We observed that mtDNA was increased 1.39- and 1.91-fold in CII cells treated with 1:10 and 1:100 (cell/PMP) ratios for 48 hours, respectively (Figure 1C). Similar results were obtained for MEC-1 cells, which exhibited a 1.3- and 1.8-fold increase of mtDNA following treatments of PMPs with 1:10 and 1:100 ratios (48 h), respectively in comparison to control cells. Altogether, these results demonstrate that PMP cargo, notably mitochondria, are efficiently transferred into CLL cells, which result in the accumulation of mitochondrial content in recipient cells in a relatively short period of time (within 24 hours).

PMPs impact CLL cell viability

Given the prominent role of mitochondria in cancer cell viability and growth, we next examined the phenotypic impact of PMP internalization on recipient CLL cancer processes. Cell viability was therefore assessed in CLL co-cultures with varying ratios of PMPs over time (24 and 48 hours) using a colorimetric cell-based assay. Accordingly, PMP co-culture with CII or MEC-1 cells induced significant cell growth, which was more pronounced after 48 hours. For example, CII and MEC-1 cells treated with PMPs (1:100) increased viability 1.9- and 1.7-fold, respectively, when compared to control cells (Figure 2A). Interestingly, raising the ratio of PMPs in CLL co-cultures (from 1:10 to 1:100) did not significantly enhance cell viability beyond the impact observed at a 1:10 ratio at 48 hours. These observations not only suggest that PMPs play a role in leukemia proliferation, but also show that a relatively small amount of PMP interactions is sufficient to induce significant CLL cell growth.

It is well established that PMP cargo encompasses a variety of bioactive content (beyond mitochondria) capable of provoking phenotypic changes in recipient target cells (22, 23). To discern the specific role of PMP mitochondria (from other bioactive cargo) in PMP-induced CLL cell growth (above), we treated CLL models with purified exogenous mitochondria organelles (Figure 2A). Technically, we made use of a platelet precursor cell line (i.e., Set2 megakaryocytes) to isolate and purify mitochondria organelles intended for CLL treatments. Here, CII and MEC-1 cells were co-cultured with different ratios (1:10 and 1:100) of purified Set2-derived mitochondria over time (24 and 48 hours) and confirmed previous observations where CLL cell viability was induced with increasing amounts of purified mitochondria. Specifically, treatments of CII and MEC-1 cells with Set2-derived mitochondria (1:100 ratio) increased viability (1.6- and 1.6-fold, respectively) after 48 hours (Figure 2B). Control experiments to validate the intracellular compartmentalization of Set2-derived mitochondria and levels of mtDNA in CLL recipient cells were also performed following mitochondria treatment using cell cytometry, fluorescence microscopy, and qPCR (Supplementary Figures 1A-C, respectively). Morphological analysis of CLL co-cultures (1:100 ratio) at various time points was also conducted by light microscopy (Figure 2C). Images of co-cultured cells show typical cell agglomeration, which is characteristic of cell growth.

Meanwhile, to better relate the direct role of mitochondria enhancement on cells proliferation, we also examined the viability of CLL cells in the presence of PMPs containing the damaged/disrupted mitochondria (Supplementary Figure 2). We used two previously proven approaches where the first one consisted of freeze-thawing the PMPs prior to the co-incubation with CLLs (62). Since mitochondria are sensitive to temperature changes, cycles of freezing and thawing causes damage to their function thus impairing the motility, plasma membrane integrity and mitochondria function of boar spermatozoa through generating excessive ROS (62). The second strategy was treating the PMPs with ROT/AmA compounds, as the mitochondrial respiratory chain complex I and III inhibitors, before co-incubation with the CLL cell groups (63, 64). Upon co-incubation of leukemic cells with frozen-thawed PMPs, we observed no significant impact on cell viability in comparison to non-treated control cells (Supplementary Figure 2A). Similar observations were noted PMPs treated with ROT/AmA prior to co-incubation with CLL cells (Supplementary Figure 2B). These results showed that the proliferative impact of PMPs on cancer cells markedly depends on the health status of PMPs mitochondria. Altogether, these findings support an important contribution for PMPs in CLL proliferation. Our results also suggest that the mitochondrial component of PMP cargo is primarily responsible for accelerated growth rates of CLL cells following PMP internalization.

PMPs impact leukemic cell bioenergetic states

Mitochondrial transfer (or "mito-transfer") is a well described phenomenon amongst cell types and has been shown to modulate recipient cell metabolic function (65–67). Since metabolic plasticity represents a hallmark of cancer progression, we investigated the impact of PMP internalization, or Set2-purified mitochondria, on several mitochondrial functions of our human leukemic cell models. First, co-cultures consisting of CLL lines (CII and MEC-1) with either PMPs or Set2-isolated mitochondria, were examined for cellular respiration through OCR using a high-resolution respirometer. We found that CLL co-cultures with PMPs (1:10) significantly increased ROUTINE (basal) respiration in both CII and MEC-1 cells (2.9- and 4.4-fold, respectively) after 48 hours when compared to controls samples (Figure 3A). These levels were even more pronounced (~2.7-fold higher for both cell lines) in 1:100 culture ratios (Figure 3A). Interestingly, co-cultures with Set2-isolated mitochondria yielded identical increases in cell

10.3389/fimmu.2023.1207631

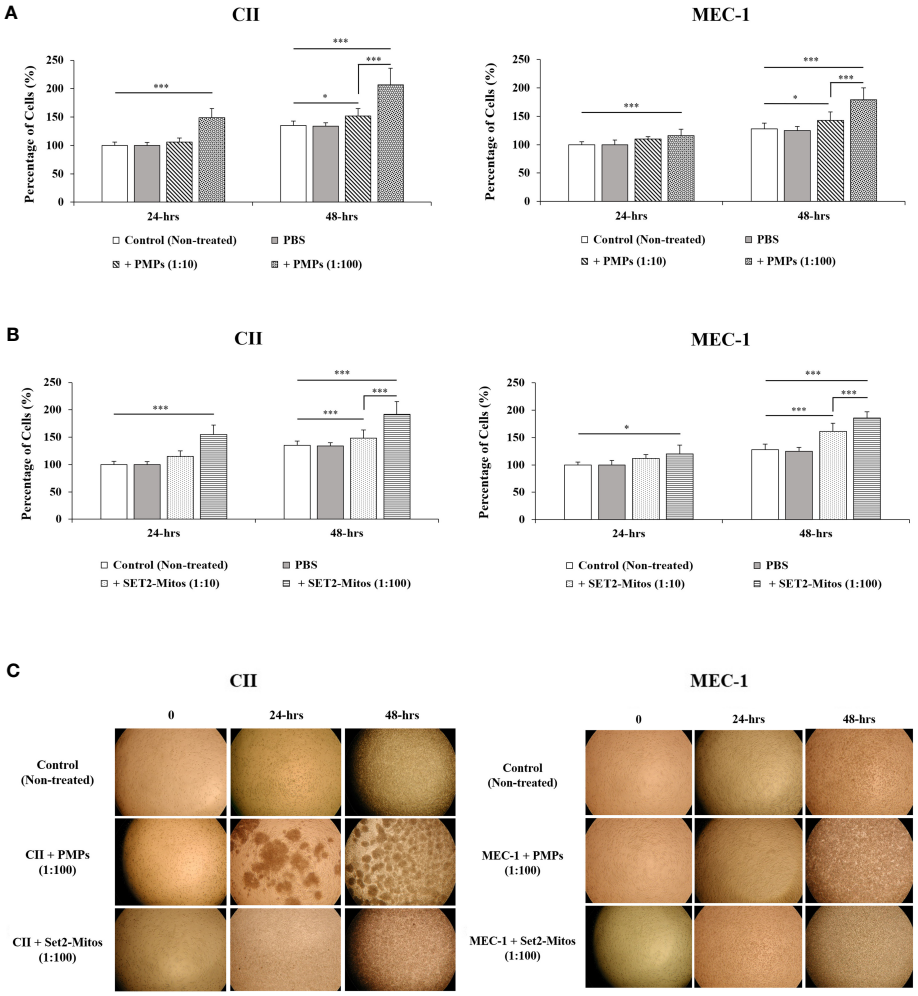

FIGURE 2
Impact of mitochondria acquisition on CLL viability. CLL cell lines were evaluated for cell viability at varying co-culture ratios (1:10 and 1:100) and incubation time (24 and 48 hours) with either **(A)** PMPs or **(B)** purified mitochondria isolated from the Set2 megakaryocytic cell line. Viability was established using a cell-based colorimetric assay (Cell Titer-Blue, Promega) combined a multi-well plate spectral analysis from a Synergy H1 Hybrid Multi-Mode Microplate Reader (Ex/Em: 560/590 nm). Each value is the mean ± SEM of six separate experiments. The asterisk (*) indicates significantly different (*$p < 0.05$, ***$p < 0.001$). **(C)** Light microscopy (40X) of CLLs co-incubations with PMPs or Set2-derived mitochondria was also performed for morphological examination.

ROUTINE respiration in comparison to PMP-treated cells (Figure 3A). These results suggest that PMP-induced basal respiration state in CLL cells is likely dependent on the transfer and function of PMP mitochondria.

We also observed that levels of non-phosphorylating resting LEAK state, after blocking the ATP synthesis with oligomycin, were also increased in PMP-treated CLL cultures, which were further accentuated with 1:100 ratios for both CII and MEC-1 cells (15.1- and 14.2-fold, respectively; Figure 3A). These increments were reciprocated in cultures treated with Set2-purified mitochondria under the same conditions (15.9- and 17.2-fold, respectively; Figure 3A). Finally, uncoupled respiratory capacity determined through the maximal capacity of the mitochondrial electron transport system (ETS), was also increased in PMP co-cultures, which was further accentuated in 1:100 culture ratios of CII and MEC-1 cells (7- and 13.4-fold, respectively) over control samples (Figure 3A). Likewise, Set2-isolated mitochondria co-cultures mimicked these increases in CII and MEC-1 cells (7.5- and 13.8-fold, respectively) in comparison to their related-control groups (Figure 3A).

To further elucidate the impact of PMPs on CLL mitochondrial-dependent functions, we examined ATP levels using bioluminescence assays. Total ATP levels in CII cells were increased 1.7- and 3.3-fold when cultured with PMPs (1:10 and 1:100, respectively) (Figure 3B). Similar ATP level increases in MEC-1 cells were also observed (2.2- and 4.1-fold) following 1:10 and 1:100 culturing ratios with PMPs, respectively (Figure 3B). Further investigation into the mechanistic source responsible for induced ATP levels, revealed that the OXPHOS pathway was mainly responsible (Figure 3B). In control experiments using Set2-derived mitochondria treatments, we observed comparable induced ATP levels suggesting that PMP-induced ATP levels in CLL cells are likely dependent on the transfer and function of PMP mitochondria.

10.3389/fimmu.2023.1207631

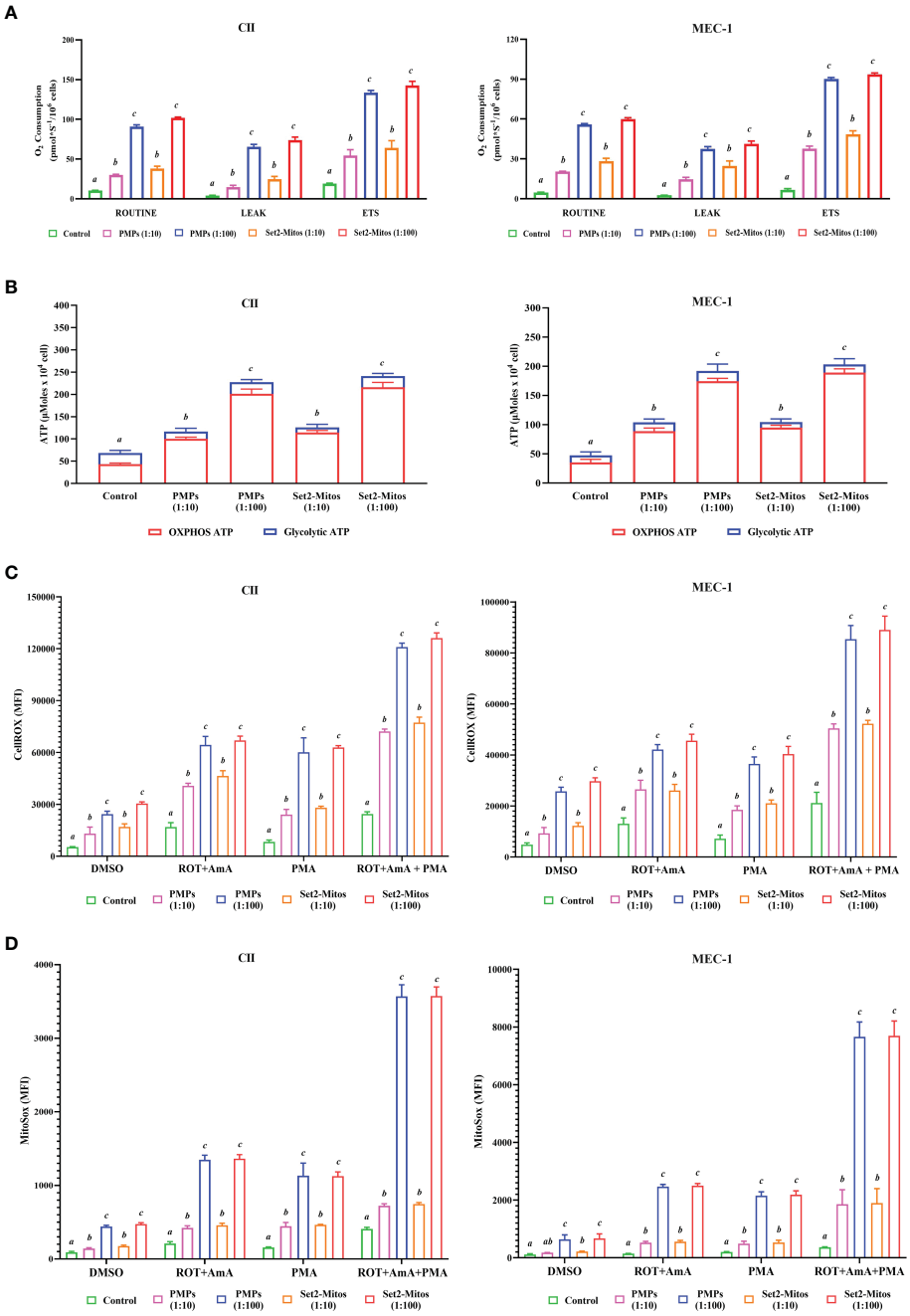

FIGURE 3
Impact of PMPs on CLL metabolic functions. CLL cell lines (CII and MEC-1) were evaluated for metabolic functions at varying co-culture ratios (1:10 and 1:100) and incubation periods (24 and 48 hours) with either PMPs or purified mitochondria isolated from the Set2 megakaryocytic cell line. **(A)** Oxygen consumption rate (OCR) was determined using an Oroboros-O2k for: ROUTINE respiration as the basal state; the non-phosphorylating resting state (LEAK respiration); and the electron transport system (ETS) capacity. **(B)** Total ATP and glycolytic ATP levels were evaluated using a firefly luciferase-based assay. Relative ATP concentrations related to specific pathways (oxidative phosphorylation/OXPHOS versus glycolysis) were determined by cell treatments to inhibit mitochondrial complexes I and III using Rotenone (ROT) and Antimycin A (AmA), respectively. **(C, D)** Cells were treated with AmA, ROT, and phorbol 12-myristate 13-acetate (PMA) as ROS inducers. Thereafter, samples were mixed with **(C)** CellROX green reagent and SYTOX Red Dead Cell Stain prior analysis by flow cytometry at Ex/Em: 508/525 nm (CellROX green) and 640/658 nm (SYTOX Red Dead Cell Stain) to determine intracellular total ROS content; or with **(D)** MitoSOX^{TM} reagent prior analysis by flow cytometry at Ex/Em: 510/580 nm to determine mitochondrial superoxide content. N-acetylcysteine (NAC) and Tert-butyl hydroperoxide (TBHP) were used as negative and positive controls, respectively. Results are expressed as the mean ± SEM of six biological experiments. One-way ANOVA followed by Tukey's multiple comparisons test show significant differences in the values presenting different superscript letters ($p < 0.05$).

Next, we examined intracellular ROS and mitochondrial superoxide levels in PMP-recipient leukemic cells treated with either rotenone (ROT, inhibitor of complex I), antimycin A (AmA, inhibitor of complex III), or phorbol 12-myristate 13-acetate (PMA, ROS inducer). The data depicted a significant increase in total ROS in CII cells co-cultured with PMPs (1:10 and 1:100) of 2.0- and 4.6-fold, respectively in comparison to total intracellular ROS levels from control cells alone (Figure 3C). To further discern the contribution of mitochondria-derived ROS production, mitochondrial superoxide was analyzed and show 1.6- and 4.8-fold increases in CII cells co-cultured with PMPs (1:10 and 1:100, respectively) when compared to their respective controls (Figure 3D). Similarity, MEC-1 treated with PMPs (1:10 and 1:100) induced 1.7- and 5.3-fold increments respectively, of total intracellular ROS (Figure 3C), where mitochondrial superoxide was increased 1.6- and 5.7-fold respectively (Figure 3D).

Given that Complex I is responsible for the transfer of electrons from NADH to ubiquinone (coenzyme Q) (68, 69) and that Complex III is responsible for the transfer of electrons from ubiquinone to cytochrome C (68), the combinatory use of inhibitors ROT and AmA is generally used to increase ROS levels (69). We therefore treated our cells with a ROT+AmA combination, which raised intracellular and mitochondrial superoxide levels by 3.8- and 6.4-fold in CII cells (1:100), respectively (Figures 3C, D). In comparison, MEC-1 intracellular ROS and mitochondrial superoxide were 3.2- and 17.2-fold higher following PMP treatments (Figure 3C, D). Upon ROS stimulation using PMA treatment (70–72), CII cells co-cultured with PMPs (1:100) enhanced intracellular ROS and mitochondria superoxide levels by 7.2- and 7.5-fold, respectively (Figures 3C, D). Likewise, PMP treated MEC-1 cells induced levels 5.1-fold (intracellular ROS) and 10.7-fold (mitochondrial superoxide), in comparison to non-treated leukemic cells (Figures 3C, D).

The maximum potential of ROS generation between study models was tested with mixtures of ROT+AmA+PMA. Intracellular ROS levels in CII cells treated with PMPs (1:100) increased 4.9-fold, whereas mitochondrial superoxide was raised 8.8-fold in comparison to control samples (Figures 3C, D). On the other hand, MEC-1 cells under these conditions raised intracellular ROS levels 4.0-fold, whereas mitochondrial superoxide increased 21.0-fold when compared to non-treated cells (Figures 3C, D).

Throughout these experiments, we also made used of Set2-derived mitochondria controls in parallel. We found that purified mitochondria treatments induced comparable levels of both intracellular ROS and mitochondrial superoxide as observed in PMP treatments (Figures 3C, D). These observations therefore suggest that total ROS production in CLL cells is likely dependent on the transfer of mitochondrial content and functions provided by PMPs. Overall, our data indicates a statistically significant increase in ROS levels, which may be attributable to either increased ROS production, or decreased antioxidant capacity of CLL cells following PMPs interaction. These results strongly suggest that PMPs enable CLL cells to gain mitochondrial-dependent functions supporting metabolic reprogramming and plasticity, which are essential for cancer malignancy.

CLL disease correlates with heightened core metabolic-related gene expression profiles

Given the benefits from the acquisition of metabolic content and function in cancer cells, we made use of bioinformatics analyses to identify the mechanisms involved in metabolic reprogramming during disease progression and the PMP treatment. Using the BisoGenet tool, a complex network of metabolic-related genes actively involved in CLL development was developed. Network genes were then filtered based on their betweenness centrality and streamed into a smaller network consisting of 160 high-degree nodes (Hubs) where 525 edges were created as potentially key players in cancer metabolism (Supplementary Figure 3). The network was then used to identify the most potential pathways encompassing these genes and highlighted: ChREBP activates metabolic gene expression (R-HSA-163765) and, the Fatty acyl-CoA biosynthesis (R-HSA-75105), as the most impacted signaling cascades in CLLs (Figure 4A). The expression levels of genes associated to these identified pathways were then applied to a cohort of CLL patients (n=442) based on their corresponding Binet staging (i.e., stage A (n)=184, stage B (n)=179, and stage C (n)=79) to define the most significant modulated genes associated with CLL disease progression. The average expression values of the profiled gene lists per patient are provided in Supplementary File S4. Through our analysis of CLL samples, we first identified an expression pattern from 17 metabolic-related genes significantly altered through disease progression (i.e., Binet stages A to C). These genes include: Hypoxia-inducible factor-alpha (HIF-A); ATP citrate lyase (ACLY); Long-chain fatty acyl-CoA ligase (ACSL1, 3 and 4); Pyruvate dehydrogenase (PDH); Fatty acid synthase (FASN); Acetyl-CoA carboxylase (ACACA); Malonyl-CoA decarboxylase (MCD); Isocitrate dehydrogenase (IDH); Fumarate hydratase (FH); Aspartate Beta-Hydroxylase (ASPH); Alpha-ketoglutarate-dependent dioxygenase (FTO); Myeloid cell leukemia-1 (MCL1); Malonyl-CoA Decarboxylase (MLYCD); Pyruvate dehydrogenase phosphatase (PDP1); and, Protein Kinase AMP-Activated Catalytic Subunit Alpha 1 (PRKAA1) (Figure 4B). These genes were then considered as metabolic reprogramming indicators for future experiments. In line with these findings, we also observed that expression levels of Transcription factor A mitochondrial (TFAM) and the Nuclear respiratory factor 1 (NRF1), two prominent factors involved in mitochondrial biogenesis, were concomitantly increased with CLL staging (Figure 4C). These results not only demonstrate that CLL progression directly correlates with rising mitochondrial content in cells; but also, with the levels of metabolic-gene expression.

Using our enrichment analysis, we then categorically sorted our lists of modulated gene expressions, along with their associated pathways, to reveal the most active signaling cascades upon the onset of CLL development (Binet stage A). For example, NF-κB and survival signals (R-HSA-209560); PKMTs methylate histone lysines (R-HSA-3214841); and Interleukin-1 processing (R-HSA-448706) were all highly activated in early stages of CLL disease (Figure 4D).

10.3389/fimmu.2023.1207631

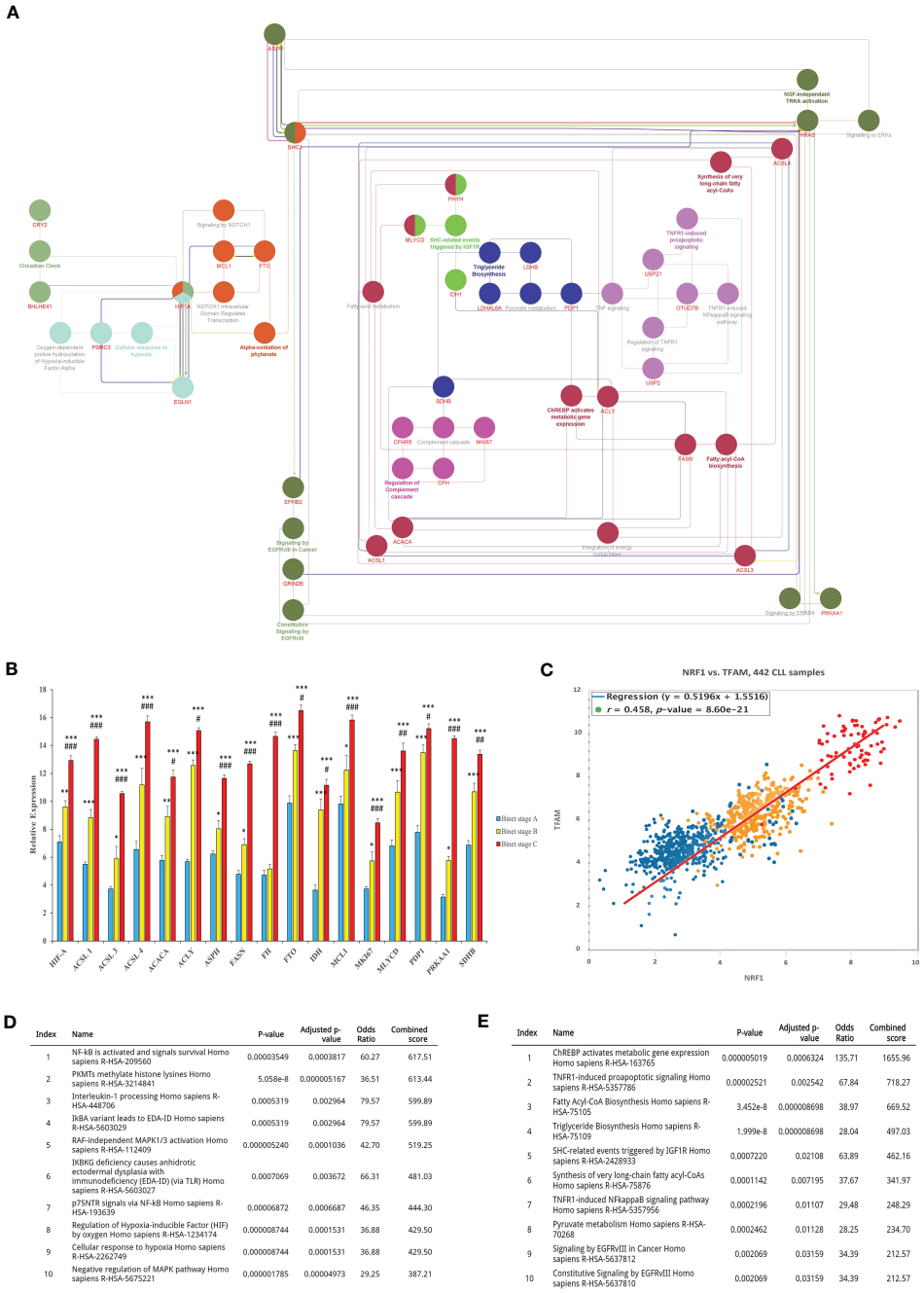

D

Index	Name	P-value	Adjusted p-value	Odds Ratio	Combined score
1	NF-kB is activated and signals survival Homo sapiens R-HSA-209560	0.00003549	0.0003817	60.27	617.51
2	PKMTs methylate histone lysines Homo sapiens R-HSA-3214841	5.058e-8	0.000005167	36.51	613.44
3	Interleukin-1 processing Homo sapiens R-HSA-448706	0.0005319	0.002964	79.57	599.89
4	IkBA variant leads to EDA-ID Homo sapiens R-HSA-5603029	0.0005319	0.002964	79.57	599.89
5	RAF-independent MAPK1/3 activation Homo sapiens R-HSA-112409	0.000005240	0.0001036	42.70	519.25
6	IKBKG deficiency causes anhidrotic ectodermal dysplasia with immunodeficiency (EDA-ID) (via TLR) Homo sapiens R-HSA-5603027	0.0007069	0.003672	66.31	481.03
7	p75NTR signals via NF-kB Homo sapiens R-HSA-193639	0.00006872	0.0006687	46.35	444.30
8	Regulation of Hypoxia-inducible Factor (HIF) by oxygen Homo sapiens R-HSA-1234174	0.000008744	0.0001531	36.88	429.50
9	Cellular response to hypoxia Homo sapiens R-HSA-2262749	0.000008744	0.0001531	36.88	429.50
10	Negative regulation of MAPK pathway Homo sapiens R-HSA-5675221	0.000001785	0.00004973	29.25	387.21

E

Index	Name	P-value	Adjusted p-value	Odds Ratio	Combined score
1	ChREBP activates metabolic gene expression Homo sapiens R-HSA-163765	0.000005019	0.0006324	135.71	1655.96
2	TNFR1-induced proapoptotic signaling Homo sapiens R-HSA-5357786	0.00002521	0.002542	67.84	718.27
3	Fatty Acyl-CoA Biosynthesis Homo sapiens R-HSA-75105	3.452e-8	0.000008698	38.97	669.52
4	Triglyceride Biosynthesis Homo sapiens R-HSA-75109	1.999e-8	0.000008698	28.04	497.03
5	SHC-related events triggered by IGF1R Homo sapiens R-HSA-2428933	0.0007220	0.02108	63.89	462.16
6	Synthesis of very long-chain fatty acyl-CoAs Homo sapiens R-HSA-75876	0.0001142	0.007195	37.67	341.97
7	TNFR1-induced NFkappaB signaling pathway Homo sapiens R-HSA-5357956	0.0002196	0.01107	29.48	248.29
8	Pyruvate metabolism Homo sapiens R-HSA-70268	0.0002462	0.01128	28.25	234.70
9	Signaling by EGFRvIII in Cancer Homo sapiens R-HSA-5637812	0.002069	0.03159	34.39	212.57
10	Constitutive Signaling by EGFRvIII Homo sapiens R-HSA-5637810	0.002069	0.03159	34.39	212.57

FIGURE 4
Bioinformatics identification and analysis of core metabolic-related genes involved in CLL progression. **(A)** Identification of key genes involved in CLL metabolism. The interaction between genes was visualized by the Cytoscape plugins BisoGenet and CentiScaPe, and subsequently annotated using the EnrichR. **(B)** Expression analysis of the most differentially expressed metabolic-related genes (DEGs) between CLL datasets were then calculated and plotted in relative expression. **(C)** Pearson Chi-square test of CLL samples was then analyzed to plot the expression levels of TFAM and NRF1 as mitochondrial biogenesis indicators in relation to Binet stages of clinical samples. **(D)** The most active signaling pathways from patients with early onset of CLL (Binet stage A), or **(E)** advanced disease (CLL Binet stage C) were also identified and listed. Each value is the mean ± SEM of six separate experiments. The asterisk (*) and number sign (#) indicate significantly different from the control group (non-PMP treated), and the 1:10 PMP-treated group, respectively (p <.05).

On the other hand, signaling pathways associated with advanced disease stages (Binet stage C) identified the pathways of ChREBP activates metabolic gene expression (R-HSA-163765), TNFR1-induced proapoptotic signaling (R-HSA-5357786), and Fatty Acyl-CoA Biosynthesis (R-HSA-75105), all which mitochondria plays a central role in advanced CLL disease (Binet stage C) (Figure 4E). These findings indicate that metabolic gene expression supporting metabolic reprogramming are tightly correlated to CLL progression and suggest that these gene profiles are likely impactful regulators of this process.

10.3389/fimmu.2023.1207631

PMPs regulate metabolic reprogramming and protection of CLL cells

Based on our results showing that PMPs enable CLL metabolic reprogramming, we investigated the potential impact of PMPs on metabolic transition as part of CLL development and progression. For this purpose, CLL cells were co-cultured with PMPs (1:100) and tested for changes in metabolic-genes expression (identified in Figure 4) associated with disease progression. These experiments were also combined with treatments of common anti-leukemia drugs (i.e., Cytarabine, Venetoclax, and Plumbagin) as these compounds elicit well-known mitochondrial inhibitory features. First, we established the median lethal dose (LD50) of anti-cancer drugs for both CII and MEC-1 cell lines as follows: ~100 nM and ~150 nM, respectively, for Cytarabine; ~50 nM and ~75 nM, respectively, for Venetoclax; and ~50 nM and ~ 75 nM, respectively, for Plumbagin (Figures 5A, B). The correlation between cell viability and metabolic-reprogramming in PMP-recipient CLL cells was then investigated using RT-qPCR to measure the relative expression levels from our panel of metabolic gene. We observed that PMP treatment of CLL cells induced the expression levels from all metabolic genes associated with advanced disease progression in both CII (Figure 5C) and MEC-1 (Figure 5D) cells with or without anti-cancer drug (LD50) treatments. For example, PMP treatment induced the expression of HIF-1A, which is known to promote the interaction between neoplastic B cells and their microenvironments (73), induces the generation of tumor-associated macrophages (TAM) (74), and participate in drug-resistance (75). HIF-1A expression was increased 4.3-fold in PMP-recipient CII cells compared to non-treated cells alone. However, this difference was increased in the presence of Cytarabine (6.9-fold), Venetoclax (7.4-fold), and Plumbagin (6.7-fold). This data demonstrates that PMPs increase the expression profiles of metabolic genes associated with CLL progression.

We further repeated this assay with CLLs co-incubated with (1:100) isolated Set2-Mitos in order to evaluate the role of mitochondria acquisition in the observed metabolic reprogramming (Supplementary Figure 5). Similar to PMP-recipient cell groups, our observations indicated a statistically significant improvement in metabolic gene expression patterns in response to Set2 mitochondria internalization into the CLL cells. Meanwhile, this expression pattern didn't markedly change in the presence of the determined LD50 concentration of Cytarabine, Venetoclax, and Plumbagin for CII and MEC-1 cells. This data demonstrates that the observed alteration in metabolic gene expression patterns of CLLs co-incubated with PMPs mostly derived from mitochondrial content increment.

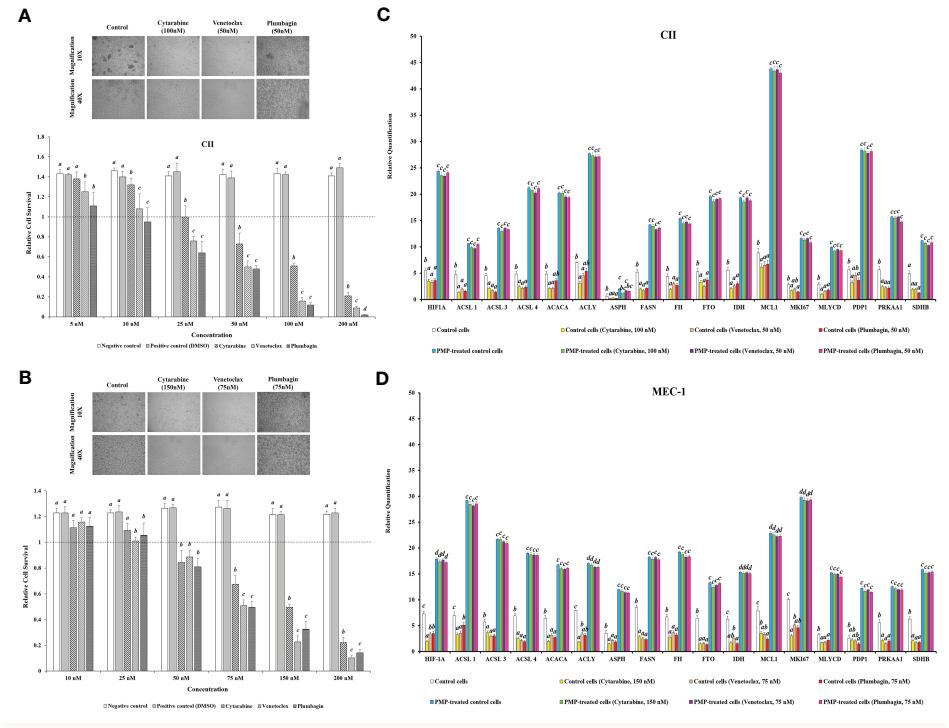

FIGURE 5
Impact of PMPs on CLL chemoresistance and metabolic gene expression. **(A)** CII and **(B)** MEC-1 cell lines were co-incubated with PMPs (1:100, 48 h) and then treated with increasing amounts of either Cytarabine, Venetoclax, and Plumbagin (5-200 nM) for 24 hours to establish the lethal doses for 50% mortality (LD50). Control groups were treated with DMSO as dilution buffer. Light microscopy of cells treated at their respective LD50 are also presented for morphological analysis. **(C, D)** Real-time PCR analysis was performed to evaluate differentially expressed metabolic-related genes (DEGs) in CLL groups in the presence of chemo-drugs where each column represents the PMP-treated/non-treated cell ratio. Control groups were treated with DMSO as dilution buffer. Results are expressed as the mean ± SEM of six biological experiments. One-way ANOVA followed by Tukey's multiple comparisons test show significant differences in the values presenting different superscript letters ($p < 0.05$).

10.3389/fimmu.2023.1207631

PMPs impact CLL cell-cycle progression and apoptosis

Reports have previously characterized CLL cells with substantially greater levels of mitochondrial mass and function when compared to healthy B-cells (11, 15). Given our observations of PMP-induced expression of metabolic genes associated with CLL disease progression, we set out to examine if this differential display in metabolic gene expression translates into altered cancer cell phenotypes associated with CLL progression. We therefore co-cultured CLL cells with PMPs (1:100 for 48 hours) and examined cell viability, growth, and programmed cell death (apoptosis) in response to anti-cancer drug treatments (LD50 for 24 hours) using Annexin-V/PI labeling. The stained cells were then analyzed by flow cytometer and sorted into four distinctive quarter zones (Q) including necrotic cells or Q1 (Anx^-/PI^+), late apoptotic or Q2 (Anx^+/PI^+), early apoptotic cells or Q3 (Anx^+/PI^-), and viable cells or Q4 (Anx^-/PI^-).

As expected, anti-cancer drug treatments induced apoptosis in both CLL models. For example, drug treatments induced early apoptosis (Q3) to 30.3% (Cytarabine), 43.5% (Venetoclax), and 48.2% (Plumbagin) in CII cells (Figure 6A). Meanwhile, drug treatments in MEC-1 cells induced early apoptotic events (Q3) by 41.6% (Cytarabine), 38.9% (Venetoclax), and 41.4% (Plumbagin) under the same conditions (Figure 6B). However, upon co-culturing conditions with PMPs (1:100, 48 hours), cells were completely refractory to drug toxicity. For example, CII cells treated with PMPs underwent early apoptosis (Q3) in only 2.2% (Cytarabine), 5.65% (Venetoclax), and 4.33% (Plumbagin) in comparison to drug-treated control cells (Figure 6A). This represents an inhibition of approximately 93.2% (Cytarabine), 87.1% (Venetoclax), and 91.1% (Plumbagin) in comparison to drug-treated control cells (without PMPs). Similar results were also obtained in MEC-1 co-cultured with PMPs where early apoptosis was inhibited by 97.8% (Cytarabine), 96.8% (Venetoclax), and 89.1% (Plumbagin) in comparison to drug-treated controls (Figure 6B). PMP treatments of CLL cells also noticeably increased the viable (Q4) population by 1.89-fold (Cytarabine), 1.85-fold (Venetoclax), and 1.74-fold (Plumbagin) when compared to the non-PMP-treated control cells (Figure 6A). Likewise, MEC-1 co-cultures with PMPs increased viability by 1.83-fold (Cytarabine), 1.85-fold (Venetoclax), and 1.87-fold (Plumbagin) when compared to drug treatments in cells alone (Figure 6B). These results demonstrate that PMP-treated CLL cells are more resistant to conventional anti-cancer drug toxicity.

To have a better conclusion, this test was also repeated with CLLs co-incubated with (1:100) isolated Set2-Mitos (Supplementary Figure 6). A similar observation has been achieved through flow cytometry assessment of cell proportions in apoptosis when leukemic cells received isolated mitochondria prior to drug treatment. Collectively, this data indicates that mitochondria acquisition in CLL cells has a major impact on cancer cells performance against the therapeutic agents.

To provide insight into the regulation of CLL cycling processes modulated by PMPs, we performed cell-cycle distribution analysis on CLL models treated (or not) with anti-cancer drugs. Our results first show that the basal proportion of the PMP-recipient CLL cells in G2/M (dividing and growing cells) phase was about 1.27-fold in

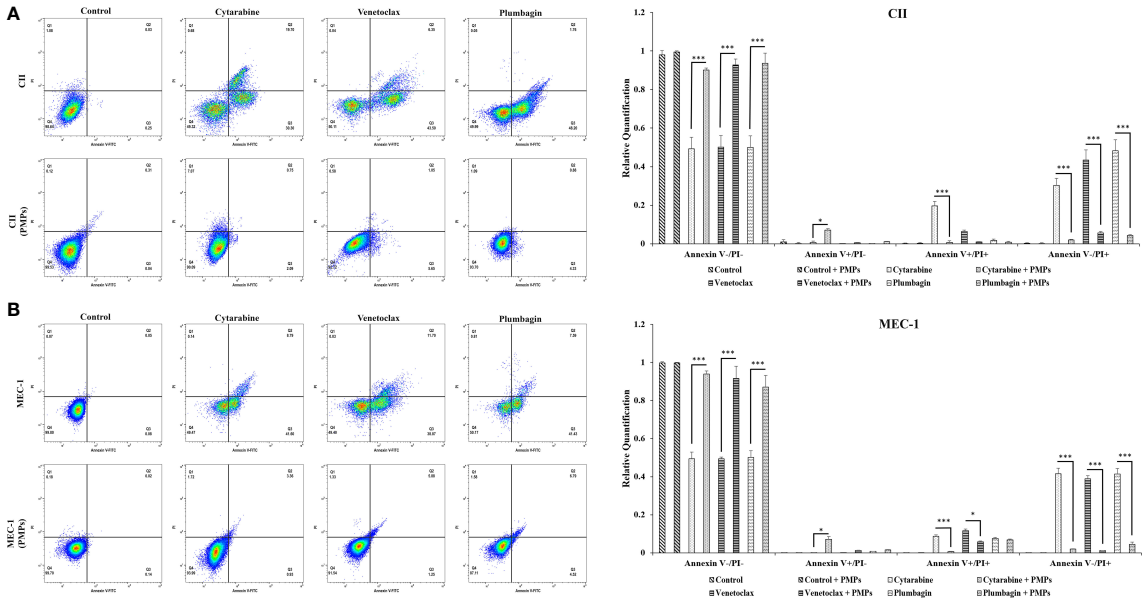

FIGURE 6
Effects of PMPs on CLL survival and apoptosis. CLL cells were co-incubated with PMPs (1:100, 48 h) prior to treatments with the cells' respective LD50 of Cytarabine, Venetoclax, and Plumbagin for 24 hours for the evaluation of drug cytotoxic events. Flow cytometry analysis in **(A)** CII and **(B)** MEC-1 cells stained with Propidium Iodide (PI, X-axis) and Annexin-FITC (X-axis) sorted cell populations according to distinctive quarter zones (Q), including the large nuclear fragments/debris or Q1 (Anx^-/PI^+), necrosis cells or Q2 (Anx^+/PI^+), apoptotic cells or Q3 (Anx^+/PI^-), and the living cells or Q4 (Anx^-/PI^-). Values for each quadrant were then plotted in relation to their respective control groups (DMSO). Each value is the mean ± SEM of six separate experiments. The asterisk (*) indicates significantly different (*$p < 0.05$, ***$p < 0.001$).

CII (Figure 7A) and 1.2-fold higher in MEC-1 (Figure 7B) when compared to non-treated control cells. These observations demonstrate that PMPs promote CLL cell cycling. Cell cycle analysis also confirmed our previous observations where toxic drug treatments of CLL cells led to an accumulation of cells in sub-G1 (<G0/G1), a phase representing cellular debris, late apoptotic, and necrotic cells. However, PMP treatments of CLL cells completely inhibited sub-G1 (<G0/G1) accumulation of both CII (Figure 7A) and MEC-1 (Figure 7B) cell models treated with anti-cancer drugs.

Furthermore, when CLL cells were co-cultured with PMPs prior to anti-cancer drug treatments, cell accumulation in G2/M was increased 10.1-fold (Cytarabine), 7.5-fold (Venetoclax), and 4.0-fold (Plumbagin) for CII cells (Figure 7A). Similar observations were noted in MEC-1 cells (Figure 7B) where cell accumulation in G2/M phase was enhanced 4.3-fold (Cytarabine), 5.4-fold (Venetoclax), and 4.4-fold (Plumbagin) when treated with PMPs). These results demonstrate that PMPs promote CLL growth and provide anticancer drug resistance.

In addition to the latter results, cell cycle analysis of CLLs incubated with mitochondria (1:100) isolated from Set2 cells also showed a statistically decrement in cells number accumulated in >G0/G1 following treatment with the LD50 dose of Cytarabine, Venetoclax, and Plumbagin chemo-drugs (Supplementary Figure 7). The data supports the notion that mitochondria acquisition *via* PMPs in CLL cells lowers sensitivity to standard leukemic treatments.

PMPs promote CLL migration and invasion properties

Given our observations that PMPs induce CLL aggressivity through enhanced growth and drug resistance, we wanted to determine the impact of PMPs on other CLL malignant processes such as migration and invasion properties. First, migration assays were performed and indicated that the mobility of leukemic cells treated with PMPs (1:100, 48 hours) was significantly increased when compared control samples without PMPs. Specifically, relative migration of CLL co-cultures was increased by 11.1- and 9.1-fold in CII and MEC-1, respectively (Figure 8A). We next evaluated migration properties in the presence of anti-cancer drug treatments. We found that the migration capacity of CLL cells co-cultured with PMPs was significantly improved following drug treatments with Cytarabine (4.5-fold), Venetoclax (6.2-fold), and Plumbagin (5.0-fold) (Figure 8A). Similar results were also obtained from MEC-1 cells where PMPs increased migration by 5.2-fold (Cytarabine), 5.5-fold (Venetoclax), and 4.0-fold (Plumbagin) when compared to drug treated control cells (Figure 8A).

To evaluate invasion potential, we made use of cell culture inserts layered with Matrigel® mixture. We found that basal invasion capacity of CLL cells co-culture with PMPs was significantly increased by 11.6- and 10.9-fold in CII and MEC-1 cells, respectively when compared to non-treated CLL cells (Figure 8B). These trends were also maintained following drug treatments where PMPs significantly increased the invasion capacity 4.3-fold (Cytarabine), 4.1-fold (Venetoclax), and 6.4-fold (Plumbagin) of CII cells. Equally, MEC-1 cells co-cultured with PMPs also exhibited increased invasion capacity following drug treatments about 5.2-fold (Cytarabine), 4.0-fold (Venetoclax), and 6.0-fold (Plumbagin) higher than their drug-treated control cells (Figure 8B). Together, these results demonstrate that PMPs promote CLL invasive features (i.e., migration and invasion) even in the presence of anti-cancer drugs.

To evaluate the role of mitochondria in these events, we performed migration/invasion analysis on CLLs incubated with Set2-derived mitochondria (1:100). We observed a significant increase of mobility (Supplementary Figure 8A) and invasiveness (Supplementary Figure 8B) following mitochondria acquisition even after treating with an LD50 dose of chemo-drugs including Cytarabine, Venetoclax, and Plumbagin in comparison to control cells. These observations highlight the importance of mitochondrial function in cancer cell resistance to anticancer drugs. Together, these results strongly suggest an impactful role for PMPs in enhanced CLL malignancy, anti-cancer drug resistance, and disease progression.

Discussion

Platelets contain various molecules that have been linked to cancer progression, including growth factors like platelet-derived growth factor (PDGF) and transforming growth factor-beta (TGF-β), cytokines such as interleukin-1 beta (IL-1β) and interleukin-6 (IL-6), chemokines like CXCL12 (SDF-1), and extracellular matrix proteins like fibronectin and vitronectin (76–78). These molecules can promote tumor cell proliferation, survival, angiogenesis, invasion, and metastasis. However, the exact roles of platelet cargos in cancer development and progression are still not fully understood and may depend on tumor type and stage (76–78). Further research is needed to elucidate the specific mechanisms involved and develop new therapeutic strategies targeting platelet-associated molecules in cancer.

It is well established that inflammation is a critical component of cancer progression (reviewed in (16)). This is due to the array of signaling mediators dictating cancer malignant processes leading to disease progression. Platelets are particularly active in these events, notably through their production of PMPs, which are reported as prominent modulators of cancer processes and progression (35, 79, 80). For example, PMPs have demonstrated a role in carcinogenesis through the direct transfer of their bioactive cargo and phenotypic trait acquisition such as invasive capacity and chemoresistance in recipient cancer cells (36, 81–83). Accordingly, we have previously reported a new subpopulation of PMPs, which encompasses functional mitochondria thus adding a new layer of complexity to the phenotypic impact in recipient cells upon PMP internalization (25, 32). Given that mitochondrial functions are an integral part of cancer processes such as cell growth, energy transduction, redox regulation, invasive capacity, and drug resistance (43–47), PMP-mediated transfer of mitochondrial content and functions represents a significant phenomenon supporting cancer progression. In this study, we report the first evidence of mitochondrial transfer (mito-transfer) in leukemia cells *via* PMPs.

10.3389/fimmu.2023.1207631

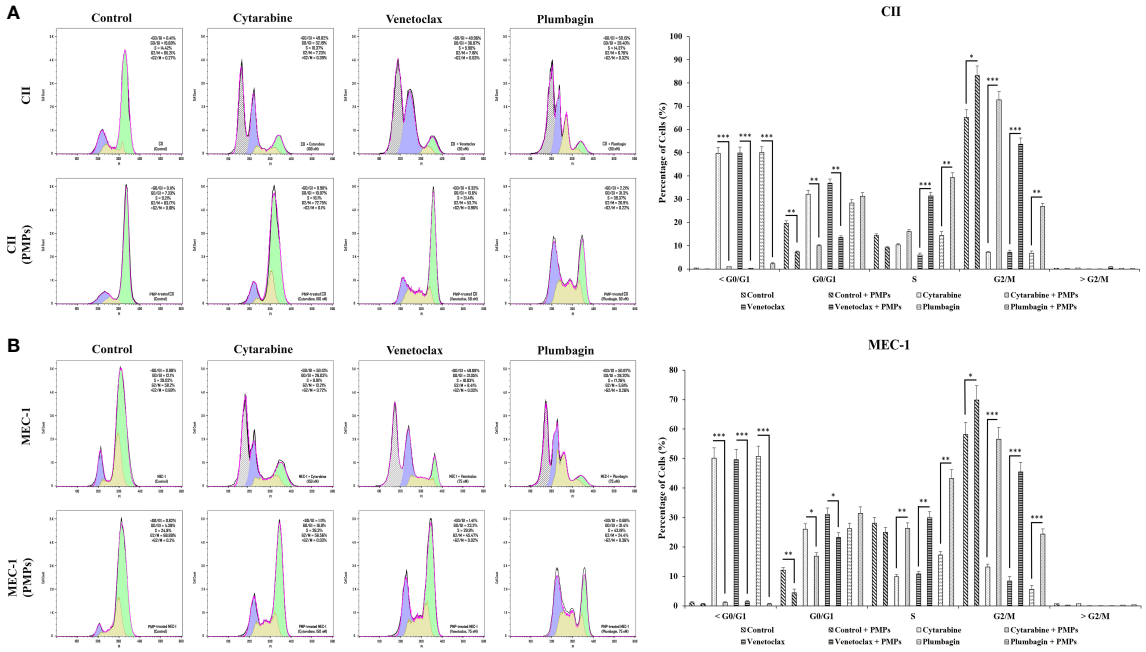

FIGURE 7
Impact of PMPs on CLL cycle progression. CLL cells were co-incubated with PMPs (1:100, 48 h) prior to treatments with the cells' respective LD50 of Cytarabine, Venetoclax, and Plumbagin for 24 hours then evaluated for cycle analysis using flow cytometry. Cell accumulation in each cell cycle phase (i.e., <G0/G1, G0/G1, S, G2/M, and >G2/M) for **(A)** CII and **(B)** MEC-1 cells stained with Propidium Iodide and RNase A was then plotted in relation to control groups treated with DMSO. Each value is the mean ± SEM of six separate experiments. The asterisk (*) indicates significantly different (*$p < 0.05$, **$p < 0.01$, ***$p < 0.001$).

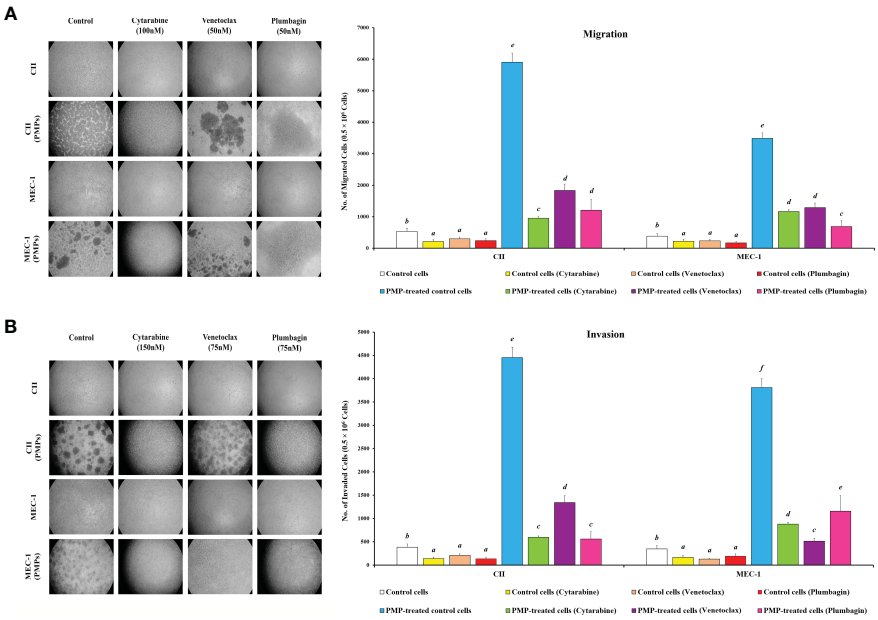

FIGURE 8
Effect of PMPs on CLL malignant processes. CLL cells were co-incubated with PMPs (1:100, 48 h) prior to treatments with the cells' respective LD50 of Cytarabine, Venetoclax, and Plumbagin for 24 hours then evaluated for **(A)** migration and **(B)** invasion capacity using 24-well ThinCerts. Control groups were treated with DMSO as dilution buffer. Light microscopy of invading cells treated at their respective LD50 are also presented for morphological analysis (left panels). Results are expressed as the mean ± SEM of 6 biological experiments. One-way ANOVA followed by Tukey's multiple comparisons test show significant differences in the values presenting different superscript letters ($p < 0.05$).

These events result in increased levels of mitochondrial content and functions, which are accompanied by metabolic reprogramming and phenotypic changes supporting CLL malignant processes essential in disease progression.

Fundamentally, metabolic adaptation is crucial for the survival of cancer cells in various microenvironments. Cancer metabolism is not simply the enhancement of a particular process, but rather a metabolic plasticity enabling cancer cells to consistently modify their metabolism to adapt to altering environmental challenges (9). This metabolic plasticity, which is generally absent in differentiated healthy cells, is a hallmark of cancer cell resilience. Accordingly, this is well demonstrated in our profiling of metabolic-gene expression patterns in CLL patients at various stages of disease (Figure 4). Our results demonstrate that CLL disease progression not only directly correlates with levels of metabolic-gene expression, but also with the amounts of mitochondrial mass in cancer cells. These observations are consistent with others reporting that mitochondrial mass and functions are intimately linked to CLL disease progression (11–15). Our results also corroborate previous studies demonstrating that CLL cells possess greater mitochondrial mass, mtDNA copy number, and functions when compared to healthy B-cells (11, 15). We further validate the relationship between mitochondria acquisition and malignant features by demonstrating enhanced CLL proliferation, drug resistance, and migration/invasion capacities following PMP co-cultures or treatments with purified mitochondria. Evidently, the acquisition of mitochondrial mass in CLL reflects the cells' extensive demand in metabolic versatility supporting phenotypic adaptation during disease progression. Fundamentally, based on the effectiveness of PMPs to increase CLL mitochondrial mass and functions (Figures 1, 3), which concomitantly leads to metabolic-gene expression and malignant CLL processes (Figure 5), PMPs solely could govern CLL disease progression. Besides, previous protein characterization of PMPs has shown that these vesicles cargo different types of proteins involved in various signaling processes (24). A superficial comparison analysis of this list with the metabolic pathways retrieved from our Bioinformatics data revealed that PMP proteins like ACLY, CD36, FASN, GNAI2, GNAQ, GNB2, GNG5, ITPR1, PPP2CA, PPP2R1A, PRKACB, PRKAR1A, PRKCA, SLC2A1 and TKT might also be involved in the metabolic reprogramming through the modulation of metabolic pathways like "ChREBP activates metabolic gene expression (R-HSA-163765)" depicted in our report. These events are substantially more impactful when considering CLL patients have increased levels of PMPs in their circulation (84). Future *in vivo* experimentation using animal models (ex: Eμ-TCL1 (85, 86)) should provide a better understanding of PMP impact on CLL cancer biology and disease progression.

Deciphering the regulatory networks of metabolic reprograming supporting cancer metastasis is extremely relevant and reflected by its attention for therapeutic targeting (46, 47, 87). PMPs are particularly noteworthy as cancer metabolic modulators as they harness multiple hallmark features enabling cancer progression (6). On one hand, PMPs package inflammatory components from their parental platelet cells, which are known to provide inflammation and signaling mediators driving malignant cancer processes (16, 18–20). On the other hand, PMPs also package functional mitochondria, which we demonstrate to foster metabolic reprogramming and cancer processes in recipient cancer cells. Although our characterization of PMP-mediated transfer of mitochondrial content and functions into cancer cells is novel, others have previously described mito-transfer phenomena mediated through extracellular vesicles from other cell types (66, 88–90). However, these findings were shown to be physiologically confined to neural and glia cell activation processes. Mito-transfer events have also been described using other routes of allocation such as tunneling nanotubes (TNT), Cx43 gap junctions, and transplantation, all of which result in recipient cell metabolic changes (65–67). Nonetheless, given that platelets represent the largest source of microparticles in the human body, PMPs therefore represent a significant means for mitochondrial acquisition into permissive cancer cells (27, 28, 91, 92).

Metabolic-related pathways in eukaryotic cells are directly affected by the number and functions of their "powerhouse" mitochondria; however, the exact impact of mitochondrial acquisition on cancer cell signaling cascades has not been fully elucidated. A study from Tan et al. (2015) has shown that the acquisition of stromal cell-derived mitochondria by mitochondria-negative (i.e., rho zero, or ρ0) cancer cells, restores cell growth and tumorigenicity *in vivo* through the activation of OXPHOS (93). In leukemia, mitochondria acquisition has been previously described in hematological lesions such as acute lymphoblastic leukemia (ALL) and acute myeloid leukemia (AML) (17, 94–96). These latter studies use bone marrow stromal cells and mesenchymal stem cells (MSCs) as mitochondria donor cells, which develop TNTs to vehicle mitochondria into hematological tumors. Following mito-transfer, recipient leukemic cells exhibit similar features to our experiments with PMPs, in terms metabolic reprogramming, enhanced ROS production, and chemoresistance (17, 94–96). Another study from Levoux et al. (2021) has examined the effects of platelet-derived mitochondria on MSCs growth and wound healing (97). Accordingly, they show that the therapeutic efficiency of MSCs in tissue injury mice models is enhanced following the treatment of platelet-derived mitochondria (97). Despite these interesting and promising results, more research is needed to further elucidate the repercussions and outcome of PMP-mediated (notably mitochondria function) effects in cancer malignancy and disease progression.

One area of study which has recently received growing attention is the role of OXPHOS activation in cancer cell survival and chemoresistance (98). Interestingly, it seems that cancer development mostly relies on the OXPHOS pathway, rather than ATP generation, by facilitating anabolism through anaplerosis to generate ROS intermediates (99). Accordingly, our data show that PMP-mediated OXPHOS enhancement in CLL cells improves leukemia resistance to commonly used drugs Cytarabine, Venetoclax, and Plumbagin. One study analyzing primary pancreatic acinar formation in mice has shown that metabolic-reprogramming and OXPHOS activation in these animals could be the result of dysregulated oncogenic KRAS (100). Moreover, it has been demonstrated that OXPHOS suppression in AML-engrafted mice can elevate cancer cell sensitivity to anti-BCL2 drug

Venetoclax and Cytarabine (101). Furthermore, they also found induced levels of mitochondrial mass and functions in CLL cells in response to the BCL-2 inhibitor drug Venetoclax. Mechanistically, they found that mitochondrial reprogramming essential for chemoresistance was mediated by MCL-1 upregulation, which led to AMP-activated protein kinase (AMPK) signaling and subsequent OXPHOS activation (102). Altogether, these studies suggest that increased mitochondrial OXPHOS activity has a crucial role in CLL survival and drug resistance. Therefore, combining the current chemotherapeutic treatment regimens with compounds targeting mitochondrial functions may provide an effective therapeutic strategy for leukemia.

Through a bioinformatics approach, we reached out to a set of metabolic-related genes in PMP-recipient CLL cells which were very similar to what was seen in cancer cells collected from CLL patients (Figure 4 and Supplementary Figure 3). Further analysis showed that this network could cause metabolic reprogramming that improved our cell model's drug resistance and survival by stimulating the oncogenic factor HIF-1. HIF-1 is a transcription factor that plays a central role in cellular adaptation to low oxygen levels (hypoxia) and regulates the expression of various genes involved in angiogenesis, metabolism reprogramming, and cell survival (103, 104). It has been well presented before that an increasing number of mitochondrial populations can potentially stimulate HIF-1 expression in cancer cells through a complex interplay of cellular signaling pathways (105). It is also vital in coordinating the interaction between neoplastic B cells and their microenvironments (106). Interestingly, the expression of HIF-1 can be upregulated by mitochondrial overgrowth and function in cells through ROS production (107). Our data showed significant ROS generation in CLL cells under PMP stimulation (Figures 3C, D). Since mitochondria are a major source of ROS generation in cells, increased mitochondrial mass or activity can result in higher levels of ROS, which in turn can stabilize HIF-1α, one of the subunits of HIF-1, by inhibiting its degradation and lead to increased HIF-1 activity and gene expression (108). The other positive impact of mitochondria enhancement on HIF-1 expression is through ETC activity which can affect cellular oxygen consumption (as already depicted in Figure 2) and result in the accumulation of hypoxia-inducible factors (Figure 5). Accordingly, a higher mitochondrial population or enhanced ETC activity may lead to an imbalance between oxygen supply and demand, triggering HIF-1 expression (109). The third possible mechanism could be through increasing the cellular metabolites like glucose and glutamine metabolism (110, 111). Changes in mitochondrial function, such as an increase in mitochondrial population, may affect the metabolic profile of cancer cells and alter the metabolism (105), which in turn, can result in the accumulation of metabolites such as succinate or fumarate (produced by SDH enzyme), which have been shown to stabilize HIF-1α and promote HIF-1 expression (105, 112). The last known possible mechanism can be the mitochondrial dynamic changes in morphology, fusion, and fission processes (113). These dynamics are regulated by specific proteins like MCL-1 (114) and result in increased HIF-1 expression (113). Despite these findings, it is important to note that the relationship between mitochondrial population and HIF-1 expression in cancer cells is complex and context-dependent. Further research is needed to elucidate the precise mechanisms underlying this relationship and identify potential therapeutic strategies targeting mitochondrial-HIF-1 interactions in CLL.

Altogether, our results strongly suggest a role for PMPs in CLL development and progression. These findings are also in line with others stating the possibility of PMP involvement in the development of primary tumors and malignancy processes (115, 116). We believe that the distinctive role of platelets in the metabolic remodeling of cancer cells (especially in advanced stages) has been underestimated, notably through PMP-mediated trafficking. This study was the first to demonstrate the impactful role of PMPs as mitochondria delivering vehicles to modulate leukemia pathogenesis. Further characterization of PMP mito-transfer may provide new avenues for strategic intervention. For example, blockade of PMP interactions may amputate cancer cell access to valuable mitochondrial content and functions essential for disease progression. More importantly, our results provide further evidence for the use of antiplatelet treatments in combination with conventional leukemia therapy to attenuate cancer progression. Further research in this area could pave the way for the design of new treatment strategies based on the targeting of cancer metabolism, particularly on mitochondrial-dependent mechanisms.

Data availability statement

The original contributions presented in the study are included in the article/Supplementary Material. Further inquiries can be directed to the corresponding author.

Ethics statement

The studies involving human participants were reviewed and approved by Institutional Review Board Statement and approval for studies involving human samples have been granted from both the Vitalité Health Network (project: CER7-3-17 Ver. 5) and the Université de Moncton (NB, Canada) (project: 1516-002) research ethics boards. The patients/participants provided their written informed consent to participate in this study.

Author contributions

Conceptualization, GR, LB, and NP. Study design and Methodology, EG and VV. Bioinformatics, and Statistical analysis, EG. Data Curation and Validation, EG. Writing of original draft, EG and GR. Review and Editing, EG, GR, VV, LB, and NP. Visualization, EG. Supervision, GR, LB, and NP. Funding acquisition, GR, LB, and NP All authors contributed to the article and approved the submitted version.

Funding

This work was supported by grants from: the New Brunswick (NB) Innovation Foundation (Grant number #RAI-0000000251); the NB Health Research Foundation (NBHRF) (Grant number #2020-LLSC-2006); the Leukemia & Lymphoma Society of Canada (Grant number #622763); by the DUO research grant program from the Vitalité Health network of NB (Grant number #DUO2022); the Canadian Cancer Society (Grant number #CHA-22); the Canadian Institutes of Health Research (CIHR-149044), the Beatrice Hunter Cancer Research Institute; and the Natural Sciences and Engineering Research Council (DDG-2020-00005 and NSERC, RGPIN-2019-05740). EG is a recipient of a fellowship salary award allocated by the MITACS Elevate program (grant number #IT21736). VV is a recipient of PhD scholarships from the NBHRF and Alexandre-Parks Foundation.

Conflict of interest

The authors declare that the research was conducted in the absence of any commercial or financial relationships that could be construed as a potential conflict of interest.

Publisher's note

All claims expressed in this article are solely those of the authors and do not necessarily represent those of their affiliated organizations, or those of the publisher, the editors and the reviewers. Any product that may be evaluated in this article, or claim that may be made by its manufacturer, is not guaranteed or endorsed by the publisher.

Supplementary material

The Supplementary Material for this article can be found online at: https://www.frontiersin.org/articles/10.3389/fimmu.2023.1207631/full#supplementary-material

SUPPLEMENTARY FIGURE 1
Interaction analysis of CLL cells with purified Set2-derived mitochondria. **(A)** Flow cytometry was performed in CLL cell lines labeled with anti-human CD19 antibody either untreated (control) or co-incubated with purified mitochondria derived from the Set2 megakaryocytic cell line labeled with MitoTracker Deep Red (MTDR). Co-incubations of CII (upper panels) or MEC-1 cells (lower panels) with purified mitochondria were performed at 1:10 and 1:100 (cell/mito) ratios for 48 hours. **(B)** CLL co-incubations (48 hours) with purified mitochondria (1:10 and 1:100) were also photographed by fluorescence microscopy. CLL cell lines were labeled with DAPI and MitoTracker™ Green FM (MTG), whereas purified mitochondria were labeled with MTDR. **(C)** Relative mitochondrial DNA copy number was obtained from cell models co-cultured with Set2-Mitos (for 24 and 48 hours) using Real-time PCR on leucine tRNA (mtDNA-tRNA-Leu). Results were normalized by nuclear DNA to reveal relative mitochondrial DNA copy number. Each value is the mean ± SEM of six separate experiments. The asterisk (*) indicates significantly different (*$p < 0.05$, **$p < 0.01$, ***$p < 0.001$).

SUPPLEMENTARY FIGURE 2
Impact of damaged mitochondria acquisition on CLL viability. CLL cell lines were evaluated for cell viability at varying co-culture ratios (1:10 and 1:100) and incubation time (24 and 48 hours) with either **(A)** frozen-thawed PMPs or **(B)** PMPs treated with Rotenone (ROT) and Antimycin A (AmA). Freeze-thaw cycling began at -6.5°C and the PMPs were cooled down to -80°C and kept 24 hours, and then warmed up to 37°C in water bath (Repeated 3 times). ROT/AmA treated PMPs were made by incubating the PMPs with 0.5μM ROT (to inhibit complex I) and 2.5μM AmA to block complex III for 1 hour. Viability was then assessed in relation to control non-treated cells (24 h). Each value is the mean ± SEM of six separate experiments. The asterisk (*) indicates significantly different (*$p < 0.05$, ***$p < 0.001$).

SUPPLEMENTARY FIGURE 3
Bioinformatics identification and analysis of core metabolic-related genes involved in CLL progression. **(A)** Identification of genes involved in CLL metabolism. The interaction between genes was visualized by the Cytoscape plugins BisoGenet and the hubs were plotted by the CentiScaPe based on their betweenness centrality. **(B)** Enrichment analysis of metabolic related signaling pathways were then configured based on identified genes (Hubs) using EnrichR. The asterisk (*) indicates significantly different (* $p <$ 0.05, **$p < 0.01$, ***$p < 0.001$).

SUPPLEMENTARY FILE 4
Metabolic gene expression values in CLL clinical samples. The expression levels of genes associated to metabolic pathways were applied to a cohort of CLL patients (n=442) based on their corresponding Binet staging (i.e., stage A (n)=184, stage B (n)=179, and stage C (n)=79) to define the most significant modulated genes associated with CLL disease progression. The average expression values of the profiled genes are listed per patient.

SUPPLEMENTARY FIGURE 5
Impact of Set2-derived mitochondria on metabolic gene expression in CLL cells. Real-time PCR analysis was performed to evaluate differentially expressed metabolic-related genes (DEGs) in **(A)** CII and **(B)** MEC-1 cells in the presence of chemo-drugs where each column represents the Set2-Mito treated/non-treated cell ratio. Control groups were treated with DMSO as dilution buffer. Results are expressed as the mean ± SEM of six biological experiments. One-way ANOVA followed by Tukey's multiple comparisons test show significant differences in the values presenting different superscript letters ($p < 0.05$).

SUPPLEMENTARY FIGURE 6
Effects of Set2-derived mitochondria on CLL survival and apoptosis. CLL cells were co-incubated with Set2-Mitos (1:100, 48 h) prior to treatments with the cells' respective LD50 of Cytarabine, Venetoclax, and Plumbagin for 24 hours for the evaluation of drug cytotoxic events. Flow cytometry analysis in **(A)** CII and **(B)** MEC-1 cells stained with Propidium Iodide (PI, X-axis) and Annexin-FITC (X-axis) sorted cell populations according to distinctive quarter zones (Q), including the large nuclear fragments/debris or Q1 (Anx^-/PI^+), necrosis cells or Q2 (Anx^+/PI^+), apoptotic cells or Q3 (Anx^+/PI^-), and the living cells or Q4 (Anx^-/PI^-). Values for each quadrant were then plotted in relation to their respective control groups (DMSO). Each value is the mean ± SEM of six separate experiments. The asterisk (*) indicates significantly different (*$p <$ 0.05, ***$p < 0.001$).

SUPPLEMENTARY FIGURE 7
Impact of Set2-derived mitochondria on CLL cycle progression. CLL cells were co-incubated with Set2-Mitos (1:100, 48 h) prior to treatments with the cells' respective LD50 of Cytarabine, Venetoclax, and Plumbagin for 24 hours then evaluated for cycle analysis using flow cytometry. Cell accumulation in each cell cycle phase (i.e., <G0/G1, G0/G1, S, G2/M, and >G2/M) for **(A)** CII and **(B)** MEC-1 cells stained with Propidium Iodide and RNase A was then plotted in relation to control groups treated with DMSO. Each value is the mean ± SEM of six separate experiments. The asterisk (*) indicates significantly different (*$p < 0.05$, **$p < 0.01$, ***$p < 0.001$).

SUPPLEMENTARY FIGURE 8
Effect of Set2-derived mitochondria on CLL malignant processes. CLL cells were co-incubated with Set2-Mitos (1:100, 48 h) prior to treatments with the cells' respective LD50 of Cytarabine, Venetoclax, and Plumbagin for 24 hours then evaluated for **(A)** migration and **(B)** invasion capacity using 24-well ThinCerts. Control groups were treated with DMSO as dilution buffer. Each value is the mean ± SEM of six separate experiments. One-way ANOVA followed by Tukey's multiple comparisons test show significant differences in the values presenting different superscript letters ($p < 0.05$).

References

1. Rassenti LZ, Huynh L, Toy TL, Chen L, Keating MJ, Gribben JG, et al. Zap-70 compared with immunoglobulin heavy-chain gene mutation status as a predictor of disease progression in chronic lymphocytic leukemia. *N Engl J Med* (2004) 351(9):893–901. doi: 10.1056/NEJMoa040857

2. Hamblin TJ, Davis Z, Gardiner A, Oscier DG, Stevenson FK. Unmutated ig V(H) genes are associated with a more aggressive form of chronic lymphocytic leukemia. *Blood* (1999) 94(6):1848–54. doi: 10.1182/blood.V94.6.1848

3. Wierda WG, O'Brien S, Wang X, Faderl S, Ferrajoli A, Do KA, et al. Prognostic nomogram and index for overall survival in previously untreated patients with chronic lymphocytic leukemia. *Blood* (2007) 109(11):4679–85. doi: 10.1182/blood-2005-12-051458

4. Hallek M, Cheson BD, Catovsky D, Caligaris-Cappio F, Dighiero G, Dohner H, et al. Iwcll guidelines for diagnosis, indications for treatment, response assessment, and supportive management of cll. *Blood* (2018) 131(25):2745–60. doi: 10.1182/blood-2017-09-806398

5. Faubert B, Solmonson A, DeBerardinis RJ. Metabolic reprogramming and cancer progression. *Science* (2020) 368(6487):1–26. doi: 10.1126/science.aaw5473

6. Hanahan D, Weinberg RA. Hallmarks of cancer: the next generation. *Cell* (2011) 144(5):646–74. doi: 10.1016/j.cell.2011.02.013

7. Chiorazzi N, Rai KR, Ferrarini M. Chronic lymphocytic leukemia. *N Engl J Med* (2005) 352(8):804–15. doi: 10.1056/NEJMra041720

8. Moreno C. Chronic lymphocytic leukemia and the warburg effect. *Blood* (2015) 125(22):3368–9. doi: 10.1182/blood-2015-04-636332

9. Abdel-Wahab AF, Mahmoud W, Al-Harizy RM. Targeting glucose metabolism to suppress cancer progression: prospective of anti-glycolytic cancer therapy. *Pharmacol Res* (2019) 150:104511. doi: 10.1016/j.phrs.2019.104511

10. Roy Chowdhury S, Banerji V. Targeting mitochondrial bioenergetics as a therapeutic strategy for chronic lymphocytic leukemia. *Oxid Med Cell Longev* (2018) 2018:2426712. doi: 10.1155/2018/2426712

11. Jitschin R, Hofmann AD, Bruns H, Giessl A, Bricks J, Berger J, et al. Mitochondrial metabolism contributes to oxidative stress and reveals therapeutic targets in chronic lymphocytic leukemia. *Blood* (2014) 123(17):2663–72. doi: 10.1182/blood-2013-10-532200

12. Zhou Y, Hileman EO, Plunkett W, Keating MJ, Huang P. Free radical stress in chronic lymphocytic leukemia cells and its role in cellular sensitivity to ros-generating anticancer agents. *Blood* (2003) 101(10):4098–104. doi: 10.1182/blood-2002-08-2512

13. Vangapandu HV, Ayres ML, Bristow CA, Wierda WG, Keating MJ, Balakrishnan K, et al. The stromal microenvironment modulates mitochondrial oxidative phosphorylation in chronic lymphocytic leukemia cells. *Neoplasia* (2017) 19(10):762–71. doi: 10.1016/j.neo.2017.07.004

14. Berard M, Mondiere P, Casamayor-Palleja M, Hennino A, Bella C, Defrance T. Mitochondria connects the antigen receptor to effector caspases during b cell receptor-induced apoptosis in normal human b cells. *J Immunol* (1999) 163(9):4655–62. doi: 10.4049/jimmunol.163.9.4655

15. Carew JS, Nawrocki ST, Xu RH, Dunner K, McConkey DJ, Wierda WG, et al. Increased mitochondrial biogenesis in primary leukemia cells: the role of endogenous nitric oxide and impact on sensitivity to fludarabine. *Leukemia* (2004) 18(12):1934–40. doi: 10.1038/sj.leu.2403545

16. Rozovski U, Keating MJ, Estrov Z. Targeting inflammatory pathways in chronic lymphocytic leukemia. *Crit Rev Oncol Hematol* (2013) 88(3):655–66. doi: 10.1016/j.critrevonc.2013.07.011

17. Wang S, Li Z, Xu R. Human cancer and platelet interaction, a potential therapeutic target. *Int J Mol Sci* (2018) 19(4):1–15. doi: 10.3390/ijms19041246

18. Lal I, Dittus K, Holmes CE. Platelets, coagulation and fibrinolysis in breast cancer progression. *Breast Cancer Res* (2013) 15(4):207. doi: 10.1186/bcr3425

19. Menter DG, Davis JS, Tucker SC, Hawk E, Crissman JD, Sood AK, et al. Platelets: "First responders" in cancer progression and metastasis. In: Gresele P, Kleiman NS, Lopez JA, Page CP, editors. *Platelets in thrombotic and non-thrombotic disorders*. Cham: Springer International Publishing (2017). p. 1111–32.

20. Menter DG, Tucker SC, Kopetz S, Sood AK, Crissman JD, Honn KV. Platelets and cancer: a casual or causal relationship: revisited. *Cancer Metastasis Rev* (2014) 33 (1):231–69. doi: 10.1007/s10555-014-9498-0

21. Heijnen HF, Schiel AE, Fijnheer R, Geuze HJ, Sixma JJ. Activated platelets release two types of membrane vesicles: microvesicles by surface shedding and exosomes derived from exocytosis of multivesicular bodies and alpha-granules. *Blood* (1999) 94(11):3791–9. doi: 10.1182/blood.V94.11.3791

22. Yanez-Mo M, Siljander PR, Andreu Z, Zavec AB, Borras FE, Buzas EI, et al. Biological properties of extracellular vesicles and their physiological functions. *J Extracell Vesicles* (2015) 4:27066. doi: 10.3402/jev.v4.27066

23. Aatonen M, Gronholm M, Siljander PR. Platelet-derived microvesicles: multitalented participants in intercellular communication. *Semin Thromb Hemost* (2012) 38(1):102–13. doi: 10.1055/s-0031-1300956

24. Capriotti AL, Caruso G, Cavaliere C, Piovesana S, Samperi R, Laganà A. Proteomic characterization of human platelet-derived microparticles. *Analytica Chim Acta* (2013) 776:57–63. doi: 10.1016/j.aca.2013.03.023

25. Duchez AC, Boudreau LH, Naika GS, Bollinger J, Belleannee C, Cloutier N, et al. Platelet microparticles are internalized in neutrophils *Via* the concerted activity of 12-lipoxygenase and secreted phospholipase A2-iia. *Proc Natl Acad Sci U.S.A.* (2015) 112 (27):E3564–73. doi: 10.1073/pnas.1507905112

26. Laffont B, Corduan A, Rousseau M, Duchez AC, Lee CH, Boilard E, et al. Platelet microparticles reprogram macrophage gene expression and function. *Thromb Haemost* (2016) 115(2):311–23. doi: 10.1160/TH15-05-0389

27. Joop K, Berckmans RJ, Nieuwland R, Berkhout J, Romijn FP, Hack CE, et al. Microparticles from patients with multiple organ dysfunction syndrome and sepsis support coagulation through multiple mechanisms. *Thromb Haemost* (2001) 85 (5):810–20. doi: 10.1055/s-0037-1615753

28. Horstman LL, Ahn YS. Platelet microparticles: a wide-angle perspective. *Crit Rev Oncol Hematol* (1999) 30(2):111–42. doi: 10.1016/S1040-8428(98)00044-4

29. Sheremata WA, Jy W, Horstman LL, Ahn YS, Alexander JS, Minagar A. Evidence of platelet activation in multiple sclerosis. *J Neuroinflamm* (2008) 5:27. doi: 10.1186/1742-2094-5-27

30. Marcos-Ramiro B, Oliva Nacarino P, Serrano-Pertierra E, Blanco-Gelaz MA, Weksler BB, Romero IA, et al. Microparticles in multiple sclerosis and clinically isolated syndrome: effect on endothelial barrier function. *BMC Neurosci* (2014) 15:110. doi: 10.1186/1471-2202-15-110

31. Boilard E, Nigrovic PA, Larabee K, Watts GF, Coblyn JS, Weinblatt ME, et al. Platelets amplify inflammation in arthritis *Via* collagen-dependent microparticle production. *Science* (2010) 327(5965):580–3. doi: 10.1126/science.1181928

32. Boudreau LH, Duchez A-C, Cloutier N, Soulet D, Martin N, Bollinger J, et al. Platelets release mitochondria serving as substrate for bactericidal group iia-secreted phospholipase A2 to promote inflammation. *Blood* (2014) 124(14):2173–83. doi: 10.1182/blood-2014-05-573543

33. Loyer X, Vion AC, Tedgui A, Boulanger CM. Microvesicles as cell-cell messengers in cardiovascular diseases. *Circ Res* (2014) 114(2):345–53. doi: 10.1161/CIRCRESAHA.113.300858

34. Tan KT, Lip GY. The potential role of platelet microparticles in atherosclerosis. *Thromb Haemost* (2005) 94(3):488–92. doi: 10.1160/TH05-03-0201

35. Al Thawadi H, Abu-Kaoud N, Al Farsi H, Hoarau-Vechot J, Rafii S, Rafii A, et al. Ve-cadherin cleavage by ovarian cancer microparticles induces beta-catenin phosphorylation in endothelial cells. *Oncotarget* (2016) 7(5):5289–305. doi: 10.18632/oncotarget.6677

36. Gong J, Luk F, Jaiswal R, Bebawy M. Microparticles mediate the intercellular regulation of microrna-503 and proline-rich tyrosine kinase 2 to alter the migration and invasion capacity of breast cancer cells. *Front Oncol* (2014) 4:220. doi: 10.3389/fonc.2014.00220

37. Badimon L, Suades R, Fuentes E, Palomo I, Padró T. Role of platelet-derived microvesicles as crosstalk mediators in atherothrombosis and future pharmacology targets: a link between inflammation, atherosclerosis, and thrombosis. *Front Pharmacol* (2016) 7:293. doi: 10.3389/fphar.2016.00293

38. Dalli J, Serhan CN. Specific lipid mediator signatures of human phagocytes: microparticles stimulate macrophage efferocytosis and pro-resolving mediators. *Blood J Am Soc Hematol* (2012) 120(15):e60–72. doi: 10.1182/blood-2012-04-423525

39. Mezentsev A, Merks RM, O'Riordan E, Chen J, Mendelev N, Goligorsky MS, et al. Endothelial microparticles affect angiogenesis in vitro: role of oxidative stress. *Am J Physiology-Heart Circulatory Physiol* (2005) 289(3):H1106–H14. doi: 10.1152/ajpheart.00265.2005

40. Mause SF, Weber C. Microparticles: protagonists of a novel communication network for intercellular information exchange. *Circ Res* (2010) 107(9):1047–57. doi: 10.1161/CIRCRESAHA.110.226456

41. Nomura S. Extracellular vesicles and blood diseases. *Int J Hematol* (2017) 105 (4):392–405. doi: 10.1007/s12185-017-2180-x

42. Preston RA, Jy W, Jimenez JJ, Mauro LM, Horstman LL, Valle M, et al. Effects of severe hypertension on endothelial and platelet microparticles. *Hypertension* (2003) 41 (2):211–7. doi: 10.1161/01.HYP.0000049760.15764.2D

43. Guerra F, Arbini AA, Moro L. Mitochondria and cancer chemoresistance. *Biochim Biophys Acta Bioenerg* (2017) 1858(8):686–99. doi: 10.1016/j.bbabio.2017.01.012

44. Vyas S, Zaganjor E, Haigis MC. Mitochondria and cancer. *Cell* (2016) 166 (3):555–66. doi: 10.1016/j.cell.2016.07.002

45. Sassano ML, van Vliet AR, Agostinis P. Mitochondria-associated membranes as networking platforms and regulators of cancer cell fate. *Front Oncol* (2017) 7:174. doi: 10.3389/fonc.2017.00174

46. Maximo V, Lima J, Soares P, Sobrinho-Simoes M. Mitochondria and cancer. *Virchows Arch* (2009) 454(5):481–95. doi: 10.1007/s00428-009-0766-2

47. Zong WX, Rabinowitz JD, White E. Mitochondria and cancer. *Mol Cell* (2016) 61(5):667–76. doi: 10.1016/j.molcel.2016.02.011

48. Kitani T, Kami D, Matoba S, Gojo S. Internalization of isolated functional mitochondria: involvement of macropinocytosis. *J Cell Mol Med* (2014) 18(8):1694–703. doi: 10.1111/jcmm.12316

49. Kheirandish-Rostami M, Roudkenar MH, Jahanian-Najafabadi A, Tomita K, Kuwahara Y, Sato T, et al. Mitochondrial characteristics contribute to proliferation and migration potency of mda-Mb-231 cancer cells and their response to cisplatin treatment. *Life Sci* (2020) 244:117339. doi: 10.1016/j.lfs.2020.117339

50. Gnaiger E. *Polarographic oxygen sensors, the oxygraph and high-resolution respirometry to assess mitochondrial function. in: mitochondrial dysfunction in drug-induced toxicity*. Dykens JAWY, editor. Hoboken: John Wiley & Sons, Inc (2008).

51. Gnaiger E. Mitochondrial pathways and respiratory control. An introduction to OXPHOS analysis. Mitochondr Physiol Network 17.18: OROBOROS MiPNet Publications, Innsbruck (2012). p. 80.

52. Livak KJ, Schmittgen TD. Analysis of relative gene expression data using real-time quantitative pcr and the 2(-delta delta C(T)) method. *Methods* (2001) 25(4):402–8. doi: 10.1006/meth.2001.1262

53. Rooney JP, Ryde IT, Sanders LH, Howlett EH, Colton MD, Germ KE, et al. Pcr based determination of mitochondrial DNA copy number in multiple species. *Methods Mol Biol* (2015) 1241:23–38. doi: 10.1007/978-1-4939-1875-1_3

54. Shannon P, Markiel A, Ozier O, Baliga NS, Wang JT, Ramage D, et al. Cytoscape: a software environment for integrated models of biomolecular interaction networks. *Genome Res* (2003) 13(11):2498–504. doi: 10.1101/gr.1239303

55. Martin A, Ochagavia ME, Rabasa LC, Miranda J, Fernandez-de-Cossio J, Bringas R. Bisogenet: a new tool for gene network building, visualization and analysis. *BMC Bioinf* (2010) 11(1):1–9. doi: 10.1186/1471-2105-11-91

56. Pinero J, Bravo A, Queralt-Rosinach N, Gutierrez-Sacristan A, Deu-Pons J, Centeno E, et al. Disgenet: a comprehensive platform integrating information on human disease-associated genes and variants. *Nucleic Acids Res* (2017) 45(D1):D833–D9. doi: 10.1093/nar/gkw943

57. Davis AP, Grondin CJ, Johnson RJ, Sciaky D, McMorran R, Wiegers J, et al. The comparative toxicogenomics database: update 2019. *Nucleic Acids Res* (2019) 47(D1): D948–D54. doi: 10.1093/nar/gky868

58. Becker KG, Barnes KC, Bright TJ, Wang SA. The genetic association database. *Nat Genet* (2004) 36(5):431–2. doi: 10.1038/ng0504-431

59. Eppig JT, Blake JA, Bult CJ, Kadin JA, Richardson JE, Mouse Genome Database G. The mouse genome database (Mgd): new features facilitating a model system. *Nucleic Acids Res* (2007) 35(Database issue):D630–7. doi: 10.1093/nar/gkl940

60. McKusick VA. Mendelian inheritance in man and its online version, omim. *Am J Hum Genet* (2007) 80(4):588–604. doi: 10.1086/514346

61. Lazar S, Goldfinger LE. Platelets and extracellular vesicles and their cross talk with cancer. *Blood* (2021) 137(23):3192–200. doi: 10.1182/blood.2019004119

62. Zhang B, Wang Y, Wu C, Qiu S, Chen X, Cai B, et al. Freeze-thawing impairs the motility, plasma membrane integrity and mitochondria function of boar spermatozoa through generating excessive ros. *BMC Vet Res* (2021) 17(1):1–9. doi: 10.1186/s12917-021-02804-1

63. Gao M-j, Cui N-h, Wang X-b. Inhibition of mitochondrial complex I leading to Nad+/Nadh imbalance in type 2 diabetic patients who developed late stent thrombosis: evidence from an integrative analysis of platelet bioenergetics and metabolomics. *Redox Biol* (2022) 57:102507. doi: 10.1016/j.redox.2022.102507

64. Donner L, Feige T, Freiburg C, Toska LM, Reichert AS, Chatterjee M, et al. Impact of amyloid-B on platelet mitochondrial function and platelet–mediated amyloid aggregation in alzheimer's disease. *Int J Mol Sci* (2021) 22(17):9633. doi: 10.3390/ijms22179633

65. Pasquier J, Guerrouahen BS, Al Thawadi H, Ghiabi P, Maleki M, Abu-Kaoud N, et al. Preferential transfer of mitochondria from endothelial to cancer cells through tunneling nanotubes modulates chemoresistance. *J Transl Med* (2013) 11:94. doi: 10.1186/1479-5876-11-94

66. Qin Y, Jiang X, Yang Q, Zhao J, Zhou Q, Zhou Y. The functions, methods, and mobility of mitochondrial transfer between cells. *Front Oncol* (2021) 11:672781. doi: 10.3389/fonc.2021.672781

67. Chang JC, Chang HS, Wu YC, Cheng WL, Lin TT, Chang HJ, et al. Mitochondrial transplantation regulates antitumour activity, chemoresistance and mitochondrial dynamics in breast cancer. *J Exp Clin Cancer Res* (2019) 38(1):30. doi: 10.1186/s13046-019-1028-z

68. Enriquez JA, Lenaz G. Coenzyme q and the respiratory chain: coenzyme q pool and mitochondrial supercomplexes. *Mol Syndromol* (2014) 5(3-4):119–40. doi: 10.1159/000363364

69. Ahmad M, Wolberg A, Kahwaji CI. *Biochemistry, electron transport chain*. Treasure Island (FL: Statpearls (2023).

70. Chang SN, Dey DK, Oh ST, Kong WH, Cho KH, Al-Olayan EM, et al. Phorbol 12-myristate 13-acetate induced toxicity study and the role of tangeretin in abrogating hif-1alpha-Nf-Kappab crosstalk in vitro and in vivo. *Int J Mol Sci* (2020) 21(23):1–22. doi: 10.3390/ijms21239261

71. Tanaka T, Kurabayashi M, Aihara Y, Ohyama Y, Nagai R. Inducible expression of manganese superoxide dismutase by phorbol 12-myristate 13-acetate is mediated by Sp1 in endothelial cells. *Arterioscler Thromb Vasc Biol* (2000) 20(2):392–401. doi: 10.1161/01.atv.20.2.392

72. Ezeamuzie CI, Taslim N. Reactive oxygen species mediate phorbol ester-stimulated camp response in human eosinophils. *Eur J Pharmacol* (2006) 543(1-3):174–80. doi: 10.1016/j.ejphar.2006.05.035

73. Valsecchi R, Coltella N, Belloni D, Ponente M, Ten Hacken E, Scielzo C, et al. Hif-1alpha regulates the interaction of chronic lymphocytic leukemia cells with the tumor microenvironment. *Blood* (2016) 127(16):1987–97. doi: 10.1182/blood-2015-07-657056

74. Colegio OR, Chu NQ, Szabo AL, Chu T, Rhebergen AM, Jairam V, et al. Functional polarization of tumour-associated macrophages by tumour-derived lactic acid. *Nature* (2014) 513(7519):559–63. doi: 10.1038/nature13490

75. Hanna BS, Ozturk S, Seiffert M. Beyond bystanders: myeloid cells in chronic lymphocytic leukemia. *Mol Immunol* (2019) 110:77–87. doi: 10.1016/j.molimm.2017.11.014

76. Gris JC, Faillie JL, Cochery-Nouvellon E, Lissalde-Lavigne G, LEFRANT JY. Isth overt disseminated intravascular coagulation score in patients with septic shock: automated immunoturbidimetric soluble fibrin assay vs. d-dimer assay. *J Thromb Haemostasis* (2011) 9(6):1252–5. doi: 10.1111/j.1538-7836.2011.04270.x

77. Joyce JA, Laakkonen P, Bernasconi M, Bergers G, Ruoslahti E, Hanahan D. Stage-specific vascular markers revealed by phage display in a mouse model of pancreatic islet tumorigenesis. *Cancer Cell* (2003) 4(5):393–403. doi: 10.1016/S1535-6108(03)00271-X

78. Labelle M, Hynes RO. The initial hours of metastasis: the importance of cooperative host–tumor cell interactions during hematogenous disseminationhost–tumor cell interactions during metastatic dissemination. *Cancer Discovery* (2012) 2 (12):1091–9. doi: 10.1158/2159-8290.CD-12-0329

79. Honn KV, Tang DG, Crissman JD. Platelets and cancer metastasis: a causal relationship? *Cancer Metastasis Rev* (1992) 11(3-4):325–51. doi: 10.1007/BF01307186

80. Harbeck N, Gnant M. Breast cancer. *Lancet* (2017) 389(10074):1134–50. doi: 10.1016/S0140-6736(16)31891-8

81. Vismara M, Zara M, Negri S, Canino J, Canobbio I, Barbieri SS, et al. Platelet-derived extracellular vesicles regulate cell cycle progression and cell migration in breast cancer cells. *Biochim Biophys Acta Mol Cell Res* (2021) 1868(1):118886. doi: 10.1016/j.bbamcr.2020.118886

82. Jaiswal R, Johnson MS, Pokharel D, Krishnan SR, Bebawy M. Microparticles shed from multidrug resistant breast cancer cells provide a parallel survival pathway through immune evasion. *BMC Cancer* (2017) 17(1):104. doi: 10.1186/s12885-017-3102-2

83. Zara M, Guidetti GF, Boselli D, Villa C, Canobbio I, Seppi C, et al. Release of prometastatic platelet-derived microparticles induced by breast cancer cells: a novel positive feedback mechanism for metastasis. *TH Open* (2017) 1(2):e155–e63. doi: 10.1055/s-0037-1613674

84. Ghosh AK, Secreto CR, Knox TR, Ding W, Mukhopadhyay D, Kay NE. Circulating microvesicles in b-cell chronic lymphocytic leukemia can stimulate marrow stromal cells: implications for disease progression. *Blood* (2010) 115 (9):1755–64. doi: 10.1182/blood-2009-09-242719

85. Bichi R, Shinton SA, Martin ES, Koval A, Calin GA, Cesari R, et al. Human chronic lymphocytic leukemia modeled in mouse by targeted Tcl1 expression. *Proc Natl Acad Sci U.S.A.* (2002) 99(10):6955–60. doi: 10.1073/pnas.102181599

86. Johnson AJ, Lucas DM, Muthusamy N, Smith LL, Edwards RB, De Lay MD, et al. Characterization of the tcl-1 transgenic mouse as a preclinical drug development tool for human chronic lymphocytic leukemia. *Blood* (2006) 108(4):1334–8. doi: 10.1182/blood-2005-12-011213

87. Weinberg SE, Chandel NS. Targeting mitochondria metabolism for cancer therapy. *Nat Chem Biol* (2015) 11(1):9–15. doi: 10.1038/nchembio.1712

88. Hayakawa K, Esposito E, Wang X, Terasaki Y, Liu Y, Xing C, et al. Transfer of mitochondria from astrocytes to neurons after stroke. *Nature* (2016) 535(7613):551–5. doi: 10.1038/nature18928

89. Gao L, Zhang Z, Lu J, Pei G. Mitochondria are dynamically transferring between human neural cells and Alexander disease-associated gfap mutations impair the astrocytic transfer. *Front Cell Neurosci* (2019) 13:316. doi: 10.3389/fncel.2019.00316

90. Davis CH, Kim KY, Bushong EA, Mills EA, Boassa D, Shih T, et al. Transcellular degradation of axonal mitochondria. *Proc Natl Acad Sci U.S.A.* (2014) 111(26):9633–8. doi: 10.1073/pnas.1404651111

91. Berckmans R, Nieuwland R, Böing A, Romijn F, Hack CE, Sturk A. Cell-derived microparticles circulate in healthy humans and support low grade thrombin generation. *Thromb Haemost* (2001) 85(4):639–49. doi: 10.1055/s-0037-1615646

92. Orozco AF, Lewis DE. Flow cytometric analysis of circulating microparticles in plasma. *Cytomet A* (2010) 77(6):502–14. doi: 10.1002/cyto.a.20886

93. Tan AS, Baty JW, Dong LF, Bezawork-Geleta A, Endaya B, Goodwin J, et al. Mitochondrial genome acquisition restores respiratory function and tumorigenic potential of cancer cells without mitochondrial DNA. *Cell Metab* (2015) 21(1):81–94. doi: 10.1016/j.cmet.2014.12.003

94. Moschoi R, Imbert V, Nebout M, Chiche J, Mary D, Prebet T, et al. Protective mitochondrial transfer from bone marrow stromal cells to acute myeloid leukemic cells during chemotherapy. *Blood* (2016) 128(2):253–64. doi: 10.1182/blood-2015-07-655860

95. Burt R, Dey A, Aref S, Aguiar M, Akarca A, Bailey K, et al. Activated stromal cells transfer mitochondria to rescue acute lymphoblastic leukemia cells from oxidative stress. *Blood* (2019) 134(17):1415–29. doi: 10.1182/blood.2019001398

96. Marlein CR, Zaitseva L, Piddock RE, Robinson SD, Edwards DR, Shafat MS, et al. Nadph oxidase-2 derived superoxide drives mitochondrial transfer from bone marrow stromal cells to leukemic blasts. *Blood* (2017) 130(14):1649–60. doi: 10.1182/blood-2017-03-772939

97. Levoux J, Prola A, Lafuste P, Gervais M, Chevallier N, Koumaiha Z, et al. Platelets facilitate the wound-healing capability of mesenchymal stem cells by mitochondrial transfer and metabolic reprogramming. *Cell Metab* (2021) 33(3):688–90. doi: 10.1016/j.cmet.2021.02.003

98. Ashton TM, McKenna WG, Kunz-Schughart LA, Higgins GS. Oxidative phosphorylation as an emerging target in cancer therapy. *Clin Cancer Res* (2018) 24 (11):2482–90. doi: 10.1158/1078-0432.CCR-17-3070

99. Porporato PE, Filigheddu N, Pedro JMB, Kroemer G, Galluzzi L. Mitochondrial metabolism and cancer. *Cell Res* (2018) 28(3):265–80. doi: 10.1038/cr.2017.155

100. Viale G, Dell'Orto P, Biasi MO, Stufano V, De Brito Lima LN, Paganelli G, et al. Comparative evaluation of an extensive histopathologic examination and a real-time reverse-Transcription-Polymerase chain reaction assay for mammaglobin and cytokeratin 19 on axillary sentinel lymph nodes of breast carcinoma patients. *Ann Surg* (2008) 247(1):136–42. doi: 10.1097/SLA.0b013e318157d22b

101. Farge T, Saland E, de Toni F, Aroua N, Hosseini M, Perry R, et al. Chemotherapy-resistant human acute myeloid leukemia cells are not enriched for leukemic stem cells but require oxidative metabolism. *Cancer Discovery* (2017) 7 (7):716–35. doi: 10.1158/2159-8290.CD-16-0441

102. Guieze R, Liu VM, Rosebrock D, Jourdain AA, Hernandez-Sanchez M, Martinez Zurita A, et al. Mitochondrial reprogramming underlies resistance to bcl-2 inhibition in lymphoid malignancies. *Cancer Cell* (2019) 36(4):369–84 e13. doi: 10.1016/j.ccell.2019.08.005

103. Semenza GL, Roth PH, Fang H-M, Wang GL. Transcriptional regulation of genes encoding glycolytic enzymes by hypoxia-inducible factor 1. *J Biol Chem* (1994) 269(38):23757–63. doi: 10.1016/S0021-9258(17)31580-6

104. Carmeliet P, Dor Y, Herbert J-M, Fukumura D, Brusselmans K, Dewerchin M, et al. Role of hif-1α in hypoxia-mediated apoptosis, cell proliferation and tumour angiogenesis. *Nature* (1998) 394(6692):485–90. doi: 10.1038/28867

105. Wallace DC. Mitochondria and cancer. *Nat Rev Cancer* (2012) 12(10):685–98. doi: 10.1038/nrc3365

106. Valsecchi R, Coltella N, Belloni D, Ponente M, Ten Hacken E, Scielzo C, et al. Hif-1α regulates the interaction of chronic lymphocytic leukemia cells with the tumor microenvironment. *Blood J Am Soc Hematol* (2016) 127(16):1987–97. doi: 10.1182%2Fblood-2015-07-657056

107. Zheng X, Narayanan S, Xu C, Angelstig SE, Grünler J, Zhao A, et al. Repression of hypoxia-inducible factor-1 contributes to increased mitochondrial reactive oxygen species production in diabetes. *elife* (2022) 11:e70714. doi: 10.7554/eLife.70714

108. Belaidi E, Morand J, Gras E, Pépin J-L, Godin-Ribuot D. Targeting the ros-Hif-1-Endothelin axis as a therapeutic approach for the treatment of obstructive sleep apnea-related cardiovascular complications. *Pharmacol Ther* (2016) 168:1–11. doi: 10.1016/j.pharmthera.2016.07.010

109. Infantino V, Santarsiero A, Convertini P, Todisco S, Iacobazzi V. Cancer cell metabolism in hypoxia: role of hif-1 as key regulator and therapeutic target. *Int J Mol Sci* (2021) 22(11):5703. doi: 10.3390/ijms22115703

110. Nagao A, Kobayashi M, Koyasu S, Chow CC, Harada H. Hif-1-Dependent reprogramming of glucose metabolic pathway of cancer cells and its therapeutic significance. *Int J Mol Sci* (2019) 20(2):238. doi: 10.3390/ijms20020238

111. Semba H, Takeda N, Isagawa T, Sugiura Y, Honda K, Wake M, et al. Hif-1α-Pdk1 axis-induced active glycolysis plays an essential role in macrophage migratory capacity. *Nat Commun* (2016) 7(1):11635. doi: 10.1038/ncomms11635

112. Koivunen P, Hirsilä M, Remes AM, Hassinen IE, Kivirikko KI, Myllyharju J. Inhibition of hypoxia-inducible factor (Hif) hydroxylases by citric acid cycle intermediates: possible links between cell metabolism and stabilization of hif. *J Biol Chem* (2007) 282(7):4524–32. doi: 10.1074/jbc.M610415200

113. Shi J, Yu T, Song K, Du S, He S, Hu X, et al. Dexmedetomidine ameliorates endotoxin-induced acute lung injury in vivo and in vitro by preserving mitochondrial dynamic equilibrium through the hif-1a/Ho-1 signaling pathway. *Redox Biol* (2021) 41:101954. doi: 10.1016/j.redox.2021.101954

114. Rasmussen ML, Kline LA, Park KP, Ortolano NA, Romero-Morales AI, Anthony CC, et al. A non-apoptotic function of mcl-1 in promoting pluripotency and modulating mitochondrial dynamics in stem cells. *Stem Cell Rep* (2018) 10(3):684–92. doi: 10.1016/j.stemcr.2018.01.005

115. Sharma D, Brummel-Ziedins KE, Bouchard BA, Holmes CE. Platelets in tumor progression: a host factor that offers multiple potential targets in the treatment of cancer. *J Cell Physiol* (2014) 229(8):1005–15. doi: 10.1002/jcp.24539

116. Varon D, Hayon Y, Dashevsky O, Shai E. Involvement of platelet derived microparticles in tumor metastasis and tissue regeneration. *Thromb Res* (2012) 130 Suppl 1:S98–9. doi: 10.1016/j.thromres.2012.08.289

Frontiers in Immunology

Explores novel approaches and diagnoses to treat immune disorders.

The official journal of the International Union of Immunological Societies (IUIS) and the most cited in its field, leading the way for research across basic, translational and clinical immunology.

Discover the latest Research Topics

See more →

Frontiers

Avenue du Tribunal-Fédéral 34
1005 Lausanne, Switzerland
frontiersin.org

Contact us

+41 (0)21 510 17 00
frontiersin.org/about/contact